



HAL
open science

Contrasting the flavors of ENSO and related trends in the tropical Pacific Ocean in recent decades

Awnesh Singh

► **To cite this version:**

Awnesh Singh. Contrasting the flavors of ENSO and related trends in the tropical Pacific Ocean in recent decades. Oceanography. Université Paul Sabatier - Toulouse III, 2012. English. NNT : . tel-00795552

HAL Id: tel-00795552

<https://theses.hal.science/tel-00795552>

Submitted on 28 Feb 2013

HAL is a multi-disciplinary open access archive for the deposit and dissemination of scientific research documents, whether they are published or not. The documents may come from teaching and research institutions in France or abroad, or from public or private research centers.

L'archive ouverte pluridisciplinaire **HAL**, est destinée au dépôt et à la diffusion de documents scientifiques de niveau recherche, publiés ou non, émanant des établissements d'enseignement et de recherche français ou étrangers, des laboratoires publics ou privés.



THÈSE

En vue de l'obtention du

DOCTORAT DE L'UNIVERSITÉ DE TOULOUSE

Délivré par l'Université Toulouse III - Paul Sabatier
Discipline ou spécialité : *Océanographie Physique*

Présentée et soutenue par *Awnesh SINGH*
Le 25 octobre 2012

Titre : *De la diversité des événements El Niño Oscillation Australe dans l'océan Pacifique tropical et des tendances climatiques associées au cours des 50 dernières années*

Title : *Contrasting the flavors of ENSO and related trends in the tropical Pacific Ocean in recent decades*

JURY

Jacqueline BOUTIN, LOCEAN/IPSL, Examinatrice
Sophie CRAVATTE, IRD/LEGOS, Examinatrice
Thierry DELCROIX, IRD/LEGOS, Directeur de thèse
Yves GOURIOU, IRD/IMAGO, Rapporteur
Eric GUILYARDI, CNRS/LOCEAN, Rapporteur
Nicholas HALL, Université Toulouse III, Examineur
Christophe MENKES, IRD/LOCEAN, Examineur
Laurent TERRAY, CERFACS, Examineur

Ecole doctorale : *ED SUD2E : Océan, Atmosphère et Surfaces Continentales*
Unité de recherche : *LEGOS*
Directeur de Thèse : *Thierry DELCROIX*
Rapporteurs : *Yves GOURIOU et Eric GUILYARDI*

Acknowledgments

How can I thank thee? Let me count the ways ...

This thesis has been compiled through the assistance of many individuals who have helped me throughout my research work. No words are sufficient to express my gratitude and appreciation to these individuals. Nonetheless, I would like to record my sincere acknowledgment for their support in the compilation of this thesis.

The invaluable guidance, advice and kindness from my honorific supervisor, Thierry Delcroix, provided a strong foundation to my research work which was essential to get this thesis up to standard. Without his help, I may not have finished my thesis successfully. I have learnt a lot from him and am greatly indebted for his acceptance of me as a PhD student. It was an unparalleled effort from him to proof-read the draft chapters and enable this research to be completed within the required timeframe. His humorous nature was always a refreshing break from scientific issues.

My sincere appreciation goes to the members of the jury for accepting the invitation to review my thesis: Yves Gouriou and Eric Guilyardi (rapporteurs), Jacqueline Boutin, Sophie Cravatte, Nick Hall, Christophe Menkes and Laurent Terray (examiners). I am immensely thankful to Sophie Cravatte for her advice and critical comments throughout the duration of this thesis project. Her suggestions greatly improved the draft manuscripts prior to submission.

I am also indebted to the Institut de Recherche pour le Développement (IRD) for giving me the opportunity to complete my PhD by awarding me a scholarship. Their financial support during my Masters project also does not go unnoticed. At this point, I would like to thank the French Consulate in Fiji for facilitating the necessary arrangements to allow me to travel to Noumea and Toulouse. My appreciation extends to the Laboratoire d'Etudes en Géophysique et Océanographie Spatiales (LEGOS) and the directors, Yves du Penohat (former) and Yves Morel (present), for the use of the laboratory facilities and providing an extra two months of financial support to defend this thesis. The administrative aspects of a PhD can be difficult at

times and I am thankful to the secretaries Brigitte Cournou, Catherine Donati, Nadine Lacroux and Martine Mena for their vital expertise and assistance during my stay at LEGOS. My appreciation goes to the University Paul Sabatier (UPS) for accepting me as an international student and accrediting my qualifications from the University of the South Pacific (USP).

It would be very difficult to mention in detail the contribution of all persons who have helped me during the course of my thesis. Nonetheless, they are (in alphabetical order): Gael Alory, Than Aung, Casamir Da-Allada, Guillaume Dencausse, Gerard Eldin, Chalapan Kaluwin, Sushil Kumar, Fabien Léger and his family, Frédéric Marin, Sylvain Ouillon, Marie-Hélène Radenac, and Zeinabou Sabatier. I also thank the members of the Océan du Large et Variabilité Climatique (OLVAC) team for their contribution during discussions about my project work. My sincere gratitude goes to all my friends, colleagues and family members who have supported me in my thesis journey.

Finally, I am greatly indebted to my family (Dad, Mum, Jyoti and Alysha) for their relentless and overwhelming support to bring me up to this point in my life. Their belief and continual encouragement has been a source of inspiration to my work and I am deeply indebted to them for standing by my side. I know I have lost valuable time with you all during this thesis project and I promise to make it up to you. I love you all and dedicate this thesis to thee.

Résumé

Comprendre les mécanismes moteurs et pouvoir anticiper l'impact environnemental du phénomène El Niño Oscillation Australe (ENOA) constituent des enjeux scientifiques et sociétaux de première importance, notamment pour les Pays Emergents. Dans cette thèse, nous avons documenté et contrasté la signature de différents types d'ENOA - dits canoniques et Modoki - pour plusieurs variables climatiques essentielles (température et salinité de surface, niveau de la mer, courant de surface, précipitation, vent de surface, ...), analysé la pertinence de la théorie dite de recharge / décharge, une des quatre théories majeures d'ENOA, à rendre compte ou non de la nature quasi oscillatoire de ces différents types et quantifié l'impact potentiel des modifications des caractéristiques majeures d'ENOA sur notre interprétation des tendances climatiques à 'long' terme pour ces variables climatiques essentielles.

Mots-clés

ENSO, ENOA, El Niño, La Niña, Océan Pacifique Tropical, *warm pool*, *SPCZ*, *ZCPS*, température de surface, salinité de surface, niveau de la mer, volume d'eau chaude, oscillateur rechargé déchargé

Table of Contents

<i>Acknowledgments</i>	<i>ii</i>
<i>Résumé</i>	<i>iv</i>
Chapter 1	1
Introduction	1
1.1 The ENSO phenomenon	1
1.2 ENSO diversity	4
1.3 The Eastern and Central Pacific ENSO debate	7
1.4 Thesis Objectives	8
1.5 Organization of Thesis	9
Chapter 2	11
Datasets and Methodology	11
2.1 Introduction	11
2.2 Data	11
2.2.1 Sea Surface Salinity (SSS)	11
2.2.2 Sea Surface Temperature (SST)	14
2.2.3 Sea Level Anomaly (SLA)	14
2.2.4 Sea Surface Currents (U)	15
2.2.5 Precipitation (P)	15
2.2.6 ENSO Indices	16
2.2.7 Simple Ocean Data Assimilation (SODA)	18
2.2.8 DRAKKAR Model	18
2.3 Methodology	19
2.3.1 Basic Data Treatment	19

2.3.2	Empirical Orthogonal Function (EOF)	20
2.3.3	Agglomerative Hierarchical Clustering (AHC)	21
2.3.4	Self-Organizing Maps (SOM)	21
2.4	Computation Platform	22
2.5	Summary	22
Chapter 3		23
	Contrasting the flavors of ENSO	23
3.1	Introduction	23
3.2	Long term mean and interannual variability	23
3.3	SST, SSS and SL signal during ENSO	24
3.3.1	SST	26
3.3.2	SSS	28
3.3.3	SL	31
3.4	Multivariate Analyses	35
3.4.1	Multivariate EOF Analysis (MVEOF)	36
3.4.2	Neural Network Analysis (NNA)	36
3.5	Summary and Discussion	41
3.6	Publication: Singh <i>et al.</i> , 2011	44
Chapter 4		61
	ENSO, WWV and the RD oscillator paradigm	61
	Preamble	61
	Submitted Manuscript	62
	Abstract	63
4.1	Introduction	64
4.2	Data and Methods	66
4.3	Observed and modeled SL and WWV changes	69
4.3.1	Observational results, 1993-2010	69

4.3.2	Model Results, 1958-2007	71
4.4	Transport contribution to the modeled WWV	75
4.4.1	Mean State	75
4.4.2	Contrasting EP and CP ENSO events	77
4.5	Conclusions and Discussion	80
4.6	References	83
	Supplementary Material	88
Chapter 5		89
	Estimating trends due to ENSO	89
5.1	Introduction	89
5.2	Trends due to ENSO: A multivariate linear regression approach	89
5.2.1	SST	91
5.2.2	SSS	93
5.2.3	SL	94
5.3	Summary and Discussion	98
5.4	Publication: Singh and Delcroix, 2011	100
Chapter 6		107
	Synthesis and Discussion	107
	Preamble	107
6.1	ENSO flavors	107
6.1.1	The 1997-98 EP El Niño	108
6.1.2	The 2002-03 CP El Niño	110
6.2	EP and CP ENSO vs. RD oscillator paradigm	110
6.2.1	EP ENSO dynamics	111
6.2.2	CP ENSO dynamics	112
6.2.3	Perspectives I	112
6.3	Trends due to EP and CP ENSO	112

6.3.1	ENSO trends in SST	113
6.3.2	ENSO trends in SSS	114
6.3.3	ENSO trends in SL	114
6.3.4	Perspectives II	115
6.4	Challenging some of my results	115
6.4.1	Data Length	116
6.4.2	EP and CP ENSO and the annual cycle	117
6.4.3	Statistical Methods	117
6.4.4	The neutral cluster	118
6.5	Final Remarks	120
References		121
Appendix		145
Appendix I	Poster: Singh <i>et al.</i> , 2011	145
Appendix II	Publication: Radenac <i>et al.</i> , 2012	146
Appendix III	Scientific News Sheet, IRD, 2012	162
Appendix IV	Résumé étendu	164
Appendix V	Thesis Journey	167
	Publications	167
	Seminars	167
	Meetings	168
	Other	168

Chapter 1

Introduction

1.1 The ENSO phenomenon

El Niño was initially a term reserved by Peruvian fishermen to explain the warm seasonal southward coastal currents that appeared along the Peru coast around Christmas. These currents are unusually intense and persistent every few years, and are associated with rainfall that literally transforms the northern Peruvian desert into a garden ([Philander, 1999](#)). Hence the term El Niño, which is Spanish for “the little boy” and refers to the *Christ child*. However, after many studies focusing on data collected and analyzed from numerous in situ and satellite data over the years, El Niño is now used to refer to the basin scale warming that occurs over the equatorial Pacific.

Following a few pioneering studies (e.g., [Hildebrandsson, 1898](#)), in a series of papers [Walker \(1923; 1924; 1928\)](#) and [Walker and Bliss \(1930; 1932; 1937\)](#) discovered that the surface atmospheric pressure fluctuated out of phase between the eastern and western halves of the tropical Pacific Ocean. Consequently, Walker coined the term Southern Oscillation to portray this east-west seesaw in Southern Pacific barometric pressure. [Bjerknes \(1966; 1969\)](#) established the link between El Niño and the Southern Oscillation and hence the name El Niño Southern Oscillation (ENSO), which is now recognized as a basin scale coupled ocean-atmosphere phenomenon in the tropical Pacific region.

ENSO is the most energetic climatic signal on interannual timescales. It originates in the tropical Pacific and as the name suggests, ENSO oscillates between anomalously warm (El Niño) and cold (La Niña) events recurring approximately every 2-7 years. El Niño and La Niña events develop in conjunction with swings in atmospheric pressure between the Indo-Pacific region and the eastern tropical Pacific. These pressure swings, or the Southern Oscillation, are related to the strength of the Pacific trade winds (see [Philander, 1990](#)). While ENSO originates from the tropical Pacific climate, it strongly affects patterns of weather variability worldwide through atmospheric teleconnections. Consequently, the term ENSO

has become synonymous with social, economic and environmental crisis in many parts of the globe, in particular for the emerging countries (Glantz, 1996; Goddard and Dille, 2005). For some countries, an ENSO event is typically associated with abnormal heat and drought whereas for others, it is persisting rains and devastating floods. Additionally, sea level in the vicinity of the Pacific Island countries can rise or drop by ~20 cm during an ENSO event (e.g., Singh and Aung, 2005). The link between the atmospheric and oceanic components during an El Niño event was brought into perspective probably starting from the milestone papers of Wyrki (1975) and Rasmusson and Carpenter (1982). Consequently, advancements in technology and scientific understanding of the tropical ocean and global atmosphere, and the unexpected arrival of the 1982-83 El Niño, led to the creation of the Tropical Oceans-Global Atmosphere (TOGA) program over the 1985-1994 period (Halpern, 1996).

TOGA's goals were to determine the predictability of the coupled ocean-atmosphere system in the tropics on seasonal to interannual time scales; to understand the mechanisms responsible for that predictability; and to establish an observing system to support climate prediction (McPhaden *et al.*, 2010). As a result, a vast array of observation systems dedicated to observing the state of the tropical Pacific Ocean, ideally in real time, have been put in place and/or internationally coordinated. Specific in situ observational programs were developed to provide these datasets, which include the Tropical Atmosphere-Ocean (TAO) array of moored buoys in the Pacific, a surface drifting buoy program, an island and coastal tide gauge network, and a volunteer observing ship network of expendable bathythermograph measurements (McPhaden *et al.*, 1998). The implementation of the TAO/Triangle Trans-Ocean Buoy Network (TRITON) array, presently maintained jointly by the Pacific Marine Environmental Laboratory (PMEL) and the Japan Agency for Marine-Earth Science and Technology (JAMSTEC), began in 1985 (with contribution from the ORSTOM/IRD centre in New Caledonia during TOGA). It was complemented by the advent of satellite altimetry data for the global ocean, also beginning in the early 1980s, with the launch of the Geodetic satellite (GEOSAT) followed by the Topex/Poseidon (in 1992), Jason (in 2001) and European Remote Sensing (ERS) series of satellite missions. The deployment of the first automated Argo floats in 2000 and the subsequent Argo international program (Roemmich *et al.*, 2009) provided the much needed subsurface temperature and salinity data, which previously were collected through Conductivity, Temperature and Depth (CTD) profilers via dedicated research cruises, Expendable Bathythermograph (XBT) and Thermosalinographs (TSGs) aboard merchant ships. The improvements in ocean data quality and frequency over

the last few decades has given much needed confidence to monitor (now in real time), analyze, understand and predict the state of the tropical ocean, and in particular, the ENSO phenomenon in more detail. Accordingly, we present here a brief and simplified summary of the sequence of events leading to the development of an El Niño.

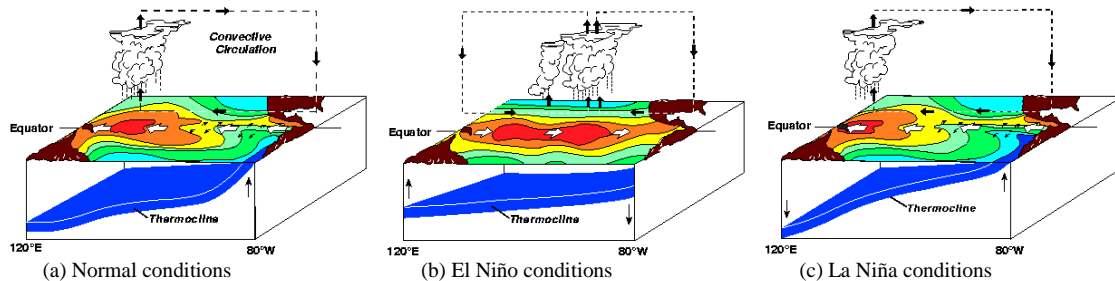


Figure 1.1 Schematic plots of the state of the tropical Pacific during (a) normal, (b) El Niño, and (c) La Niña conditions. The contour plots illustrate the sea surface temperature with red (blue) denoting warmer (cooler) temperatures. Thick black (white) arrows denote the wind (surface currents) direction. [Adapted from http://www.pmel.noaa.gov/tao/el_nino/nino-home.html]. Note that the World Meteorological Organization (WMO) officially defines an event as an El Niño or La Niña when SST anomalies in the Niño3.4 region exceed $\pm 0.5^\circ\text{C}$ for at least three consecutive months.

During normal conditions (Fig. 1.1a) and prior to the onset of an El Niño, strong southeast trade winds over the central Pacific intensifies the South Equatorial Current (SEC) resulting in an accumulation of warm waters in the western equatorial Pacific and an east-west slope in the thermocline (and reversed slope in sea level). The relaxation of these trades in synchrony with the appearance of westerlies in the western equatorial Pacific during the onset stage of El Niño, leads to an eastward release of the accumulated waters, which results in anomalous warming of waters in the central equatorial Pacific and deepening of the thermocline there. Bjerknes positive feedback between the ocean and atmosphere further enhances the westerlies in the west resulting in warmer sea surface temperature (SST) anomalies extending from the central Pacific towards the South American coast. Because of the change in the surface pressure, the fully developed El Niño alters the normal atmospheric Walker circulation resulting in an eastward shift of precipitation anomalies from the western to the central equatorial Pacific (Fig. 1.1b). In addition, the regions of wind stress convergence in the northern and southern hemispheres are also modified. The Inter Tropical Convergence Zone (ITCZ) and South Pacific Convergence Zone (SPCZ) move southwards and north-eastwards, respectively, thereby modifying the regions of precipitation. During La Niña (Fig. 1.1c), the southeast trade winds intensify further than during normal conditions. This pushes the warm waters further into the far western equatorial Pacific thereby strengthening the east-west gradient in thermocline depth (and sea level). The region of anomalous precipitation

shifts further westwards and the ITCZ and SPCZ regions move northwards and south-westwards, respectively, of its normal position.

As noted above, our understanding of ENSO has greatly improved since the 1990s thanks to the development of dedicated observing (in situ and satellite) systems. Most of the progress also comes from specific process studies, analytical and modeling studies, and relevant theories (e.g., see the special TOGA issue of the *Journal of Geophysical Research* published in 1998; and [Clarke, 2008](#)). Among those theories, one group has especially been proposed to account for the observed quasi-oscillatory nature of ENSO, while another group conjectures that ENSO may be a stable (and not self-sustained) mode triggered by stochastic wind forcing. In the former group, four major theories have been proposed for the oscillatory nature of ENSO: the delayed oscillator ([Suarez and Schopf, 1988](#); [Battisti and Hirst, 1989](#)), the advective-reflective oscillator ([Picaut et al., 1997](#)), the western Pacific oscillator ([Weisberg and Wang, 1997](#)), and the recharge-discharge oscillator ([Jin, 1997](#)). Basically, the above group of theories rely on the fact that after an El Niño reaches its peak phase, negative feedbacks are required to terminate the growth of the positive SST anomalies and possibly reverse it into a La Niña. Motivated by the existence of these different oscillator models, [Wang \(2001\)](#) proposed a unified oscillator model, which includes the physics of all four ENSO oscillator models. A schematic diagram (and explanation) of the unified oscillator model is illustrated in [Fig. 1.2](#).

1.2 ENSO diversity

Several features contribute to the diversity of El Niño. These include its amplitude (e.g., [Li et al., 2011](#)), duration (e.g., [Glantz et al., 1991](#)), onset time (e.g., [Wang, 1995](#)), strength (e.g., [Wolter and Timlin, 1998](#)), phasing with the seasonal cycle (e.g., [Jin et al., 1994](#)), eastward/westward propagation of SST anomalies along the equator (e.g., [Wang, 1995](#); [McPhaden and Zhang, 2009](#)), asymmetry between El Niño and La Niña in terms of duration (e.g., [Okumura and Deser, 2010](#)) and spatial patterns (e.g., [Yu and Kim, 2011](#)), and more recently, the location of SST anomalies (e.g., [Ashok et al., 2007](#)). To exemplify the diversity of El Niño using the Niño3.4 index, [Fig. 1.3](#) shows the difference in amplitude and duration for El Niño events over the past few decades in the tropical Pacific. In addition, [Fig. 1.4](#) shows the difference in onset times for El Niño events during a similar period. These features illustrate what had been stated more than 35 years ago by [Wyrтки \(1975\)](#) that “no two El Niño

events are quite alike". Other indices have since been proposed to further classify and tentatively discriminate between ENSO events; these are detailed in Chapter 2.

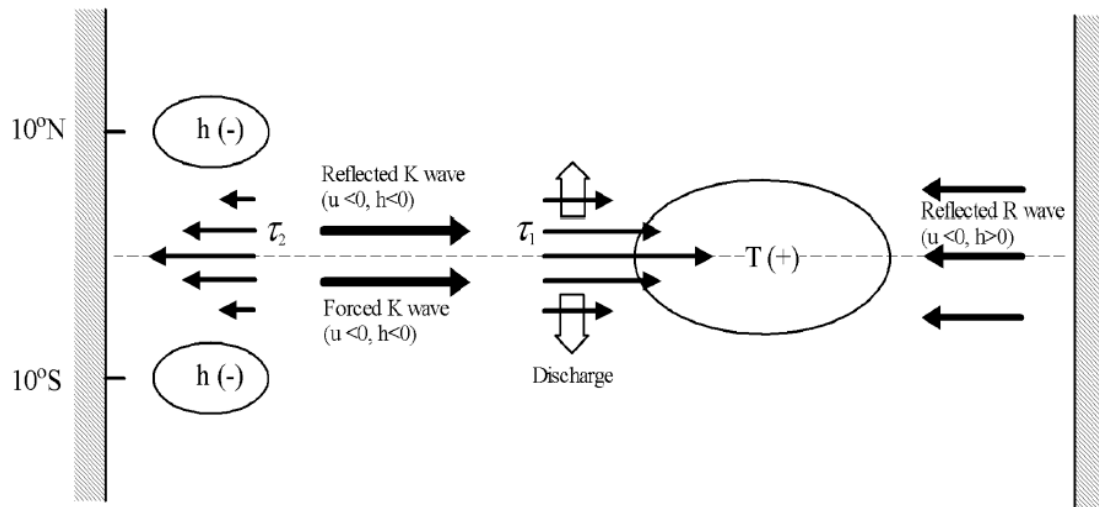


Figure 1.2 Schematic diagram of the unified oscillator for ENSO. Bjerknes positive ocean-atmosphere feedback leads the equatorial central/eastern Pacific to a warm state (El Niño). Four negative feedbacks, required to turn the warm state around, are (1) reflected Kelvin wave at the ocean western boundary, (2) discharge process due to Sverdrup transport, (3) western Pacific wind-forced Rossby wave, and (4) reflected Rossby wave at the ocean eastern boundary. These negative feedbacks correspond to the delayed oscillator, the recharge oscillator, the western Pacific oscillator, and the advective-reflective oscillator. The unified oscillator suggests that all of the four negative feedbacks may work together, with different respective contribution for each event, in terminating El Niño warming. The four ENSO oscillators are special cases of the unified oscillator. [Adapted from Wang and Picaut, 2004]

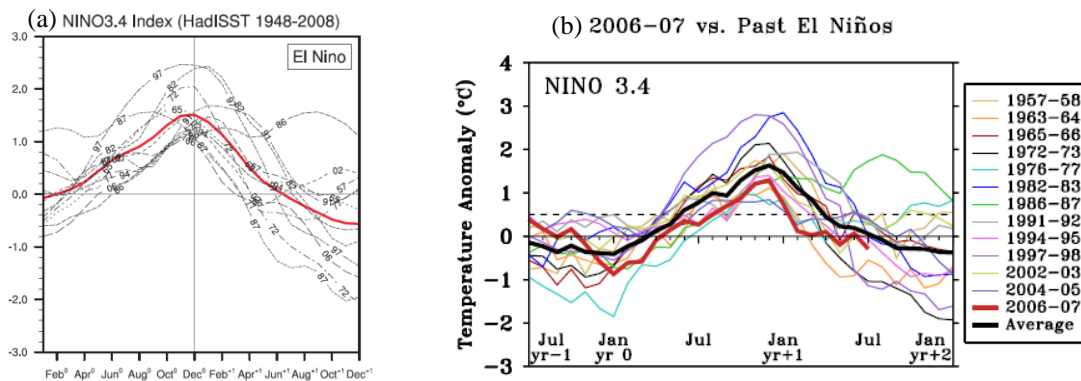


Figure 1.3 (a) Time series of the Niño3.4 index overlaid from Jan⁰ to Dec⁺¹ for El Niño during 1948-2008 based on HadISST. The thick red line is the composite time series. [Adapted from Okumura and Deser, 2010] (b) Niño3.4 index for El Niño events since 1957-1958 to 2006-2007. Time series are split into 2.5 year segments starting July the year before the peak warm anomaly (Jul yr-1) and ending January approximately one year after the peak anomaly (Jan yr+2). Dashed horizontal line indicates the 0.5°C threshold for the definition of El Niño warm anomalies. The thick black line is the average Niño3.4 anomaly based on the twelve previous El Niños from 1957-1958 to 2004-2005. [Adapted from McPhaden, 2008]

Differences in the Onset of El Niño Events

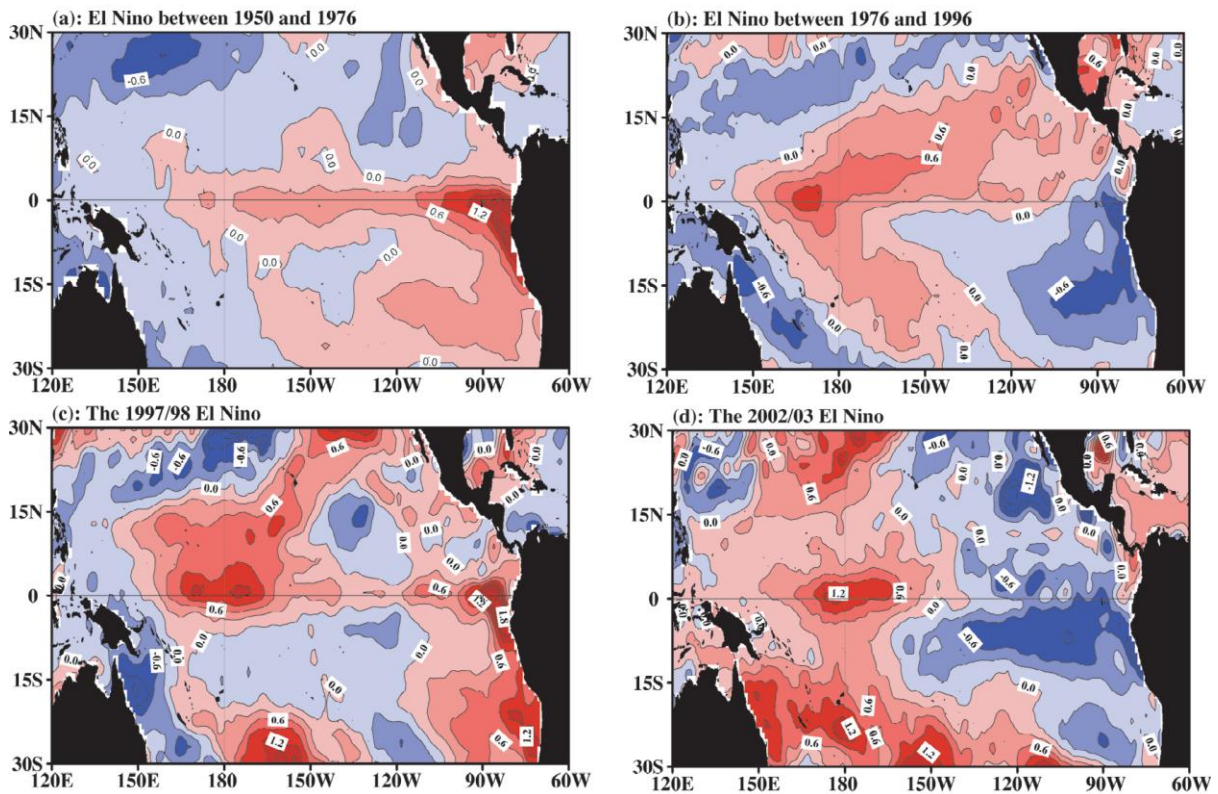


Figure 1.4 SST anomaly composites showing the differences in the onset of El Niño over the last five decades. (a) El Niño between 1950 and 1976, (b) El Niño between 1977 and 1996, (c) the 1997-98 El Niño, and (d) the 2002-03 El Niño. The composites are calculated by averaging the SST anomalies during March-May of the El Niño year. Since the 2002-03 El Niño started earlier, its composite used the SST anomalies of December 2001 to February 2002. [Adapted from Wang and Picaut, 2004]

Numerous studies have used both observational and model data to test the previously mentioned oscillatory theories and their relevance to explain ENSO. However, it should be noted that these theories were proposed more than a decade ago, before the recent enhanced attention given to an *argued* different type of El Niño, variously termed as *Dateline El Niño* (Larkin and Harrison, 2005a,b), *El Niño Modoki* (Ashok *et al.*, 2007), *Warm Pool El Niño* (Kug *et al.*, 2009) or *Central Pacific El Niño* (Kao and Yu, 2009), and hereafter referred to as CP El Niño. This “new” flavor of El Niño has added a new dimension to the ENSO climatic puzzle as it has maximum SST anomalies (relative to the mean monthly climatology) confined to the central equatorial Pacific, in contrast with the variously called *traditional*, *canonical*, *conventional*, *cold tongue* or *Eastern Pacific El Niño* (hereafter referred to as EP El Niño), when they occur in the eastern Pacific (see Fig. 1.5). In addition, the global climatic impacts due to EP and CP El Niño events have been shown to differ. For example, Kim *et al.* (2009) showed that the relative increased frequency and landfall potential of North Atlantic

tropical cyclones on the coast of the Gulf of Mexico and Central America is associated with CP El Niño rather than EP El Niño. [Weng *et al.* \(2009\)](#) indicated that there is an increased transport of moisture from the tropics to higher latitudes during CP El Niño than during EP El Niño due to the increased poleward extent of the tripolar pattern of boomerang-shaped SST, precipitation and upper-level divergent wind anomalies in the eastern Pacific.

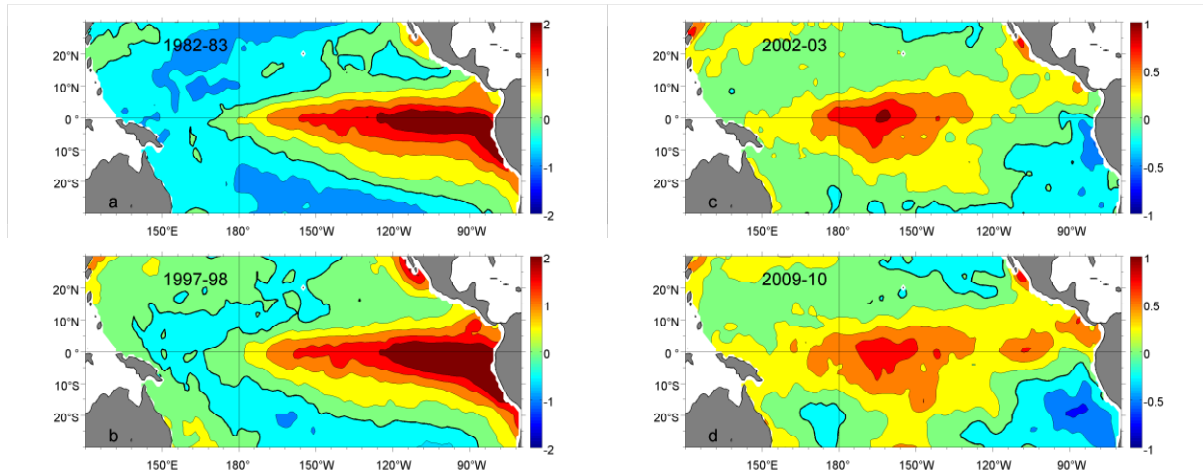


Figure 1.5 SST anomalies (with respect to the 1971-2000 mean monthly climatology) in the tropical Pacific during the December-January-February months for the EP El Niño events in (a) 1982-83 and (b) 1997-98, and the CP El Niño events in (c) 2002-03 and (d) 2009-10. Units are in °C. Thick black contour lines in the spatial patterns denote the 0 line. Note the different color scales in the plots.

1.3 The Eastern and Central Pacific ENSO debate

The apparent changing pattern of El Niño in recent decades has sparked widespread scientific interest into the causes of these “unusual” warming patterns. With the consequent increase in research on CP El Niño events, numerous questions have been put forward including whether or not: (a) observation- and model-based data are long enough ([Stevenson *et al.*, 2010](#)) and whether statistical methods are “reliable” to get robust statistics ([Kao and Yu, 2009](#); [Kug *et al.*, 2009](#); [Choi *et al.*, 2011](#); [Yu and Kim, 2011](#); [Kim *et al.*, 2012](#)); (b) there is an increased occurrence of CP El Niño in recent years ([Lee and McPhaden, 2010](#); [Horii *et al.*, 2012](#); [Kim *et al.*, 2012](#); [McPhaden, 2012](#); [Xiang *et al.*, 2012](#)); (c) there is a link between CP El Niño and global warming ([Nicholls, 2008](#); [Yeh *et al.*, 2009](#); [Collins *et al.*, 2010](#); [Newman *et al.*, 2011](#)), and/or between CP El Niño and changes in the mean/background state of the tropical Pacific ([Fedorov and Philander, 2000](#); [Guilyardi, 2006](#); [Okumura and Deser, 2010](#); [Choi *et al.*, 2011](#); [McPhaden *et al.*, 2011](#); [Kim *et al.*, 2012](#)); (d) climate models, providing long time series for the pre- and post-industrial periods, are trustworthy to simulate CP El Niño ([van Oldenborgh](#)

et al., 2005; Leloup *et al.*, 2008; Guilyardi *et al.*, 2009; Choi *et al.*, 2011; Delcroix *et al.*, 2011; Ham and Kug, 2012; Kim and Yu, 2012); and (e) CP El Niños actually exist (Lian and Chen, 2012), to name a few. The diversity of these questions provides evidence that understanding ENSO dynamics remains a considerable challenge (Vecchi and Wittenberg, 2010) to the scientific community.

1.4 Thesis Objectives

Many studies have used SST to stress the differences between (EP and CP) ENSO events since the climatic impacts are sensitive to details of the surface warming/cooling of the equatorial Pacific (Palmer and Mansfield, 1984) via varying teleconnections, and because SST is by far the best observed oceanic variable. However, using different variables (e.g., sea level anomaly, surface wind stress, subsurface temperature, precipitation, outgoing long-wave radiation) to document ENSO clearly gives different perspectives rather than using SST alone to understand its behaviour, impacts and how it works. An essential climatic variable of the global climate observing system (Global Climate Observing System, 2004; see also Lagerloef *et al.*, 2008) that is also affected by (and may impact) the ENSO cycle is sea surface salinity (SSS). Indeed, precipitation patterns and heat fluxes are modified in the course of an El Niño or La Niña, affecting SSS, which may in turn modify the ocean mixed layer depth and impact ENSO thermodynamics and dynamics. Moreover, anomalous surface currents have been observed during CP El Niño (Kug *et al.*, 2009) and we can expect these currents to imprint on the distribution of SSS given the main role of zonal salt advection in the equatorial band on ENSO time scales (Picaut *et al.*, 2001).

Furthermore, the intriguing and socially-relevant topic on the influence of anthropogenic and natural effects on climate change has been widely documented (e.g., IPCC, 2007). In line with this, various studies have used different variables to estimate the contribution of climate change and/or climate modes such as ENSO and the Pacific Decadal Oscillation (PDO) on the observed long-term trends (e.g., Cravatte *et al.*, 2009 used sea surface salinity; Compo and Sardeshmukh, 2010 used sea surface temperature; Merrifield and Maltrud, 2011 used sea level; Zhang *et al.*, 2007 used precipitation; Gillet *et al.*, 2003 used sea level pressure; Jones *et al.*, 2003 used atmospheric temperature; Santer *et al.*, 2003 used tropopause height; Barnett *et al.*, 2005 used ocean heat content). However, to our knowledge, no study has yet quantified the respective effects of the different flavors of ENSO on the long-term trends, with the

exception of Lee and McPhaden (2010) who used satellite-derived SST to attribute the observed warming trends in the western Pacific warm pool region to the increased intensity and frequency of CP El Niño events.

Hence, as a complement to previous studies, the major objectives of this study were:

1. for the first time, to tentatively contrast and explain the different flavors of ENSO using SSS;
2. to differentiate the flavors of ENSO in terms of dynamics and whether one of the leading theories for the oscillatory nature of ENSO, the recharge-discharge oscillator paradigm, can account for the EP and CP ENSO features; and
3. to quantify the effects of the different flavors of ENSO on the long-term freshening/salting trends in SSS, as a possible input to the broad question of how to discriminate natural climate variability from observed climate change.

These key objectives were further extended during the course of this study to include the climate variables SST and sea level (SL). These are also presented, however, no manuscript has been submitted and/or published on these results so far.

1.5 Organization of Thesis

This thesis manuscript is organized and presented as follows:

- Chapter 2 gives a detailed description of the various observational and model datasets used for this study and the methodology employed to analyze these datasets.
- Chapter 3 attempts to contrast the different flavors of ENSO using the essential climate variables sea surface temperature, sea surface salinity and sea level. Different methods are used to verify that the results are robust. A paper published in the *Journal of Geophysical Research* focusing on sea surface salinity is included.
- Chapter 4 uses both observational and model data to test if one of the leading theories on the oscillatory nature of ENSO, the recharge-discharge oscillator

paradigm, can explain the new flavor of ENSO. A paper submitted to *Deep Sea Research: Part I*, focusing on warm water volume variability and transport dynamics is incorporated within this chapter.

- Chapter 5 estimates and quantifies the effects of the different flavors of ENSO on the long-term sea surface temperature, sea surface salinity and sea level trends observed in the tropical Pacific region. A paper published in *Geophysical Research Letters* focusing on sea surface salinity is included as well.
- Chapter 6 reviews the results of this study. A brief summary of the contributions of the present study to the understanding of the climate dynamics in the tropical Pacific is presented. In addition, some challenges and perspectives for future work are discussed.
- An appendix section is also included, which comprises of a poster presented at international meetings, a paper published in relation to a parallel study to contrast the flavors of ENSO using chlorophyll, a monthly scientific news sheet published by the IRD, and final comments on this thesis journey.

The major objective of any kind of study is to add something new to already existing knowledge on a particular topic. Consequently, this study aims to build on the pioneering and extensive works on ENSO, and in particular, to differentiate the flavors of ENSO using sea surface salinity and other essential climatic variables. In addition, the mechanisms responsible for the different observed signatures will be investigated and possible explanations will be proposed. Furthermore, one of the leading theories for the oscillatory nature of ENSO will be tested to see if it can explain the observed changes in ENSO behaviour. The ENSO and non-ENSO related effects on warming, freshening and sea level trends will also be examined. To begin this study, however, reliable data and methodology are crucial. These are discussed in the following chapter.

Chapter 2

Datasets and Methodology

2.1 Introduction

The availability of reliable, long-term and accurate data is of vital importance in climate studies, or any study for that matter. Erroneous data can lead to meaningless results and inappropriate conclusions can be derived accordingly. We therefore make use of data that has been properly documented for its source, methods of acquisition and data processing. Consequently, some data may have error estimates attached to them. We believe that all data (and methodology) that have been outlined below are “robust” in a sense that they have been, in some way, tested and utilized in many previous studies. This gives us additional assurance on the reliability of the data products used here. In addition, prior use of these data products and methodologies provide key information that helps assess their relative strengths and/or weaknesses. In this chapter, we highlight the use of in situ, satellite-derived and model-derived oceanic data with a few sets of atmospheric data as well.

2.2 Data

2.2.1 Sea Surface Salinity (SSS)

The sea surface salinity (SSS) data was obtained from the gridded product of [Delcroix *et al.* \(2011\)](#) for the tropical Pacific region (120°E-70°W, 30°S-30°N), which were derived from surface samples and Thermosalinographe (TSG) measurements through the Voluntary Observing Ship (VOS) programs, mainly from the French Sea Surface Salinity Observations Service (<http://www.legos.obs-mip.fr/observations/sss>), together with hydrocasts, STD and CTD measurements collected during research cruises, conductivity/temperature sensors on TAO/TRITON moorings and Argo floats. Details about the steps of combining the SSS data originating from these different sources can be found in [Delcroix *et al.* \(2011\)](#). An optimal interpolation procedure ([de Mey and Menard, 1989](#)) was adapted to obtain one value per month from 1950-2008 on a 1° longitude × 1° latitude grid. As the SSS data coverage is

greatly time dependent, each grid point has an associated error indicating the confidence we can have on the SSS product at one particular month. This error is given as a percentage of the interannual variance at that point (see Fig. 2.1). When there is no SSS data available, the error is 100% and the SSS gridded value is equal to the monthly climatological SSS. In their analysis using a similar product, Cravatte *et al.* (2009) used an arbitrary value of 60% to define the error threshold. Initial sensitivity studies found that using 80% as the error threshold does not significantly change the results presented below and we therefore choose to use this value in our analysis as the spatial coverage is wider. Accordingly, regions where the errors exceed 80% of the SSS variance have not been included in the analysis.

Recently, a new version of the SSS product was released. The major differences from the earlier version mentioned above are the extension of the time series to 2009 and the addition of newly obtained SSS data for previous years. Consequently, although it is tempting to use the new version in the present study, discrepancies may arise when comparing with results that were published using the earlier version (Singh *et al.*, 2011; Singh and Delcroix, 2011). In addition, some data analysis procedures are very sensitive to small changes in data (e.g., the agglomerative hierarchical clustering procedure which will be described later). However, it should be noted that recently Chen *et al.* (2012) derived similar results for the interannual SSS variability as those obtained by Singh *et al.* (2011) using the new version of the SSS product. We choose to use the 1950-2008 earlier version in the present project.

Salinity will be referred to using pss-78 (practical salinity scale-1978) in this study. The Thermodynamic Equation of Seawater – 2010 (TEOS-10), which has been adopted by the Intergovernmental Oceanographic Commission to replace Equation of State 1980 (EOS-80) as the official description of seawater, uses absolute salinity (S_A) as opposed to practical salinity (S_P) to describe the salt content of seawater (www.teos-10.org). Therefore, ocean salinities now have units of $g\ kg^{-1}$. However, because S_A is linearly related to S_P (Eq. 2.1; Millero *et al.*, 2008), the differences are negligible between the two scales in terms of the anomalies and hence we will continue to use the pss-78 scale.

$$S_A = \left(\frac{35.16504}{35} \right) g.kg^{-1} \times S_P \quad (2.1)$$

For the SSS in situ data (measured in pss), the mean difference in salinity between the two scales is 0.16 for the entire dataset, with the absolute scale being the larger of the two.

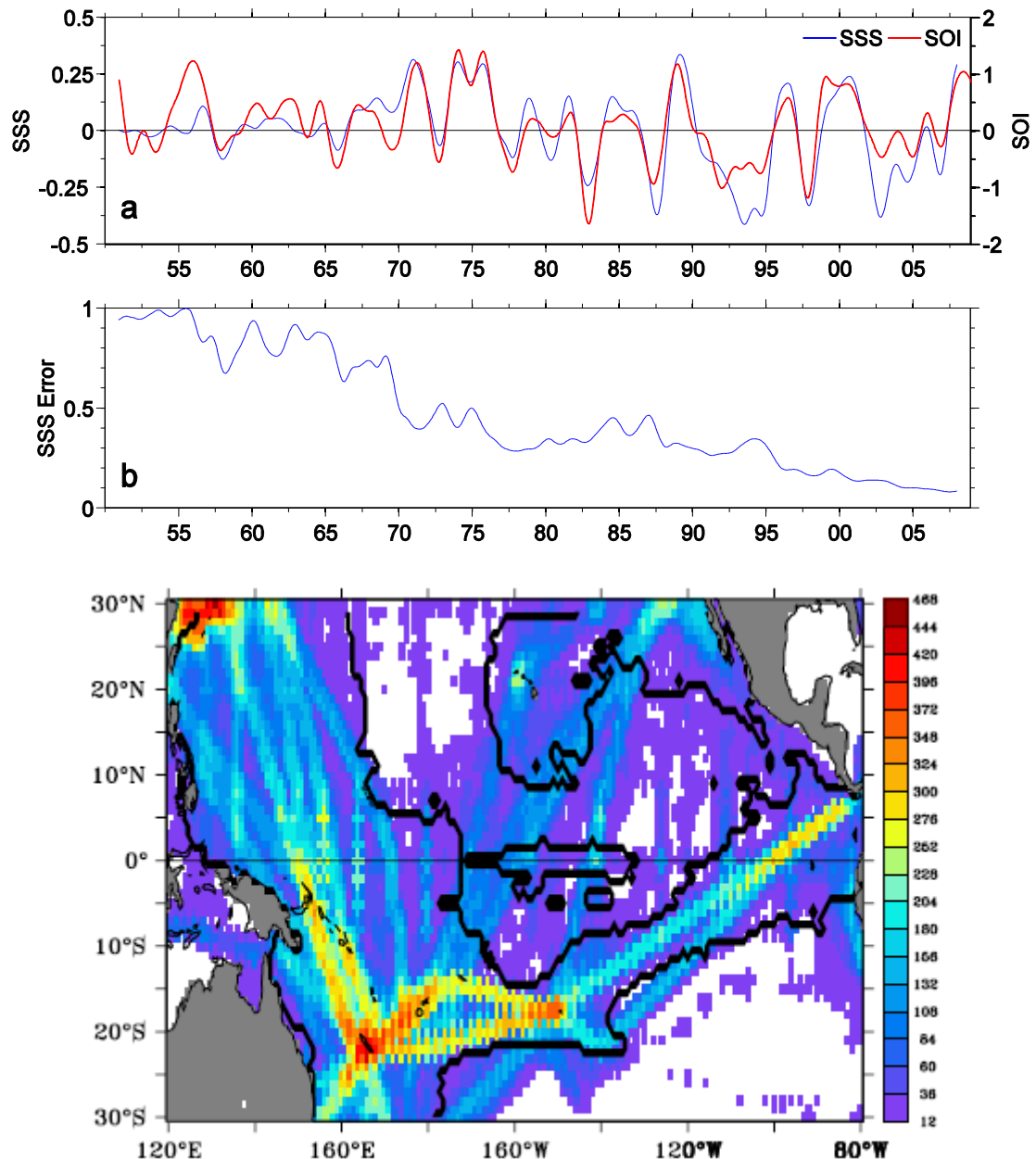


Figure 2.1 (a) Mean SSS anomaly (in blue; left vertical axis) averaged in the western equatorial Pacific region (150°E-170°W, 2°S-2°N) and the SOI (in red; right vertical axis), illustrating the regional ENSO signature in SSS (see Chapter 5). The SSS anomalies are relative to the 1971-2000 mean monthly climatology. (b) The corresponding mean SSS errors. Note the lack of interannual SSS variability in (a) at the beginning of the time series is spurious and actually reflects a poor data density distribution (error > 0.8). The time series are smoothed with a 25-months Hanning filter for clarity. “Units” for SSS anomaly is pss. [Adapted from Singh and Delcroix, 2011] (c) Number of months of SSS observations from 1955 to 2003. The heavy black line delimits the region where the calculations of trends, for example, are reliable. [Adapted from Cravatte *et al.*, 2009]

2.2.2 Sea Surface Temperature (SST)

For sea surface temperature (SST), we chose to use the Met Office Hadley Centre for Climate Prediction and Research sea ice and sea surface temperature dataset (HadISST1; Rayner *et al.*, 2003), available monthly from 1870 until present and which has the same 1° grid size as the SSS product. The Extended Reconstructed Sea Surface Temperature version 3 (ERSSTv3; Smith and Reynolds, 2003) and extended Kaplan version 2 (Kaplan *et al.*, 1998) datasets that are available on 2° and 5° grids, respectively, were also tested. Some differences between the datasets are evident before 1950 due to different historical bias adjustments, for example. However, we found no significant differences on interannual timescales (see Fig. 2.2) for our intended period of study (1950 onwards) and will focus on the HadISST dataset henceforth. We restrict the spatial and temporal domain for the data to be the same as that for the SSS data.

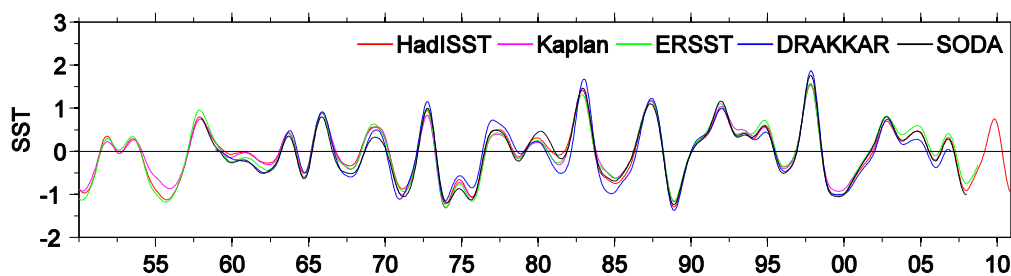


Figure 2.2 Mean SST anomaly for the 1950-2010 period in the Niño3.4 region (170°W - 120°W , 5°S - 5°N) relative to the 1971-2000 mean monthly climatology for HadISST (in red), Kaplan (in magenta), ERSST (in green), DRAKKAR (in blue) and SODA (in black) datasets. The time series are smoothed with a 25-months Hanning filter for clarity. Units are in $^\circ\text{C}$.

2.2.3 Sea Level Anomaly (SLA)

The remotely sensed homogeneous monthly sea level anomalies (SLA) were obtained in combining data from the ERS, ENVISAT, GEOSAT, Jason and Topex/Poseidon series of satellite reference missions (Ducet *et al.*, 2000) and are available from the Aviso website (<http://www.aviso.oceanobs.com>) on a $\frac{1}{4}^\circ$ cartesian grid from December 1992 to July 2011. The anomalies are monthly averages, which are calculated with respect to a seven year (1993-1999) mean. These are further processed here by removing the mean monthly climatology over the 1993-2010 period. The SLA data is an important component in climate studies, especially in the tropical Pacific because it is an alias for warm water volume (WWV), which is defined as the areal integral of warm water above the 20°C isotherm (see Chapter 4). The limited availability of subsurface observations in the tropical Pacific further

stresses the usefulness of SLA especially in studying interannual variability (e.g., [Bosc and Delcroix, 2008](#)).

2.2.4 Sea Surface Currents (U)

The surface currents (U) were acquired from the Ocean Surface Currents Analyses – Real time (OSCAR) product, which is available on a 1° grid monthly from October 1992 to July 2009 and includes both the geostrophic and Ekman components ([Bonjean and Lagerloef, 2002](#)). The near real-time currents are derived from satellite altimeter and scatterometer data. We also tested the Centre of Topography of the Oceans and the Hydrosphere (CTOH) surface currents product, which is available on a $\frac{1}{4}^\circ$ resolution grid weekly from 1999-2008 and also includes the geostrophic and Ekman components ([Sudre and Morrow, 2008](#)). However, due to the shorter data length (begins in 1999) and its emphasis on regions of mid to high latitudes, we chose the OSCAR product over the CTOH product. In addition to these two products, we tested the surface geostrophic currents (u_g) product available from Aviso (<http://www.aviso.oceanobs.com>), which is available on a $\frac{1}{4}^\circ$ grid weekly from October 1992 to July 2009.

2.2.5 Precipitation (P)

The precipitation (P) data used is from the Global Precipitation Climatology Project (GPCP) version 2.1 combined precipitation dataset ([Adler et al., 2003](#)) of monthly means from combined satellite and station data on a 2.5° grid that is available from 1979 to present. This product is re-gridded on a 1° grid using triangle-based linear interpolation based on a Delaunay triangulation ([Barber et al., 1996](#)) and constrained to the tropical Pacific region to have the same dimensions as the SSS product. We also tested the CPC Merged Analysis of Precipitation (CMAP; [Xie and Arkin, 1997](#)) and NCEP/NCAR Reanalysis 1 ([Kalnay et al., 1996](#)) precipitation products that are also available on a 2.5° grid from 1979 and 1948, respectively. Comparison studies on these products (e.g., [Janowiak et al., 1998](#); [Gruber et al., 2000](#); [Lim and Ho, 2000](#); [Xie et al., 2003](#)) show that differences arise mostly in the source of the input data and merging algorithms. We choose to use the GPCP product in this study. The evaporation (E) product from the objectively analyzed air-sea fluxes (OAFlux) for the global ocean ([Yu, 2007](#)), produced by the Woods Hole Oceanographic Institute (WHOI), was also tested and we found no significant difference regarding the conclusions derived below on interannual time scales between using P only and P-E.

2.2.6 ENSO Indices

Many oceanic and atmospheric indices have been defined to characterize ENSO events. Some of the traditional indices include the atmospheric Southern Oscillation Index (SOI), which measures the normalized difference in sea level pressures between Tahiti and Darwin (see Fig. 2.3), and the oceanic Niño indices, which are mean SST anomalies in different spatial regions: Niño1+2 (80°W-90°W, 10°S-0°), Niño3 (150°W-90°W, 5°S-5°N), Niño4 (160°E-150°W, 5°S-5°N) and Niño3.4 (170°W-120°W, 5°S-5°N; see Fig. 2.3). These indices have been widely used in climate studies and have also been compared with each other (e.g., Rasmusson and Carpenter, 1982; Deser and Wallace, 1987; Trenberth and Stepaniak, 2001; Hanley *et al.*, 2003). The Climate Prediction Centre (CPC) of NOAA's National Centre for Environmental Prediction (NCEP) defines ENSO using the Oceanic Niño Index (ONI), which is a 3-month running mean of NOAA ERSST version 3b SST anomalies in the Niño3.4 region with respect to the 1971-2000 base period. To be classified as an El Niño/La Niña, the ONI must exceed $\pm 0.5^{\circ}\text{C}$ for at least five consecutive months. The official definition of ENSO adopted by the WMO in 2005 states that an event can be classified as an El Niño/La Niña when the SST anomalies in the Niño3.4 region exceed $\pm 0.5^{\circ}\text{C}$ for at least 3 consecutive months. The SOI anomalies used are departures from the 1951-1980 base period and are calculated as 3-month running means of the normalized difference between the normalized Tahiti and Darwin sea level pressures. Both these datasets (Niño indices and the SOI) were obtained from the CPC website (<http://www.cpc.noaa.gov/data/indices>).

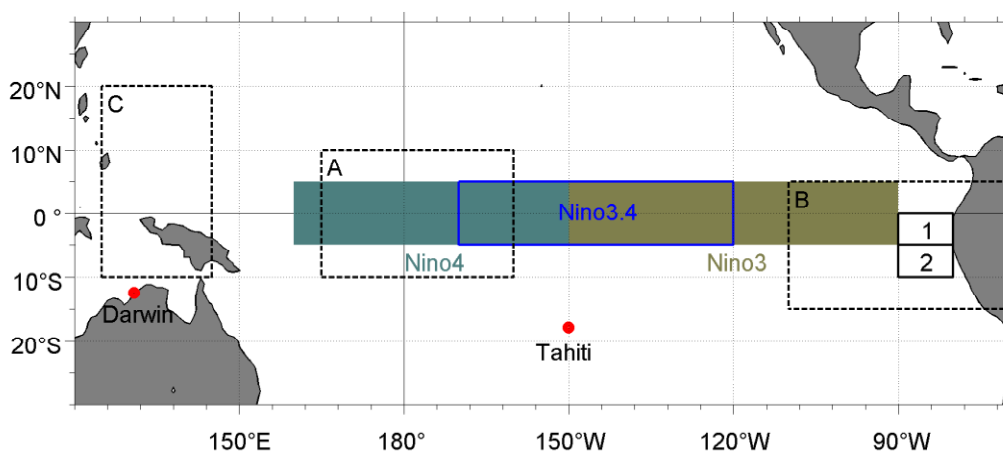


Figure 2.3 Map of the tropical Pacific showing the Niño1+2, Niño3, Niño3.4 and Niño4 regions (solid rectangular blocks) and the A, B and C EMI regions (dashed rectangular blocks). The SOI is calculated from the normalized difference in sea level pressures between Darwin and Tahiti (shown by the red dots).

Klaus Wyrski postulated more than 35 years ago that “... *no two El Niño events are quite alike*” (Wyrski, 1975). An example of this situation is illustrated in Fig. 1.5, which shows that the maximum anomalous surface warming of oceanic waters in the tropical Pacific region occur at different locations and with different magnitudes during the 1982-83/1997-98 and 2002-03/2009-10 El Niño events. Hence, while there is an official WMO definition of ENSO, there is currently no consensus in the scientific community as to which of the many ENSO indices best captures the ENSO phases. Although SST anomalies in the Niño regions have been used as an index to classify ENSO, the choice of which index to use in ENSO studies is dependent upon the phase of ENSO (Wang, 1995; Hanley *et al.*, 2003; Kumar *et al.*, 2004; Bunge and Clarke, 2009). Consequently, numerous indices have been proposed to characterize the different flavors of ENSO. Some of these include the Trans-Niño Index (TNI; Trenberth and Stepaniak, 2001) and the El Niño Modoki Index (EMI; Ashok *et al.*, 2007). The TNI is defined as the normalized difference between the normalized anomalies in the Niño1+2 and Niño4 regions, while the EMI is defined as the area-averaged SST anomaly in region A (165°E-140°W, 10°S-10°N) minus half the sum of the area-averaged SST anomaly in regions B (110°W-70°W, 15°S-5°N) and C (125°E-145°E, 10°S-20°N; see Fig. 2.3). We used both TNI and EMI indices which were obtained, respectively, from the NOAA (http://www.esrl.noaa.gov/psd/gcos_wgsp/Timeseries/Data/tni.long.data) and JAMSTEC (<http://w3.jamstec.go.jp/frcgc/research/d1/iod/DATA/emi.monthly.txt>) websites.

More recently, ENSO indices have been proposed by Ren and Jin (2011) that can distinguish between Eastern Pacific (EP) and Central Pacific (CP) types of ENSO. The Niño Cold Tongue (N_{CT}) and Niño Warm Pool (N_{WP}) indices are successfully able to capture the two types of ENSO in addition to the two types of El Niño events (Fig. 2.4). The two indices are empirically calculated from the Niño3 and Niño4 SST anomalies to fit the observations and are almost orthogonal at zero lag (see Eq. 2.2). We calculate these indices from the Niño3 and Niño4 region anomalies obtained from the CPC website.

$$\begin{cases} N_{CT} = N_3 - \alpha N_4 \\ N_{WP} = N_4 - \alpha N_3 \end{cases} \quad \alpha = \begin{cases} 2/5, & N_3 N_4 > 0 \\ 0, & \text{otherwise} \end{cases} \quad (2.2)$$

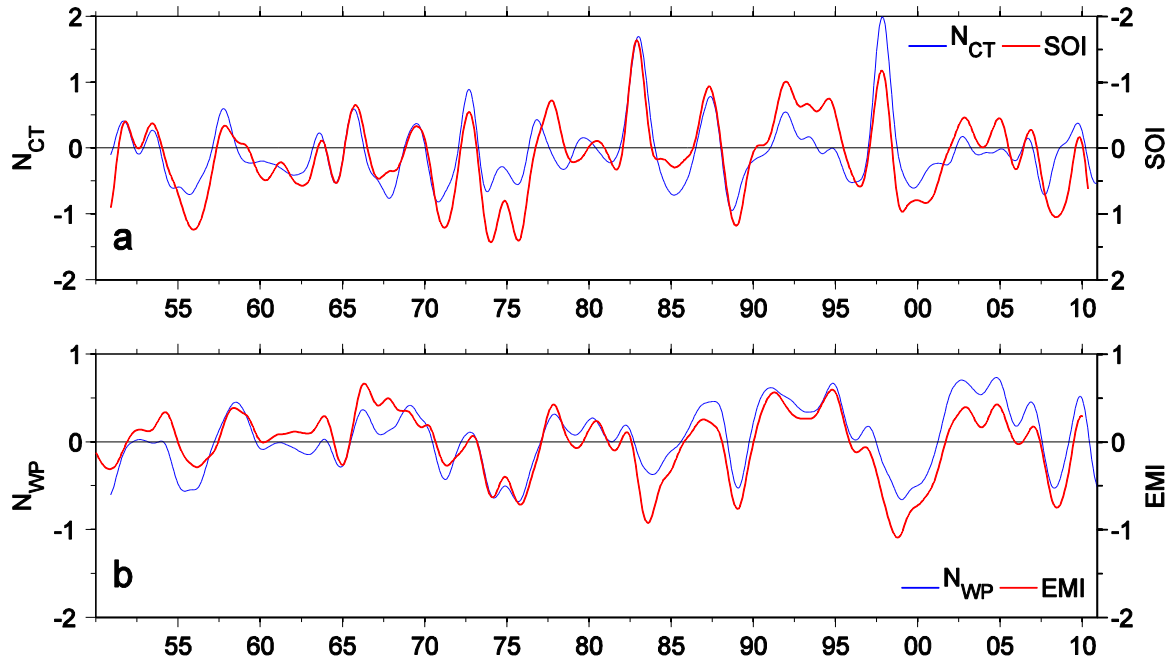


Figure 2.4 (a) N_{CT} (in blue) and SOI (in red) and (b) N_{WP} (in blue) and EMI (in red) over the 1950-2010 period. Note the reversed scale for the SOI. The time series are smoothed with a 25-months Hanning filter for clarity. Units for N_{CT} , N_{WP} and EMI are in $^{\circ}\text{C}$.

2.2.7 Simple Ocean Data Assimilation (SODA)

The Simple Ocean Data Assimilation (SODA) 2.2.4 reanalysis product is an assimilation of observed sea level, temperature and salinity data into an Ocean General Circulation Model (OGCM) and is jointly managed by the University of Maryland and Texas A&M University. The product spans the 1871-2008 period and covers the global ocean with an average resolution of $0.25^{\circ} \times 0.4^{\circ} \times 40$ vertical levels (Carton and Giese, 2008). This product was re-gridded on a 1° horizontal grid for the tropical Pacific region while maintaining the vertical resolution. The data, which is available freely from <http://soda.tamu.edu/>, includes zonal and meridional wind stress (τ_x and τ_y , respectively), absolute zonal, meridional and vertical current velocities, temperature, salinity and sea surface height. We use data from 1950 onwards.

2.2.8 DRAKKAR Model

The DRAKKAR model simulation ORCA-R025.L75-G85 forced by DRAKKAR Forcing Set #4.3 with ECMWF 40-year reanalysis (ERA40) base has outputs of temperature, salinity, sea surface height, and horizontal and vertical velocities amongst other variables (Barnier *et al.*, 2006). The data is distributed on a $\frac{1}{4}^{\circ}$ grid at 5-day averaged intervals from 1958-2007. We

re-gridded this product on a 1° horizontal grid by 1 month (using monthly mean and linear interpolation along the time and space axes) while conserving the vertical resolution of 47 levels (with 31 levels in the upper 200 m). The DRAKKAR configurations are routinely evaluated against in situ observations by the DRAKKAR group. We perform extra evaluation in this project, for example, see [Fig. 2.2](#) for the SST anomaly in the Niño3.4 region and Chapter 4, where the DRAKKAR model data was used in the study of warm water volume (WWV) variability on ENSO timescales.

2.3 Methodology

2.3.1 Basic Data Treatment

Before performing statistical analysis using methods outlined in the following sections, and those that are used in the later chapters, it is necessary to perform some basic data treatment. Because we are interested in the ENSO (interannual) signal, it is convenient to filter the data from the “very high” and “very low” frequencies to bracket as much as possible the 1-7 year ENSO frequency band. First, to remove the “very low” frequency variability, we removed a linear trend (the best straight-fit line) over the prescribed length of the respective dataset. And second, we removed the high frequency variability by removing the mean monthly climatology and applied smoothing using a 13-months Hanning filter to remove any remaining seasonality. This 13-months Hanning filter passes almost no signal at periods of 6 months and shorter and so looks appropriate since the duration of some ENSO events was found to be less than 1 year (e.g., [Kao and Yu, 2009](#)). An alternative would be to use a 25-months Hanning filter (see [Fig. 2.5](#)), as used by some authors. Note, however, that using a 25-months Hanning filter on a time series with the long-term mean removed gives essentially the same result as when using a 13-months Hanning filter with the mean monthly climatology removed. Using the former approach, we lose 12 months of data at the beginning and end of the time series compared to only 6 months when using the latter approach, and thus our choice of using the latter approach. The Hanning filter also has the advantage of removing a variable annual cycle rather than a constant annual cycle over the length of the time series (e.g., [Delcroix, 1998](#)). A constant annual cycle has the disadvantage that variations in seasonal behaviour become mixed up with longer-term interannual variations in the mean ([Pezzulli et al., 2005](#)).

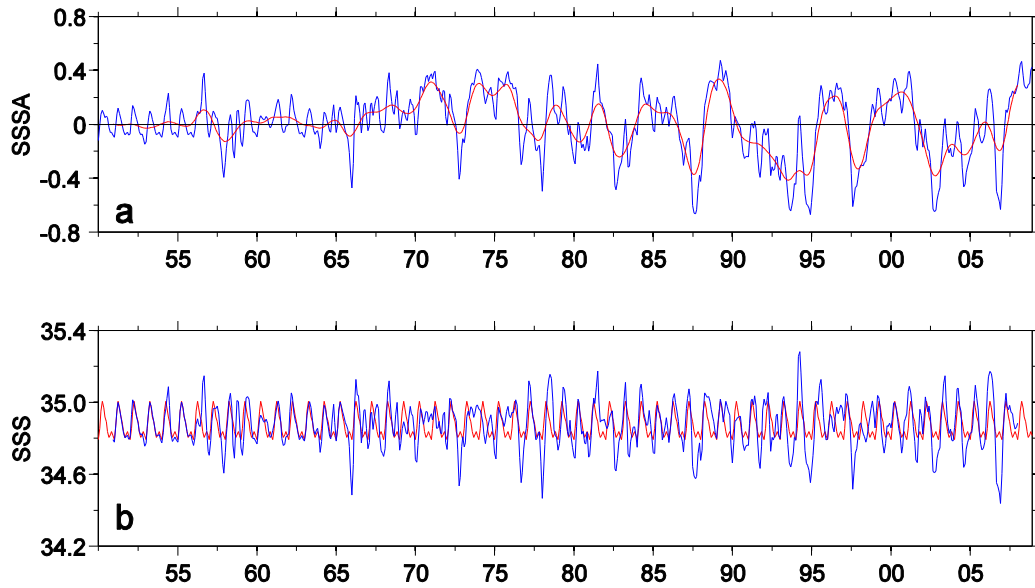


Figure 2.5 (a) SSS averaged in the western equatorial Pacific region (150°E - 170°W , 2°S - 2°N) with the long-term mean (34.87 pss) removed (in blue) and a 25-months Hanning filter applied (in red). (b) The constant annual cycle obtained from the mean monthly climatology (in red) and the variable annual cycle obtained from the difference between the original and the 25-months Hanning filtered SSS data (in blue). The mean is removed over the 1971-2000 period.

2.3.2 Empirical Orthogonal Function (EOF)

The Empirical Orthogonal Function (EOF) procedure is a data reduction method that provides a compact description of the spatial and temporal variability of a data series in terms of orthogonal functions (or EOF modes), of which the first few usually explain most of the variance and *may* be linked to possible dynamical mechanisms. However, no direct physical or mathematical relationship necessarily exists between the statistical EOFs and any related dynamical modes (see [Emery and Thompson, 2001](#) and references therein). Each EOF mode is comprised of a standing oscillation (or mode of variability) coupled with a time series coefficient (known as Principle Component, PC) whose product describes the oscillation related with that EOF mode. A measure of variance is associated with each EOF mode to emphasize its importance relative to the other modes. This measure of variance is important in deciding which EOF modes to retain and which to discard. Significance tests, as those described by [North *et al.* \(1982\)](#), also need to be conducted as a *rule of thumb* to ensure that the EOF modes are not contaminated by its nearest neighbours.

2.3.3 Agglomerative Hierarchical Clustering (AHC)

Agglomerative Hierarchical Clustering (AHC) allows large datasets to be reduced to smaller numbers of mutually exclusive groups, with any loss of information being quantified (Ward, 1963). In the AHC process, the Euclidean distance (shortest distance between two points) between each pair of singletons (or unique elements of a dataset) is calculated to measure their (dis)similarity. The *Ward* criterion uses this Euclidean distance to merge each pair of singleton(s) and (or) already merged singleton(s) based on the least sum of squared distance between the singleton(s) and (or) the centroid of the cluster. This ensures maximum *similarity* within the cluster of elements and maximum *dissimilarity* with elements of other clusters. The process is repeated agglomeratively (from the bottom-up) until the entire dataset is merged into one cluster. The clustering procedure can be represented by a dendrogram (upside-down) tree, which shows the clustering at each successive step. The abscissa shows the unique cluster numbers and the ordinate indicates the height. The horizontal lines link the clusters while the vertical lines denote the distance between each pair of clusters being merged. Consequently, to identify the main modes of variability, it suffices to *cut* the dendrogram horizontally so as to represent the entire dataset using only a few merged unique clusters which can be physically explained (similar to using an EOF procedure where only the first few dominant modes are used). This cut-off can be defined arbitrarily so as to optimally maximize the similarity *within* the cluster and the dissimilarity *between* clusters. Statistical significance tests for the aggregation of the individual monthly maps into clusters, not performed here, can be done using the Monte Carlo (Hope, 1968) or bootstrap (Thompson, 1993) methods.

2.3.4 Self-Organizing Maps (SOM)

Self-Organizing Maps (SOM; Kohonen, 1989) is a non-linear neural network based on unsupervised learning. Its function is to represent large datasets on a regular low-dimensional grid in a synthetic way while conserving their topology. In this objective method, the input data is linked to a predefined map of neurons via weight vectors. The map of neurons, often called Kohonen map, has all the neurons fully connected to their closest neighbours. This conservation of a topological order is the fundamental property of the SOM. It allows two neighbouring neurons to be represented by two close weight vectors in the space of the input data, and conversely, two close observations in the input data are projected onto two close neurons on the map. The weight vectors are randomly initialized as a first step and then the

SOM is trained (as it is an iterative algorithm). During the training process, each observation in the input data is associated to their best representative neuron according to the Euclidean distance. The weight vectors linked to the neurons are then updated depending on the assigned observations and their neighbouring neurons. Finally, when the computed weight vectors converge to a stabilized map, determined by how well they agree with the input data, an ensemble of neurons (synthetic indices) representing all possible scenarios is obtained. At this point, each observation in the input data (input layer) is associated to one neuron only (output layer) via a weight vector.

2.4 Computation Platform

Data analysis of large datasets, especially model output, requires fast processors combined with reliable and high level analysis software. From the many available choices, we chose to use the Matrix Laboratory (MATLAB) high-level technical computing language (version 2009b). As its name suggests, MATLAB stores data in its workspace as matrices. Because of this unique data storage method, general functions may be written to address a particular type of problem. A collection of these functions constitute a toolbox, which can be used on any machine running MATLAB. The *Neural Network Toolbox* proved to be a very useful and efficient tool when performing neural network analysis (NNA). Many other toolboxes were used that made data analysis relatively simple. Consequently, all analyses were done using MATLAB mainly because of its ability to handle large sets of data (limited only by the size of computer memory), the availability of numerous statistical toolboxes, high quality of graphical display, online support, exchange of information and solutions with fellow users (at LEGOS), help forums and simplicity of use.

2.5 Summary

We make use of various data processing techniques, most of which have been described above. These include the commonly used EOF analysis, the adequately used AHC technique and less frequently used in climates studies SOM procedure. Various statistical methods were used in the course of this study and are presented in the following chapters. The idea to use different statistical methods was primarily to ensure that the derived physical interpretations were not method-dependent. The more unique and appropriate methods were used in the attached publications.

Chapter 3

Contrasting the flavors of ENSO

3.1 Introduction

This chapter roots on the published manuscript by [Singh *et al.* \(2011\)](#) attached at the end of this chapter, in which we contrast the different flavors of ENSO in terms of SSS observations. We supplement the study here by using different methods and also use different climate variables (other than SSS) to characterize the different ENSO signatures. The data processing for each variable is described in the respective sections. A parallel study was also conducted using chlorophyll anomalies, the results of which are published in [Radenac *et al.* \(2012\)](#) and attached in Appendix II.

3.2 Long term mean and interannual variability

The mean structures for SST, SSS, P and surface U were first analyzed in order to set the context prior to focusing on the interannual variability. This analysis is not repeated here as it is given in [Singh *et al.* \(2011\)](#); see their section 3 and Fig. 2). We then detrend and calculate anomalies, which are defined here as departures from the mean monthly climatology, for each variable. The detrended anomalies are calculated over the periods 1977-2008 (for SST and SSS), 1979-2008 (for P), 1993-2008 (for U), 1993-2010 (for SL from the Aviso product) and 1958-2007 (for SL from the DRAKKAR product). A 13-months Hanning filter is then applied to the detrended anomalies to remove any remaining seasonality.

The regions of maximum interannual variability for each variable, which are calculated as the standard deviation of the detrended low-pass filtered anomalies, are shown in [Fig. 3.1](#). The regions of maximum SST anomaly (SSTA) variability reflect the well-known signature of ENSO with maxima extending from the South American coast to the central Pacific region along the equator ([Fig. 3.1a](#)). Some variability is also seen in the northeast Pacific. Regions of high SSS anomaly (SSSA) variability can be seen in the western equatorial Pacific, SPCZ region and in the far eastern equatorial Pacific off Panama ([Fig. 3.1b](#)). The region of high

variability extending from the SPCZ to the South American coast coincides with the observations collected along the shipping lanes (see Fig. 1 in [Delcroix *et al.*, 2011](#)) and could be an artifact related to the relatively high data density. This region does not appear in the analysis of ARGO data collected during the more limited 2004-2011 period ([Roemmich and Gilson, 2011](#); their Fig. 1). The precipitation anomalies (PA) show maximum variability concentrated chiefly in the warm pool region and along the equatorial, ITCZ and SPCZ regions ([Fig. 3.1c](#)). The zonal current anomalies (UA) display high variability over the entire equatorial region with a tendency to be slightly north of the equator ([Fig. 3.1d](#)). The SLA variability is concentrated in three main regions: in the central-eastern equatorial, northwestern and southwestern Pacific for both the Aviso ([Fig. 3.1e](#)) and DRAKKAR ([Fig. 3.1f](#)) modeled data.

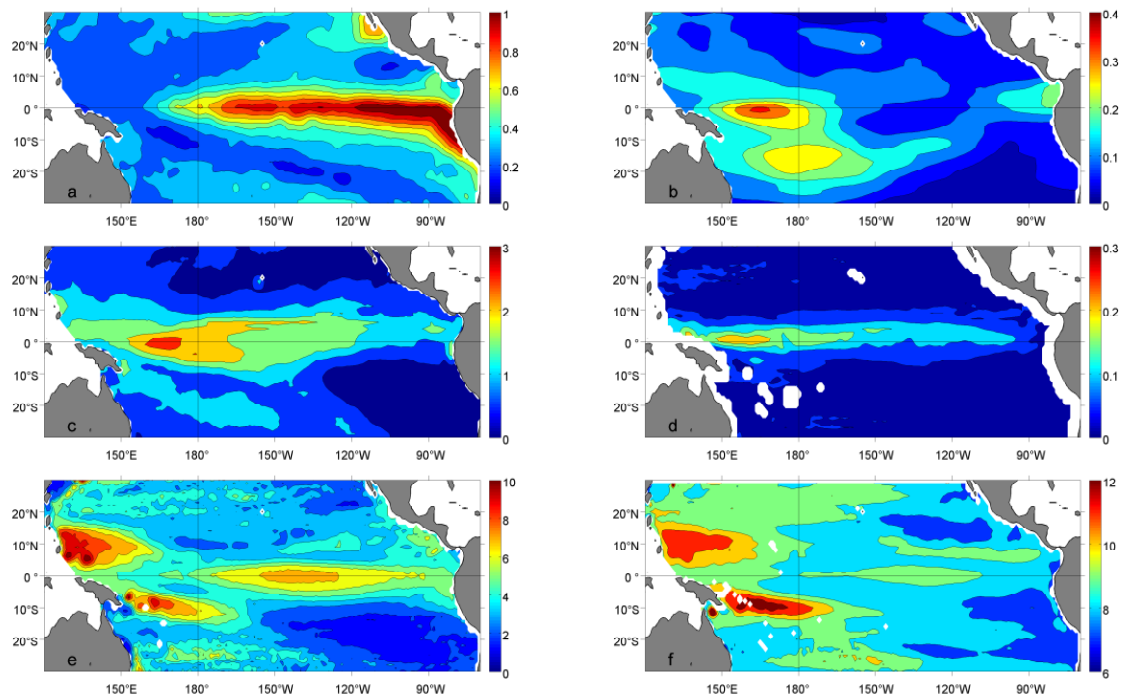


Figure 3.1 Standard deviations of the anomalies of (a) SST over 1977-2008 (in $^{\circ}\text{C}$), (b) SSS over 1977-2008 (in ps), (c) P over 1979-2008 (in mm day^{-1}), (d) U over 1993-2008 (in m s^{-1}), (e) SL over 1993-2010 (from Aviso; in cm), and (f) SL over 1958-2007 (from DRAKKAR; in cm) in the tropical Pacific region. The anomalies are calculated after the trends and mean monthly climatology are removed over their respective periods.

3.3 SST, SSS and SL signal during ENSO

Various statistical methods have been employed previously to determine the variability of climate variables on interannual timescales. Some of these have been used repeatedly in

climate studies (e.g., EOF analysis) while others less frequently (e.g., AHC and SOM). In this study, we attempt to characterize the ENSO signal using singular EOF, combined regression-EOF, multivariate EOF, AHC and SOM. The combined regression-EOF analysis method is a two-step procedure which involves firstly, regression of the climate variable onto a climate index and secondly, an EOF analysis on the residuals obtained from the regression analysis. The residuals are defined as the difference between the variable and the reconstructed variable (which are calculated from the regression coefficients). We use the N_{CT} and N_{WP} indices (see Chapter 2) as the regression indices. The statistical results for each variable using the EOF and combined regression-EOF, and AHC analyses are detailed in [Tables 3.1 and 3.2](#), respectively, while the similarities and/or differences in using the different procedures for each variable are briefly summarized at the end of each respective section.

Table 3.1 Statistical results of the singular EOF and combined regression-EOF analyses on SST, SSS and SL anomalies.

Method	Specifications	SST (1977-2008)			SSS (1977-2008)			SL (1993-2010)		
		EOF1	EOF2	EOF3	EOF1	EOF2	EOF3	EOF1	EOF2	EOF3
EOF analysis	% var.	57.0	13.5	5.5	28.6	13.2	12.4	42.4	15.3	8.3
	# R_{lag} (N_{CT})	0.94 ₀	0.33 ₃	0.24 ₆	0.78 ₄	0.33 ₋₆	0.36 ₅	0.82 ₀	0.77 ₇	-0.55 ₋₃
	R_{lag} (N_{WP})	-0.36 ₂	0.82 ₋₁	0.33 ₋₂	0.51 ₅	0.55 ₋₅	-0.56 ₃	0.58 ₁	-0.64 ₋₅	0.61 ₅
Combined regression-EOF analysis	% var. (N_{WP}^*)	61.5	7.6	4.6	27.8	15.0	9.7	40.6	14.0	6.9
	R_{lag} (N_{CT})	0.97 ₀	0.18 ₀	0.36 ₆	0.86 ₂	0.34 ₋₅	0.28 ₋₆	0.95 ₀	0.88 ₈	0.13 ₋₆
	R_{lag} (N_{WP})	-0.15 ₋₆	-0.04 ₋₆	-0.22 ₋₆	0.15 ₋₆	0.23 ₋₆	0.40 ₆	-0.15 ₋₆	-0.23 ₋₆	-0.56 ₆
	% var. (N_{CT}^*)	36.3	13.0	7.6	20.5	16.3	10.8	30.9	17.2	7.0
	R_{lag} (N_{CT})	0.14 ₋₆	-0.47 ₆	0.33 ₋₆	0.14 ₆	0.47 ₆	-0.34 ₆	-0.22 ₆	0.88 ₈	-0.25 ₋₆
	R_{lag} (N_{WP})	0.87 ₀	0.49 ₋₄	0.1 ₋₆	0.76 ₁	-0.55 ₋₆	0.19 ₆	0.93 ₁	0.31 ₅	0.26 ₆

The correlations of the principle component (PC) with the ENSO index (in parentheses) are the maximum correlations (R) at a given lag (in subscript). A positive lag means that the index leads the PC. Values in blue are those for which the EOF spatial pattern can be physically explained and are discussed in the following sections.

* The lag between the regression indices (in parentheses) and SSS, SST and SL used in the combined regression-EOF analysis was 3, 0 and 0 months, respectively.

Table 3.2 Percentage occurrences of Eastern Pacific (EP) and Central Pacific (CP) El Niño (EN) and La Niña (LN) events from the AHC performed on SST, SSS and SL anomalies.

	EPEN	CPEN	EPLN	CPLN	*Neutral
SST (1977-2008)	12%	44%	34%	10%	-
SSS (1977-2008)	8%	34%	33%	8%	18%
SL (1993-2010)	5%	56%	35%	4%	-

* The neutral cluster from the AHC analysis is shown only for the analysis on SSS anomalies.

The AHC method, like the EOF, has the advantage of not using a priori, in this case an ENSO index, to determine the final result. This method has been used previously in climate studies (e.g., Vincent *et al.*, 2009). Kao and Yu (2009) used this method to confirm their combined regression-EOF analysis on SST anomalies in the tropical Pacific (see their Fig. 4). In addition, we also used a sophisticated SOM technique, which is based on neural networks. Leloup *et al.* (2007) used this method to characterize ENSO. We used this method to characterize the different flavors of ENSO.

3.3.1 SST

The analyses for SST covers the period 1977-2008 over the domain 120°E - 70°W , 30°S - 30°N . The results of the EOF analysis is summarized and shown in Fig. 3 in Singh *et al.* (2011) while the results of the combined regression-EOF analysis is shown in Fig. 3.2 and the AHC analysis in Fig. 3.3. A generalized discussion on the observed results is then presented.

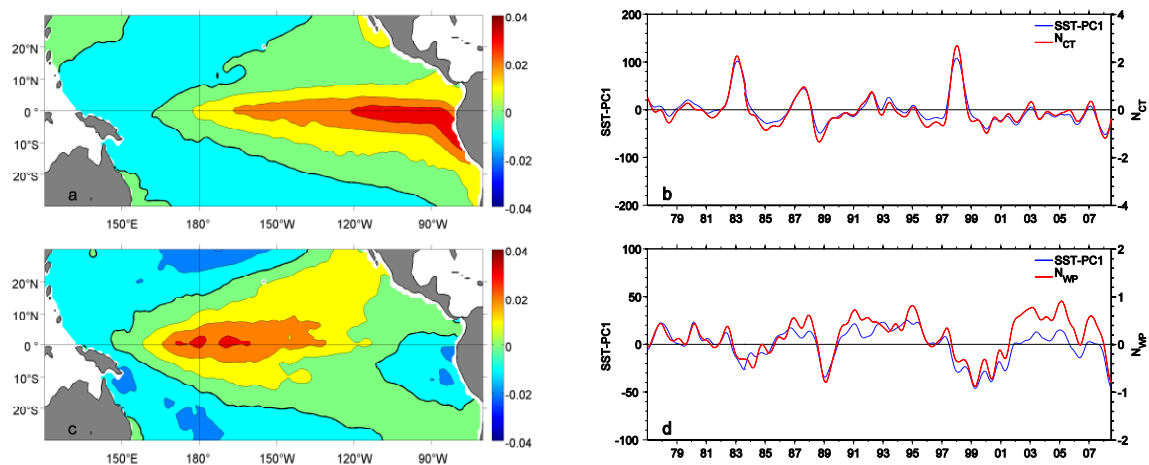


Figure 3.2 Spatial patterns for EOF1 on SSTA after regressing with (a) N_{WP} and (c) N_{CT} and (b and d) their corresponding time functions (in blue). The units are defined so that the product between the spatial patterns and the corresponding time functions denote $^{\circ}\text{C}$. The red lines in the time functions denote the 25-months Hanning filtered N_{CT} (in b) and N_{WP} (in d), scaled on the right vertical axis. Thick black contour lines in the spatial patterns denote the 0 line.

The EOF on the residuals obtained from the regression of SST anomalies on N_{CT} and N_{WP} indices allows for the orthogonal separation of the different flavors of ENSO. Fig. 3.2 shows that using N_{CT} (N_{WP}) as the regression index in the combined regression-EOF procedure results in the leading EOF modes to capture the CP (EP) ENSO signals in SST, which are similar to the results obtained by Kao and Yu (2009) in using a similar method. The EP ENSO signal (Fig. 3.2a) is characterized by SST anomalies extending from the South

American coast towards the central Pacific along the equator. The CP ENSO signal (Fig. 3.2c) shows that the SST anomalies are confined to the central equatorial Pacific and extend northeastwards to the Central American coast. The spatial patterns for EP (CP) ENSO are similar to the EP (CP) ENSO signals in EOF1 (EOF2) on the original SST anomalies (see Fig. 3 in Singh *et al.*, 2011). The statistical analysis is provided in Table 3.1.

Four clusters are identified from the dendrogram (Fig. 3.3a) using the AHC procedure on SST anomalies. The spatial patterns of these four clusters (Fig. 3.3c-f) are similar to the EP and CP ENSO patterns obtained from the combined regression-EOF analysis. The clusters in Fig. 3.3d&f show SST anomalies attached to the South American coast and extending along the equator. Fig. 3.3c&e show clusters which have their SST anomalies located in the central equatorial Pacific. The resemblance of these clusters to the positive and negative phases of EOF1 from the combined regression-EOF analysis in Fig. 3.2, and their timing (Fig. 3.3b), tend to confirm that clusters 1-4 represent the CP La Niña (CPLN), EP La Niña (EPLN), CP El Niño (CPEN) and EP El Niño (EPEN) signals, respectively. The statistical analysis is provided in Table 3.2. If the cutting level in the dendrogram is shifted down (Fig. 3.3a), cluster 4 splits into two clusters that both show similar spatial patterns but differ in magnitude. This is because one cluster represents the two very strong EP El Niño events of 1982-83 and 1997-98 while the other cluster represents the mixed El Niño events in 1987-88 and 1991-92 (see also Fig. 3.14m&p).

The similarity between the results from each procedure above, plus their agreement with previous studies, makes us gain confidence in the use of the combined regression-EOF and AHC procedures to extract the ENSO signal. However, we also stress that the EOF and combined regression-EOF analyses assume symmetry in the spatial patterns between El Niño and La Niña events, while this is not necessarily the case when using the AHC procedure as the clusters obtained are aggregated from individual monthly maps. A good example that illustrates this can be found in the following section.

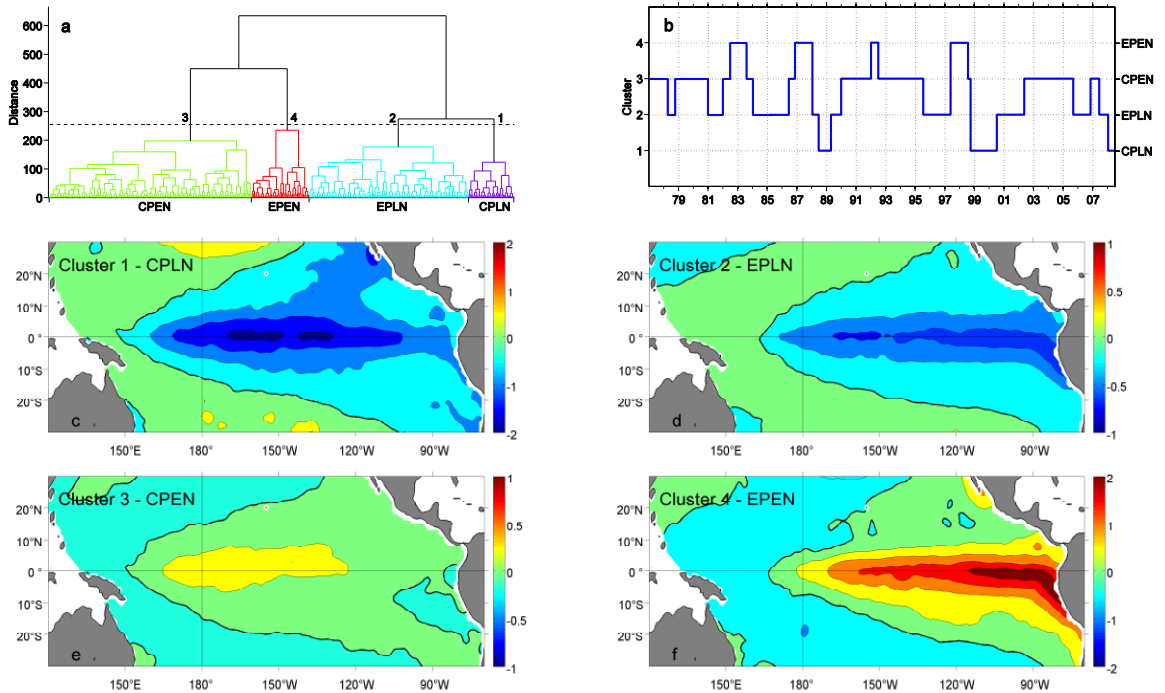


Figure 3.3 (a) Dendrogram resulting from the AHC performed on SSTA. The ordinate labels the inter-cluster distance. The dashed line indicates the cutting level ensuing in four clusters being identified. (b) The cluster time series showing which cluster best represents the SSTA pattern at a particular time. Spatial patterns from the AHC on SSTA with (c) cluster 1 denoting CPLN, (d) cluster 2 denoting EPLN, (e) cluster 3 denoting CPEN and (f) cluster 4 denoting EPEN conditions. Thick black contour lines in the spatial patterns denote the 0 line. Note the different color scales in the spatial patterns. Units in the spatial patterns are in $^{\circ}\text{C}$.

3.3.2 SSS

An EOF (Fig. 3.4), combined regression-EOF (Fig. 3.5) and AHC (Fig. 5 in Singh *et al.*, 2011, complemented by Fig. 3.6 below) analyses were performed on the SSS anomalies over the period 1977-2008 and covering the region 120°E - 70°W , 30°S - 30°N . The statistical results are summarized in Tables 3.1 and 3.2. It should be noted that the AHC method is very sensitive to the input parameters, including period, region, error threshold, trends present and level of smoothing applied to the SSS data. However, the spatial patterns extracted near the top of the dendrogram tree are robust; the only minor differences arise in the time series of the clusters. Noting the regions of maximum interannual variability from Fig. 3.1b, we use the AHC analysis for the region delimited by 120°E - 70°W , 20°S - 10°N , 80% error threshold and January 1977-July 2008 period.

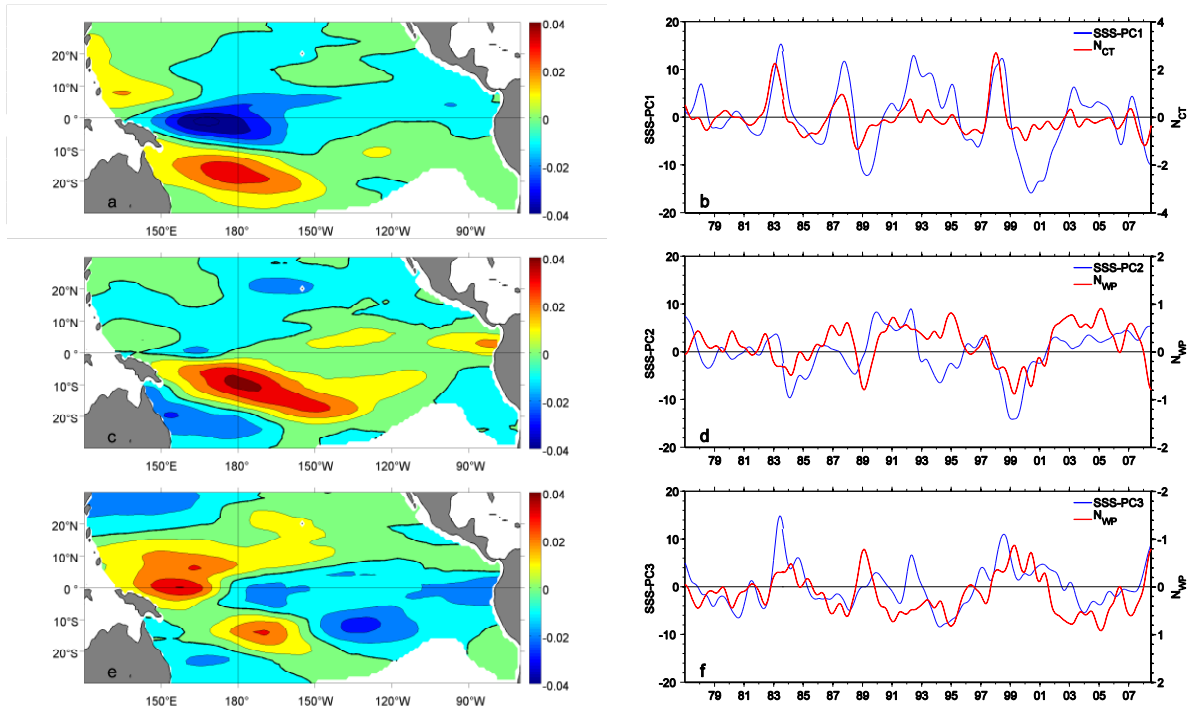


Figure 3.4 Spatial patterns for (a) EOF1, (c) EOF2 and (e) EOF3 and (b, d and f) their corresponding time functions (in blue) for the first, second and third modes of the EOF on SSSA, respectively. The units are defined so that the product between the spatial patterns and the corresponding time functions denote pss. The red lines in the time functions denote the 25-months Hanning filtered N_{CT} (in b) and N_{WP} (in d and f), scaled on the right vertical axis. Note the reversed vertical scale in (f). The blanked areas in the southeastern tropical Pacific in the spatial patterns indicate regions where the errors in SSS are larger than 80% and are not used in the analysis. Thick black contour lines in the spatial patterns denote the 0 line.

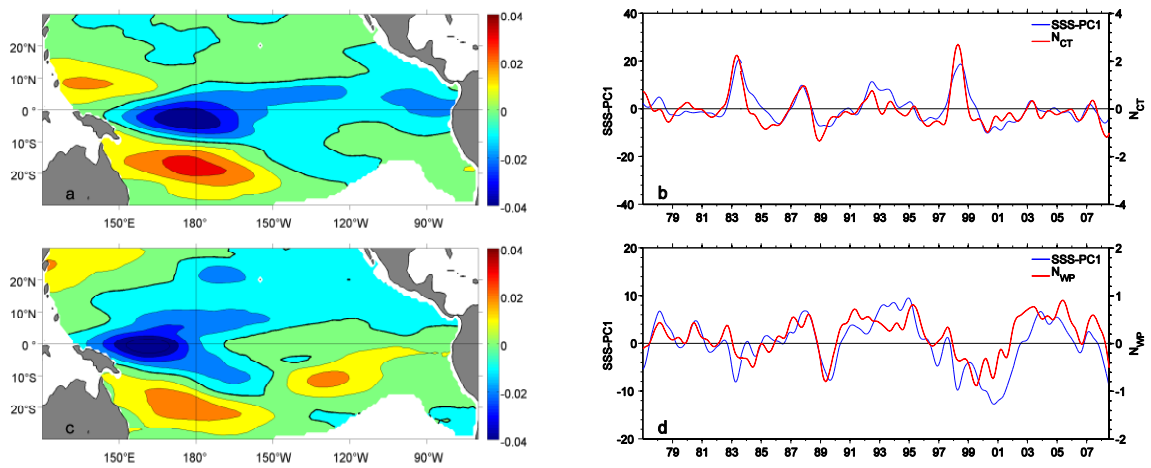


Figure 3.5 Spatial patterns for EOF1 on SSSA after regressing with (a) N_{WP} and (c) N_{CT} and (b and d) their corresponding time functions (in blue). The units are defined so that the product between the spatial patterns and the corresponding time functions denote pss. The red lines in the time functions denote the 25-month Hanning filtered N_{CT} (in b) and N_{WP} (in d), scaled on the right vertical axis. The blanked areas in the southeastern tropical Pacific in the spatial patterns indicate regions where the errors in SSS are larger than 80% and are not used in the analysis. Thick black contour lines in the spatial patterns denote the 0 line.

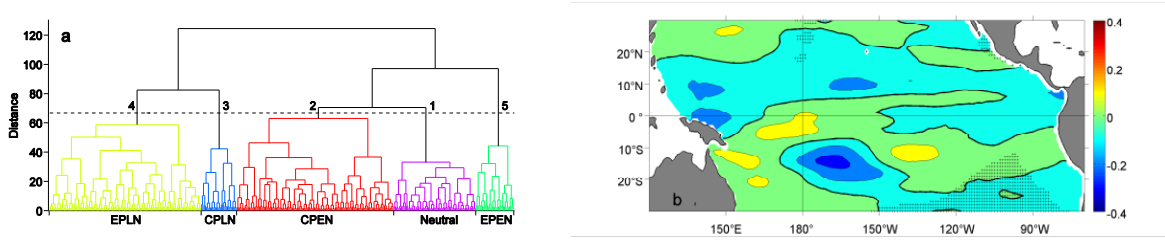


Figure 3.6 (a) Dendrogram resulting from the AHC performed on SSSA. The ordinate labels the inter-cluster distance. The dashed line indicates the cutting level ensuing in five clusters being identified. (b) Spatial pattern from the AHC on SSSA denoting neutral conditions. The regions shaded in black, mainly located in the southeastern tropical Pacific, denote regions where the error in SSS is larger than 80%. Thick black contour lines in the spatial pattern denote the 0 line. Units in the spatial pattern are in pss.

As discussed in Singh *et al.* (2011) and shown in Fig. 3.4a, EOF1 on SSS shows freshening (saltening) concentrated in the western-central equatorial Pacific region with maximum anomalies just west of 180° during EPEN (EPLN). Anomalous saltening during EPEN (EPLN) can be seen in the SPCZ region south of the freshening (saltening) maxima mentioned above and in the far western Pacific north of the equator. Similar results are obtained from the combined regression-EOF analysis using N_{WP} as the regression index (Fig. 3.5a). However, the second and third modes from the singular EOF analysis could not be distinguished in a statistically significant way. EOF1 accounts for 28.6% of the interannual variability while EOF2 and EOF3 individually account for 13.2% and 12.4%, respectively. Because of the closeness of the eigenvalues for EOF2 and EOF3, a test of significance (Eq. 3.1; North *et al.*, 1982) is applied to determine if these two EOFs are well separated from each other. The EOFs are not well separated if the equation is satisfied.

$$\delta\lambda \approx \lambda \cdot \sqrt{2/N} \quad (3.1a)$$

$$\Delta\lambda \leq \delta\lambda \quad (3.1b)$$

where λ is the eigenvalue, $\Delta\lambda$ is the difference between two neighboring eigenvalues, $\delta\lambda$ is the standard error associated with the eigenvalue and N is the sample size. Using the above test for EOF2 and EOF3 with $N=379/25$ (379 is the number of months and 25 is the de-correlation time scale), we obtain values of $\Delta\lambda=0.008$ and $\delta\lambda=0.048$ thereby satisfying Eq. 3.1b resulting in the EOFs not being able to be distinguished in a statistically significant way and thus probably do not extract (or more likely extract a mixture of) real physical phenomenon. In comparison, for EOF1 and EOF2, we obtain values of $\Delta\lambda=0.15$ and $\delta\lambda=0.10$

showing that these two EOFs are well separated. Because they are not statistically significant, EOF2 and EOF3 will not be discussed any further.

We make use of the combined regression-EOF analysis in an attempt to extract the CP ENSO signature in SSS. Using N_{CT} index, the dominant EOF mode (Fig. 3.5c) shows the freshening in the western equatorial Pacific shifted about 20° in longitude westward compared to during EPEN (Fig. 3.5a) while the saltening in the SPCZ and far western Pacific are still evident. However, the amplitude of the signal is reduced by almost 50% in comparison to EPEN. The high correlation with N_{WP} (Table 3.1) suggests that this is the CP ENSO signature in SSS.

An AHC analysis was also performed on the SSS anomalies to confirm (or not) the above results. Five clusters were identified from the dendrogram tree (Fig. 3.6a) and these are discussed in Singh *et al.* (2011). A neutral cluster that was also identified is illustrated in Fig. 3.6b.

The SSS analyses shown above remind us that not all statistical procedures can be used to determine the dominant modes of variability. On one hand, EOFs, the most commonly used statistical method for instance, was not able to properly discriminate the different flavors of ENSO using SSS in a statistically significant way. A combined regression-EOF analysis proved successful in accomplishing this task. However, it should be noted that this method requires a priori, in this case, an ENSO index, to extract the dominant modes. On the other hand, the AHC technique was adequately able to discriminate the different flavors of ENSO *without* using a priori *and* unlike the EOF, which results in N modes depending on the number of observations, the AHC can be defined to output a specific number of aggregated clusters that can be physically explained *and* does not extract unrealistic symmetrical spatial patterns like an EOF analysis would do. A similar situation was encountered by Radenac *et al.* (2012) where the EOF method was unsuccessful in discriminating the flavors of ENSO in chlorophyll but the AHC proved to be effective.

3.3.3 SL

As with the analyses on SST and SSS, an EOF (Fig. 3.7), combined regression-EOF (Figs. 3.8 and 3.9) and AHC (Fig. 3.10) analyses were performed on SL anomalies for the period 1993-2010 over the domain 120°E - 70°W , 30°S - 30°N . The statistical results are summarized in Tables 3.1 and 3.2. A generalized discussion on the observed results is then presented.

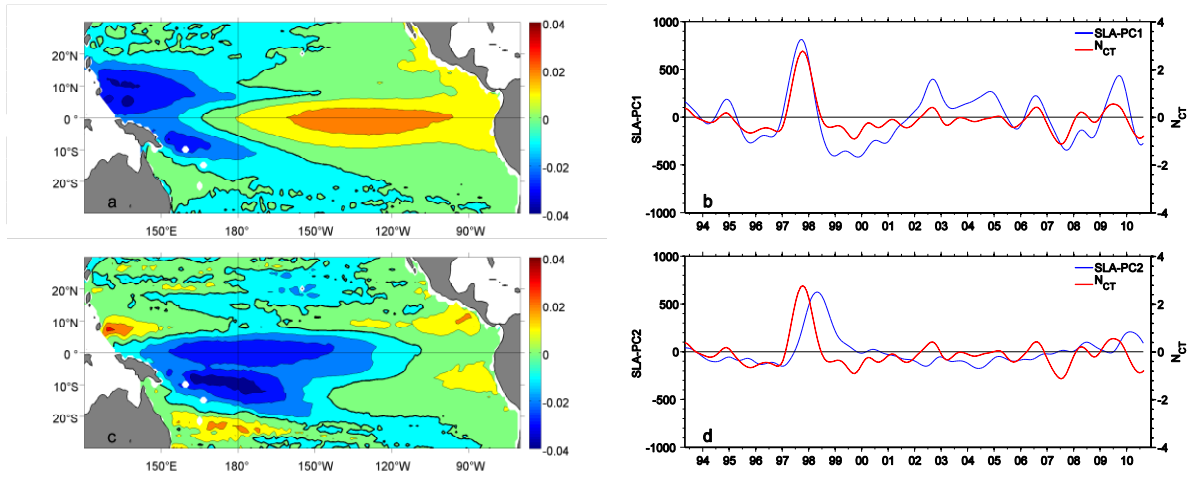


Figure 3.7 Spatial patterns for (a) EOF1 and (c) EOF2 and (b and d) their corresponding time functions (in blue) for the first and second modes of the EOF on SLA, respectively. The units are defined so that the product between the spatial patterns and the corresponding time functions denote cm. The red lines in the time functions denote the 25-months Hanning filtered N_{CT} scaled on the right vertical axis. Thick black contour lines in the spatial patterns denote the 0 line.

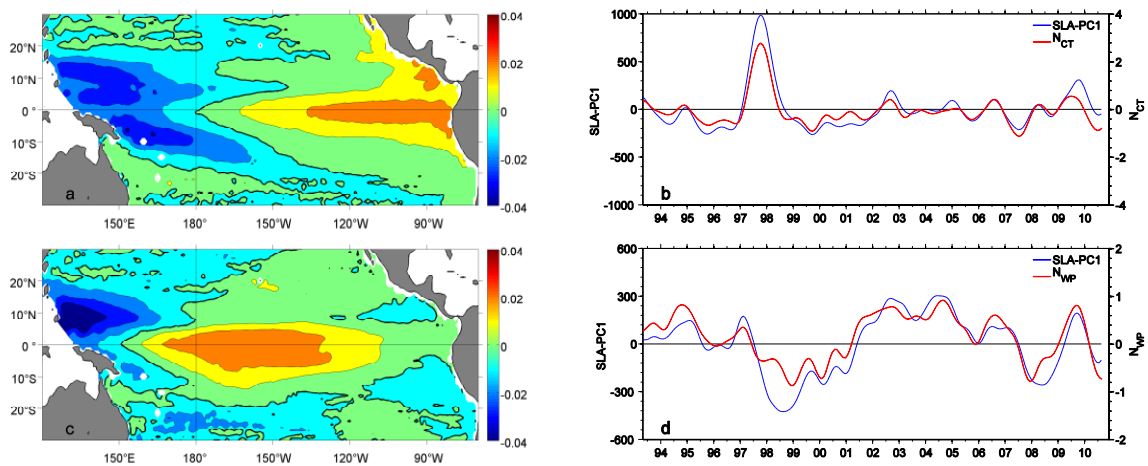


Figure 3.8 Spatial patterns for EOF1 after regressing with (a) N_{WP} and (c) N_{CT} and (b and d) their corresponding time functions (in blue) for the first mode of the EOF on SLA. The units are defined so that the product between the spatial patterns and the corresponding time functions denote cm. The red lines in the time functions denote the 25-months Hanning filtered N_{CT} (in b) and N_{WP} (in d) scaled on the right vertical axis. Thick black contour lines in the spatial patterns denote the 0 line.

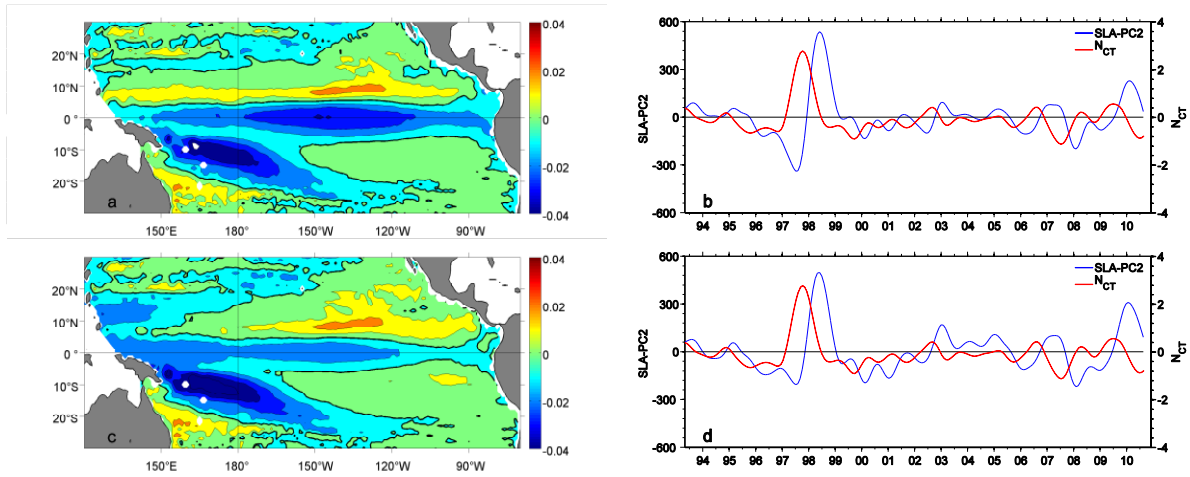


Figure 3.9 Spatial patterns for EOF2 after regressing with (a) N_{CT} and (c) N_{WP} and (b and d) their corresponding time functions (in blue) for the second mode of the EOF on SLA. The units are defined so that the product between the spatial patterns and the corresponding time functions denote cm. The red lines in the time functions denote the 25-months Hanning filtered N_{CT} scaled on the right vertical axis. Thick black contour lines in the spatial patterns denote the 0 line.

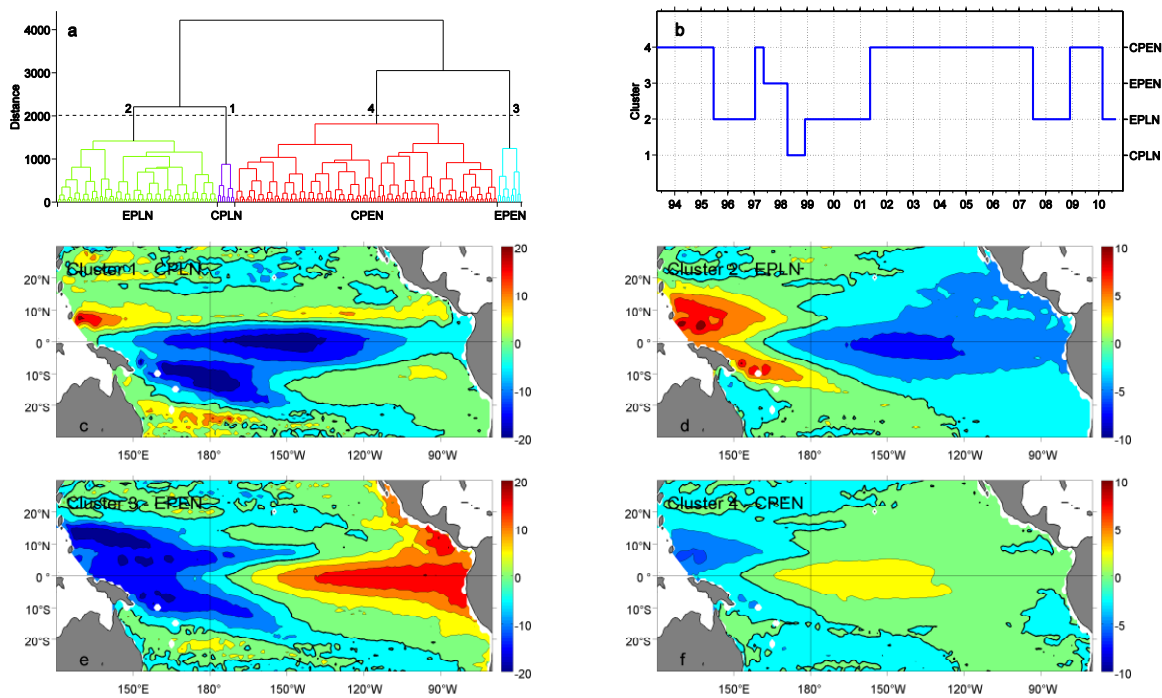


Figure 3.10 (a) Dendrogram resulting from the AHC performed on SLA. The ordinate labels the inter-cluster distance. The dashed line indicates the cutting level ensuing in four clusters being identified. (b) The cluster time series showing which cluster best represents the SLA pattern at a particular time. Spatial patterns from the AHC on SLA with (c) cluster 1 denoting CPLN, (d) cluster 2 denoting EPLN, (e) cluster 3 denoting EPEN and (f) cluster 4 denoting CPEN conditions. Thick black contour lines in the spatial patterns denote the 0 line. Note the different color scales in the spatial patterns. Units in the spatial patterns are in cm.

The well-known signature of ENSO in SLA with an equatorial east-west seesaw pivoted near 180° is evident from EOF1 in Figs. 3.7a and 3.8a and from clusters 2 and 3 in Fig. 3.10d&e, respectively (see also Delcroix, 1998 and references therein). Note that both the positive and negative phases of ENSO are derived in the EOF and combined regression-EOF analyses, which fluctuates according to their respective PC. From the singular EOF, combined regression-EOF (with N_{WP}) and AHC analyses, we can identify the 1997-98 El Niño and the 1995-96, 1999-2001, 2007-08 and 2010 La Niña events. Generally, the positive (negative) SLA during El Niño (La Niña) is trapped around the equator in the eastern half of the Pacific. In contrast, the negative (positive) SLA during El Niño (La Niña) are present in two patches in the far western Pacific centered near 140°E , 5°N and 160°E , 5°S and extend eastwards following the location of the ITCZ and SPCZ, respectively. Using a multivariate EOF analysis with wind stress and similar SLA data, Alory and Delcroix (2002) found similar signatures in SLA during ENSO, but for a shorter period (1993-1999). From the high correlations of the PC with N_{CT} ($R > 0.8$), we believe that this denotes the EP ENSO signature in SLA. It should be noted that although they show almost spatial symmetry (even from the AHC analysis which are discussed later), the amplitude of the EP La Niña signal is about 50% of that during EP El Niño.

From the EOF analysis, EOF2 (Fig. 3.7c) shows negative loadings present in the western-to-central equatorial and SPCZ regions and an almost meridional seesaw pattern with a fulcrum along the 5°N latitude. Relatively weak positive loadings can be observed in the far eastern and western regions off the equatorial region. Interestingly, this EOF mode shows large negative SLA variability after the very strong 1997-98 (only EP) El Niño for the 1993-2010 period (Fig. 3.7d). The opposite phase of this mode seems to show weak positive SLA in the equatorial and SPCZ regions. It should be noted that higher EOF modes individually account for less than 9% of the variance (see Table 3.1) and cannot be physically explained. PC1 from the combined regression-EOF analysis (with N_{CT} ; Fig. 3.8d) shows a more balanced symmetry when compared to PC2 from the EOF analysis (Fig. 3.7d). This means that the EOF1 pattern (Fig. 3.8c) is not dominated by a single event but several events, which however assume symmetry in the spatial patterns. This mode shows positive loadings broadly spread over the central-equatorial Pacific region and negative loadings in the far western Pacific just north of the equator. A similar pattern with positive SLA in the central-equatorial Pacific region is extracted from the AHC analysis (Fig. 3.10f). This cluster (and positive phase from EOF1 in Fig. 3.8c) coincides with the 1993-95, 2002-03, 2004-05, 2006-07 and

2009-10 CP El Niño events and we refer to this cluster as the CP El Niño cluster. Note that the negative phase from EOF1 in Fig. 3.8c is not included in this definition yet although the amplitude of the signal from the PC is quite large (Fig. 3.8d). The reason for this is explained later.

Interestingly, EOF2 from the combined regression-EOF analysis using N_{CT} and N_{WP} are both very similar to each other and probably extract the same phenomenon (Fig. 3.9). The spatial patterns show negative loadings encompassed between 10°S-5°N over the entire equatorial band with the negative loadings also extending over the SPCZ region. Positive loadings poleward of 5°N along the ITCZ region defines the meridional seesaw along this latitude. The PCs show high maximum correlations with N_{CT} with the later leading the former by 8 months (see Table 3.1). The spatial patterns show maximum positive (negative) SLA in the equatorial band and over the SPCZ region at the onset (decay) of the 1997-98 El Niño. This implies a recharge of the equatorial band before an El Niño and a discharge after. This discharge is clearly evident in cluster 1 from the AHC analysis in 1998 (Fig. 3.10c). This, together with the negative phase of EOF1 in Fig. 3.8c constitutes the after EP El Niño signal in SLA (see Chapter 4 for more detailed analyses). Note that the after EP El Niño signal from the combined regression-EOF analysis is spread over two EOF modes. This is not the case when using AHC, which is able to clearly extract the after EP El Niño pattern. It should be noted that shifting the cutting level in the dendrogram down (Fig. 3.10a) results in cluster 4 splitting into a cluster which resembles a relatively slightly stronger CPEN cluster and a weak neutral cluster.

3.4 Multivariate Analyses

The above singular EOF, combined regression-EOF and AHC analyses were all performed on the climate variables individually, with the exception of the combined regression-EOF analysis which used the Niño indices (N_{CT} and N_{WP}) in the regression part of the analysis. To see how the variability of each variable behaves with respect to the other, we used two multivariate analyses techniques: a multivariate EOF and a more sophisticated neural network analysis. These are detailed in the following sections.

3.4.1 Multivariate EOF Analysis (MVEOF)

Using standardized SST and SSS data, we performed a multivariate EOF analysis to extract the dominant modes of interannual variability in both SST and SSS simultaneously. It should be noted that the temporal length for each variable used in the analysis was the same. We used a lag of 3 months with SST leading SSS, as estimated from the EOF analysis in Figs. 3 and 4 in Singh *et al.* (2011) as well as from a visual detection of the peak anomalies on printed monthly mean maps. The results of EOF1 for SST and SSS from the multivariate EOF analysis (not shown here) are in agreement with EOF1 of the individual singular EOFs, respectively. It should be noted that both EOF1 spatial patterns vary according to the same time function. The results for EOF2 and higher modes from the multivariate EOF analysis are inconclusive, probably due to the unresolved second and third modes for the EOF on SSS (see Fig. 3.4). Hence, this procedure was not used any further. Note that we did not use SLA data as the length of the record (1993-2010) is almost half that of the 1977-2008 period we used for the SST and SSS data.

3.4.2 Neural Network Analysis (NNA)

A neural network analysis (NNA) is performed using self-organizing maps (SOM) and three climate indices, which generally sum up the state of the tropical Pacific on ENSO timescales. These indices are the N_{CT} , N_{WP} and Niño3.4 indices, which characterize EP ENSO, CP ENSO and ENSO (as a whole), respectively. The Niño3.4 index, officially adapted by WMO to define ENSO, characterizes ENSO as either El Niño or La Niña but does not further classify them as EP or CP events. The Niño3.4 index is calculated from the partial areas of both Niño3 and Niño4 regions, which in turn are used to calculate N_{CT} and N_{WP} indices (see Eq. 2.2). The Niño3.4 index aptly resembles the zonal displacements of the eastern edge of the western Pacific warm pool (see Picaut *et al.*, 2001), characterized by the longitude position of the 2°S-2°N averaged 28°C surface isotherm (SST_{28} ; Fig. 3.11), and is highly correlated with the later ($R=0.86$ with Niño3.4 leading by 1 month using unfiltered data). Because of the above features of the Niño3.4 index, we shall refer to it as an index for mixed ENSO events (following Kug *et al.*, 2009). In a similar study using NNA, Leloup *et al.* (2007) used the Niño1+2, Niño3.4 and Longi28 (analogous to what we call SST_{28}) over the period 1950-2002. Note that SST_{28} is not defined during a few months of the two very strong

EP El Niño events of 1982-83 and 1997-98 because of widespread warming (greater than 28°C) over the entire equatorial region.

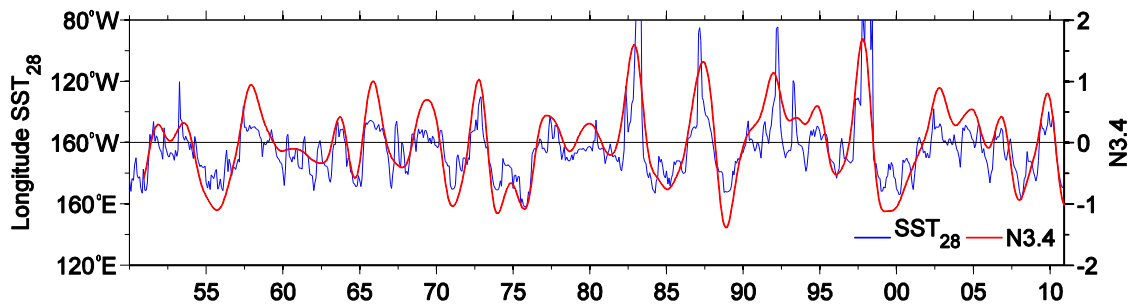


Figure 3.11 Time series of the longitude of the 2°S - 2°N averaged 28°C isotherm (SST_{28}) signifying the eastern edge of the warm pool in the tropical Pacific (in blue) and the Niño3.4 index (in red; units is $^{\circ}\text{C}$). Note that SST_{28} is not defined during the very strong 1982-83 and 1997-98 El Niño events as waters warmer than 28°C occupy the entire equatorial band. A 25-months Hanning filter is applied to the Niño3.4 index for clarity.

To remove any seasonality, the input indices (N_{CT} , N_{WP} and Niño3.4) were further smoothed using a 13-months Hanning filter. We use the 1977-2007 period (shortened by 1 year at the end of the record) to ensure later that the SSS field can be fully extracted. After many trials, the maximum neuron map size (7×7 hexagonal map) was determined to fittingly cover the input data (372×3 observations; see Fig. 3.12). Using a larger map results in more detailed information but it also leaves some neurons empty in the space of the observations. A smaller map gives more general information. Our choice allows for an optimal resolution of the neuron map. The hexagonal arrangement allows for a minimum (maximum) of 2 (6) nearest neighbors as opposed to other arrangements which are not so highly connected. The SOM was trained over 10,000 iterations; no difference was noticed when a higher number of iterations was used.

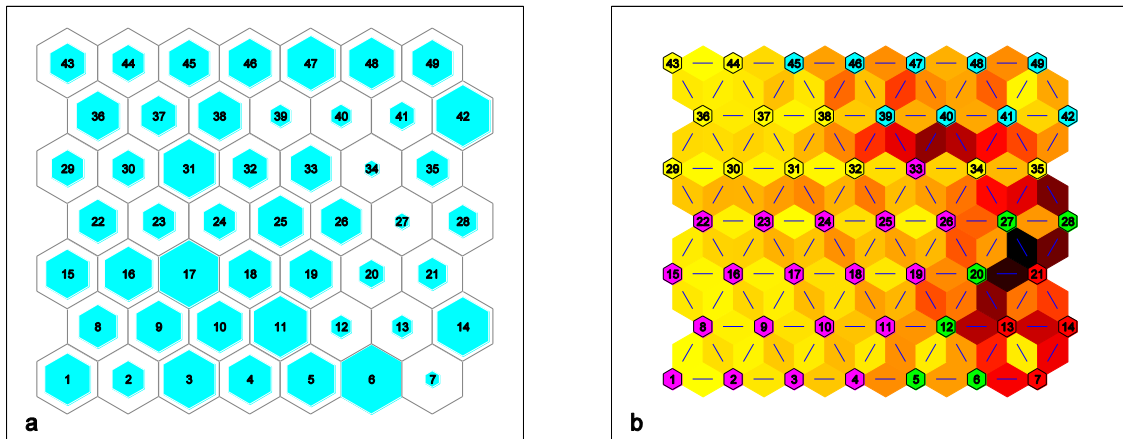


Figure 3.12 (a) Kohonen map displaying the SOM topology (numbers specify neuron number) and neuron cardinality showing the proportion of observations projected onto each neuron (in cyan; see Fig. 3.14 for the number of hits on each neuron). (b) SOM neighbor weight distances indicating the distance between neighboring neurons. Hexagons (numbered 1-49) represent the neurons. Each neuron is color coded to represent which cluster it belongs to from the AHC performed on the neurons (see Fig. 3.14). Blue lines connect neighboring neurons while the colors in regions containing the blue lines indicate the distances between the neurons: darker (lighter) colors represent larger (smaller) distances.

Our choice of the size of the neuron map is justified as all neurons are occupied within the space of the observations. The size of the hexagons in Fig. 3.12a (in cyan) represents the number of hits of observations on each neuron. A large (small) size means that a large (small) number of observations are represented by the particular neuron. The sum of the number of hits on all the neurons is equal to the temporal size of the observations (i.e., 372). After the SOM is trained, the sampling needs to be checked to ensure that the weight vectors are suitably able to represent the observations. Fig. 3.13a-c shows a scatter plot of the observations (black crosses) and the weight vectors (red dots). The nearest neighbors are connected by the straight lines (in blue). It can be seen for all three plots that the weight vectors homogeneously wrap up all the observations. Therefore, the neurons are successful in capturing a majority of the information contained in the observations. The contribution of each input index to the neuron topology is shown in Fig. 3.13d-e, while the total contribution is illustrated in Fig. 3.12b.

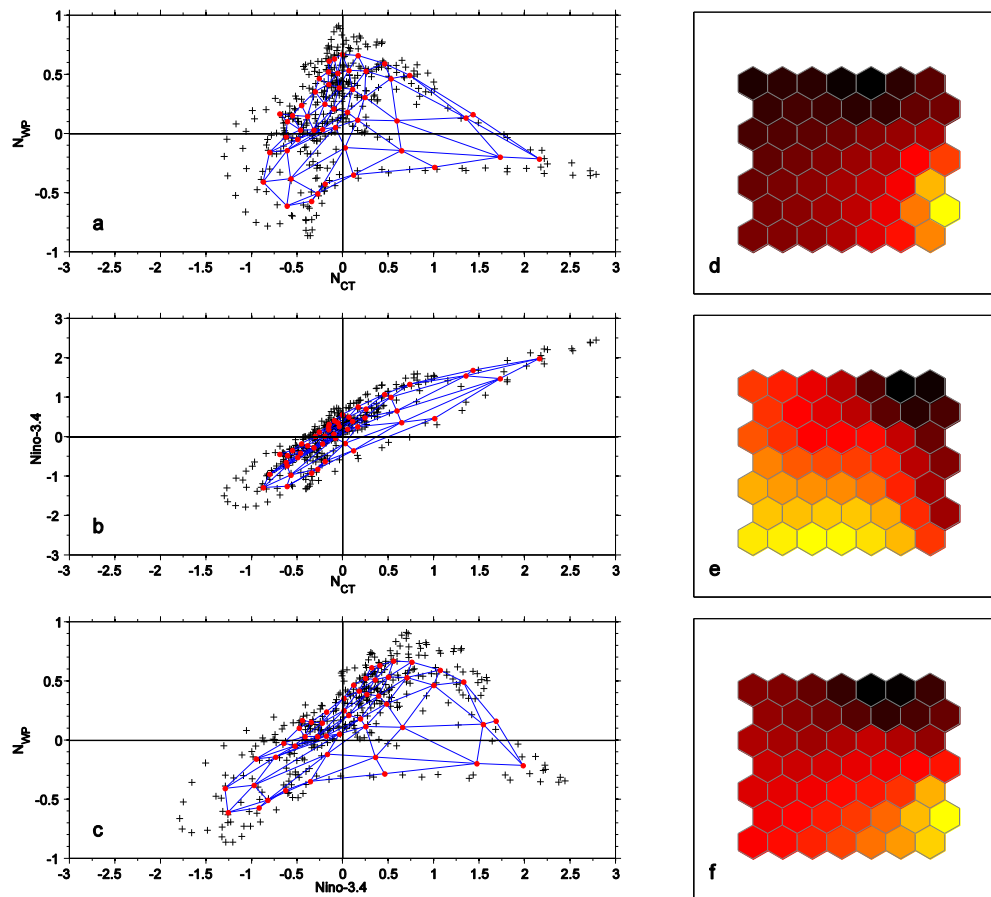


Figure 3.13 (left column) The location of observations (black crosses) and weight vectors (red dots connected by blue lines) between (a) N_{CT} and N_{WP} , (b) N_{CT} and $Ni\tilde{no}3.4$ and (c) N_{WP} and $Ni\tilde{no}3.4$ indices. The units are in $^{\circ}C$. (right column) The weight planes connecting each observation of (d) N_{CT} , (e) N_{WP} and (f) $Ni\tilde{no}3.4$ to each neuron. Darker (lighter) colors represent larger (smaller) distances.

From the NNA, a reduction of the data space is realized. The neurons, however, need to be aggregated as there is more than one neuron which may represent a single phenomenon. To achieve this, we perform an AHC analysis on the neurons. Each neuron contains information about the timing and number of observations it represents. This, combined with information on the distances between the neurons (weight vectors), is fed into the clustering procedure. The resulting dendrogram and neuron classification is shown in Fig. 3.14a&b. The information on the timing of the observations contained in each neuron can be extracted to obtain a general time series of the neuron clusters (Fig. 3.14c), which can then be used to extract the spatial patterns of SST, SSS and SL anomalies (Fig. 3.14d-r).

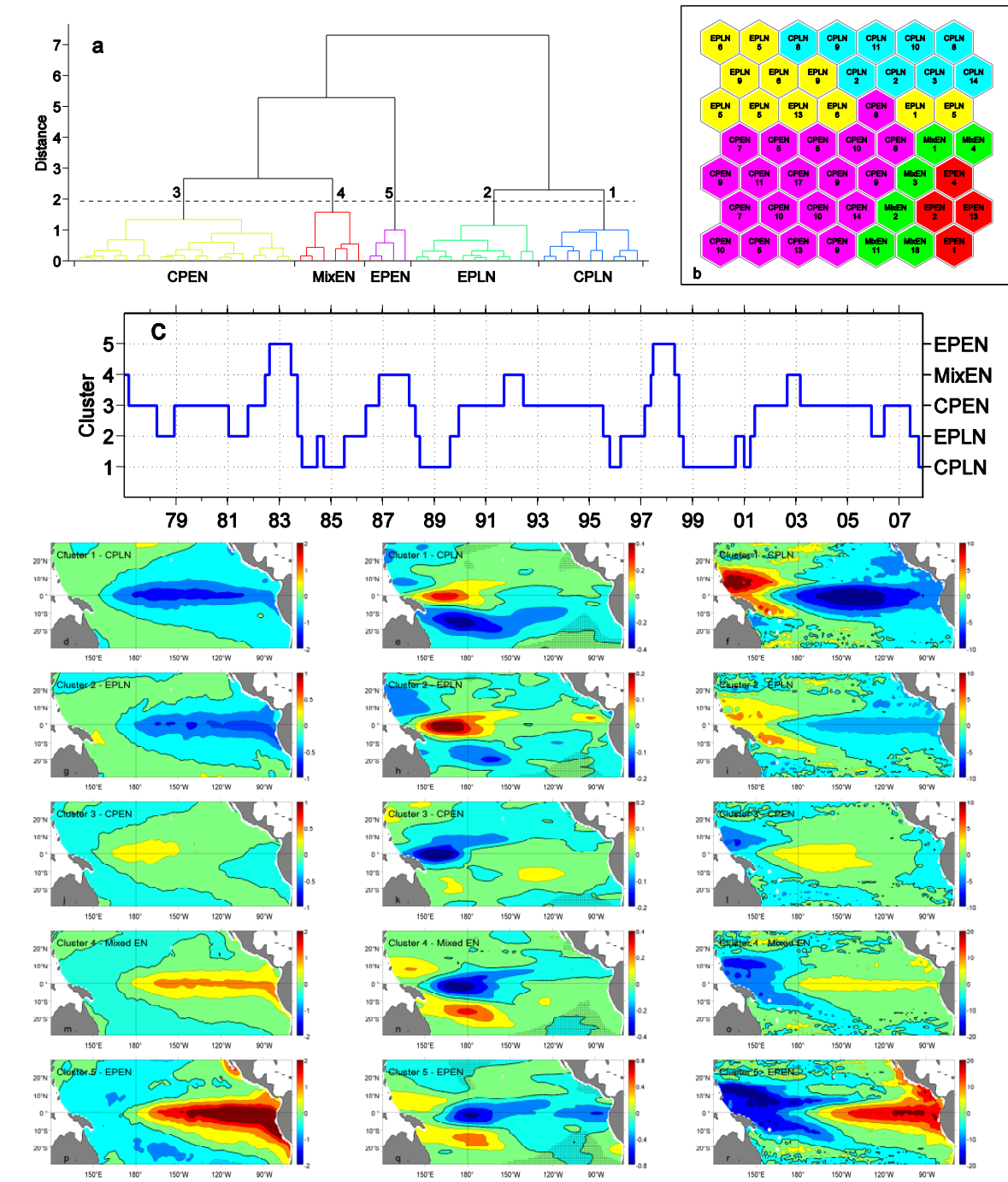


Figure 3.14 (a) Dendrogram resulting from the AHC performed on the neurons. The ordinate labels the inter-cluster distance. The dashed line indicates the cutting level ensuing in five clusters being identified. (b) The neuron grouping showing which neurons uniquely belong to each cluster. The numbers on each neuron indicate the number of hits. (c) The cluster time series showing which cluster best represents the neurons at a particular time. Spatial patterns of SSTA (first column; in $^{\circ}\text{C}$), SSSA (second column; in pss) and SLA (third column; in cm) extracted from the AHC on the neurons with (d-f) cluster 1 denoting CPLN, (g-i) cluster 2 denoting EPLN, (j-l) cluster 3 denoting CPEN, (m-o) cluster 4 denoting mixed EN and (p-r) cluster 5 denoting EPEN conditions. The lag used to extract the spatial patterns from the cluster time series is zero for SSTA and SLA and 3 months for SSSA. Note the different color scales in the spatial patterns. The regions shaded in black in the plots for SSS, mainly located in the southeastern tropical Pacific, denote regions where the error in SSS is larger than 80%. Thick black contour lines in the spatial patterns denote the 0 line.

From the AHC analysis, five clusters are obtained which represent EP and CP El Niño and La Niña events as well as mixed El Niño events. The EP and CP ENSO clusters are very similar, if not the same, with those obtained earlier using the singular EOF, combined regression-EOF and AHC analyses. This gives us confidence in the use of SOM to efficiently and effectively extract the climatic signal on interannual timescales. The mixed El Niño cluster is probably a consequence of using the Niño3.4 index, which cannot discriminate between EP and CP El Niño events on its own. As a consequence, the two very strong El Niño events over the past few decades, the 1982-83 and 1997-98 EP El Niño events, are singled out in the EP El Niño cluster. As would then be expected, the mixed El Niño clusters have similar spatial patterns to the EP El Niño cluster with generally reduced magnitudes in SST, SSS and SL anomalies.

3.5 Summary and Discussion

Both ENSO similarities and differences have been analyzed in the last three decades with numerous results pointing out the many dissimilarities of ENSO events, including their strength, onset time, phasing with the seasonal cycle, duration, eastward or westward propagation of SST anomalies in the equatorial band (e.g., [Wang, 1995](#)), and more recently the recent detection of a possible new type of El Niño (e.g., [Larkin and Harrison, 2005a,b](#)), referred to here as central Pacific (CP) El Niño events. In line with this, the aim of this chapter was to further contrast ENSO features in the tropical Pacific using SST, SSS and SL observations using different statistical methods. A parallel study was also conducted to contrast the different ENSO signatures using sea surface chlorophyll observations from satellite measurements.

Using singular EOF, combined regression-EOF and agglomerative hierarchical clustering (AHC) on SST, SSS and SL anomalies, we showed that the timing of what have been recently called the eastern Pacific (EP) and CP El Niño and La Niña events using each climate variable generally agree with each other. It should be noted, however, that differentiating clearly between EP and CP ENSO flavors is a difficult exercise, depending on the method used, and noting that some years may even be classified as “mixed” events (e.g., [Kug *et al.*, 2009](#); their Fig. 1). Of course, not all statistical methods may be appropriate and/or reliable, for example, the EOF analysis on SSS anomalies failed to correctly extract the CP ENSO signature. However, consistent results were obtained using other statistical methods.

The SST signature during EP and CP El Niño were briefly described in Chapter 1 using the 1982-83, 1997-98, 2002-03 and 2009-10 El Niño events as representative examples (see [Fig. 1.5](#)). We obtained basically the same signature using the different statistical methods outlined above, noting that the La Niña signature during EP and CP events are almost symmetrical to the El Niño events. In brief, the EP El Niño (La Niña) signature shows maximum anomalous warming (cooling) extending from the South American coast along the equator to the central Pacific region. In contrast, the CP El Niño (La Niña) signature has maximum anomalous warming (cooling) concentrated in the central Pacific flanked by weaker anomalies on either side of the maxima. These results are in agreement with previous studies using similar statistical analysis and/or datasets (e.g., [Ashok et al., 2007](#); [Leloup et al., 2007](#); [Kao and Yu, 2009](#)).

To somewhat paraphrase the results published in [Singh et al. \(2011\)](#), EP and CP El Niño (La Niña) events result in a SSS freshening (saltening) in the western half of the equatorial Pacific and a SSS increase (decrease) in the SPCZ mean area. The EP and CP El Niño events, however, have distinct quantitative SSS signatures. In the equatorial Pacific (say 2°S-2°N), EP El Niño events are characterized by a maximum SSS freshening (~-1 pss) near the dateline and a strong (~30° longitude) eastward displacements of the 34.8 pss isohaline materializing the eastern edge of the low-salinity warm pool waters. During CP El Niño events, the maximum SSS freshening is shifted westward by about 15° longitude and the eastward displacements of the 34.8 pss isohaline are only about half the EP El Niño amplitude. [Kug et al. \(2009\)](#) found similar differences between Warm Pool and Cold Tongue El Niño events (analogous to our CP and EP El Niño) in terms of SST, precipitation, atmospheric vertical motion and surface zonal wind anomalies: the anomalies are shifted to the west during Warm Pool El Niño compared to those associated with the Cold Tongue El Niño. This results in rather homogeneous SSS within 150°E-170°W during EP El Niño events, contrasting with non-homogeneous SSS between the western (150°E-170°E) and eastern (170°E-170°W) halves of the warm pool during CP El Niño events (with the western half being ~0.2 pss fresher). In the far western equatorial Pacific, results are also contrasted: EP El Niño events result in a saltening, whereas CP El Niño in a freshening of the surface waters. Besides, in the SPCZ mean area, EP El Niño events are characterized by a well-marked increase (~+1 pss) in SSS, which is about 2-3 times less during CP El Niño events. The differences in SSS anomalies in the western and eastern halves of the warm pool and in the SPCZ region during EP and CP ENSO events allows us to define two possible metrics

(see Fig. 13 in [Singh et al., 2011](#)): one which can fairly well distinguish between EP and CP ENSO events (SSS ENSO Index) and another, which can also discriminate EP from CP El Niño events (SSS El Niño Index). These indices are only “indices” and so not 100% perfect. As an example, in the above-noted figure, the discrepancy in the SSS El Niño Index in 2002-03 can be attributed to the fact that although the AHC procedure classifies the 2002-03 El Niño as a CP El Niño, the location of the negative SSS anomaly in the equatorial western Pacific during 2002-03 is displaced further east of what the CP El Niño cluster shows. The location of the negative anomaly (only) agrees with that in the EP El Niño cluster, and thus the reason for the discrepancy in the SSS El Niño Index during 2002-03. Further studies on the evolution and termination of the 2002-03 El Niño can be found in the works of [McPhaden \(2004\)](#) and [Vecchi and Harrison \(2003\)](#), respectively. A detailed discussion on the main mechanisms responsible for the ENSO signatures in SSS can be found in [Singh et al. \(2011\)](#) at the end of this chapter.

The EP and CP ENSO signature in SLA is reminiscent of a zonal and meridional seesaw, respectively. During EP El Niño, the release of warm waters from the western to the eastern equatorial Pacific results in a reduced zonal thermocline slope leading to anomalous warming (cooling) in the eastern (western) half of the Pacific. This results in a zonal seesaw pattern in SLA pivoted around 180°. During EP La Niña, the strengthening of the trade winds allows for the buildup of warm waters in the far western Pacific and equatorial upwelling in the eastern Pacific, which results in a stronger thermocline slope and a zonal seesaw pattern opposite in sign to that during EP El Niño. In contrast, the CP El Niño (La Niña) signature in SLA indicates a recharge (discharge) of the equatorial band resulting in positive (negative) SLA almost over the entire equatorial region. Generally, the positive (negative) SLA during CP El Niño (La Niña) extends up to 15°S while it is mirrored by negative (positive) SLA north of around 5°N. This meridional seesaw pattern was also found in the study of [Alory and Delcroix \(2002\)](#) using multivariate EOF analysis and similar SLA data. A detailed analysis of these patterns and the mechanisms responsible are further discussed in Chapter 4.

As a final comment, there is no doubt that the mechanisms responsible for the different flavors of ENSO, as observed in many oceanic and atmospheric variables, need to be further scrutinized to possibly explain their occurrence. Major theories have previously been put forward to explain, at least, the oscillatory nature of ENSO. However, these theories were proposed more than a decade ago, before the recent enhanced attention given to the CP type

of ENSO. Consequently, we believe appropriate to tentatively analyze the EP and CP signature of ENSO in terms of dynamics from ENSO theories. This is the next step in this project and which is addressed in the next chapter.

3.6 Publication: Singh *et al.*, 2011

The following article was published in *Journal of Geophysical Research* in 2011 as part of this PhD thesis.

Singh, A., Delcroix, T., and Cravatte, S. (2011). Contrasting the flavors of El Niño-Southern Oscillation using sea surface salinity observations, *Journal of Geophysical Research*, **116**(C06016), doi:10.1029/2010JC006862.

Contrasting the flavors of El Niño-Southern Oscillation using sea surface salinity observations

Awnesh Singh,¹ Thierry Delcroix,¹ and Sophie Cravatte¹

Received 3 December 2010; revised 25 February 2011; accepted 9 March 2011; published 23 June 2011.

[1] The recent detection of a central Pacific type of El Niño has added a new dimension to the El Niño-Southern Oscillation climatic puzzle. Sea surface salinity (SSS) observations collected during 1977–2008 in the tropical Pacific are used to contrast the three eastern Pacific (EP) (1982–1983, 1991–1992, 1997–1998) and seven central Pacific (CP) (1977–1978, 1986–1988, 1990–1991, 1992–1995, 2002–2003, 2004–2005, 2006–2007) types of El Niño events, as well as the six EP (1985–1986, 1988–1989, 1995–1996, 1999–2001, 2005–2006, 2007–2008) and two CP (1983–1984, 1998–1999) types of La Niña events. The EP El Niño events result in large (~30° longitude) eastward displacements of the eastern edge of the low-salinity warm pool waters in the equatorial band, a resulting well-marked SSS freshening (~−1) near the dateline, and a SSS increase (~+1) below the mean position of the South Pacific Convergence Zone (SPCZ). The CP El Niño events are characterized by smaller (50%) eastward displacements of the eastern edge, a ~15° longitude westward shift of the equatorial SSS freshening, and a comparatively reduced (~50%) SSS increase in the SPCZ. A qualitative analysis indicates that changes in zonal currents and precipitation can account for the observed contrasted signature in SSS. Eastward current anomalies appear over most of the equatorial band during EP El Niño events. In contrast, there is a tendency for zonal current convergence slightly west of the dateline during CP El Niño events, consistent with the confinement of the warm/fresh pool in the western central equatorial basin, the related quasi-inexistent northeastward migration of the SPCZ, and associated heavy precipitation regime.

Citation: Singh, A., T. Delcroix, and S. Cravatte (2011), Contrasting the flavors of El Niño-Southern Oscillation using sea surface salinity observations, *J. Geophys. Res.*, 116, C06016, doi:10.1029/2010JC006862.

1. Introduction

[2] The El Niño-Southern Oscillation (ENSO) phenomenon is the strongest climatic signal on an interannual time scale and greatly affects the world population [Goddard and Dilley, 2005; McPhaden *et al.*, 2006]. The ENSO comprises warm (El Niño) and cold (La Niña) episodes, with a returning time scale ranging from 2 to 7 years. The main properties of these two episodes are sometimes described as being negatively related, to the first order, but more interestingly, the properties differ within each episode. This was especially studied for the El Niño episodes which, at least, can vary in terms of phasing with the seasonal cycle [e.g., Jin *et al.*, 1994], strength [e.g., Wolter and Timlin, 1998], duration [e.g., Glantz *et al.*, 1991], onset time [e.g., Wang, 1995], and eastward or westward displacement of sea surface temperature (SST) anomalies along the equator [e.g., Wang, 1995; McPhaden and Zhang, 2009]. The recent detection of a “new type” of El Niño, termed as “Dateline El Niño” [Larkin and Harrison, 2005a], “El Niño Modoki”

[Ashok *et al.*, 2007], “Warm Pool El Niño” [Kug *et al.*, 2009] or “central Pacific El Niño” [Kao and Yu, 2009], and hereafter referred to as the CP El Niño, has added a new dimension to the ENSO climatic puzzle. During this new type of El Niño, the maximum SST Anomalies (SSTA) are confined in the central equatorial Pacific, in contrast with the variously called “traditional,” “canonical,” “conventional,” “cold tongue” or “eastern Pacific” El Niño (hereafter referred to as the EP El Niño), when they occur in the eastern Pacific. Interestingly, the CP El Niño has been shown to be more intense in recent years [Lee and McPhaden, 2010], and could be more frequent in a warming climate [Yeh *et al.*, 2009].

[3] Different methods and numerous indices have been used to document the occurrence and diversity of ENSO, and to classify the different types of El Niño. Perhaps the most commonly used indices to document ENSO are the atmospheric Southern Oscillation Index (SOI) and the oceanic Niño-1+2, Niño-3, Niño-3.4 and Niño-4 SST indices [e.g., Rasmusson and Carpenter, 1982; Trenberth, 1984, 1997]. Other indices have also been developed for specific process studies [e.g., Delcroix, 1998; Leloup *et al.*, 2007; Meyers *et al.*, 2007; Wolter and Timlin, 1998]. Most of these indices vary *rather* consistently with each other, as detailed

¹IRD/LEGOS, UMR 5566, Toulouse, France.

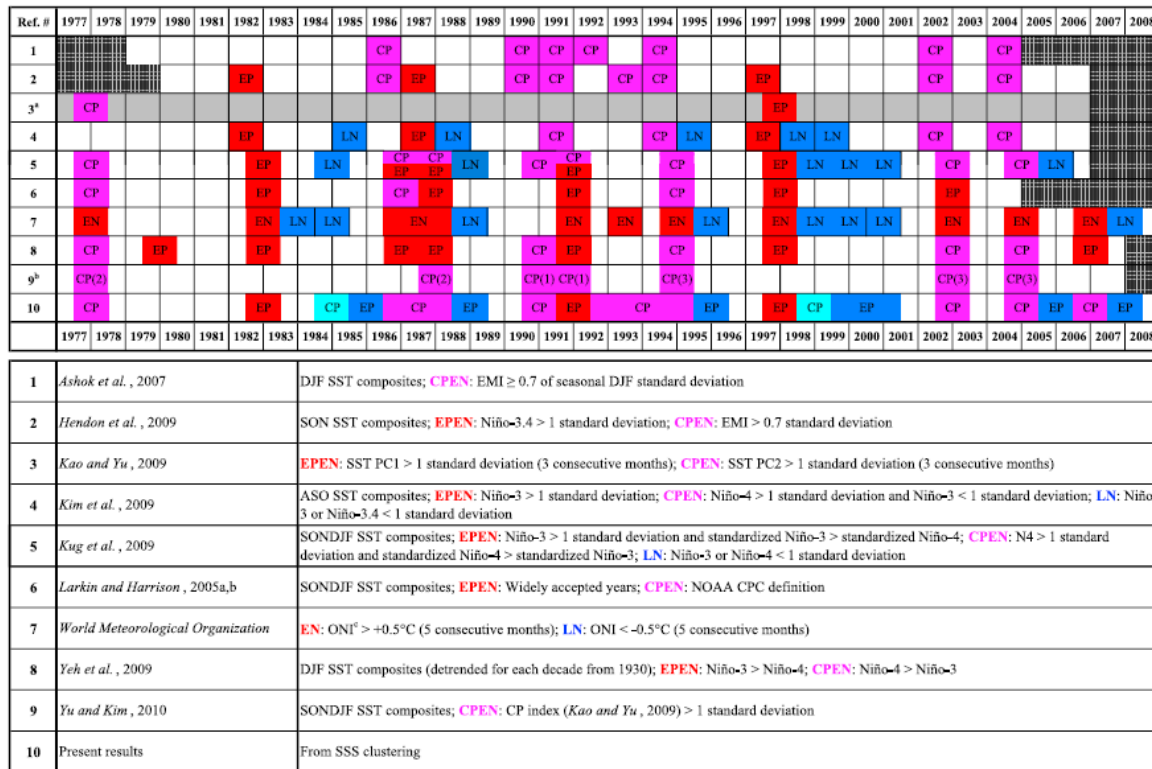


Figure 1. Years of eastern Pacific (EP) and central Pacific (CP) El Niño (EN) (in red and pink) and La Niña (LN) (in blue and turquoise) events as defined by the various references and their criteria (at the bottom image). Dark hatched boxes show that the period was not analyzed by the respective authors. Light hatched boxes show that the period was analyzed but the authors did not classify the events. The acronym DJF stands for December-January-February, etc. The superscript a means these authors only classified two events as examples of EPEN and CPEN events. Further analysis from their work was done by Yu and Kim [2010]. The superscript b means only CPEN events were analyzed and subsequently divided into three classes. The superscript c means ONI is the World Meteorological Organization defined Oceanic Niño Index, which is defined as the 3 month running means of SSTA in the Niño-3.4 region.

for a few of them by Deser and Wallace [1987] and Hanley et al. [2003]. Yet, as a useful reference, the World Meteorological Organization (WMO), in 2005, has adopted a definition of El Niño and La Niña events based on the analysis of Niño-3.4 SSTA. The WMO years of the 1977–2008 events are given in Figure 1. In addition, to classify the different types of ENSO, new SST-based indices have been proposed recently to characterize the CP El Niño, including the Trans-Niño Index (TNI) [Trenberth and Stepaniak, 2001], El Niño Modoki Index (EMI) [Ashok et al., 2007] and CP Index [Kao and Yu, 2009]. Depending on the method and SST-based index used, the years identified as EP or CP El Niño may slightly differ, as summarized in Figure 1.

[4] Studies have shown that different ENSO episodes, including EP and CP El Niño events, have different impacts on weather and climate, at both global and regional scales [Larkin and Harrison, 2005b; Weng et al., 2007; Ashok et al., 2009a, 2009b; Cai and Cowan, 2009; Hendon et al., 2009; Kim et al., 2009; Vincent et al., 2009; Yeh et al., 2009; Chen and Tam, 2010]. Most of them have used SST to stress

the differences between ENSO episodes since the climatic impacts are sensitive to details of the surface warming (or cooling) of the equatorial Pacific [Palmer and Mansfield, 1984] via varying teleconnections, and because SST is by far the best observed oceanic variable. Interestingly, some of them have used variables other than SST involved in the ENSO cycle. For example, looking at recent publications only, Bosc and Delcroix [2008] and Kug et al. [2009] used sea level anomalies (SLA) as an alias for warm water volume (WWV) to differentiate between ENSO events, Kao and Yu [2009] identified the anomalous surface wind stress and vertical temperature structure associated with the EP and CP types of El Niño, Yeh et al. [2009] and Kug et al. [2009] found different signatures in precipitation anomalies during EP and CP El Niño events, while Chiodi and Harrison [2010] used outgoing longwave radiation (OLR) in the equatorial Pacific to distinguish between El Niño events.

[5] Using different variables to document ENSO clearly gives different perspectives rather than using SST only to understand its behavior, impacts and how it works. An

essential variable of the global climate observing system [Global Climate Observing System, 2004; see also Lagerloef *et al.*, 2008] that is also affected by the ENSO cycle is sea surface salinity (SSS). Indeed, precipitation patterns and heat fluxes are modified in the course of an El Niño or La Niña, affecting SSS. Moreover, anomalous surface currents have been simulated during CP El Niño [Kug *et al.*, 2009], and we can expect these currents to imprint on the distribution of SSS given the main role of zonal salt advection in the equatorial band at the ENSO time scale [Picaut *et al.*, 2001]. Hence, as a complement to previous studies, the goal of this paper is, for the first time, to contrast and tentatively explain the different flavors of ENSO using SSS.

[6] The rest of the paper is organized as follows. Section 2 describes the data and methodology. Section 3 recalls the mean structures for SST, SSS, precipitation (P) and zonal currents (U). Section 4 sets the context regarding EP and CP ENSO based on an Empirical Orthogonal Function (EOF) analysis on SST and then analyzes the ENSO-related SSS variability with an EOF analysis, Agglomerative Hierarchical Clustering (AHC), and representative examples of ENSO events. Section 5 discusses the main mechanisms likely responsible for observed ENSO-related SSS variations. Section 6 summarizes and discusses the findings of this study.

2. Data Sets and Methodology

[7] The SSS data were obtained from the 1° longitude by 1° latitude and 1 month gridded product of Delcroix *et al.* [2011] for the tropical Pacific region (30°S–30°N, 120°E–70°W) and from 1950 to 2008. This product is derived from data originating from Voluntary Observing Ships, TAO/TRITON moorings, CTD and Argo profilers. As the SSS coverage data is greatly time dependant, each grid point has an associated error indicating the confidence we can have on the SSS product at one particular month. This error is given as a percentage of the interannual variance at that point. When there is no SSS data available, the error is 100% and the SSS gridded value is equal to the monthly climatological SSS. In our analyses, we wish to exclude the grid points where too few data are available, and we consider somewhat arbitrarily that we can trust the SSS gridded product value if the error is less than the 80% threshold. In their analysis with a similar product, Cravatte *et al.* [2009] used an arbitrary value of 60% to define the error threshold. Initial sensitivity studies found that using 60% or 80% as the error threshold did not significantly change our results. Accordingly, regions where the mean error is less than 80% as well as data starting from 1977 only (due to poor data coverage before the mid 1970s) were used in our analysis. For SST, we chose to use the Met Office Hadley Centre for Climate Prediction and Research sea ice and sea surface temperature data set 1 (HadISST1) [Rayner *et al.*, 2003], available monthly from 1870 until present and with the same grid size as the SSS product. The Extended Reconstructed Sea Surface Temperature (ERSST) [Smith and Reynolds, 2003] and Kaplan [Kaplan *et al.*, 1998] data sets were also tested in addition to the HadISST1 product, and we found that there is not much difference in the end results for the low-

frequency variations. We restricted the spatial and temporal domain for the SST data to be the same as that for the SSS data.

[8] The precipitation data used is from the Global Precipitation Climatology Project (GPCP) version 2.1 combined precipitation data set [Huffman *et al.*, 2009] of monthly means from combined satellite and station data on a 2.5° grid that is available from 1979 to present. This product is regridded on a 1° grid using triangle-based linear interpolation based on a Delaunay triangulation [Barber *et al.*, 1996] and constrained to the tropical Pacific region. We also tested the NCEP/NCAR Reanalysis 1 precipitation product [Kalnay *et al.*, 1996] available from 1948, and while there are not significant differences between the two products, we selected to show results from GPCP for our specified region because no precipitation observations are assimilated in the reanalysis product [Janowiak *et al.*, 1998]. The surface (0–30 m) currents are derived from the Ocean Surface Currents Analyses-Real time (OSCAR) product, which is available on a 1° grid monthly from October 1992 [Bonjean and Lagerloef, 2002]. We also tested the Centre of Topography of the Oceans and the Hydrosphere (CTOH) [Sudre and Morrow, 2008] and Archiving, Validation and Interpretation of Satellite Oceanographic data (AVISO) surface currents products and got basically the same results as with the OSCAR product. The Websites for downloading all the gridded fields we used are given below in the Acknowledgments paragraph.

[9] All data sets were detrended (except for the zonal currents as the time series are too short) over the 1977–2008 period for SSS and SST, and 1979–2008 for precipitation. This proved necessary as, for example, the freshening trend observed in the warm pool over the last 30 years [Delcroix *et al.*, 2007; Cravatte *et al.*, 2009] could have been (mis) interpreted as a sign of increased intensity or occurrence of El Niño events. Yet, it is also possible that part of the observed linear trends in SST and SSS in the central equatorial Pacific are due to an increase of El Niño intensity in the central Pacific, as suggested by Lee and McPhaden [2010] for SST and discussed in section 6 for SSS.

[10] A number of different data analysis procedures were then performed on the anomalies (relative to the mean monthly climatology) in order to characterize the different ENSO signatures. These include time filtering using different filter lengths, EOF analysis [e.g., Emery and Thomson, 2001], linear regressions of anomalies onto ENSO indices (e.g., Niño-1+2 and Niño-4 SSTA), combined regression-EOF analysis (as used by Kao and Yu [2009]), neural network analysis [Kohonen, 1989] and agglomerative hierarchical clustering (AHC) [Kohonen, 1989]. We choose to discuss results derived from the well-known EOF analysis and less frequently used AHC technique only. These two techniques were performed on 13 months Hanning filtered anomalies. This filter passes almost no signal at periods of 6 months and shorter and so looks appropriate since the duration of CP ENSO was found to be less than 1 year [e.g., Ashok *et al.*, 2007; Weng *et al.*, 2007; Kao and Yu, 2009].

[11] In the AHC procedure, each singleton (defined as a monthly anomaly map) is initially merged with another according to the smallest Euclidean distance between each pair of singletons. Each resulting merged cluster is then

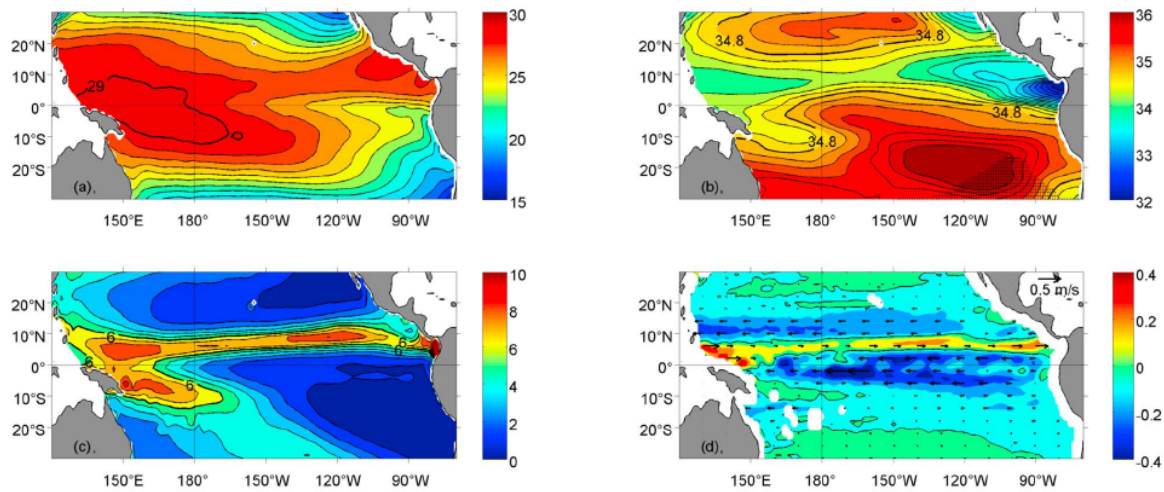


Figure 2. Mean structures of (a) SST, (b) SSS, (c) precipitation, and (d) zonal currents in the tropical Pacific region. The heavy contour lines in Figures 2a–2c represent the 29°C isotherm, 34.8 isohaline, and 6 mm d⁻¹ isohyet, respectively. The contour spacing is 1°C, 0.2, and 1 mm d⁻¹ in Figures 2a–2c, respectively. The regions shaded in black in the southeastern tropical Pacific in Figure 2b denote regions where the normalized error in SSS is larger than 80% and that are not used in the analysis. Positive values in Figure 2d denote eastward currents.

paired with another merged cluster according to the *Ward* [1963] criterion (which is analogous to the Euclidean distance for singletons). This procedure was repeated until the remaining two clusters were finally merged into the complete data set. The clustering procedure can be represented by a dendrogram, which illustrates the fusions made at each successive step of the analysis and the linkage (separation) distance between each successive clustering. Further examples on the use of the above clustering technique can be found in the work by *Kao and Yu* [2009] and *Vincent et al.* [2009].

3. Mean Structures

[12] The mean structures for SST, SSS, precipitation and zonal currents fields are first reminded in Figure 2. For SST, the presence of a smooth temperature gradient along the equatorial region distinguishes the warm pool (characterized here by SST greater than 29°C) in the west from the equatorial upwelling region in the east. High SST bands are found along the Inter Tropical Convergence Zone (ITCZ) north of the equator and in the South Pacific Convergence Zone (SPCZ), which is obliquely oriented along the north-west-southeast axis in the southwest tropical Pacific. The poleward decrease in SST is evident from ~15°–20° latitude. The mean SSS structure shows low-salinity waters observed under the ITCZ and SPCZ and in the western equatorial Pacific. A strong minimum in SSS is also observed in the far eastern Pacific within 5°N–10°N, south of the eastern warm pool. Two high-salinity cores are found northwest of Hawaii and in the vicinity of Tahiti. In the equatorial region, SSS increases westward from the Americas to the central Pacific

and then decreases farther to the west, with the 34.8 isohaline lying close to the eastern edge of the warm pool. High precipitation (>6 mm d⁻¹) is found in the ITCZ and SPCZ regions, which are linked together in the western Pacific just north of the equator in the warm pool area. Regions deficient in precipitation are observed in the northeastern and southeastern tropical Pacific. For zonal currents, the westward flowing north equatorial current (NEC) and south equatorial current (SEC) are most evident in the 10°N–15°N and 10°S–5°N bands with maximum magnitudes around 0.30 m s⁻¹ and 0.55 m s⁻¹, respectively. The eastward flowing north equatorial counter current (NECC) lies in the 5°N–10°N band with maximum amplitudes close to 0.47 m s⁻¹. Its much weaker (maximum amplitude of 0.1 m s⁻¹) southern counterpart, the South Equatorial Counter Current (SECC) is also visible at around 10°S–5°S, east of the Solomon Islands.

4. SST and SSS Signal During ENSO

4.1. EOF Analysis

[13] To set the context, especially regarding the signature of EP and CP ENSO, Figures 3 and 4 show the results of an EOF analysis performed on 13 months Hanning filtered SST and SSS anomalies. The first EOF on SST accounts for 56.9% of the interannual variance. The spatial pattern (Figure 3) shows anomalous SST warming off the South American coast extending toward the central Pacific along the equatorial region. Its time function (SST-PC1) is highly correlated with the 13 months Hanning filtered SOI ($R = -0.91$; SOI leading by 1 month). The second EOF on SST accounts for 13.6% of the interannual variance. The spatial

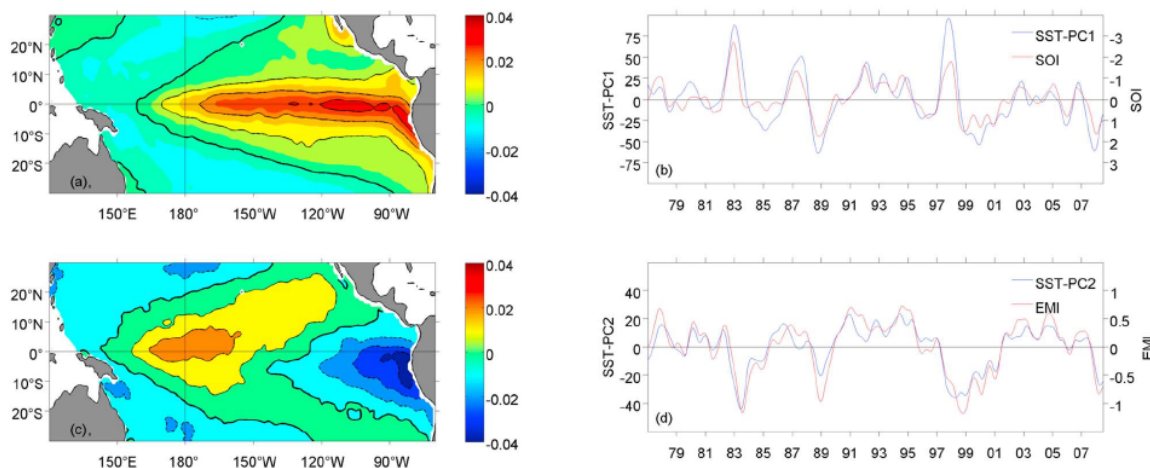


Figure 3. Spatial structures for (a) EOF1 and (c) EOF2 and (b and d) their corresponding time functions (in blue) for the first and second modes of the EOF on SSTA, respectively. The units are defined so that the product between the spatial pattern and the corresponding time function denotes degree Celsius. Note the different vertical scales for the time functions. The red lines in the time functions denote the 13 months Hanning filtered SOI (in Figure 3b) and EMI (in Figure 3d), scaled on the right vertical axis. Note the reversed vertical scale for the SOI.

pattern shows a large meridional “horseshoe pattern” of warm SSTA in the central Pacific region flanked by cold SSTA in the eastern equatorial Pacific and, to a lesser extent, in the far western basin. Its time function (SST-PC2) shows high correlation with the 13 months Hanning filtered EMI ($R = 0.94$; SST-PC2 leading by 1 month), noting that the variations in SST EOF2 are about half of those from SST EOF1. Note that the EMI is defined as: $[SSTA]_A - (0.5 \times ([SSTA]_B + [SSTA]_C))$, where the square brackets represent the area averaged SST anomalies over the regions A ($165^\circ\text{E}–140^\circ\text{W}$, $10^\circ\text{S}–10^\circ\text{N}$), B ($110^\circ\text{W}–70^\circ\text{W}$, $15^\circ\text{S}–5^\circ\text{N}$) and C ($125^\circ\text{E}–145^\circ\text{E}$, $10^\circ\text{S}–20^\circ\text{N}$) [Ashok et al., 2007]. According to Ashok et al. [2007], the spatial patterns of SST EOF1 and EOF2 associated with the positive phase of their time functions are characteristic of EP and CP El Niño, respectively.

[14] The first EOF for SSS accounts for 28.6% of the interannual variance. The spatial pattern (Figure 4) shows

negative loadings in the western central equatorial Pacific region with maximum values west of the dateline (up to 0.043), and positive loadings with maxima (around 0.036) found further south in the SPCZ region. Its time function (SSS-PC1) is highly correlated with SST-PC1 ($R = 0.91$; SST-PC1 leading by 3 months). Negative (positive) loadings in Figure 4a thus indicate a decrease (increase) of SSS during El Niño events, and vice versa during La Niña events. These SSS EOF1 results are in agreement with those of Delcroix [1998] who found similar patterns using data from 1976 to 1992 only, though our confidence is strengthened in the present analysis in which we double the record length. By analogy with SST EOF1, it is tempting to conclude that this SSS EOF1 characterizes the SSS signature of EP ENSO. The second and third SSS EOFs extract a total of 25.6% ($13.2 + 12.4$) and are not shown here. Although their time functions are well correlated with SST-PC2 ($R = 0.44$ and $R = 0.75$) at zero lag, a simple test of significance

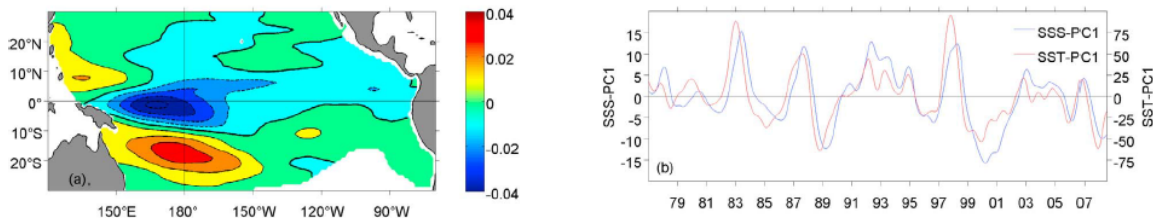


Figure 4. (a) Spatial structure and (b) corresponding time function (in blue) for the first mode of the EOF on SSSA. The red line in the time function denotes SST-PC1, as in Figure 3b, scaled on the right vertical axis. The white areas in the southeastern tropical Pacific in Figure 4a denote regions where the normalized error in SSS is larger than 80% and are not used in the analysis.

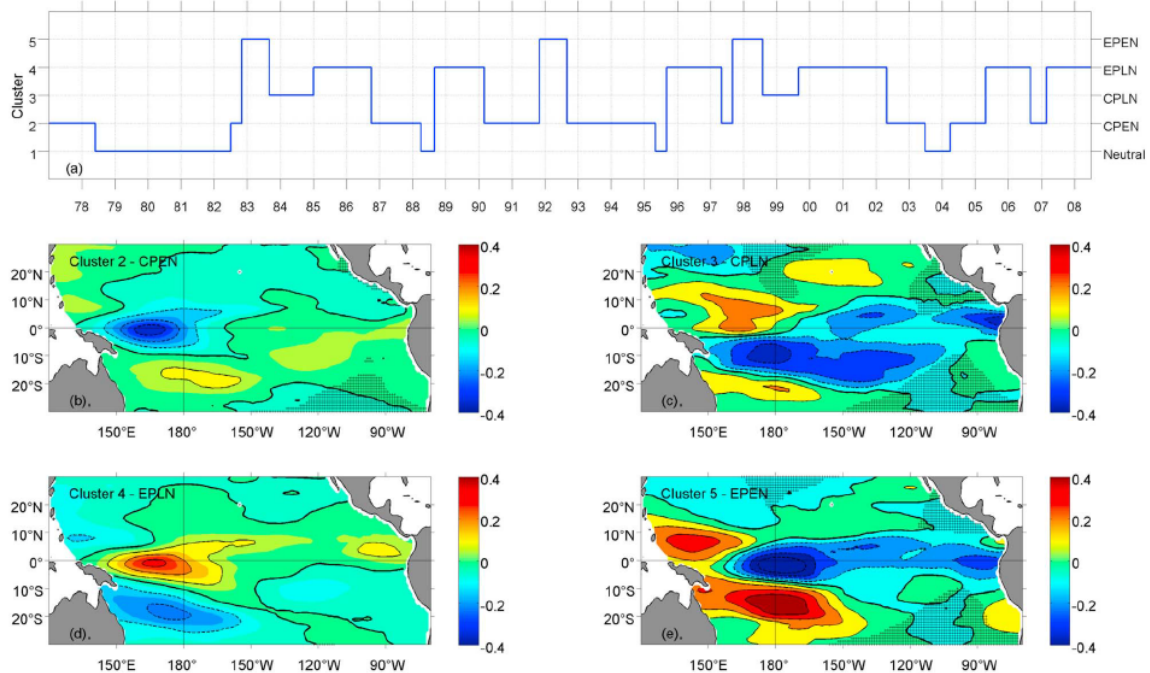


Figure 5. (a) The cluster time series shows which cluster best represents the SSSA pattern at a particular time. The abscissa labels denote the beginning of the year. Spatial structures from the agglomerative hierarchical clustering technique on SSSA with (b) cluster 2 showing CP El Niño conditions, (c) cluster 3 showing CP La Niña conditions, (d) cluster 4 showing EP La Niña conditions, and (e) cluster 5 showing EP El Niño conditions. The regions shaded in black, mainly located in the southeastern tropical Pacific, denote regions where the normalized error in SSS is larger than 80%.

[North *et al.*, 1982] applied to the eigenvalues shows that these EOFs cannot be distinguished in a statistically significant way and thus probably do not extract (or extract a mixture of) real physical phenomena.

4.2. AHC Analysis

[15] The advantage of the above EOF analysis is that it provides a compact description of the spatial and temporal variability of SST and SSS. Noteworthy, it implicitly assumes symmetry in the spatial patterns of the El Niño and La Niña events denoted by the positive and negative phases of the EOF time functions, respectively. As discussed in a few papers [e.g., Larkin and Harrison, 2002] and in the following paragraphs, the El Niño and La Niña spatial patterns are however not strictly symmetrical. Moreover, the EOF analysis on SSS suggests that the CP ENSO signal is likely spread, at least, over the second and third EOF modes. Given these EOF limitations, an AHC analysis was performed on the low-pass filtered monthly SSS Anomaly (SSSA) maps in an attempt to better discriminate the signature of EP and CP ENSO in SSS.

[16] The AHC technique was found to be rather sensitive to the selected SSS data coverage and data processing. Hence, we show only robust clusters that appear whatever the used error thresholds (tested from 60% to 80%), spatial coverage (from 20°S–10°N to 30°S–30°N and 120°E–70°W), and low-pass filter lengths (from 13 to 25 months).

Five clusters for a total of 379 maps were identified at the top of the dendrogram tree (not shown here) using 80% as the maximum SSS error and 13 months Hanning filtered SSSA maps in the region 20°S–10°N, 120°E–70°W. As discussed below, the five clusters characterize the neutral, EP and CP El Niño and EP and CP La Niña conditions, and occur approximately 18%, 8%, 34%, 33% and 8% of the time, respectively.

[17] The cluster time series together with the cluster maps in terms of SSS are shown in Figure 5. The spatial pattern of the fourth cluster (Figure 5d) shows high positive SSS anomalies (maximum of 0.33) located mostly west of the dateline in the equatorial region and a strong freshening (maximum of 0.23) located south of the mean SPCZ position. The timing of that cluster 4 (1985–1986, 1988–1989, 1995–1996, 1999–2001, 2005–2006 and 2007–2008) indicates that this pattern characterizes the EP La Niña signal in SSS (according to SST-PC1). The spatial pattern of cluster 1 (not shown here) is somewhat similar to cluster 4 with smaller SSS anomalies, and occurs during periods when the ENSO signal is the weakest (also according to SST-PC1 and SST-PC2). Similarities between clusters 1 and 4 thus suggest that this cluster is characteristic of neutral conditions, and that the La Niña situation could be interpreted simply as an enhanced neutral situation [e.g., Meyers *et al.*, 2007]. The pattern in cluster 5 (Figure 5e) roughly shows opposite signs to the pattern in clusters 1 or 4. Its timing represents the very

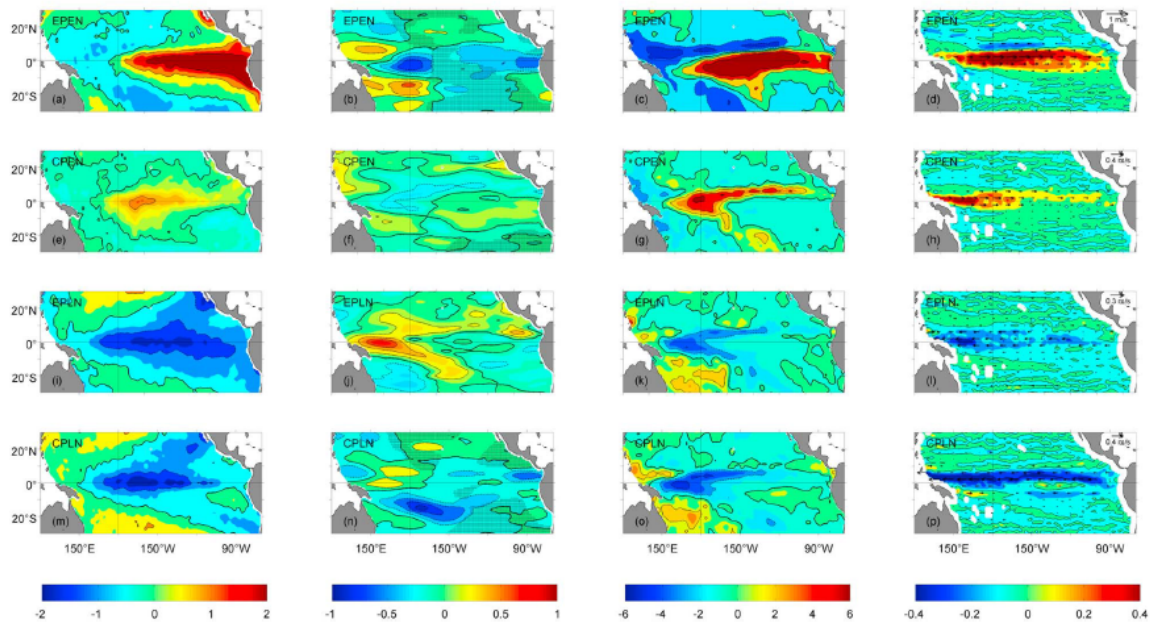


Figure 6. Three monthly DJF averages of SSTA (first column), SSSA at 3 months lag (second column), precipitation anomalies at zero lag (third column), and zonal currents anomalies at 3 months lead (fourth column) for the (a–d) 1997–1998 EP El Niño, (e–h) 2002–2003 CP El Niño, (i–l) 2007–2008 EP La Niña, and (m–p) 1998–1999 CP La Niña. The regions shaded in black in the second column denote regions where the normalized error in SSS is larger than 80%. Units are as in Figure 2.

strong 1982–1983 and 1997–1998 and strong 1991–1992 EP El Niño events, thus we conclude that this cluster extracts the EP El Niño signal. Interestingly, these three events correspond to the only El Niño events associated with the occurrence of deep atmospheric convection ($OLR < 230 \text{ W m}^{-2}$) lasting at least half a year in the central equatorial Pacific [Chiodi and Harrison, 2010]. The maximum negative SSS anomalies (0.51) for these events are centered close to the equator and the dateline, and high-salinity cores are found in the SPCZ region and north of Papua New Guinea with maximum amplitudes of 0.51 and 0.35, respectively. Cluster 3 (Figure 5c) shows negative SSS anomalies zonally oriented over the SPCZ region (maximum of 0.37) and sandwiched between two positive anomaly regions: one centered west of the dateline in the equatorial region (maximum of 0.29) and the other approximately between 30°S and 20°S (maximum of 0.21). In the equatorial region, higher salinities are confined west of $\sim 165^\circ\text{W}$ while lower salinities are evident to extend southeastward from the SPCZ region. The timing of this cluster occurs during 1983–1984 and 1998–1999, after the two very strong EP El Niños in 1982–1983 and 1997–1998 (consistent with findings by Yu *et al.* [2010b]) and before the EP La Niña events of 1985–1986 and 1999–2001, respectively, and thus this cluster represents the CP La Niña signal in SSS. A reduction in the amplitudes of the SSS anomalies is seen in cluster 2 (Figure 5b), as compared to the EP El Niño in cluster 5 (Figure 5e), especially in the SPCZ region (maximum of 0.36) and with a $\sim 15^\circ$ westward displacement of the low-salinity core in equatorial region as compared to cluster 5.

The timing of cluster 2 coincides with those of CP El Niño events in 1977–1978, 1986–1988, 1990–1991, 1992–1995, 2002–2003, 2004–2005 and 2006–2007, according to the dates of positive values of SST-PC2 or EMI in Figure 3. Interestingly, the frequency of CP El Niño (cluster 2) does not increase significantly with time during the 30 year period from 1977 to 2008 (e.g., in Figure 5a, 16% and 17% of CP El Niño events occurred in the first and second halves of that period, respectively), as could occur under global warming as suggested by Yeh *et al.* [2009] and Lee and McPhaden [2010] using SST. Note, however, that the few numbers of sampled EP and CP El Niño events prevents us to be firmly conclusive in this matter.

4.3. Representative Examples

[18] To further help reduce the possibility that the SSS patterns in Figures 4 and 5 are artificial results of the statistical EOF and AHC analyses, the two left columns in Figure 6 shows DJF (December to the following February) composites of SSTA, and MAM (March–April–May) composites for SSS anomalies for the 1997–1998 EP El Niño, 2002–2003 CP El Niño, 2007–2008 EP La Niña and 1998–1999 CP La Niña events. The 3 months SST/SSS lag has been estimated from the EOF analysis in Figures 3 and 4, as well as from a visual detection of the peak anomalies on monthly mean maps. Reassuringly, these four presented examples, as well as others not shown here, are quite consistent with the AHC analysis. The remaining subtle differences between each example and its corresponding ENSO type in the AHC analysis, however, remind us of the

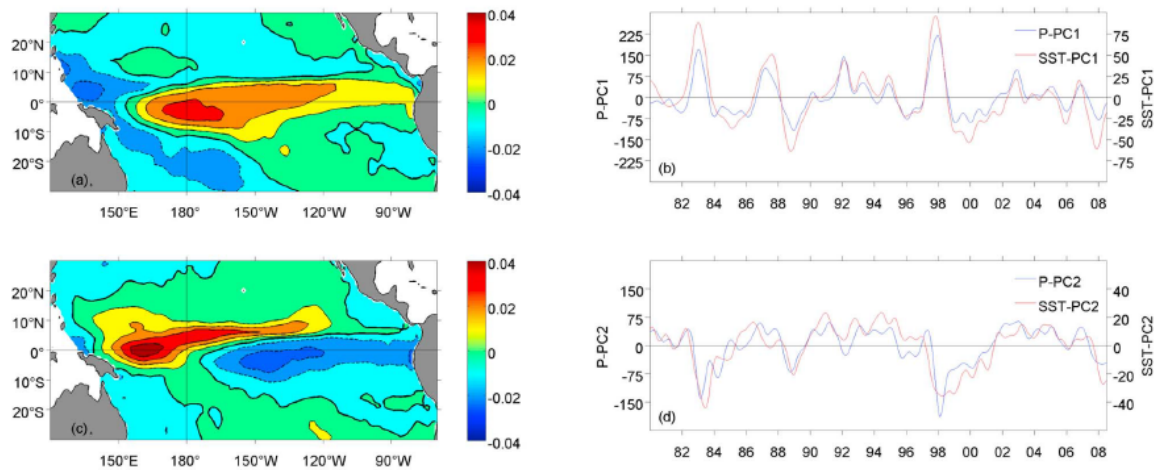


Figure 7. (a-d) Same as Figure 3 but for the precipitation anomalies. The units are defined so that the product between the spatial pattern and the corresponding time function denotes mm d^{-1} . Note the different vertical scales for the time functions. The red lines in the time functions denote SST-PC1 (in Figure 7b) and SST-PC2 (in Figure 7d), scaled on the right vertical axis.

uniqueness of each individual event, at least in terms of SST and SSS. In addition, these examples confirm, if needed, that the SST and SSS spatial patterns are not quite symmetrical during the El Niño and La Niña events (e.g., compare Figures 6a and 6i and Figures 6b and 6j).

5. Proposing Mechanisms Responsible for Contrasted ENSO-Related SSS Changes

[19] The contrasted ENSO signals observed in SSS result from the different contributions of terms involved in the salt conservation equation in the salinity mixed layer. These terms, however, cannot be quantitatively computed with confidence using observational data. Hence, as an alternative approach, this section qualitatively discusses how precipitation and zonal currents, the main two terms affecting SSS changes [e.g., *Picaut et al.*, 2001; *Gouriou and Delcroix*, 2002; *Vialard et al.*, 2002], might induce the observed contrasted signals. An EOF analysis on precipitation and zonal currents is first presented to get a general view, and we then focus on the equatorial region and SPCZ mean areas where the maximum ENSO-related SSS changes are observed. Statistical tests based on the work by *North et al.* [1982] indicate the presented EOF1 and EOF2 are well separated and are thus likely representative of real physical phenomena, as supported by the representative examples portrayed in the two right columns of Figure 6.

5.1. Precipitation and Zonal Currents Signal During ENSO

[20] The spatial patterns of P EOF1 (Figure 7a), which accounts for 39.9% of the total variance, shows positive loadings concentrated in the central equatorial Pacific region (between $\sim 170^\circ\text{E}$ and 165°W with maximum loadings of 0.037) and expanding to the east over the ITCZ region ($\sim 5^\circ\text{N}$). Negative loadings can be found in the far western equatorial Pacific (maximum of 0.025) and extending

southeastward over the SPCZ region. The spatial pattern for P EOF2 (Figure 7c), showing 22.8% of the total variance, illustrates that the positive maximum loadings (0.046) in the equatorial region tend to be west of the dateline and $\sim 15^\circ$ – 20° of longitude westward of the positive maximum loadings found in P EOF1. However, the tendency for the positive loadings to appear north of the equator still remains. Noteworthy, the negative loadings that were present over the SPCZ region in P EOF1 have disappeared in P EOF2. Negative loadings (maximum of 0.026) are found east of the dateline extending toward the South American coast along the equatorial region. The principal components of P EOF1 (P-PC1) and P EOF2 (P-PC2) show high positive correlations of $R = 0.94$ and $R = 0.82$ with SST-PC1 (at zero lag) and SST-PC2 (with P-PC2 leading by 1 month), respectively. This implies that the two P EOFs represent the EP and CP ENSO signals, respectively, with positive loadings in Figures 7a and 7c denoting enhanced precipitation during EP and CP El Niño events. As also noticed by *Larkin and Harrison* [2005b], the precipitation signature of EP and CP El Niño can thus be dramatically different for Pacific countries, especially in the southwestern tropical region where precipitation changes are much smaller during CP events, and in the central and eastern equatorial region where they are of opposite signs. Consistent results were derived by computing correlation coefficients between precipitation changes versus the principle components of the SST EOFs [*Kao and Yu*, 2009], and by making composites of individual events [*Kug et al.*, 2009] (also shown here in Figure 6).

[21] The time functions and spatial patterns of U EOF1 and U EOF2, which account for 48.6% and 11.4% of the variance, respectively, are shown in Figure 8 (recall that the zonal currents time series start in 1992 only). As was found above for precipitation, there are high correlations of U-PC1 and U-PC2 with SST-PC1 ($R = 0.80$; U-PC1 leading by

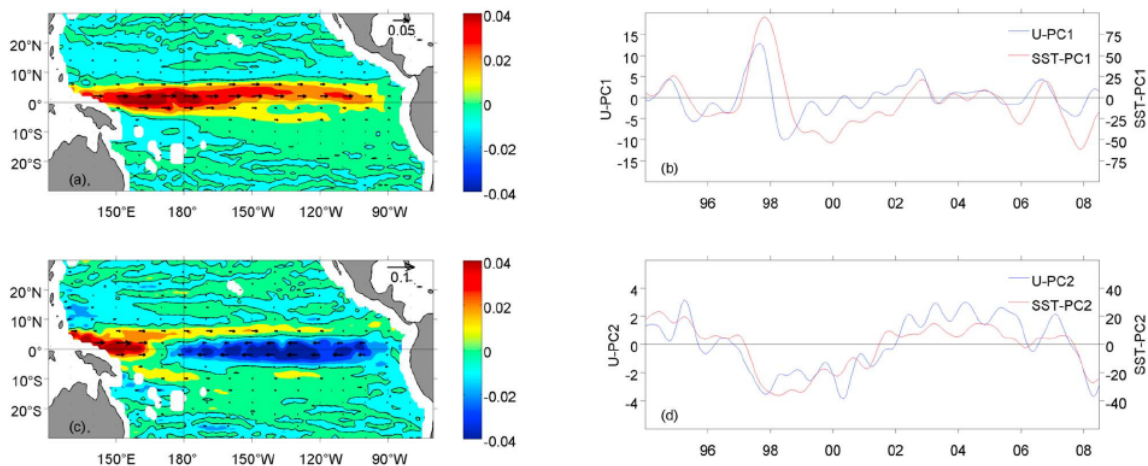


Figure 8. (a–d) Same as Figure 3 but for the surface zonal current anomalies. The units are defined so that the product between the spatial pattern and the corresponding time function denotes m s^{-1} , and positive values represent eastward current anomalies. The red lines in the time functions denote SST-PC1 (in Figure 8b) and SST-PC2 (in Figure 8d), scaled on the right vertical axis.

4 months) and SST-PC2 ($R = 0.87$; SST-PC2 leading by 1 month), respectively. This indicates that U EOF1 and U EOF2 are representative of the EP and CP ENSO signals, correspondingly. During EP El Niño, eastward current anomalies dominate most of the equatorial region, with a tendency for the maximum amplitudes to appear slightly north of the equator east of $\sim 160^\circ\text{W}$. During CP El Niño, the eastward anomalies over the far western equatorial Pacific region remain with maximum loadings greater than 0.050 (as in U EOF1). There is, however, a reversal of the current anomalies east of about 160°E – 170°E in the equatorial region (with maximum negative loadings of 0.046) so that the U EOF2 resembles the mean zonal currents field (Figure 2d). Such a reversal is crucial as it means a convergence of surface current anomalies near 175°E favoring the confinement of the warm and fresh pool in the western central basin as observed during CP El Niño [see also Kug *et al.*, 2009, Figure 9] (also shown here in Figure 6h). Away from the equatorial band, small eastward current anomalies tend to dominate in the NECC and over the entire south Pacific region.

[22] Generally, in the equatorial band, the EOF analysis suggests that for the EP El Niño (cluster 5 in Figure 5e), eastward equatorial zonal current anomalies bring in low-salinity waters from the far western equatorial Pacific into the central equatorial region. This combined with the high precipitation anomaly east of about 150°E , further lowers the salinity in this region, consistent with the findings of Delcroix and Picaut [1998]. For the CP El Niño (cluster 2 in Figure 5b), the low-salinity waters in the far western equatorial Pacific are consistent in space with the reduced zonal extension of anomalous eastward zonal currents and high precipitation. Similarly, the westward zonal current anomalies and rainfall deficit east of the dateline are in agreement with the higher salinity found in the region. In the SPCZ region, the precipitation deficit combined with the

hint for small westward current anomalies in the western Pacific (due to the northeastward displacement of the SPCZ; see section 5.3) results in increased salinity during EP El Niño, as found by Gouriou and Delcroix [2002]. In contrast, weaker precipitation deficit and eastward current anomalies tend to dominate the entire Pacific region south of about 8°S during CP El Niño. As a result, higher than average salinity waters remain as during EP El Niño but with reduced magnitude due to the SPCZ position near its normal position (see section 5.3).

5.2. SSS Changes in the Equatorial Region

[23] In addition to the above EOF analyses, Figure 9 illustrates the tight relationships between the 2°S – 2°N averaged SSS, precipitation and zonal currents over their respective measurement periods. The zonal displacements of the eastern edge of the warm pool, characterized by the 34.8 isohaline positions, agree well with both the zonal current direction and heavy precipitation location, corroborating earlier results obtained for different time periods [Delcroix and Picaut, 1998; Picaut *et al.*, 1996, 2001]. As expected from U EOF, Figure 9 also indicates that eastward current anomalies extend further to the east during the EP (1997–1998) than during the CP El Niño events (1992–1995, 2002–2003, 2004–2005 and 2006–2007), with CP El Niño events showing a current convergence in the western central basin.

[24] The 2°S – 2°N averaged positions of the 34.8 isohaline for eleven El Niño and nine La Niña events of the years 1977–2008 are compared in Figures 10a and 10b, respectively. The mean position of the 34.8 isohaline (heavy black line) reaches its maximum eastward position (MEP) of $\sim 175^\circ\text{W}$ during November of the El Niño year, and its maximum westward position (MWP) of $\sim 155^\circ\text{E}$ during May of the La Niña year. During the EP El Niños, the MEP of the 34.8 isohaline is further east of the mean position. In con-

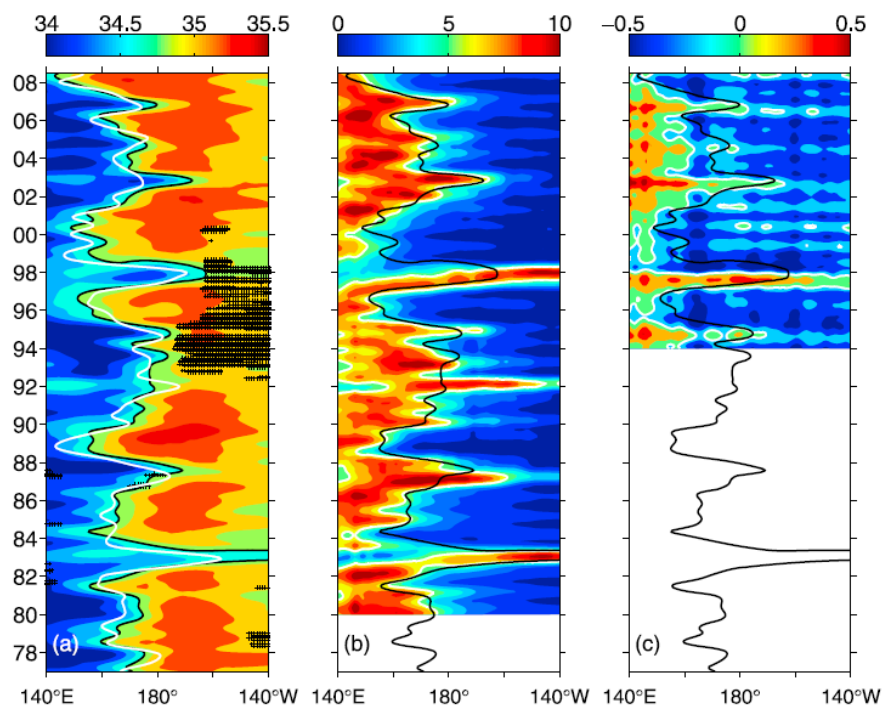


Figure 9. Time-longitude distribution of 2°S–2°N averaged (a) SSS, (b) precipitation, and (c) zonal currents showing the 34.8 isohaline position in continuous black, and overlaid in white are the SOI (in Figure 9a), 6 mm d⁻¹ isohyet (in Figure 9b), and 0 m s⁻¹ isotack (in Figure 9c).

trast, during CP El Niño, the MEP of the 34.8 isohaline lies west of the mean isohaline position. It is interesting to note that the timing of the MEP of the 34.8 isohaline generally occurs before the peak of the mean isohaline position during CP El Niño's in contrast to the EP El Niño's. The CP La

Niña events generally peak before the EP La Niña events. In general, CP ENSO events peak earlier than EP ENSO events while the MEP (MWP) of the 34.8 isohaline show greater displacements from the mean isohaline position during EP rather than during CP El Niño (La Niña) events.

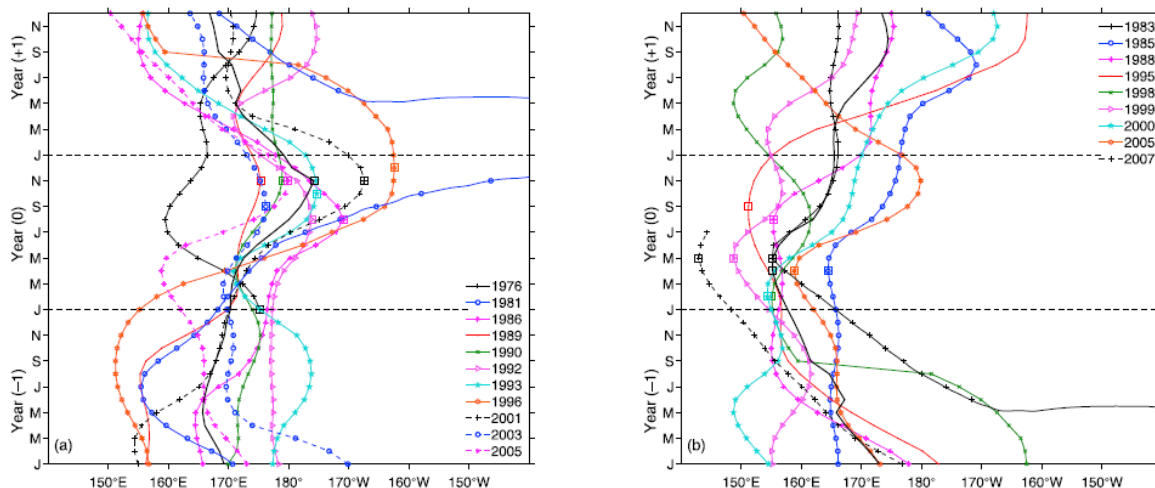


Figure 10. Zonal displacements of the 2°S–2°N averaged 34.8 isohaline position during (a) eleven El Niño events and (b) nine La Niña events. Year (0) represents the year of the peak El Niño/La Niña, and Year (-1) and Year (1) represent the year before and after, respectively. The years indicated in the legend correspond to Year (-1). The heavy black line shows the mean isohaline position for the eleven El Niño events in Figure 10a and nine La Niña events in Figure 10b.

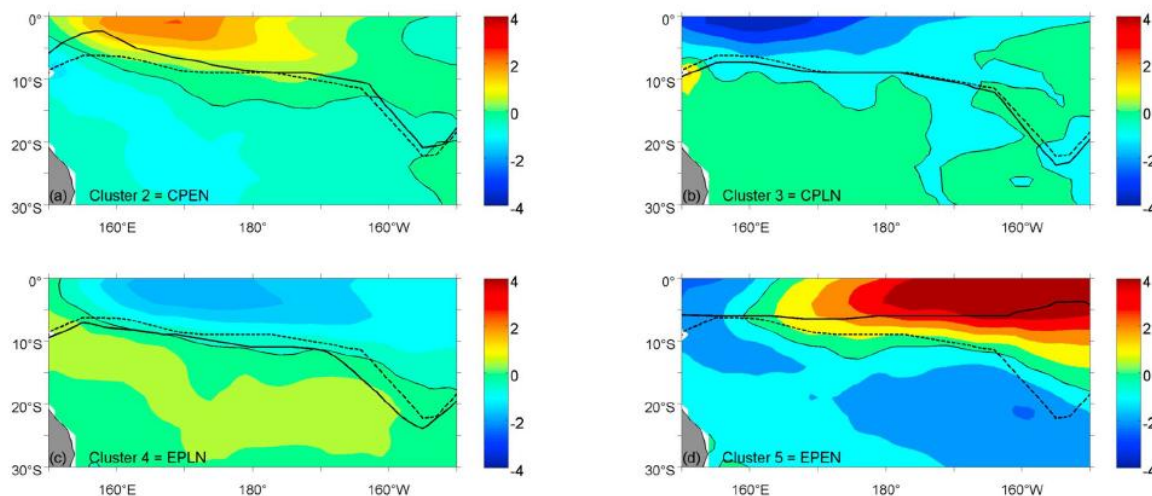


Figure 11. The spatial structures of the precipitation anomalies extracted from the SSS cluster time series in Figure 5 with precipitation leading by 3 months, (a) with cluster 2 showing CP El Niño conditions, (b) cluster 3 showing CP La Niña conditions, (c) cluster 4 showing EP La Niña conditions, and (d) cluster 5 showing EP El Niño conditions. Superimposed are the mean SPCZ positions estimating from precipitation data for the entire data length (dashed black line) and during the respective cluster timing (continuous black line).

5.3. SSS Changes in the SPCZ Region

[25] The correlation between EOF1 principal components of SSS and precipitation is maximum when precipitation is leading SSS by 3 months. Using this lag, we extracted the precipitation signal from the SSS cluster time series (Figure 5) for each cluster from 1980 to 2008 and averaged it (as was done to obtain the SSS clusters) for the southwestern

tropical region (0° – 30° S, 150° E– 150° W). The mean position of the SPCZ for each cluster was then calculated by averaging the position of maximum precipitation for each map that makes up the cluster. The mean SPCZ position over the entire time series was calculated in a similar way. The resulting precipitation patterns corresponding to the SSS clusters are shown in Figure 11, together with the mean

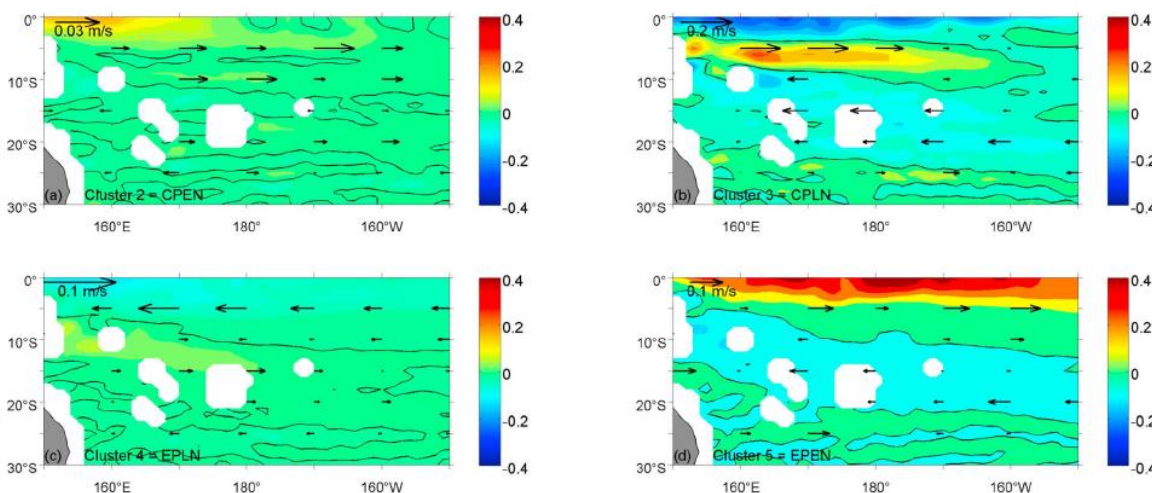


Figure 12. The spatial structures of the zonal currents anomalies extracted from the SSS cluster time series in Figure 5 with zonal currents leading by 7 months, with (a) cluster 2 showing CP El Niño conditions, (b) cluster 3 showing CP La Niña conditions, (c) cluster 4 showing EP La Niña conditions, and (d) cluster 5 showing EP El Niño conditions. Note the different scales for the zonal currents arrows: 0.03 m s^{-1} in Figure 12a, 0.2 m s^{-1} in Figure 12b, and 0.1 m s^{-1} in Figures 12c and 12d. Positive values denote eastward current anomalies.

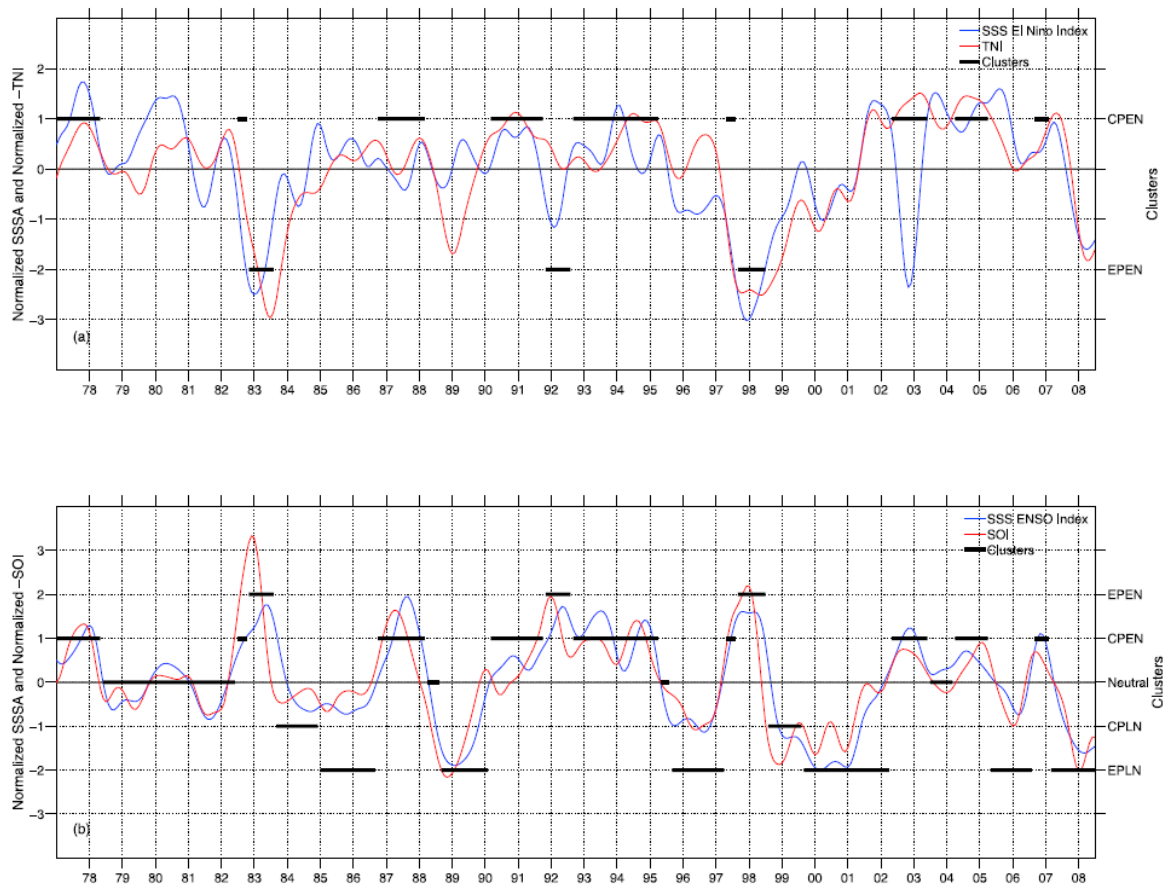


Figure 13. Time series of (a) the SSS El Niño Index and (b) the SSS ENSO Index in blue with the 13 months Hanning filtered SOI and TNI superimposed in red (in Figures 13a and 13b, respectively), and the timing of the SSS clusters in black (see Figure 5). See section 5.4 for the definition of both indices.

SPCZ positions over the entire data length and for each cluster.

[26] The La Niña signal (Figures 11b and 11c) is consistent with the SSSA pattern (Figures 5c and 5d) with negative correlations, respectively, north and south of the SPCZ position. The pattern is reversed during CP and EP El Niño as can be seen in Figures 11a and 11d, respectively. Noteworthy, the SPCZ position does not move as far to the north during CP El Niño as during EP El Niño and, as expected from the derived precipitation changes, the positive SSS anomalies are reduced in magnitude.

[27] The SPCZ position found above is similar to findings by Vincent [1994], Folland *et al.* [2002] and Gouriou and Delcroix [2002], but only for EP El Niño and La Niña events. Recently, Vincent *et al.* [2009] further characterized the SPCZ position into four different structures using three monthly austral summer precipitation composites over the 1979–2002 period. We reinforce their work by obtaining similar results for the SPCZ position but further stress that this is strongly characterized by the different SSSA structures during EP and CP El Niño and La Niña.

[28] As was done with the precipitation anomalies, the zonal currents anomalies in the SPCZ region were also extracted from the SSS cluster time series with zonal currents leading SSS by 7 months (based on the EOF principal components in SSS and zonal current); the results are shown in Figure 12. In general, the zonal currents anomalies complement the precipitation anomalies (Figure 11) in explaining the SSS signal (Figures 5b–5d) in the SPCZ region with eastward (westward) zonal currents anomalies bringing in fresher (saltier) waters from the southwestern (eastern) tropical Pacific (see the mean SSS structure in Figure 2b).

5.4. Defining ENSO Metrics With SSS

[29] The EOF and AHC procedures indicate that the main difference during EP and CP ENSO is the appearance of contrasted SSS patterns in the equatorial part of the warm pool and along the mean SPCZ position. Because of this we identify three regions in the western half of the tropical Pacific: the first region (A) is delimited between 2°S – 2°N and 150°E – 170°E , the second (B) between 2°S – 2°N and 170°E – 170°W and the third (C) between 160°E – 160°W and

25°S–10°S. The normalized difference (B-A) between the normalized average SSSA in the first two regions results in an index (Figure 13a), henceforth called the SSS El Niño Index, which is fairly able to distinguish EP El Niño events from CP El Niño events (except in 2003). In fact it has a high negative correlation of $R = -0.7$ with the TNI (defined as the normalized difference between the normalized SST anomalies averaged in the Niño-1+2 and Niño-4 regions) lagging by 2 months. In addition, because the SSS signature in the SPCZ area is also different during El Niño and La Niña episodes, the normalized difference (C-(A+B)) between the normalized average SSSA in the third (SPCZ) region and the sum of the normalized average SSSA in the first two (equatorial) regions (Figure 13b), hereafter called the SSS ENSO Index, allows us to discriminate between El Niño (positive anomalies) and La Niña (negative anomalies) events, in agreement with the WMO definition in Figure 1. Actually, it has a high correlation of $R = -0.88$ with the SOI leading by 2 months. Moreover, both indices correspond fairly well with the SSS cluster time series in Figure 5, suggesting that the SSS El Niño Index (SSS ENSO Index) could also be used as an indicator for EP and CP El Niño (and La Niña) events.

6. Conclusion and Discussion

[30] The analyses of resemblances and dissimilarities between ENSO events are both important for improving the understanding of ENSO physics, predicting regional and global climate impacts, and estimating the effects of global warming on ENSO features. Accordingly, both ENSO similarities and differences have been analyzed in the last three decades, probably starting from the milestone papers of Wyrski [1975] and Rasmusson and Carpenter [1982]. As stated 35 years ago by K. Wyrski: “no two El Niño events are quite alike.” Since then, numerous results have pointed out the many dissimilarities of ENSO events [e.g., Wang, 1995], including the recent detection of a new type of El Niño variously called Dateline, Warm Pool, central Pacific or El Niño Modoki events [Harrison and Larkin, 1998; Larkin and Harrison, 2005a, 2005b; Ashok et al., 2007; Kao and Yu, 2009; Kug et al., 2009]. In line with this, the aim of this paper was to contrast ENSO features in the tropical Pacific, for the first time using SSS observations, as collected during 1977–2008.

[31] Using EOF and AHC analyses on SSS, and comparing with ENSO-related SST features, we showed that the eastern Pacific (EP) El Niño events in SSS appear in 1982–1983, 1991–1992, and 1997–1998, the central Pacific (CP) El Niño events in 1977–1978, 1986–1988, 1990–1991, 1992–1995, 2002–2003, 2004–2005 and 2006–2007, the EP La Niña events in 1985–1986, 1988–1989, 1995–1996, 1999–2001, 2005–2006 and 2007–2008, and the CP La Niña events in 1983–1984 and 1998–1999. It should be noted, however, that clearly differentiating the two EP and CP El Niño and La Niña flavors is a difficult exercise, depending on the method used (see Figure 1), and noting that some years may even be classified as “mixed” events [e.g., Kug et al., 2009, Figure 1]. In general, EP and CP El Niño (La Niña) events result in a SSS freshening (saltening) in the western half of the equatorial Pacific and a SSS increase (decrease) in the SPCZ mean area. The EP and CP

El Niño events, however, have distinct quantitative SSS signatures. In the equatorial Pacific (say 2°S–2°N), EP El Niño events are characterized by a maximum SSS freshening (~ -1) near the dateline and a strong ($\sim 30^\circ$ longitude) eastward displacements of the 34.8 isohaline materializing the eastern edge of the low-salinity warm pool waters. During CP El Niño events, the maximum SSS freshening is shifted westward by about 15° longitude and the eastward displacements of the 34.8 isohaline are only about half the EP El Niño amplitude. Kug et al. [2009] found similar differences between Warm Pool and Cold Tongue El Niños (analogous to our CP and EP El Niño) in terms of SST, precipitation, atmospheric vertical motion and surface zonal wind anomalies: the anomalies are shifted to the west during Warm Pool El Niño compared to those associated with the Cold Tongue El Niño. This results in rather homogeneous SSS within 150°E–170°W during EP El Niño events, contrasting with nonhomogeneous SSS between the western (150°E–170°E) and eastern (170°E–170°W) halves of the warm pool during CP El Niño events (with the western half being ~ 0.2 fresher). In the far western equatorial Pacific, results are also contrasted: EP El Niño result in a saltening, whereas CP El Niño in a freshening of the surface waters. Besides, in the SPCZ mean area, EP El Niño events are characterized by a well-marked increase ($\sim +1$) in SSS, which is about 2–3 times less during CP El Niño events. As a practical application, we showed that computing SSS differences between the western and eastern parts of equatorial part of the warm pool, as well as between the warm pool and the SPCZ mean areas, which we define as the SSS El Niño and SSS ENSO Indices, could be used as possible indicators of (EP and CP) El Niño and La Niña events, potentially enriching the list of simple ENSO metrics to benchmark climate model skills.

[32] A qualitative analysis of the two main terms of the SSS balance strongly suggests that zonal advection by surface currents and precipitation changes are the main mechanisms responsible for the ENSO signatures in SSS. In the equatorial band, the zonal displacements of the eastern edge of the warm pool (i.e., the 34.8 isohaline) are remarkably consistent with the zonal current anomalies, as demonstrated earlier (see Picaut et al. [2001] for a review). Notable differences in zonal currents, however, show up between EP and CP El Niño events. During EP El Niño events, eastward current anomalies appear chiefly from the western to the central eastern equatorial Pacific, consistently with the strong eastward displacements of low-salinity warm pool waters. In contrast, during CP El Niño events, there is a tendency to have a zonal current convergence slightly west of the dateline, consistent with the reduced eastward displacements and, more generally, with the confinement of the warm/fresh pool in the central Pacific basin. The strong eastward displacements of the warm/fresh pool in the equatorial band during EP El Niño events lead to an important northeastward shift of the SPCZ ($\sim 5^\circ$ – 7° latitude for the eastern part) which induces rainfall deficit and related SSS increase at the mean SPCZ position. In contrast, the central Pacific confinement of the warm/fresh pool during CP El Niño events yields to small ($\sim 1^\circ$ – 2° latitude) equatorward shifts of the SPCZ and to moderate SSS increase at the mean SPCZ position.

[33] It has been suggested by *Kao and Yu* [2009] that EP ENSO fits well with the evolution described by the delayed oscillator theory of ENSO, while it is likely that local atmospheric forcing is important to CP ENSO. Accordingly, *Yu et al.* [2010a] showed that their Type 1 SST variability (analogous to our EP El Niño) in the central Pacific results from the zonal advection of thermocline-controlled SST variations from the eastern equatorial Pacific whereas their Type 2 variability (analogous to our CP El Niño) is linked to the northeastern subtropics through surface wind forcing and associated atmosphere–ocean heat fluxes (primarily the latent heat flux) and surface ocean advection. As discussed above, our analysis of SSS changes in the equatorial band during ENSO also suggests that one of the main SSS differences between EP and CP El Niño events result from the different roles of zonal current anomalies, in particular with the zonal currents anomalies favoring the warm pool confinement in the central Pacific during CP El Niño events. The question then remains as to why zonal currents differ so drastically between EP and CP events? One possibility that first comes to mind is the wind stress forcing. As noted by *Kao and Yu* [2009], westerly wind anomalies covered a large part of the tropical Pacific during EP El Niño events, whereas they are limited to its western central part during CP El Niño events. Both instances of westerly anomalies are located west of the maximum related warm SST anomalies, in close agreement with a Gill-type model. Further studies should be carried out to differentiate these coupling processes. Another possibility is that the barrier layer (BL) may be responsible for the different zonal currents anomalies. Model results have shown that its existence in the equatorial part of the warm pool may affect zonal currents [*Vialard et al.*, 2002] and/or ENSO development [*Maes et al.*, 2006]. Previous studies actually suggest a tendency for a thick BL to be associated with the two EP El Niño events in 1991–1992 and 1997–1998, noting that we cannot conclude for the third EP El Niño event in 1982–1983 given the poor data density at that time [*Ando and McPhaden*, 1997; *Maes and Behringer*, 2000; *Vialard et al.*, 2002; *Bosc et al.*, 2009]. Yet, another possibility for the different zonal currents anomalies is the role of equatorial waves. As discussed in previous papers [e.g., *Delcroix and Picaut*, 1998; *Picaut and Delcroix*, 1995], the zonal displacements of the eastern edge of the warm/fresh pool chiefly result from the combined effects of wind-forced and reflected first baroclinic equatorial Kelvin and first meridional mode Rossby waves. The confinement of the warm/fresh pool in the central Pacific basin during CP El Niño events should thus necessarily reflect a specific combination of these waves.

[34] Another interesting question is to what extent changes in the number and amplitude of ENSO events, as well as the respective occurrence of EP and CP events, might contribute to long-term SSS trends, as discussed by *Compo and Sardeshmukh* [2010] and *Lee and McPhaden* [2010] for SST. We showed above from *detrended* SSS time series that CP, as compared to EP El Niño events, are characterized by an increased freshening in the far western equatorial Pacific and a reduced saltening in the SPCZ mean area. Taken as a whole, this can be viewed as a relative freshening of the western half of the tropical Pacific. Hence, assuming that the frequency of CP events will increase with global warming [*Yeh et al.*, 2009], we would thus observe an ENSO-related

enhancement of the long-term freshening trends observed in the western half of the tropical Pacific [*Delcroix et al.*, 2007; *Cravatte et al.*, 2009]. Caution will thus be required to properly discriminate natural (ENSO) from anthropogenic (trend) climate changes in long-term SSS records: a generic question in today's climate research.

[35] **Acknowledgments.** This work is a contribution to the GLOSCAL ESA/SMOS proposal supported by CNES. We benefited from numerous observed data sets made freely available, and those which are used in this manuscript include the Hadley Centre Sea Ice and Sea Surface Temperature (<http://www.metoffice.gov.uk/hadobs/hadisst/>), French Sea Surface Salinity Observation Service (<http://www.legos.obs-mip.fr/en/observations/sss/>), Global Precipitation Climatology Project (<http://www.esr.noaa.gov/psd/data/gridded/data.gpcp.html>), Southern Oscillation Index (<http://www.cpc.ncep.noaa.gov/data/indices/soi/>), El Niño Modoki Index (http://www.jamstec.go.jp/frcgc/research/d1/iod/modoki_home.html), Trans-Niño Index (http://www.cgd.ucar.edu/cas/catalog/climind/TNI_N34/index.html), and Ocean Surface Current Analyses-Real time (<http://www.oscar.noaa.gov/datadisply/>) data sets. One of us (A.S.) benefits from a Ph.D. grant from the Institut de Recherche pour le Développement (IRD). We also thank the three anonymous reviewers for their constructive comments.

References

- Ando, K., and M. J. McPhaden (1997), Variability of surface layer hydrography in the tropical Pacific, *J. Geophys. Res.*, *102*(C10), 23,063–23,078, doi:10.1029/97JC01443.
- Ashok, K., S. K. Behera, S. A. Rao, H. Weng, and T. Yamagata (2007), El Niño Modoki and its possible teleconnection, *J. Geophys. Res.*, *112*, C11007, doi:10.1029/2006JC003798.
- Ashok, K., S. Izuka, S. A. Rao, N. H. Saji, and W.-J. Lee (2009a), Processes and boreal summer impacts of the 2004 El Niño Modoki: An AGCM study, *Geophys. Res. Lett.*, *36*, L04703, doi:10.1029/2008GL036313.
- Ashok, K., C.-Y. Tam, and W.-J. Lee (2009b), ENSO Modoki impact on the Southern Hemisphere storm track activity during extended austral winter, *Geophys. Res. Lett.*, *36*, L12705, doi:10.1029/2009GL038847.
- Barber, C. B., D. P. Dobkin, and H. Huhdanpaa (1996), The quickhull algorithm for convex hulls, *Trans. Math. Software*, *22*(4), 469–483, doi:10.1145/235815.235821.
- Bonjean, F., and G. S. E. Lagerloef (2002), Diagnostic model and analysis of the surface currents in the tropical Pacific Ocean, *J. Phys. Oceanogr.*, *32*(10), 2938–2954, doi:10.1175/1520-0485(2002)032<2938:DMAAOT>2.0.CO;2.
- Bosc, C., and T. Delcroix (2008), Observed equatorial Rossby waves and ENSO-related warm water volume changes in the equatorial Pacific Ocean, *J. Geophys. Res.*, *113*, C06003, doi:10.1029/2007JC004613.
- Bosc, C., T. Delcroix, and C. Maes (2009), Barrier layer variability in the western Pacific warm pool from 2000 to 2007, *J. Geophys. Res.*, *114*, C06023, doi:10.1029/2008JC005187.
- Cai, W., and T. Cowan (2009), La Niña Modoki impacts Australia autumn rainfall variability, *Geophys. Res. Lett.*, *36*, L12805, doi:10.1029/2009GL037885.
- Chen, G., and C.-Y. Tam (2010), Different impacts of two kinds of Pacific Ocean warming on tropical cyclone frequency over the western North Pacific, *Geophys. Res. Lett.*, *37*, L01803, doi:10.1029/2009GL041708.
- Chiodi, A. M., and D. E. Harrison (2010), Characterizing warm-ENSO variability in the equatorial Pacific: An OLR perspective, *J. Clim.*, *23*(9), 2428–2439, doi:10.1175/2009JCLI3030.1.
- Compo, G. P., and P. D. Sardeshmukh (2010), Removing ENSO-related variations from the climate record, *J. Clim.*, *23*(8), 1957–1978, doi:10.1175/2009JCLI2735.1.
- Cravatte, S., T. Delcroix, D. Zhang, M. McPhaden, and J. Leloup (2009), Observed freshening and warming of the western Pacific warm pool, *Clim. Dyn.*, *33*(4), 565–589, doi:10.1007/s00382-009-0526-7.
- Delcroix, T. (1998), Observed surface oceanic and atmospheric variability in the tropical Pacific at seasonal and ENSO timescales: A tentative overview, *J. Geophys. Res.*, *103*(C9), 18,611–18,633, doi:10.1029/98JC00814.
- Delcroix, T., and J. Picaut (1998), Zonal displacement of the western equatorial Pacific “fresh pool,” *J. Geophys. Res.*, *103*(C1), 1087–1098, doi:10.1029/97JC01912.
- Delcroix, T., S. Cravatte, and M. J. McPhaden (2007), Decadal variations and trends in tropical Pacific sea surface salinity since 1970, *J. Geophys. Res.*, *112*, C03012, doi:10.1029/2006JC003801.

- Delcroix, T., G. Alory, S. Cravatte, T. Corrège, and M. McPhaden (2011), A gridded sea surface salinity data set for the tropical Pacific with sample applications (1950–2008), *Deep Sea Res., Part 1*, 58(1), 38–48, doi:10.1016/j.dsr.2010.11.002.
- Deser, C., and J. M. Wallace (1987), El Niño events and their relation to the Southern Oscillation: 1925–1986, *J. Geophys. Res.*, 92(C13), 14,189–14,196, doi:10.1029/JC092iC13p14189.
- Emery, W. J., and R. E. Thomson (2001), *Data Analysis Methods in Physical Oceanography*, 2nd ed., Elsevier Sci., Amsterdam.
- Folland, C. K., J. A. Renwick, M. J. Salinger, and A. B. Mullan (2002), Relative influences of the Interdecadal Pacific Oscillation and ENSO on the South Pacific Convergence Zone, *Geophys. Res. Lett.*, 29(13), 1643, doi:10.1029/2001GL014201.
- Glantz, M. H., R. W. Katz, and N. Nicholls (1991), *Teleconnections Linking Worldwide Climate Anomalies*, Cambridge Univ. Press, Cambridge, U. K.
- Global Climate Observing System (2004), Implementation plan for the global observing system for climate in support of the UNFCCC: Executive summary, *Rep. GCOS-92(ES)*, 29 pp., World Meteorol. Organ., Geneva, Switzerland.
- Goddard, L., and M. Dillely (2005), El Niño: Catastrophe or opportunity, *J. Clim.*, 18(5), 651–665, doi:10.1175/JCLI-3277.1.
- Gouriou, Y., and T. Delcroix (2002), Seasonal and ENSO variations of sea surface salinity and temperature in the South Pacific Convergence Zone during 1976–2000, *J. Geophys. Res.*, 107(C12), 3185, doi:10.1029/2001JC000830.
- Hanley, D. E., M. A. Bourassa, J. J. O'Brien, S. R. Smith, and E. R. Spade (2003), A quantitative evaluation of ENSO indices, *J. Clim.*, 16(8), 1249–1258, doi:10.1175/1520-0442(2003)16<1249:AQEOEI>2.0.CO;2.
- Harrison, D. E., and N. K. Larkin (1998), El Niño–Southern Oscillation sea surface temperature and wind anomalies, 1946–1993, *Rev. Geophys.*, 36(3), 353–399, doi:10.1029/98RG00715.
- Hendon, H. H., E. Lim, G. Wang, O. Alves, and D. Hudson (2009), Prospects for predicting two flavors of El Niño, *Geophys. Res. Lett.*, 36, L19713, doi:10.1029/2009GL040100.
- Huffman, G. J., R. F. Adler, D. T. Bolvin, and G. Gu (2009), Improving the global precipitation record: GPCP Version 2.1, *Geophys. Res. Lett.*, 36, L17808, doi:10.1029/2009GL040000.
- Janowiak, J. E., A. Gruber, C. R. Kondragunta, R. E. Livezey, and G. J. Huffman (1998), A comparison of the NCEP–NCAR reanalysis precipitation and the GPCP rain gauge–satellite combined dataset with observational error considerations, *J. Clim.*, 11(11), 2960–2979, doi:10.1175/1520-0442(1998)11<2960:ACOTNN>2.0.CO;2.
- Jin, F.-F., J. D. Neelin, and M. Ghil (1994), El Niño on the Devil's Staircase: Annual subharmonic steps to chaos, *Science*, 264(5155), 70–72, doi:10.1126/science.264.5155.70.
- Kalnay, E., et al. (1996), The NCEP/NCAR 40-year reanalysis project, *Bull. Am. Meteorol. Soc.*, 77(3), 437–471, doi:10.1175/1520-0477(1996)077<0437:TNYRP>2.0.CO;2.
- Kao, H.-Y., and J.-Y. Yu (2009), Contrasting eastern-Pacific and central-Pacific types of ENSO, *J. Clim.*, 22(3), 615–632, doi:10.1175/2008JCLI2309.1.
- Kaplan, A., M. A. Cane, Y. Kushnir, A. C. Clement, M. B. Blumenthal, and B. Rajagopalan (1998), Analyses of global sea surface temperature 1856–1991, *J. Geophys. Res.*, 103(C9), 18,567–18,589, doi:10.1029/97JC01736.
- Kim, H.-M., P. J. Webster, and J. A. Curry (2009), Impact of shifting patterns of Pacific Ocean warming on North Atlantic tropical cyclones, *Science*, 325(5936), 77–80, doi:10.1126/science.1174062.
- Kohonen, T. (1989), *Self-Organization and Associative Memory*, 3rd ed., Springer, New York.
- Kug, J.-S., F.-F. Jin, and S.-I. An (2009), Two types of El Niño events: Cold tongue El Niño and warm pool El Niño, *J. Clim.*, 22(6), 1499–1515, doi:10.1175/2008JCLI2624.1.
- Lagerloef, G., et al. (2008), The Aquarius/SAC-D mission: Designed to meet the salinity remote-sensing challenge, *Oceanography*, 21(1), 68–81.
- Larkin, N. K., and D. E. Harrison (2002), ENSO warm (El Niño) and cold (La Niña) event life cycles: Ocean surface anomaly patterns, their symmetries, asymmetries, and implications, *J. Clim.*, 15(10), 1118–1140, doi:10.1175/1520-0442(2002)015<1118:EWENOA>2.0.CO;2.
- Larkin, N. K., and D. E. Harrison (2005a), Global seasonal temperature and precipitation anomalies during El Niño autumn and winter, *Geophys. Res. Lett.*, 32, L16705, doi:10.1029/2005GL022860.
- Larkin, N. K., and D. E. Harrison (2005b), On the definition of El Niño and associated seasonal average U.S. weather anomalies, *Geophys. Res. Lett.*, 32, L13705, doi:10.1029/2005GL022738.
- Lee, T., and M. J. McPhaden (2010), Increasing intensity of El Niño in the central-equatorial Pacific, *Geophys. Res. Lett.*, 37, L14603, doi:10.1029/2010GL044007.
- Leloup, J. A., Z. Lachkar, J.-P. Boulanger, and S. Thiria (2007), Detecting decadal changes in ENSO using neural networks, *Clim. Dyn.*, 28, 147–162, doi:10.1007/s00382-006-0173-1.
- Maes, C., and D. Behringer (2000), Using satellite-derived sea level and temperature profiles for determining the salinity variability: A new approach, *J. Geophys. Res.*, 105(C4), 8537–8547, doi:10.1029/1999JC900279.
- Maes, C., K. Ando, T. Delcroix, W. S. Kessler, M. J. McPhaden, and D. Roemmich (2006), Observed correlation of surface salinity, temperature and barrier layer at the eastern edge of the western Pacific warm pool, *Geophys. Res. Lett.*, 33, L06601, doi:10.1029/2005GL024772.
- McPhaden, M. J., and X. Zhang (2009), Asymmetry in zonal phase propagation of ENSO sea surface temperature anomalies, *Geophys. Res. Lett.*, 36, L13703, doi:10.1029/2009GL038774.
- McPhaden, M. J., S. E. Zebiak, and M. H. Glantz (2006), ENSO as an integrating concept in Earth science, *Science*, 314(5806), 1740–1745, doi:10.1126/science.1132588.
- Meyers, G., P. McIntosh, L. Pigot, and M. Pook (2007), The years of El Niño, La Niña, and interactions with the tropical Indian Ocean, *J. Clim.*, 20(13), 2872–2880, doi:10.1175/JCLI4152.1.
- North, G. R., T. L. Bell, R. F. Cahalan, and F. J. Moeng (1982), Sampling errors in the estimation of empirical orthogonal functions, *Mon. Weather Rev.*, 110(7), 699–706, doi:10.1175/1520-0493(1982)110<0699:SEITEO>2.0.CO;2.
- Palmer, T. N., and D. A. Mansfield (1984), Response of two atmospheric general circulation models to sea-surface temperature anomalies in the tropical east and west Pacific, *Nature*, 310, 483–485, doi:10.1038/310483a0.
- Picaut, J., and T. Delcroix (1995), Equatorial wave sequence associated with warm pool displacements during the 1986–1989 El Niño–La Niña, *J. Geophys. Res.*, 100(C9), 18,393–18,408, doi:10.1029/95JC01358.
- Picaut, J., M. Ioualalen, C. Menkes, T. Delcroix, and M. J. McPhaden (1996), Mechanism of the zonal displacements of the Pacific warm pool: Implications for ENSO, *Science*, 274(5292), 1486–1489, doi:10.1126/science.274.5292.1486.
- Picaut, J., M. Ioualalen, T. Delcroix, F. Masia, R. Murtugudde, and J. Vialard (2001), The oceanic zone of convergence on the eastern edge of the Pacific warm pool: A synthesis of results and implications for El Niño–Southern Oscillation and biogeochemical phenomena, *J. Geophys. Res.*, 106(C2), 2363–2386, doi:10.1029/2000JC900141.
- Rasmusson, E. M., and T. H. Carpenter (1982), Variations in tropical sea surface temperature and surface wind fields associated with the Southern Oscillation/El Niño, *Mon. Weather Rev.*, 110(5), 354–384, doi:10.1175/1520-0493(1982)110<0354:VITSST>2.0.CO;2.
- Rayner, N. A., D. E. Parker, E. B. Horton, C. K. Folland, L. V. Alexander, D. P. Rowell, E. C. Kent, and A. Kaplan (2003), Global analyses of sea surface temperature, sea ice, and night marine air temperature since the late nineteenth century, *J. Geophys. Res.*, 108(D14), 4407, doi:10.1029/2002JD002670.
- Smith, T. M., and R. W. Reynolds (2003), Extended reconstruction of global sea surface temperatures based on COADS data (1854–1997), *J. Clim.*, 16(10), 1495–1510, doi:10.1175/1520-0442-16.10.1495.
- Sudre, J., and R. A. Morrow (2008), Global surface currents: A high-resolution product for investigating ocean dynamics, *Ocean Dyn.*, 58(2), 101–118, doi:10.1007/s10236-008-0134-9.
- Trenberth, K. E. (1984), Signal versus noise in the Southern Oscillation, *Mon. Weather Rev.*, 112(2), 326–332, doi:10.1175/1520-0493(1984)112<0326:SVNITS>2.0.CO;2.
- Trenberth, K. E. (1997), The definition of El Niño, *Bull. Am. Meteorol. Soc.*, 78(12), 2771–2777, doi:10.1175/1520-0477(1997)078<2771:TDOENO>2.0.CO;2.
- Trenberth, K. E., and D. P. Stepaniak (2001), Indices of El Niño evolution, *J. Clim.*, 14(8), 1697–1701, doi:10.1175/1520-0442(2001)014<1697:LIOENO>2.0.CO;2.
- Vialard, J., P. Delecluse, and C. Menkes (2002), A modeling study of salinity variability and its effects in the tropical Pacific Ocean during the 1993–1999 period, *J. Geophys. Res.*, 107(C12), 8005, doi:10.1029/2000JC000758.
- Vincent, D. G. (1994), The South Pacific Convergence Zone (SPCZ): A review, *Mon. Weather Rev.*, 122(9), 1949–1970, doi:10.1175/1520-0493(1994)122<1949:TSPCZA>2.0.CO;2.
- Vincent, E. M., M. Lengaigne, C. E. Menkes, N. C. Jourdain, P. Marchesio, and G. Madec (2009), Interannual variability of the South Pacific Convergence Zone and implications for tropical cyclone genesis, *Clim. Dyn.*, 36, 1–16, doi:10.1007/s00382-009-0716-3.
- Wang, B. (1995), Interdecadal changes in El Niño onset in the last four decades, *J. Clim.*, 8(2), 267–285, doi:10.1175/1520-0442(1995)008<0267:ICIENO>2.0.CO;2.

- Ward, J. H. (1963), Hierarchical grouping to optimize an objective function, *J. Am. Stat. Assoc.*, 58(301), 236–244, doi:10.2307/2282967.
- Weng, H., K. Ashok, S. K. Behera, S. A. Rao, and T. Yamagata (2007), Impacts of recent El Niño Modoki on dry/wet conditions in the Pacific rim during boreal summer, *Clim. Dyn.*, 29, 113–129, doi:10.1007/s00382-007-0234-0.
- Wolter, K., and M. S. Timlin (1998), Measuring the strength of ENSO events: How does 1997/98 rank?, *Weather*, 53, 315–324.
- Wyrtki, K. (1975), El Niño: The dynamic response of the equatorial Pacific Ocean to atmospheric forcing, *J. Phys. Oceanogr.*, 5(4), 572–584, doi:10.1175/1520-0485(1975)005<0572:ENTDRO>2.0.CO;2.
- Yeh, S.-W., J.-S. Kug, B. Dewitte, M.-H. Kwon, B. P. Kirtman, and F.-F. Jin (2009), El Niño in a changing climate, *Nature*, 461(7263), 511–514, doi:10.1038/nature08316.
- Yu, J.-Y., and S. T. Kim (2010), Three evolution patterns of central-Pacific El Niño, *Geophys. Res. Lett.*, 37, L08706, doi:10.1029/2010GL042810.
- Yu, J.-Y., H.-Y. Kao, and T. Lee (2010a), Subtropics-related interannual sea surface temperature variability in the central equatorial Pacific, *J. Clim.*, 23, 2869–2884, doi:10.1175/2010JCLI3171.1.
- Yu, J.-Y., H.-Y. Kao, T. Lee, and S. T. Kim (2010b), Subsurface ocean temperature indices for central-Pacific and eastern-Pacific types of El Niño and La Niña events, *Theor. Appl. Climatol.*, 103, 337–344, doi:10.1007/s00704-010-0307-6.
- S. Cravatte, T. Delcroix, and A. Singh, IRD/LEGOS, UMR 5566, 14 Avenue Edouard Belin, F-31400 Toulouse, France. (awnesh.singh@legos.obs-mip.fr)

ENSO, WWV and the RD oscillator paradigm

Preamble

Chapter 4 is mainly based on a manuscript by [Singh and Delcroix \(2012\)](#) submitted to *Deep Sea Research: Part I* (on 30 September 2012). The essence of this manuscript is to test the applicability of one of the leading theories for the oscillatory nature of ENSO, the recharge-discharge oscillator paradigm proposed by [Jin \(1997\)](#), to account for the different EP and CP flavors of ENSO. A schematic diagram for this oscillator is illustrated in [Fig. 4.S1](#) with a brief description in the caption.

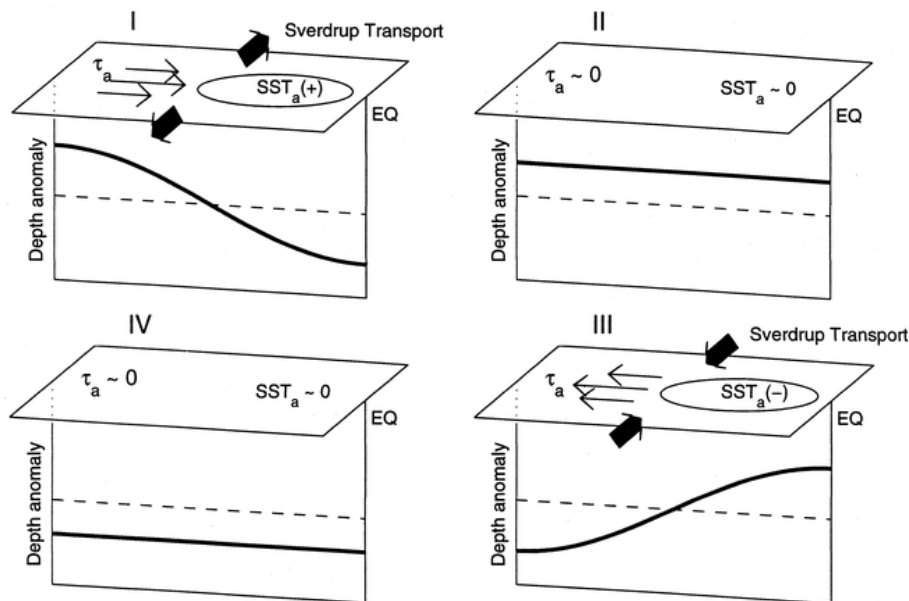


Figure 4.S1 Schematic diagram of the recharge/discharge oscillator for ENSO illustrating the four phases of the recharge/discharge oscillation: (I) the warm phase, (II) the warm to cold transition phase, (III) the cold phase, and (IV) the cold to warm transition phase. During the warm phase of ENSO, the divergence of Sverdrup transport associated with equatorial central Pacific westerly wind anomalies and equatorial eastern Pacific warm SST anomalies results in the discharge of equatorial heat content. The discharge of equatorial heat content leads to a transition phase in which the entire equatorial Pacific thermocline depth is anomalously shallow due to the discharge of equatorial heat content. This anomalous shallow thermocline at the transition phase allows anomalous cold waters to be pumped into the surface layer by climatological upwelling and then leads to the cold phase. The converse occurs during the cold phase of ENSO. [Adapted from [Meinen and McPhaden, 2000](#)]

Submitted Manuscript

The following sections are an extended version (with supplementary material at the end of the chapter) of a submitted manuscript.

Singh, A., and Delcroix, T. (2012). Eastern and Central Pacific ENSO and their relationships to the recharge/discharge oscillator paradigm, *Deep Sea Research: Part I*, submitted.

Eastern and Central Pacific ENSO and their relationships to the recharge/discharge oscillator paradigm

Awnesh Singh and Thierry Delcroix

Abstract

One of the leading theories to explain the oscillatory nature of ENSO is the recharge-discharge paradigm, which roots on warm waters exchanged between the equatorial and off-equatorial regions. This study tests the relevance of this theory to account for the Eastern and recently mediated Central Pacific El Niño events. The recharge-discharge of the equatorial Pacific, measured here as changes in Warm ($>20^{\circ}\text{C}$) Water Volume (WWV), is analyzed using monthly 1993-2010 sea level anomaly (a proxy for WWV) obtained from altimetry, and a validated 1958-2007 DRAKKAR simulation. An Agglomerative Hierarchical Clustering (AHC) technique performed on the observed and modeled WWV shows the existence of five distinct clusters, which characterize the Eastern Pacific (EP) and Central Pacific (CP) El Niño, La Niña, after EP El Niño and neutral conditions. The AHC results, complemented with an analysis of 3-month composites of typical EP and CP El Niño events, indicate that the equatorial band WWV discharge during CP is not as pronounced as during EP El Niño. To understand the differences, we analyze the balance of horizontal mass transport accounting for changes in WWV. The analysis indicates an overall poleward transport during EP El Niño, which is not the case during CP El Niño. Instead, a compensating effect with a poleward (equatorward) transport occurring in the western (eastern) Pacific is evident, in line with changes in the zonal thermocline slopes. The WWV changes are discussed with respect to the conceptual phases of the recharge-discharge oscillator paradigm.

4.1 Introduction

The El Niño Southern Oscillation (ENSO) phenomenon is the most energetic climate signal on interannual timescales with a quasi-cyclic period of 2-7 years. It has been given strong attention in the science and decision-making community for more than three decades owing to its complex dynamics and notable socio-economic impacts (e.g., [Philander, 1990](#); [Clarke, 2008](#)). Our understanding of ENSO has greatly improved in the 1990s thanks to the development of dedicated observing systems, relevant theories, and key analytical and modeling studies (e.g., [McPhaden *et al.*, 2006](#)). One group of theories has especially been proposed to account for the quasi-oscillatory nature of ENSO, while another group conjectures that ENSO may be a stable (and not self-sustained) mode triggered by stochastic wind forcing. The former group of theories includes the delayed action, western Pacific, advective-reflective, recharge-discharge and unified oscillators, with each oscillator involving a specific negative feedback to account for the termination of El Niño (see [Wang and Picaut, 2004](#) for a review of ENSO mechanisms).

The above-noted first group of ENSO theories were proposed more than a decade ago based on the observations of canonical El Niño events (e.g., [Rasmusson and Carpenter, 1982](#)), and hence chiefly focus on the 3-5 years oscillatory aspects of ENSO. In other words, they did not consider what is sometimes now presented as a “new” and more frequent type of El Niño, variously called Dateline El Niño, El Niño Modoki, Warm Pool or Central Pacific El Niño ([Larkin and Harrison, 2005a,b](#); [Ashok *et al.*, 2007](#); [Kao and Yu, 2009](#); [Kug *et al.*, 2009](#)). This raises the question of whether these theories are adequately able to describe Central Pacific ENSO events. Hence, as a first step in addressing that question, the present paper aims to assess whether or not one of these theories, namely the recharge-discharge (RD) oscillator paradigm, can account for the canonical and Central Pacific El Niño events and/or if it can be used to contrast the two types of events.

Let us first briefly review the main features of the different flavors of ENSO and of the RD oscillator. Basically, the canonical, cold-tongue or Eastern Pacific (EP) El Niño is characterized by anomalous sea surface temperature (SST) warming extending along the equator from the South American coast to the central Pacific ([Rasmusson and Carpenter, 1982](#)). In contrast, the “recently detected” Central Pacific (CP) El Niño has anomalous warm SST concentrated in the central equatorial Pacific region. Different structures during these

contrasting episodes have also been observed in other climate variables including wind stress and subsurface temperature (Kao and Yu, 2009), precipitation (Yeh *et al.*, 2009), sea level (Kug *et al.*, 2009), heat content (Kug *et al.*, 2010), sea surface salinity (Singh *et al.*, 2011) and chlorophyll (Radenac *et al.*, 2012).

The RD oscillator paradigm roots on the early results of Wyrтки (1985) and, to name a few, was further highlighted by Jin (1997), Meinen and McPhaden (2000), and Clarke *et al.* (2007). For convenience, the RD has been measured as variations of the volume of water warmer than 20°C in the tropical Pacific (named as Warm Water Volume (WWV)). According to Jin (1997), there is a general tendency for an east-west redistribution followed (preceded) by a discharge (recharge) of WWV in the equatorial band during El Niño (La Niña). Results based on observations and models indicate that such WWV changes are mainly controlled by meridional and zonal advectons with an overall relatively small contribution from vertical advection (Meinen and McPhaden, 2000; 2001; Meinen, 2005; Clarke *et al.*, 2007; Bosc and Delcroix, 2008; Brown and Fedorov, 2010; Lengaigne *et al.*, 2012). Changes in WWV usually lead changes in the Niño3.4 SST, and so can interestingly be used as a possible predictor for ENSO onset (McPhaden, 2003). As exemplified in Fig. 4.1 for the 1980-2010 period (see Section 4.2 for the data origin), WWV leads the Niño3.4 SST index by 6 months with a maximum correlation of $R=0.71$. Noteworthy, changes in WWV and Niño3.4 SST are reduced in amplitude and this correlation looks slightly higher ($R=0.81$) for the 2000-2010 period, when CP ENSO prevails, with a reduced lag of 3 months (see also McPhaden, 2012; Horii *et al.*, 2012).

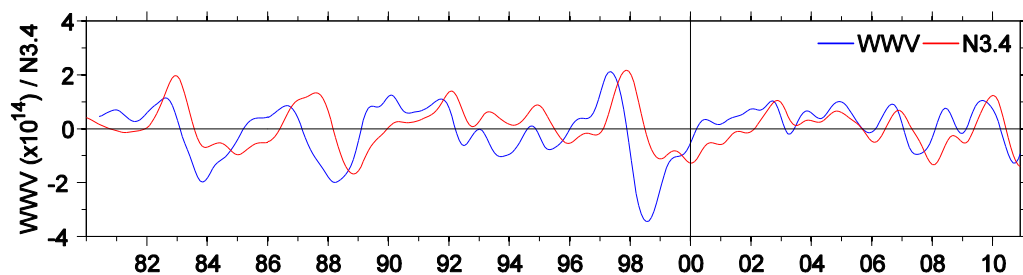


Figure 4.1 WWV anomaly averaged in the region 5°S-5°N, 120°E-80°W (in blue) and Niño3.4 index defined as the average SST anomaly in the region 5°S-5°N, 170°W-120°W (from HadISST; in red) for the period 1980-2010. Both time series have been smoothed with a 13-months Hanning filter for clarity. The WWV data was downloaded from <http://www.pmel.noaa.gov/tao/elNiño/wwv/>. Units for WWV anomaly and Niño3.4 index are 10^{14} m^3 and °C, respectively.

As mentioned earlier, the different flavors of El Niño have been contrasted in terms of climate variables. Also, numerous modeling studies did look at the mechanisms involved in ENSO (e.g., Mechoso *et al.*, 2003; van Oldenborgh *et al.*, 2005) but, to our knowledge, did not further distinguish the different flavors of El Niño in terms of oscillatory modes. In this study, we attempt to differentiate EP and CP El Niño in terms of dynamics and especially examine whether or not WWV, and therefore the RD paradigm, can account for CP ENSO features. The rest of the manuscript is organized as follows: Section 4.2 describes the data and methodology; Section 4.3 describes the observational and model results; Section 4.4 attempts to explain the main mechanisms likely responsible for the contrasted ENSO signatures; and a discussion and conclusion follow in Section 4.5.

4.2 Data and Methods

We use two observational and two modeling datasets for this study. The first observational dataset is the Met Office Hadley Centre for Climate Prediction and Research sea ice and sea surface temperature dataset 1 (HadISST1; Rayner *et al.*, 2003), available monthly from 1870 until present on a 1° horizontal grid. From this, we computed the well-known Niño3 (150°W - 90°W , 5°S - 5°N), Niño4 (160°E - 150°W , 5°S - 5°N) and Niño3.4 (170°W - 120°W , 5°S - 5°N) SST indices, the first two of which are also used to calculate the Niño cold tongue (N_{CT}) and Niño warm pool (N_{WP}) indices (using $\alpha=0.4$) following Ren and Jin (2011). The second observational dataset is the remotely sensed sea level anomalies (SLA) which were obtained in combining data from the ERS, ENVISAT, GEOSAT, Jason and TOPEX/Poseidon series of satellite missions (Ducet *et al.*, 2000). The monthly SLA, calculated with respect to a seven year (1993-1999) mean, are available from AVISO (<http://www.aviso.oceanobs.com>) on a $\frac{1}{4}^\circ$ cartesian grid and from December 1992 to June 2011 at the time of writing. The SLA are further re-gridded on a 1° horizontal grid using linear interpolation. SLA is an important component in ENSO-related studies more so because it is an excellent alias for WWV changes (e.g., Meinen, 2005). The SLA were converted into WWV anomalies (using $\rho/\Delta\rho=180$) following the approach of Bosc and Delcroix (2008).

The short observational period of the altimetry-based SLA does not cover many ENSO events and we therefore also make use of two simulations. These simulations allow us to calculate the WWV directly from the 20°C isotherm (Z_{20}) at each grid point. The first modeling dataset is obtained from the DRAKKAR simulation ORCA-R025.L75-G85 forced

by DRAKKAR Forcing Set #4.3 with the European Centre for Medium-Range Weather Forecasts (ECMWF) 40-year reanalysis (ERA40) base and has outputs of temperature, salinity, sea surface height, and horizontal and vertical velocities data amongst other variables (Barnier *et al.*, 2006). The data is distributed on a $\frac{1}{4}^\circ$ grid at 5-day averaged intervals from 1958-2007. We re-gridded this product on a 1° horizontal grid by 1 month (using monthly mean and linear interpolation along the temporal and spatial axes) while conserving the vertical resolution of 47 levels (with 31 levels in the upper 200 m). We also tested a second modeling dataset, the Simple Ocean Data Assimilation (SODA) 2.2.4 reanalysis product (Carton and Giese, 2008), which is an assimilation of observed data into an Ocean General Circulation Model (OGCM). Here, we choose to present results obtained from the DRAKKAR product only, noting that using the SODA product gave us similar conclusions.

Focusing on the interannual time scale, the datasets were detrended and their mean monthly climatology removed over the 1993-2010 period for the observed SLA (and derived WWV), and over the 1958-2007 period for the modeled WWV. The anomalies were then smoothed using a 13-months Hanning filter as it passes almost no signal at periods of 6 months and shorter and so looks appropriate since the duration of CP ENSO was found to be less than 1 year (e.g., Ashok *et al.*, 2007; Weng *et al.*, 2007; Kao and Yu, 2009). The data analysis was restricted to the tropical Pacific region delimited by 120°E - 70°W , 15°S - 15°N as isotherms spreading beyond these meridional boundaries result in a diffused thermocline (Wyrtki and Kilonsky, 1984); the ocean then poorly behaves like a 1.5-layer ocean system meaning that SLA cannot be used as a good proxy for WWV anymore (see Meinen, 2005; his Fig. 4). We did not use regions in the far western tropical Pacific north of Australia and west of Papua New Guinea and extending to the South China Sea.

In addition to the overall evaluation performed in Barnier *et al.* (2006), the DRAKKAR simulation was further evaluated regarding its capability to simulate the SST (taken at 0.5 m depth), the WWV tendency, the link between Niño3.4 SST and WWV, and the horizontal transports involved in WWV changes. The correlation coefficient between the monthly 1958-2007 observed and modeled Niño3.4, N_{CT} and N_{WP} SST time series is $R=0.97$, $R=0.96$ and $R=0.87$, respectively (not shown here). The observed SLA-derived, in situ temperature-derived (Meinen and McPhaden, 2000; hereafter MM00) and model-derived WWV tendencies computed over the 5°S - 5°N , 120°E - 80°W region are compared in Fig. 4.2. The correlations at zero lag (ratio of standard deviations) between the SLA-derived and in situ

temperature-derived WWV tendency is 0.82 (1.06), SLA-derived and model-derived WWV tendency is 0.93 (0.82), and model-derived and in situ temperature-derived WWV tendency is 0.93 (1.36). The correlation coefficient between the 1958-2007 modeled WWV (tendency) and Niño3.4 SST time series is $R=0.68$ ($R=-0.84$) with the WWV leading by 6 months (at zero lag; not shown here).

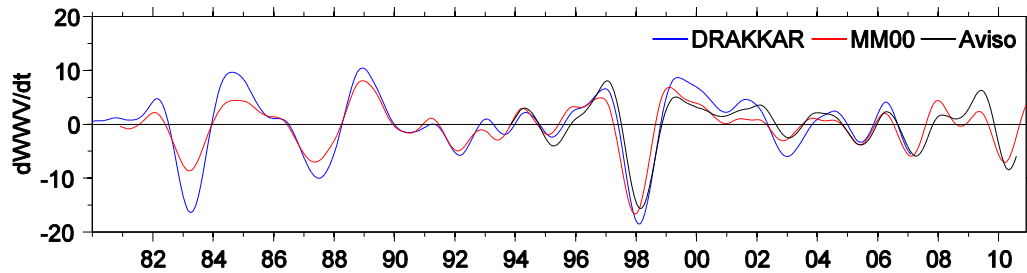


Figure 4.2 The 1980-2010 WWV tendency term for the region bounded by latitudes 5°S and 5°N , and longitudes 120°E and 80°W using DRAKKAR modeled data (in blue), observational data from Aviso (in black) and Meinen and McPhaden (2000; hereafter MM00; in red). All time series have been smoothed with a 25-months Hanning filter for clarity. Units are in Sverdrups.

As discussed in the Introduction section, the WWV tendency in a given equatorial box is chiefly balanced by the horizontal mass transports across those box boundaries. The Ekman and total horizontal transports were then computed from the surface wind stress and horizontal velocity profiles, respectively, while the geostrophic transports were inferred from the total minus the Ekman transports (hence with no assumption regarding the reference level). Note that the net horizontal transport was not divided onto Ekman and geostrophic transports within 5°S - 5°N to avoid computation of strong discontinuity at the equator where the Coriolis parameter goes to zero. With this caveat, we validate with observations from Meinen and McPhaden (2001; hereafter referred to as MM01), the horizontal transports for the equatorial Pacific region using the DRAKKAR dataset for the 1993-1999 period. The correlations and ratio of standard deviations between the model and observed data for the total, geostrophic and Ekman meridional transports across 8°S and 8°N , and the total zonal transports across 156°E and 95°W are shown in Table 4.1. Note that the data processing used was the same as MM01. The high correlation between the observed and modeled SST, WWV tendency and horizontal transport terms gives us extra confidence in the ability of the routinely-validated DRAKKAR product to realistically simulate the state of the tropical Pacific during ENSO.

We use an Agglomerative Hierarchical Clustering (AHC) procedure to characterize the main ENSO signature in SL and WWV anomalies. In the AHC process, the Euclidean distance between each pair of singletons (monthly maps) is calculated to measure their (dis)similarity. The Ward criterion uses this Euclidean distance to merge each pair of singleton based on the least sum of squared distance between them. This ensures maximum similarity within the cluster of elements and maximum dissimilarity with elements of other clusters. The process is repeated agglomeratively until the entire dataset is merged into one cluster. We gain confidence in the use of this method as it has been successfully applied to climate and biological studies before (e.g., [Kao and Yu, 2009](#); [Vincent *et al.*, 2009](#); [Singh *et al.*, 2011](#), [Radenac *et al.*, 2012](#)) and further stress that it does not require a priori to extract the dominant modes of variability and does not extract unrealistic symmetrical El Niño/La Niña (EN/LN) patterns like an EOF analysis would do, for example.

Table 4.1 Correlation coefficients between the meridional (across 8°N and 8°S) and zonal (across 156°E and 95°W) transports calculated above the 20°C isotherm from observations and DRAKKAR model data using the same data processing as in [Meinen and McPhaden \(2001](#); hereafter **MM01**) for the 1993-1999 period. The values in parentheses represent the ratio of standard deviations (SD) between the two time series: SD-observations / SD-model. Sections at 8°N and 8°S extend from 156°E to 95°W, and sections at 156°E and 95°W from 8°S to 8°N. The Ekman transports used from **MM01** were those from the ECMWF product.

Section	Ekman Transports	Geostrophic Transports	Total Transport
8°N	0.85 (0.96)	0.91 (0.89)	0.85 (0.85)
8°S	0.91 (1.01)	0.97 (1.43)	0.90 (1.19)
156°E	-	-	0.76 (0.61)
95°W	-	-	0.80 (0.75)

4.3 Observed and modeled SL and WWV changes

4.3.1 Observational results, 1993-2010

The AHC procedure was performed on the observed SLA for the May 1993-January 2011 period (note the first and last 5 months of the December 1993-June 2011 time period cannot be analyzed using a 13-months low pass filter). The resulting cluster time series and the spatial clusters for SLA are shown in [Fig. 4.3](#). Five clusters for a total of 213 observations (months) were identified at the top of the dendrogram tree (not shown; see supplementary material [Fig. 4.S2](#)). These five clusters mostly characterize a central equatorial Pacific discharge and an off-equatorial recharge in the far west (cluster 1), a western-central

equatorial Pacific and SPCZ discharge and a recharge in the off-equatorial far eastern Pacific (cluster 2), a neutral situation (cluster 3-not shown), a central equatorial Pacific recharge and an off-equatorial discharge in the far west (cluster 4 – roughly symmetrical to cluster 1) and a zonal seesaw with an equatorially-trapped maximum in the eastern half and off-equatorial minima in the western half of the basin (cluster 5), and occur 34%, 4%, 19%, 40% and 3% of the time, respectively. The comparison between the cluster time series and the normalized N_{CT} and N_{WP} indices (Fig. 4.3a) suggests that these clusters chiefly represents La Niña-type (LN), after EP El Niño-type (AEPEN), CP El Niño-type (CPEN) and EP El Niño-type (EPEN) situations for clusters 1, 2, 4 and 5, respectively. We shall use this nomenclature henceforth to refer to these clusters.

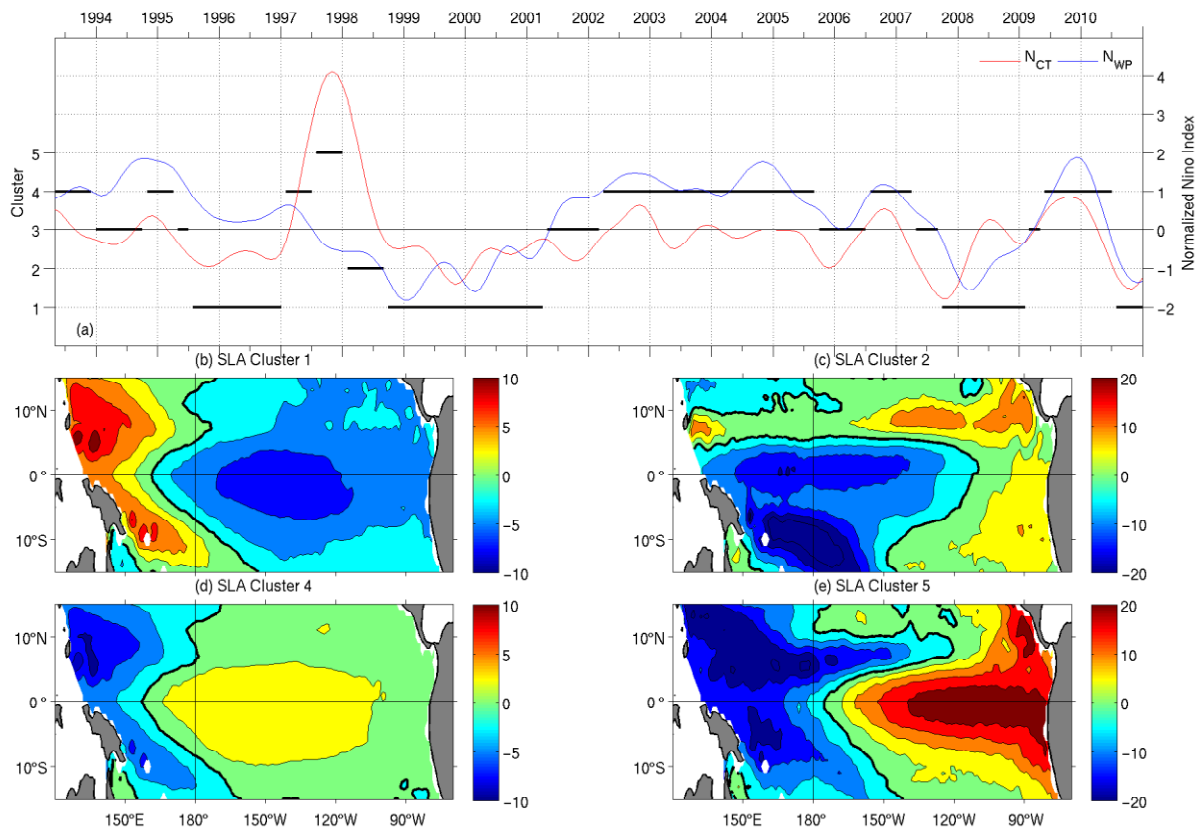


Figure 4.3 (a) The cluster time series showing which cluster best represents the observed SLA pattern at a particular time for the period 1993-2010 (in black; left vertical axis). Superimposed are the normalized N_{CT} (in red) and N_{WP} (in blue) indices (scaled on the right vertical axis). The abscissa labels denote the beginning of the year. Spatial patterns from the AHC on SLA with (b) cluster 1 denoting La Niña-type (LN), (c) cluster 2 denoting after EP El Niño-type (AEPEN), (d) cluster 4 denoting CP El Niño-type (CPEN) and (e) cluster 5 denoting EP El Niño-type (EPEN) situations. Thick black contour lines in the spatial patterns denote the 0 line. Note the different color scales for the plots. Units for SLA are in cm. The SLA (in cm) can be converted to WWV anomaly (in m^3) using a factor approximately equal to 2.2×10^{10} .

The EPEN and AEPEN spatial patterns (Fig. 4.3e&c, respectively) are similar to those obtained by Alory and Delcroix (2002) using multivariate EOF for a shorter time period (1992-1999; see their Figs. 2&7, respectively). The negative SLA evidenced in the SPCZ region during AEPEN is due to shoaling of the thermocline resulting from upwelling favorable wind stress curl (Picaut *et al.*, 2002; see their Fig. 8). The zonal seesaw pattern during EPEN (Fig. 4.3e) is also evident during LN (Fig. 4.3b) but with opposite signs and much weaker magnitudes and with the fulcrum at around 170°E instead of 170°W. Such a zonal seesaw during EPEN corresponds to a displacement of the western Pacific warm waters to the central and eastern basins and so to a reduced thermocline slope in the equatorial band. It should be noted that the amplitude of the SLA pattern for AEPEN is almost 3 times that for LN. The CPEN pattern (Fig. 4.3d), almost symmetrical to the LN pattern, shows positive SLA mostly from the east to the west, except in the far western Pacific, with maximum SLA in the central equatorial Pacific region. Again, it should however be noted that the amplitude of the maximum SLA during CPEN is only ~15% of that during EPEN. Although the SLA signature of CPEN is weaker than for EPEN, the reduced amplitude is also due to the effect of aggregating the six CPEN events as compared to only one very strong EPEN event that occur over the 1993-2010 period in the AHC.

As further discussed below, it is worth pointing out that the changing SLA slope in the equatorial band during CPEN yields to a zonal gradient of the SLA which is eastward (westward) to the west (east) of the maximum SLA and can result in geostrophic poleward (equatorward) transports by meridional divergence (convergence). In contrast, the zonal gradient of the SLA is eastward only during EPEN and thus results in poleward geostrophic transports from the east to the west of the basin.

4.3.2 Model Results, 1958-2007

To extend the short observational-based time series, we repeated the AHC technique to the 1958-2007 model-derived WWV using the same data processing as was done for the observed SLA-derived WWV data. The WWV cluster time series and the spatial patterns of the modeled WWV are shown in Fig. 4.4.

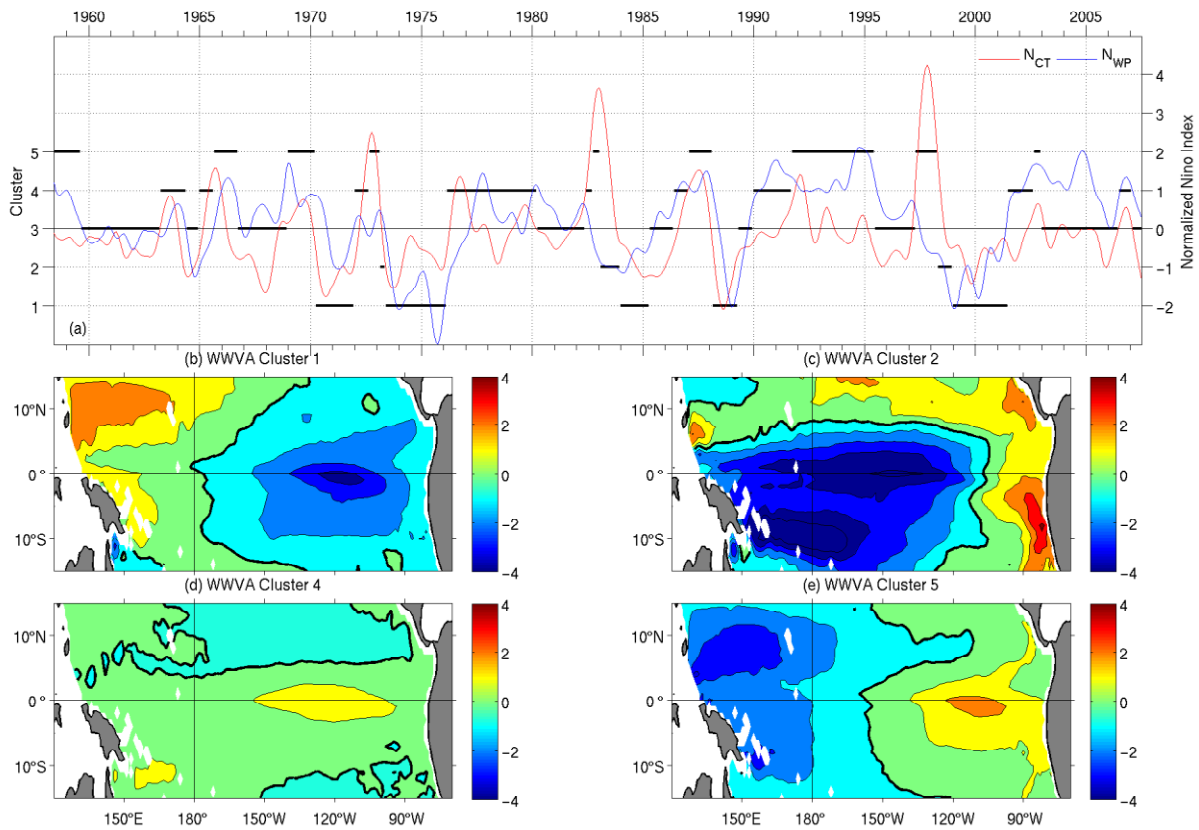


Figure 4.4 (a) The cluster time series showing which cluster best represents the model-derived WWV anomaly pattern at a particular time for the period 1958-2007 (in black; left vertical axis). Superimposed are the normalized N_{CT} (in red) and N_{WP} (in blue) indices (scaled on the right vertical axis). The abscissa labels denote the beginning of the year. Spatial patterns from the AHC on WWV anomaly with (b) cluster 1 denoting La Niña-type (LN), (c) cluster 2 denoting after EP El Niño-type (AEPEN), (d) cluster 4 denoting CP El Niño-type (CPEN) and (e) cluster 5 denoting EP El Niño-type (EPEN) situations. Thick black contour lines in the spatial patterns denote the 0 line. Units for WWV anomaly are 10^{11} m^3 .

From the AHC on WWV anomalies, five distinct clusters from the 590 sets of observations (months) were identified and these are still representative of a central equatorial Pacific discharge and an off-equatorial recharge in the far west (cluster 1), a western-central equatorial Pacific and SPCZ discharge and a recharge in the off-equatorial far eastern Pacific (cluster 2), a neutral situation (cluster 3 – not shown), a central equatorial Pacific recharge (cluster 4) and a zonal seesaw (cluster 5 – almost symmetrical to cluster 1) and occur 19%, 4%, 33%, 23% and 21% of the time, respectively. Because of the close similarity of these clusters to the ones derived from observed SLA (but for a shorter period; Fig. 4.3), and relying on the comparison between the cluster time series and the EP/CP indices (Fig. 4.4a), we will use the same naming conventions for the clusters here. Cluster 2, which represents AEPEN conditions (Fig. 4.4c), shows the equatorial and SPCZ discharge with positive anomalies to the north of a meridional fulcrum situated near 5°N . The negative anomalies

occupy most of the equatorial band (except in the far eastern Pacific), extend up to 15°S in the western Pacific, and are much larger in amplitude over the SPCZ region than in the equatorial region. This mass depletion of warm water in the equatorial and SPCZ regions occurs directly after the strong 1972-73 and very strong 1982-83 and 1997-98 EPEN events (represented by cluster 5; Fig. 4.4e) and is followed by LN (represented by cluster 1; Fig. 4.4b). In terms of dynamics, this means that the eastward sloping thermocline anomaly during EPEN in the central Pacific results in a mass discharge in the central equatorial region thereby shoaling the thermocline there. The EPEN and LN spatial patterns are similar to those obtained from observations in Fig. 4.3e&b, respectively, with oppositely signed zonal seesaws. Interestingly, the CPEN cluster (Fig. 4.4c) shows a mass accumulation of warm water that extends from 5°N to 10°S.

The cluster time series implies that after the strong 1972-73 and very strong 1982-83 and 1997-98 EPEN events, an AEPEN event follows which shows a WWV discharge in the equatorial band. It also shows that a recharge of the equatorial band (CPEN) occurs prior to any EPEN event (except during 1997-98). These results are consistent with results obtained from the observed SLA analysis earlier and the RD paradigm. However, there is no discharge signal occurring after any CPEN event strongly suggesting that CPEN does not fit the RD oscillator paradigm.

To further detail the EP and CP El Niño features with respect to the RD paradigm, we have plotted and analyzed the chronology of model-derived WWV anomaly for all EP and CP El Niño events, as well as the anomalous depths of the 20°C thermocline (Z_{20}) in the equatorial band that we compared to the conceptual phases of the RD oscillator. These are illustrated in Fig. 4.5 for the 1997-98 EP and 2002-03 CP El Niño periods. The 1997-98 EPEN event shows a positive WWV anomaly increasing in magnitude as it progresses from the central to the eastern equatorial Pacific. The almost initially flat thermocline anomaly gradually tilts to have an eastward slope by Oct-Dec 1997, when there is a sharp east-west contrast in the WWV anomaly signature pivoted at around 160°W along the equator. The negative WWV anomaly in the west then moves eastward and poleward signifying a discharge of warm waters from the western-central Pacific equatorial region resulting in a shallower thermocline anomaly by Oct-Dec 1998. Meanwhile the positive WWV anomaly in the east is forced to move poleward along the South American coast and tends to move westward along and above the 10° latitudes.

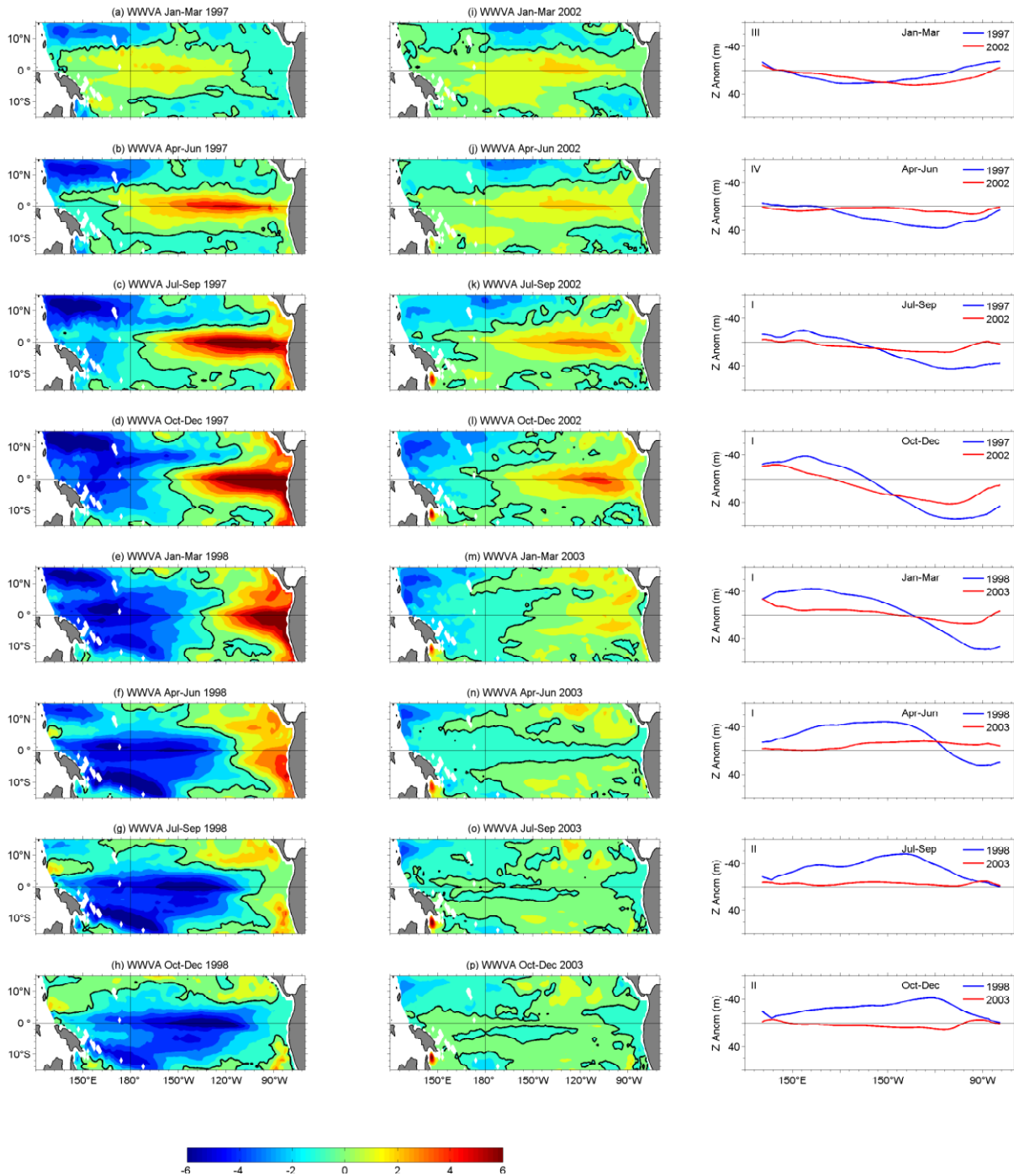


Figure 4.5 3-month composites of model-derived WWV anomaly for the periods (a-h) Jan 1997-Dec 1998 (first column) and (i-p) Jan 2002-Dec 2003 (second column). (third column) The corresponding anomalous depth of the 20°C thermocline (Z_{20}) for each 3-month WWV anomaly composite. The depth anomalies are departures from the 1971-2000 mean thermocline depth averaged between 2°S-2°N and are smoothed with a 5° longitude running mean (positive values denote a deeper thermocline). The roman numerals represent the modified Jin (1997) conceptual model phase of ENSO (as illustrated in MM00). Phases I and III represent El Niño and La Niña phases, while phases II and IV represent the discharged and recharged phases, respectively. Thick black contour lines in the spatial patterns denote the 0 line. Units for WWV and depth anomalies are 10^{11} m^3 and m, respectively.

For the 2002-03 CPEN event, the situation during 2002 is somewhat similar to that in 1997 except for the reduced magnitude of the WWV anomaly buildup in the east. Consequently, the anomalous eastward sloping thermocline tilt during Oct-Dec 2002 is not as pronounced as during Oct-Dec 1997. The east-west seesaw is pivoted at around 180° , about 20° in longitude westward of the position during Oct-Dec 1997. The poleward transport of the positive WWV anomaly in Jan-Mar 2003 results in a depletion of warm waters from the equatorial band. However, this discharge is not as pronounced as during the 1997-98 event, which is reflected in the near zero thermocline anomaly. This suggests that the discharge during the 2002-03 CPEN was clearly different from that during the 1997-98 EPEN. By the end of 2003, the equatorial basin shows a slightly positive thermocline anomaly in huge contrast to the largely negative anomaly during the end of 1998. The WWV anomaly is almost the same in Oct-Dec 2003 as it was in Jan-Mar 2002. In comparison, the 1997-98 WWV anomaly for the same months show pronounced symmetry. It is tempting to conclude from these results that the 1997-98 EP (2002-03 CP) El Niño does (not) fit the RD oscillator paradigm. A more detailed study of the transport contribution to the WWV anomaly is presented below to understand the dynamical processes taking place in the equatorial region during EP and CP ENSO.

4.4 Transport contribution to the modeled WWV

To understand the RD process in the equatorial Pacific, it is important to understand the WWV variations, and consequently, the mass balance of horizontal transports of warm water. This is done here in two steps using model data: (1) to set the context by looking at the mean state (and standard deviation) of the horizontal transports across different boundaries, and (2) contrasting the EP and CP El Niño signature in horizontal transports across these boundaries.

4.4.1 Mean State

Previously published estimates of horizontal mass transports accounting for WWV tendency were sometimes performed in separating the entire equatorial box in two or three sub-regions (e.g., [Brown and Fedorov, 2010](#)). Choosing the eastern and western limits of those sub-regions is not straightforward and may appear somewhat arbitrary. As an alternative, we computed the mean transports entering the equatorial region across 5°S and 5°N in running 31° longitude regions between 120°E and 70°W ([Fig. 4.6](#)). As stated in [Section 4.2](#), we calculate the total horizontal transports above the 20°C isotherm, the Ekman transports from

the model wind stress, and the geostrophic transports as the total minus Ekman transports (except within 5°S - 5°N for the later).

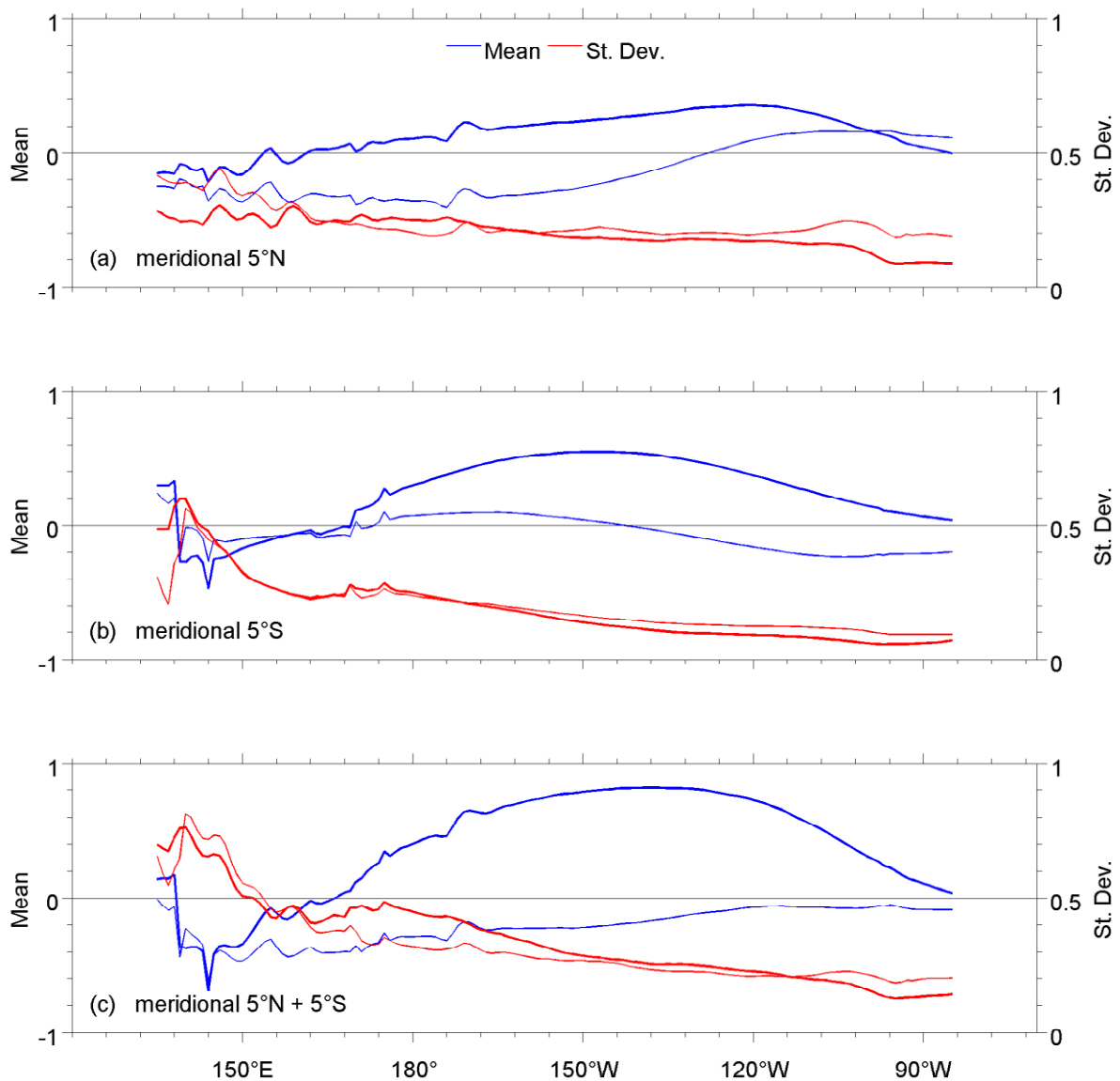


Figure 4.6 Mean (in blue; left vertical axis) and standard deviation (in red; right vertical axis) of model-derived meridional (a) transport across 5°N , (b) transport across 5°S and (c) total transport entering across 5°N and 5°S computed above the 20°C isotherm depth and for 31° longitude moving boxes. The thin (thick) lines represent the mean meridional total (geostrophic) transports. The abscissa is centered on the 31° longitude moving box. Positive values indicate transports entering the equatorial band. Mean values are calculated over the 1958-2007 period. Units are in Sverdrups per degree longitude.

The inferred mean meridional geostrophic transports are into the equatorial region across both 5°S and 5°N along the central and eastern Pacific, consistent with the mean east-west slope of the thermocline, with maximum variability in the western Pacific. The mean total meridional transports across 5°N show a recharge of the equatorial band in the eastern Pacific

and a discharge in the central and western Pacific. The mean absolute meridional transports across 5°S show a recharge of the equatorial band in the central Pacific and a discharge in the western and eastern Pacific. The total mean geostrophic (absolute) meridional transports across both 5°S and 5°N shows a recharge (discharge) of the equatorial band over the central and eastern Pacific and a discharge in the western Pacific. The mean meridional Ekman transports (not shown) shows poleward discharge across 5°S and 5°N , consistent with the mean westward blowing trade winds, and opposes the geostrophic transports, as sketched more than 30 years ago (e.g., [Wyrki, 1981](#)). For the zonal transports, the mean transports are calculated between 5°S and 5°N at each longitudinal position. The mean total zonal transports are westward over the central and eastern Pacific, in line with the South Equatorial Current (SEC), and eastward in the western Pacific with a mean zonal convergence within 160°E - 180°E (not shown), consistent with the mean position estimated from the convergence of surface drifters ([Picaud *et al.*, 1996](#)). Maximum variability for the zonal transports is seen in the western and central Pacific regions (not shown). The total mean transports across 5°N , 5°S , 156°E and 95°W (not shown) are close to zero indicating that the vertical mass transports across the 20°C are one order of magnitude smaller than the horizontal transports in changing the WWV.

4.4.2 Contrasting EP and CP ENSO events

To obtain the WWV signature during ENSO, we use a linear regression analysis using normalized N_{CT} and N_{WP} indices, which characterize EP and CP events, respectively. We use the 5°S and 5°N latitudes as the southern and northern limits of our equatorial box, respectively, and calculate the signal in 31° longitude moving boxes from the western to the eastern Pacific coasts. For WWV, gradients obtained from the regression indicate the well-known zonal seesaw centered at around 150°W during EP ENSO (red curve in [Fig. 4.7a](#)). It shows that the WWV anomaly has opposite signs on either side of this fulcrum, indicating a mass transfer from the west to the east during EP El Niño. The maximum positive WWV anomaly is closer to the South American coast compared to during CP ENSO (blue curve in [Fig. 4.7a](#)), where the maxima is smaller in magnitude and broadly spread in the central eastern basin. The zonal seesaw, which is still evident during CP ENSO, has a weaker slope and the fulcrum is shifted about 15° in longitude westward compared to during EP ENSO.

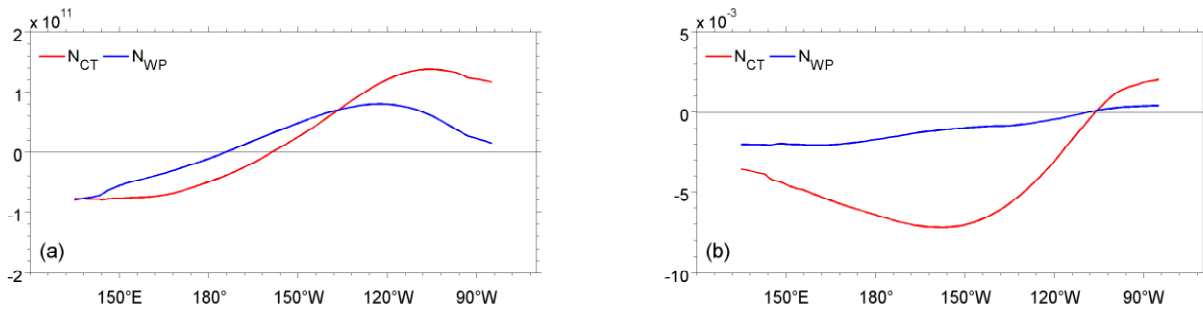


Figure 4.7 Gradients obtained from the regression of normalized Niño cold tongue (N_{CT} , in red) and Niño warm pool (N_{WP} , in blue) indices with model-derived (a) mean WWV anomaly averaged between $5^{\circ}S$ - $5^{\circ}N$ and (b) the corresponding mean WWV tendency. The regressions were performed on averages computed in running 31° longitude boxes. The abscissa is centered on the 31° longitude moving box. Note the different scales in the plots. Units are $m^3 \text{ }^{\circ}C^{-1}$ in (a) and Sverdrups $^{\circ}C^{-1}$ per degree longitude in (b).

A similar regression analysis was performed between N_{CT} and N_{WP} indices versus the WWV tendency, as a way to infer the related incoming and outgoing mass transport balance during EP and CP ENSO. Interestingly, results show a huge mass discharge over the entire equatorial region during EP El Niño (red curve in Fig. 4.7b), contrasting with a weak mass discharge during CP El Niño (blue curve Fig. 4.7b). The RD paradigm hence again does not seem to apply during CP El Niño events.

The regression analysis was extended to the individual transports entering the equatorial box from the south ($5^{\circ}S$) and north ($5^{\circ}N$). The meridional geostrophic transports during EP and CP ENSO across both $5^{\circ}S$ and $5^{\circ}N$ show similar behavior, with the transport across $5^{\circ}S$ showing a larger effect than its northern counterpart (thick lines in Fig. 4.8a&b; note the different scales). There is geostrophic discharge of warm water almost over the entire equatorial band during EP (except in the far west) while it is restricted to the region west of about $160^{\circ}W$ and peaking at $170^{\circ}E$ during CP El Niño. East of about $160^{\circ}W$, geostrophic recharge of the equatorial band is seen during CP El Niño. This indicates that there is some sort of compensating effect of the meridional geostrophic transports into the equatorial region during CP El Niño, hence the weak overall discharge of WWV (Fig. 4.7b), which is not evident during EP El Niño. The total meridional geostrophic transports into the box also reflect the above scenario (Fig. 4.8c). The discharge of the equatorial band in the western basin during CP El Niño is indicative of an eastward sloping thermocline, and the recharge in the eastern basin of a westward sloping thermocline, as was evidenced in the SLA observations (Fig. 4.3d).

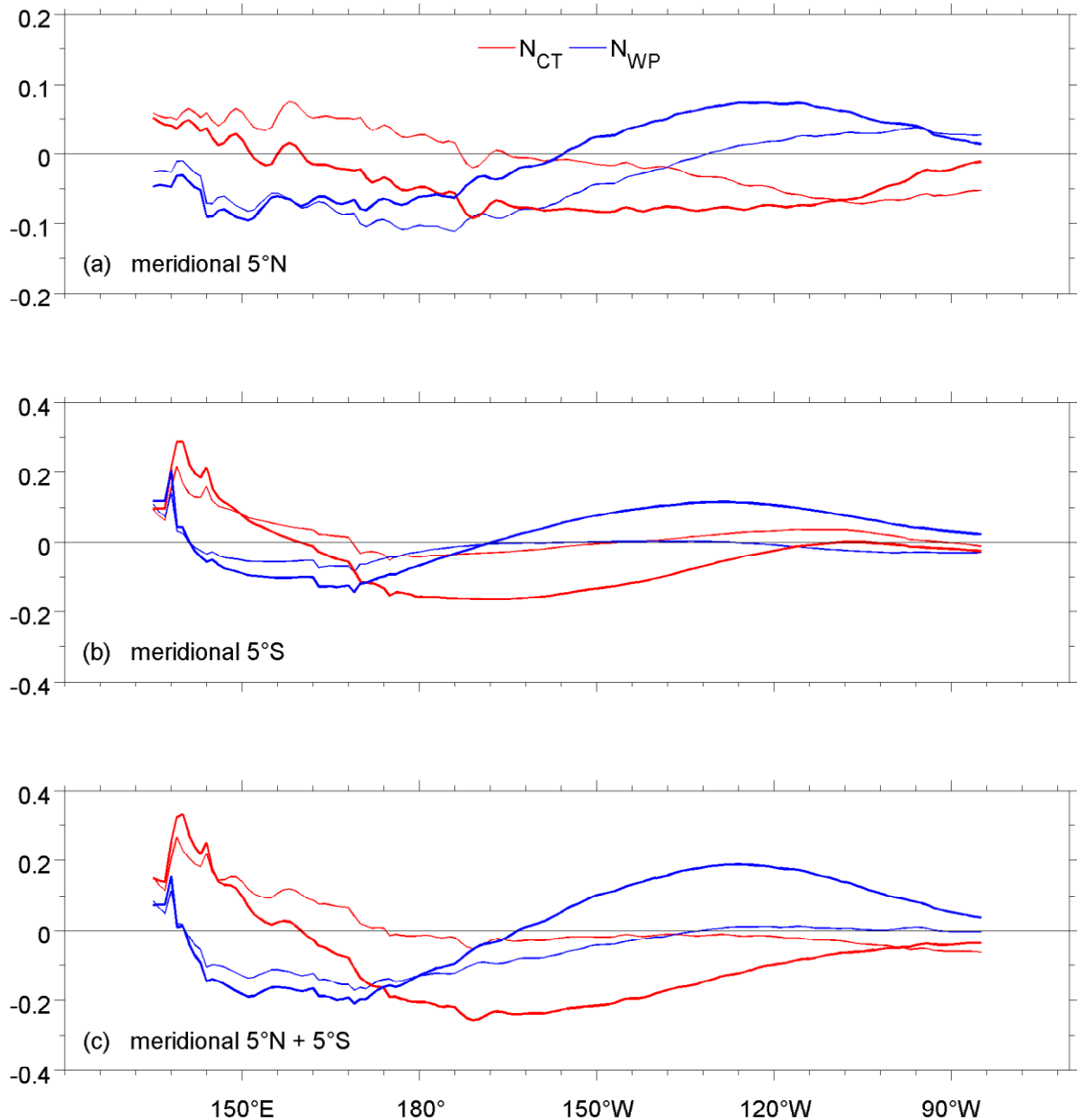


Figure 4.8 Gradients obtained from the regression of normalized Niño cold tongue (N_{CT} , in red) and Niño warm pool (N_{WP} , in blue) indices with model-derived mean meridional transports entering across (a) $5^\circ N$, (b) $5^\circ S$ and (c) $5^\circ S$ and $5^\circ N$. The regressions were performed on averages computed in running 31° longitude boxes. The thin (thick) lines represent the absolute (geostrophic) transports. The abscissa is centered on the 31° longitude moving box. Note the different scales in the plots. All transports were computed above the $20^\circ C$ isotherm depth. Units are in Sverdrups $^\circ C^{-1}$ per degree longitude.

The absolute zonal transports during EP El Niño are eastward over the entire equatorial region (not shown). In comparison, the absolute zonal transports show opposite signs on either side of about $170^\circ W$ during CP El Niño. In particular it shows there is mass convergence with eastward transports to the west and westward transports to the east, in agreement with the analysis of 1994-2008 observed surface currents during CP El Niño

events (Singh *et al.*, 2011; their Fig. 8). The total horizontal transports in the equatorial region generally show a discharge (recharge) during EP (CP) El Niño (also not shown).

4.5 Conclusions and Discussion

The El Niño Southern Oscillation (ENSO) is a climate signal which occurs at interannual time scales in the tropical Pacific Ocean. It oscillates between warm (El Niño) and cold (La Niña) phases with the origin, development and decay of each episode being different from each other. Four major theories have been proposed more than a decade ago to explain the quasi-periodic nature of ENSO (see Wang and Picaut, 2004). This raises the question whether the basic processes involved in these ENSO theories are still appropriate to describe the features of the recently-evidenced “new” CP type of El Niño. One of the leading theories which we analyzed in this study is the recharge-discharge (RD) oscillator paradigm.

The recharge and discharge can be measured as changes of sea level and related Warm (>20°C) Water Volume (WWV) in the equatorial band. Using an agglomerative hierarchical clustering (AHC) procedure, we first characterize the eastern Pacific (EP) and CP El Niño signal using 1993-2010 SLA derived from satellite altimetry. The EP El Niño signature shows a zonal seesaw with positive anomalies in the eastern Pacific and negative anomalies in the western Pacific. This is similar to the findings of Alory and Delcroix (2002; and references therein) who found this as the dominant signal using a multivariate EOF analysis on SLA but for a shorter period. The CP El Niño (La Niña) pattern is reminiscent of a mass recharge (discharge) in the central Pacific while a western-central equatorial and SPCZ discharge characterizes the after EP El Niño signal. This later signal occurs once only during 1993-2010 – after the very strong EP El Niño in 1997-98, and represents a mass discharge of warm waters. We find basically the same ENSO signatures using the AHC procedure complemented with an analysis of 3-month composites of EP and CP El Niño events when studying the 1958-2007 WWV computed directly from the DRAKKAR model product.

The previous and present results show that changes in WWV of an equatorial box (5°S-5°N) result chiefly from the horizontal transports computed above the 20°C isotherm depth across the box boundaries. The transports at play during the recharge-discharge process were then analyzed, contrasting the EP and CP transport characteristics. This was done by regressing the meridional and zonal transports entering the equatorial band with the Niño Cold Tongue (N_{CT}) and Niño Warm Pool (N_{WP}) indices (Ren and Jin, 2011). Our findings indicate that

there is a mass discharge (recharge) over the entire equatorial band occurring during EP El Niño (La Niña), in line with the recharge-discharge paradigm proposed by [Jin \(1997\)](#), with the meridional geostrophic transports being more pronounced across 5°S than at 5°N.

The CP ENSO signature is drastically different in terms of recharge-discharge and related horizontal transports. Interestingly, it shows both a recharge and discharge occurring simultaneously. During CP El Niño, there is a recharge of the equatorial band in the eastern Pacific and a discharge in the western Pacific. This creates a compensating effect which results in a reduced recharge-discharge during CP El Niño as when compared to EP El Niño. Part of these results were also found in the works of [Hasegawa et al. \(2006\)](#) who contrasted the discharge of the equatorial heat content in terms of ‘A-type’ and ‘B-type’ El Niño events based on subsurface ocean temperature dataset for the 1955-2003 period, and in the works of [Kug et al. \(2009; 2010\)](#) based on composite analysis of sea level and heat content from reanalysis data for the 1970-2005 period and a 500-year preindustrial simulation from a coupled global circulation model, respectively.

The zonal total transport of warm waters is eastward (westward) during EP El Niño (La Niña) over most of the equatorial region; In contrast, that transport in the equatorial band shows a convergence during CP El Niño occurring in the central basin at around 170°W. Similar results for the mixed layer zonal currents were found by [Kug et al. \(2009\)](#) and [Singh et al. \(2011\)](#) using assimilated and observed data for the 1980-2005 and 1992-2008 periods, respectively.

From our results, it is tempting to conclude that the recharge-discharge oscillator proposed by [Jin \(1997\)](#) does not apply to CP El Niño. This is probably the reason why CP El Niño is not followed by La Niña events, in contrast to EP El Niño which are followed by La Niña ([Kug et al., 2009](#)). The different behaviors of the RD oscillator during EP and CP El Niño raise interesting and open questions. As far as the RD oscillator paradigm is concerned, should CP El Niño events be called “El Niño” events? What are the origins of the different EP and CP El Niño discharge processes? How is it related to the location of SST anomalies ([Larkin and Harrison, 2005a,b](#); [Kug et al., 2010](#)) and zonal wind stress anomalies ([Kug et al., 2009](#)) and consequently different equatorial Kelvin and Rossby wave signatures that modify the zonal thermocline slope and so the geostrophic RD processes ([Bosc and Delcroix, 2008](#); [Dewitte et al., 2012](#); their Fig. 5)? Is the CP signature an intrinsic part of ENSO, a possible special case

of the unified oscillator (Wang, 2001), and/or an expression of the global warming signal (Yeh *et al.*, 2011)? Why do we reach different conclusions regarding the ability to predict EP and CP El Niño events (Hendon *et al.*, 2009; Kim *et al.*, 2009)? How is the predictability of recent CP ENSO events influenced by the reduced amplitude of WWV (Horii *et al.*, 2012; McPhaden, 2012)? These are questions that remain to be answered in addition to testing the relevance of the other oscillator theories to account for CP El Niño features.

Acknowledgements

This work is a contribution to the Solwara proposal supported by the French ANR. We benefited from freely available datasets, including SLA from Aviso (<http://www.aviso.oceanobs.com/en/data/products/sea-surface-height-products/global/msla>), WWV from PMEL (<http://www.pmel.noaa.gov/tao/elNiño/wwv/>), gridded Hadley Centre Sea Ice and Sea Surface Temperature dataset (<http://www.metoffice.gov.uk/hadobs/hadisst/>), and the SODA assimilation dataset (http://soda.tamu.edu/assim/SODA_2.2.4/). We do thank B. Barnier and J.-M. Molines from LEGI, Grenoble, for making available the latest DRAKKAR model output. Comments from S. Cravatte were appreciated. One of us (A.S.) benefits from a PhD grant from the French Institut de Recherche pour le Développement (IRD).

4.6 References

- Alory, G., Delcroix, T. (2002). Interannual sea level changes and associated mass transports in the tropical Pacific from TOPEX/Poseidon data and linear model results (1964-1999), *Journal of Geophysical Research*, **107**(C10), 1-22, doi:10.1029/2001JC001067.
- Ashok, K., Behera, S. K., Rao, S. A., Weng, H., Yamagata, T. (2007). El Niño Modoki and its possible teleconnections, *Journal of Geophysical Research*, **112**(C11), 1-27, doi:10.1029/2006JC003798.
- Barnier, B., Madec, G., Penduff, T., Molines, J. -M., Treguier, A. -M., le Sommer, J., Beckmann, A., Biastoch, A., Böning, C., Dengg, J., Derval, C., Durand, E., Gulev, S., Remy, E., Talandier, C., Theetten, S., Maltrud, M., McClean, J., de Cuevas, B. (2006). Impact of partial steps and momentum advection schemes in a global ocean circulation model at eddy-permitting resolution, *Ocean Dynamics*, **56**, 543-567, doi:10.1007/s10236-006-0082-1.
- Bosc, C., Delcroix, T. (2008). Observed equatorial Rossby waves and ENSO-related warm water volume changes in the equatorial Pacific Ocean, *Journal of Geophysical Research*, **113**(C6), 1-14, doi:10.1029/2007JC004613.
- Brown, J. N., Fedorov, A. V. (2010). Estimating the diapycnal transport contribution to warm water volume variations in the tropical Pacific Ocean, *Journal of Climate*, **23**(2), 221-237, doi:10.1175/2009JCLI2347.1.
- Carton, J. A., Giese, B. S. (2008). A reanalysis of ocean climate using Simple Ocean Data Assimilation (SODA), *Monthly Weather Review*, **136**(8), 2999-3017, doi:10.1175/2007MWR1978.1.
- Clarke, A. J. (2008). *An introduction to the dynamics of El Niño and the Southern Oscillation*, Academic Press, London.
- Clarke, A. J., van Gorder, S., Colantuono, G. (2007). Wind stress curl and ENSO discharge/recharge in the equatorial Pacific, *Journal of Physical Oceanography*, **37**(4), 1077, doi:10.1175/JPO3035.1.
-

- Dewitte, B., Vasquez-Cuervo, J., Goubanova, K., Illig, S., Takahashi, K., Cambon, G., Purca, S., Correa, D., Gutierrez, D., Sifeddine, A., Ortlieb, L. (2012). Change in El Niño flavours over 1958-2008: Implications for the long-term trend of the upwelling off Peru, *Deep Sea Research II*, doi:10.1016/j.dsr2.2012.04.011.
- Ducet, N., le Traon, P., Y., Reverdin, G. (2000). Global high-resolution mapping of ocean circulation from TOPEX/Poseidon and ERS-1 and -2, *Journal of Geophysical Research*, **105**(C8), 19477-19498, doi:10.1029/2000JC900063.
- Hasegawa, T., Horii, T., Hanawa, K. (2006). Two different features of discharge of equatorial upper ocean heat content related to El Niño events, *Geophysical Research Letters*, **33**, L02609, doi:10.1029/2005GL024832.
- Hendon, H. H., Lim, E., Wang, G., Alves, O., Hudson, D. (2009). Prospects for predicting two flavors of El Niño, *Geophysical Research Letters*, **36**, 1-6, doi:10.1029/2009GL040100.
- Horii, T., Ueki, I., Hanawa, K. (2012). Breakdown of ENSO predictors in the 2000s: Decadal changes of recharge/discharge-SST phase relation and atmospheric intraseasonal forcing, *Geophysical Research Letters*, **39**, L10707, doi: 10.1029/2012GL051740.
- Jin, F. -F. (1997). An equatorial ocean recharge paradigm for ENSO. Part I: Conceptual model, *Journal of the Atmospheric Sciences*, **54**(7), 811-829, doi:10.1175/1520-0469(1997)054<0811:AEORPF>2.0.CO;2.
- Kao, H. -Y., Yu, J. -Y. (2009). Contrasting Eastern-Pacific and Central-Pacific types of ENSO, *Journal of Climate*, **22**(3), 615-632, doi:10.1175/2008JCLI2309.1.
- Kug, J. -S., Choi, J., An, S. -I., Jin, F. -F., Wittenberg, A. T. (2010). Warm Pool and Cold Tongue El Niño events as simulated by the GFDL 2.1 Coupled GCM, *Journal of Climate*, **23**(5), 1226-1239, doi:10.1175/2009JCLI3293.1.
- Kug, J. -S., Jin, F. -F., An, S. -I. (2009). Two types of El Niño Events: Cold Tongue El Niño and Warm Pool El Niño, *Journal of Climate*, **22**(6), 1499-1515, doi:10.1175/2008JCLI2624.1.
-

- Larkin, N. K., Harrison, D. E. (2005). Global seasonal temperature and precipitation anomalies during El Niño autumn and winter, *Geophysical Research Letters*, **32**(16), 1-4, doi:10.1029/2005GL022860.
- Lengaigne, M., Hausmann, U., Madec, G., Menkes, C., Vialard, J., Molines, J. M. (2012). Mechanisms controlling warm water volume interannual variations in the equatorial Pacific: diabatic versus adiabatic processes, *Climate Dynamics*, **38**, 1031-1046, doi:10.1007/s00382-011-1051-z.
- McPhaden, M. J. (2003). Tropical Pacific Ocean heat content variations and ENSO persistence barriers, *Geophysical Research Letters*, **30**(9), 1-4, doi:10.1029/2003GL016872.
- McPhaden, M. J. (2012). A 21st century shift in the relationship between ENSO SST and warm water volume anomalies, *Geophysical Research Letters*, **39**, 1-5, doi:10.1029/2012GL051826.
- McPhaden, M. J., Zebiak, S. E., Glantz, M. H. (2006). ENSO as an integrating concept in Earth Science, *Science*, **314**(5806), 1740-1745, doi:10.1126/science.1132588.
- Mechoso, C. R., Neelin, J. D., Yu, J. -Y. (2003). Testing simple models of ENSO, *Journal of the Atmospheric Sciences*, **60**(2), 305-318, doi:10.1175/1520-0469(2003)060<0305:TSMOE>2.0.CO;2.
- Meinen, C. S. (2005). Meridional extent and interannual variability of the Pacific Ocean tropical-subtropical warm water exchange, *Journal of Physical Oceanography*, **35**(3), 323-335, doi:10.1175/JPO-2694.1.
- Meinen, C. S., McPhaden, M. J. (2000). Observations of warm water volume changes in the equatorial Pacific and their relationship to El Niño and La Niña, *Journal of Climate*, **13**(20), 3551-3559, doi:10.1175/1520-0442(2000)013<3551:OOWWVC>2.0.CO;2.
- Meinen, C. S., McPhaden, M. J. (2001). Interannual variability in warm water volume transports in the equatorial Pacific during 1993-99, *Journal of Physical Oceanography*, **31**(5), 1324-1345, doi:10.1175/1520-0485(2001)031<1324:IVIWWV>2.0.CO;2.

- Philander, S. G. (1990). *El Niño, La Niña, and the Southern Oscillation*, Academic Press, San Diego.
- Picaut, J., Hackert, E., Busalacchi, A. J., Murtugudde, R., Lagerloef, G. S. E. (2002). Mechanisms of the 1997-1998 El Niño-La Niña, as inferred from space-based observations, *Journal of Geophysical Research*, **107**(C5), 1-16, doi:10.1029/2001JC000850.
- Picaut, J., Ioualalen, M., Menkes, C., Delcroix, T., McPhaden, M. J. (1996). Mechanism of the zonal displacements of the Pacific warm pool: Implications for ENSO, *Science*, **274**(5292), 1486-1489, doi: 10.1126/science.274.5292.1486.
- Radenac, M. -H., Léger, F., Singh, A., Delcroix, T. (2012). Sea surface chlorophyll signature in the tropical Pacific during Eastern and Central Pacific ENSO events, *Journal of Geophysical Research*, **117**, 1-15, doi:10.1029/2011JC007841.
- Rasmusson, E. M., Carpenter, T. H. (1982). Variations in tropical sea surface temperature and surface wind fields associated with the Southern Oscillation/El Niño, *Monthly Weather Review*, **110**(5), 354-384, doi:10.1175/1520-0493(1982)110<0354:VITSST>2.0.CO;2.
- Rayner, N. A., Parker, D. E., Horton, E. B., Folland, C. K., Alexander, L. V., Rowell, D. P., Kent, E. C., Kaplan, A. (2003). Global analyses of sea surface temperature, sea ice, and night marine air temperature since the late nineteenth century, *Journal of Geophysical Research*, **108**(D14), 1-22, doi:10.1029/2002JD002670.
- Ren, H. -L., Jin, F. -F. (2011). Niño indices for two types of ENSO, *Geophysical Research Letters*, **38**, 1-5, doi:10.1029/2010GL046031.
- Singh, A., Delcroix, T., Cravatte, S. (2011). Contrasting the flavors of El Niño-Southern Oscillation using sea surface salinity observations, *Journal of Geophysical Research*, **116**, 1-16, doi:10.1029/2010JC006862.
- van Oldenborgh, G. J., Philip, S. Y., Collins, M. (2005). El Niño in a changing climate: A multi-model study, *Ocean Science*, **1**, 81-95.

- Vincent, E. M., Lengaigne, M., Menkes, C. E., Jourdain, N. C., Marchesiello, P., Madec, G. (2009). Interannual variability of the South Pacific Convergence Zone and implications for tropical cyclone genesis, *Climate Dynamics*, **36**, 1-16, doi:10.1007/s00382-009-0716-3.
- Wang, C. (2001). A Unified Oscillator Model for the El Niño-Southern Oscillation, *Journal of Climate*, **14**, 98-115, doi:10.1175/1520-0442(2001)014<0098:AUOMFT>2.0.CO;2.
- Wang, C., Picaut, J. (2004). Understanding ENSO Physics – A review, *Geophysical Monograph Series*, **147**, 21-48.
- Weng, H., Ashok, K., Behera, S. K., Rao, S. A., Yamagata, T. (2007). Impacts of recent El Niño Modoki on dry/wet conditions in the Pacific rim during boreal summer, *Climate Dynamics*, **29**, 113-129, doi:10.1007/s00382-007-0234-0.
- Wyrtki, K. (1981). An estimate of equatorial upwelling in the Pacific, *Journal of Physical Oceanography*, **11**(9), 1205-1214, doi:10.1175/1520-0485(1981)011<1205:AEOEUI>2.0.CO;2.
- Wyrtki, K. (1985). Water displacements in the Pacific and the genesis of El Niño cycles, *Journal of Geophysical Research*, **90**(NC4), 7129-7132, doi:10.1029/JC090iC04p07129.
- Wyrtki, K., Kilonsky, B. (1984). Mean water and current structure during the Hawaii-to-Tahiti shuttle experiment, *Journal of Physical Oceanography*, **14**(2), 242-254, doi:10.1175/1520-0485(1984)014<0242:MWACSD>2.0.CO;2.
- Yeh, S. -W., Kug, J. -S., Dewitte, B., Kwon, M. -H., Kirtman, B. P., Jin, F. -F. (2009). El Niño in a changing climate, *Nature*, **461**(7263), 511-514, doi:10.1038/nature08316.
- Yeh, S. -W., Kirtman, B. P., Kug, J. -S., Park, W., Latif, M. (2011). Natural variability of the central Pacific El Niño event on multi-centennial timescales, *Geophysical Research Letters*, **38**, L02704, doi:10.1029/2010GL045886.

Supplementary Material

The following figures are supplementary material for the manuscript above. The explanations and links to the manuscript are detailed in the figure captions.

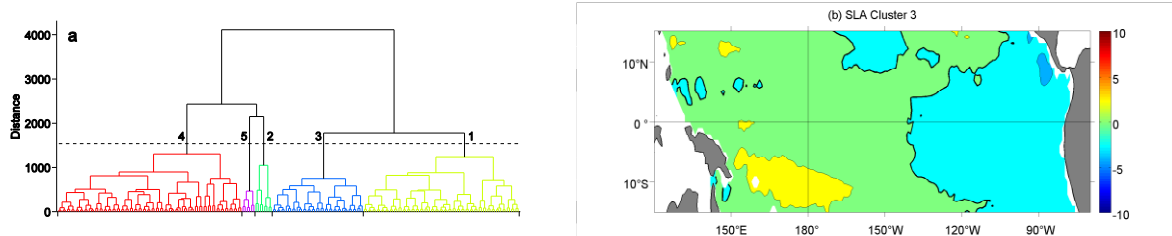


Figure 4.S2 (a) Dendrogram resulting from the AHC performed on SL anomalies for the period 1993-2010 in Fig. 4.3. The ordinate labels the inter-cluster distance. The dashed line indicates the cutting level ensuing in five clusters being identified. (b) Spatial pattern from the AHC on SLA denoting neutral conditions. Thick black contour lines in the spatial pattern denote the 0 line. Units in the spatial pattern are in cm.

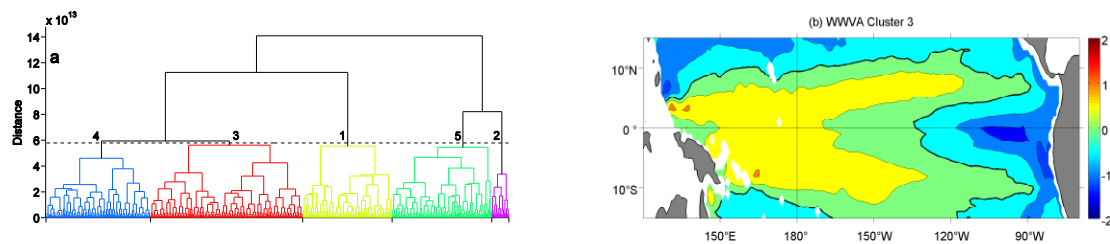


Figure 4.S3 (a) Dendrogram resulting from the AHC performed on WWV anomalies derived using DRAKKAR modeled data for the period 1958-2007 in Fig. 4.4. The ordinate labels the inter-cluster distance. The dashed line indicates the cutting level ensuing in five clusters being identified. (b) Spatial pattern from the AHC on SLA denoting neutral conditions. Thick black contour lines in the spatial pattern denote the 0 line. Units in the spatial pattern are in m^3 .

Chapter 5

Estimating trends due to ENSO

5.1 Introduction

The scientific rationale for estimating trends due to ENSO is reminded in Chapter 1. In line with this, the present chapter roots on the results presented in [Singh and Delcroix \(2011\)](#) attached at the end of this chapter. These authors attempt to distinguish the respective contributions of the different flavors of ENSO, which were detailed in the Chapter 3, on the long-term SSS trends observed in the tropical Pacific over the past 50 years making use of in situ SSS measurements. A simple linear regression model was used for this analysis and here, as a complement, we make use of this method to determine the contributions of EP and CP ENSO on the long-term SST and SL trends.

5.2 Trends due to ENSO: A multivariate linear regression approach

Various methods can be used to isolate the effects of ENSO from the long-term trends. As summarized in [Singh and Delcroix \(2011\)](#), probably the most frequently used method to capture the ENSO component is based on least squares linear regression, lagged or not, onto ENSO indices (e.g., [Jones, 1989](#); [Kelly and Jones, 1996](#); [Cane *et al.*, 1997](#); [Latif *et al.*, 1997](#); [Santer *et al.*, 2001](#); [Solomon and Newman, 2011](#)). Another way could be to first band-pass filter the data in an assumed 2- to 7-year ENSO band to remove the high and low frequency variability, respectively, and then to perform an EOF analysis to obtain (and further filter out) the ENSO signal (e.g., [Cane *et al.*, 1997](#)). However, this method assumes that the entire ENSO signal is contained within the 2-7 year band, and none outside it. Moreover, using an EOF analysis may result in leakage of the signal (e.g., [Singh *et al.*, 2011](#); [Radenac *et al.*, 2012](#)), especially with the trends being spread over several modes. To resolve this issue, a trend-EOF analysis ([Hannachi, 2007](#)) could be used, which involves an EOF performed on the time positions of the sorted observations (inverted ranks) rather than on direct observations. The result is a dominant mode which displays the space-time pattern of the long-term non-linear trend present in the data. Higher modes reflect the remaining dominant

signals (e.g., ENSO) but may have non-significant trends present in their principle components (e.g., [Barbosa and Andersen, 2009](#)). Initial tests show that an EOF performed after removing a *linear* trend (as shown in Chapter 3) has results similar to those when an EOF is performed with the *non-linear* trend (obtained from trend-EOF) removed. An alternative but more sophisticated approach would be to identify ENSO using dynamical eigenvectors that are most important in the observed evolution of ENSO events, as was proposed by [Compo and Sardeshmukh \(2010\)](#) on tropical SST evolution. These authors argue that ENSO should be viewed as a dynamical process rather than just a “number” (e.g., SST anomalies in the Niño3.4 region).

None of these methods are fully satisfactory (see [Compo and Sardeshmukh, 2010](#)). Hence, for the sake of simplicity, we choose to use a simple multivariate linear regression model (see [Amemiya, 1974](#)) which will further allow us to tentatively isolate the respective impacts of CP and EP ENSO events. Similar regression models have been used in climate studies before, for example, [Lean and Rind \(2008\)](#) used multiple regression to distinguish the simultaneous effects of natural (ENSO, volcanic aerosols and solar irradiance) and anthropogenic forcing on surface temperatures for the period 1889-2006, [Fyfe et al. \(2011\)](#) predicted decadal trends in global mean surface temperature during 1961-2010 using multivariate regression on dynamically induced atmospheric variability, ENSO, and the effects of explosive volcanic eruptions, and [Izumo et al. \(2010\)](#) used bilinear regression to estimate the contribution of warm water volume (WWV) and the Indian Ocean Dipole (IOD) on ENSO over the 1981-2009 period.

The multivariate least squares linear regression technique is used to isolate the respective effects of EP and CP ENSO on SST, SSS and SL from the long-term variability. We use N_{CT} and N_{WP} indices to distinguish between EP and CP ENSO as they are almost orthogonal at zero lag (see Chapter 2). The anomalies of SST, SSS and SL were first calculated with respect to the mean monthly climatology, computed over 1971-2000 for SST and SSS, and over 1993-2010 (1971-2000) for SL derived from Aviso (SODA and DRAKKAR). All anomalies were then regressed onto a linear function of time, N_{CT} and N_{WP} using [Eq. 5.1](#).

$$\underbrace{Var_{x,y}(t)}_I = \underbrace{\alpha_{x,y}.t}_II + \underbrace{\beta_{x,y}.N_{CT}(t-\Delta t)}_III + \underbrace{\gamma_{x,y}.N_{WP}(t-\Delta t)}_IV + \underbrace{\xi_{x,y}}_V \quad (5.1)$$

where $Var_{x,y}$ are the SST, SSS or SL anomalies at any point (x,y) , α , β and γ are the coefficients obtained after regressing $Var_{x,y}$ onto time t , N_{CT} and N_{WP} , respectively, Δt represents the lag between $Var_{x,y}$ and the ENSO indices, ζ are the residuals obtained from the regression analysis and k is a constant. Trends at each grid point were then calculated for terms I to V in Eq. 5.1, which we will refer to as the overall, non-ENSO, EP-ENSO, CP-ENSO and residual trends, respectively. A Student's t -test was also performed on the trends to test their significance at the 95% confidence level.

5.2.1 SST

The multivariate linear regression for SST covers the period 1955-2008. The value of Δt in Eq. 5.1 was set to zero to indicate no lag between SST and the ENSO indices. The values of the regression coefficients β and γ , denoting the EP and CP ENSO signatures in SST, respectively, indicates an increase of SST concentrated in the eastern-to-central and central equatorial Pacific region during EP and CP El Niño events, respectively, and vice versa during La Niña events (Fig. 5.1). These SST changes reflect the well-known spatial signatures of EP and CP ENSO, as expected, and are remarkably similar to those obtained from the combined regression-EOF analysis on SST anomalies in Fig. 3.2. This reinforces our confidence in the use of the multivariate regression technique to isolate the respective effects of EP and CP ENSO on the long-term warming/cooling trends in the tropical Pacific.

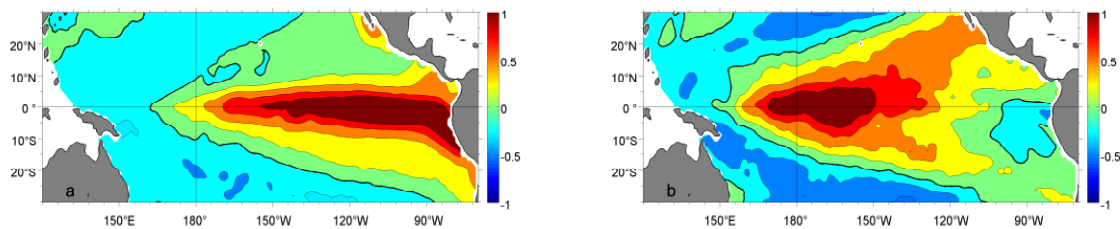


Figure 5.1 Coefficient estimates of (a) β and (b) γ after regressing SST anomalies with N_{CT} and N_{WP} indices, respectively (see Eq. 5.1). Positive values thus indicate an increase of SST during EP or CP El Niño events and vice versa during La Niña events. There are no units for these coefficient estimates as the coefficients are proportional to N_{CT} and N_{WP} . Thick black contour lines in the spatial patterns denote the 0 line.

The trends obtained from terms I to IV in Eq. 5.1 are shown in Fig. 5.2, while the trends obtained from residual term are not shown because they cannot be physically explained and are not significant at the 95% confidence level. It should be noted that the EP ENSO trends are also not significant at the 95% confidence level. The trends due to CP ENSO show maximum warming reaching magnitudes of $0.4 \text{ }^\circ\text{C}/50 \text{ years}$ in the central basin and are

similar in pattern to the CP ENSO signature in SST (Fig. 3.2c). The non-significant effect of the EP ENSO trends is evident in the overall (EP+CP) ENSO trends pattern, which prominently reflects the trends due to CP ENSO. The non-ENSO long-term trends are very similar to the overall trends (with/without the residuals and/or ENSO terms) with maximum warming in the western Pacific warm pool and SPCZ regions and in the eastern basin north and south of the equator. Non-ENSO long-term cooling trends (up to -0.75 °C/50 years) are observed in the central-eastern equatorial Pacific. The existence of this non-ENSO long-term cooling trends in the meridionally confined region of the eastern equatorial Pacific has been shown by various authors using different datasets, methods and/or periods of analysis (e.g., Lau and Weng, 1999; Chen *et al.*, 2008; Guan and Nigam, 2008; Barbosa and Andersen, 2009; Cravatte *et al.*, 2009). Clement *et al.* (1996) and Cane *et al.* (1997) attribute these cooling trends to be a coupled response to uniform radiative forcing while Compo and Sardeshmukh (2010) attributes them to an enhancement of surface easterlies (therefore strengthening of the Walker circulation) and equatorial upwelling over the eastern Pacific in response to the strong ENSO-unrelated recent warming of the Indian and west Pacific Oceans. Whatever the cause, it is clear from the present results that the ENSO-related warming trends, chiefly attributable to CP ENSO, act to compensate these long-term cooling trends observed in the central-eastern equatorial Pacific. However, the period over which the trends are calculated should be kept in mind.

Using 30-year running trends of SSS anomalies in predefined boxes encompassing the warm pool and SPCZ regions, Singh and Delcroix (2011) illustrated that linear trends are sensitive over the period in which they are calculated, as expected. We perform a similar analysis with SST anomalies in the Niño3 and Niño4 regions where we observe contrasting results in the long-term trends. The results (Fig. 5.3) show warming trends in the Niño4 region, except in the early part of the record. The Niño3 region also shows warming trends, however, there is a hint that the sign of the trends change in the early 1990s. The reason for this change in the behavior of trends, if confirmed with ongoing data collection, is not analyzed here and clearly deserves further investigation. The changing amplitude and sign of the trends, from -0.5 to 1 °C/50 years, warns us that our present results, although based on rather long record lengths, may change and thus should be viewed with caution when choosing different time periods (Singh and Delcroix, 2011).

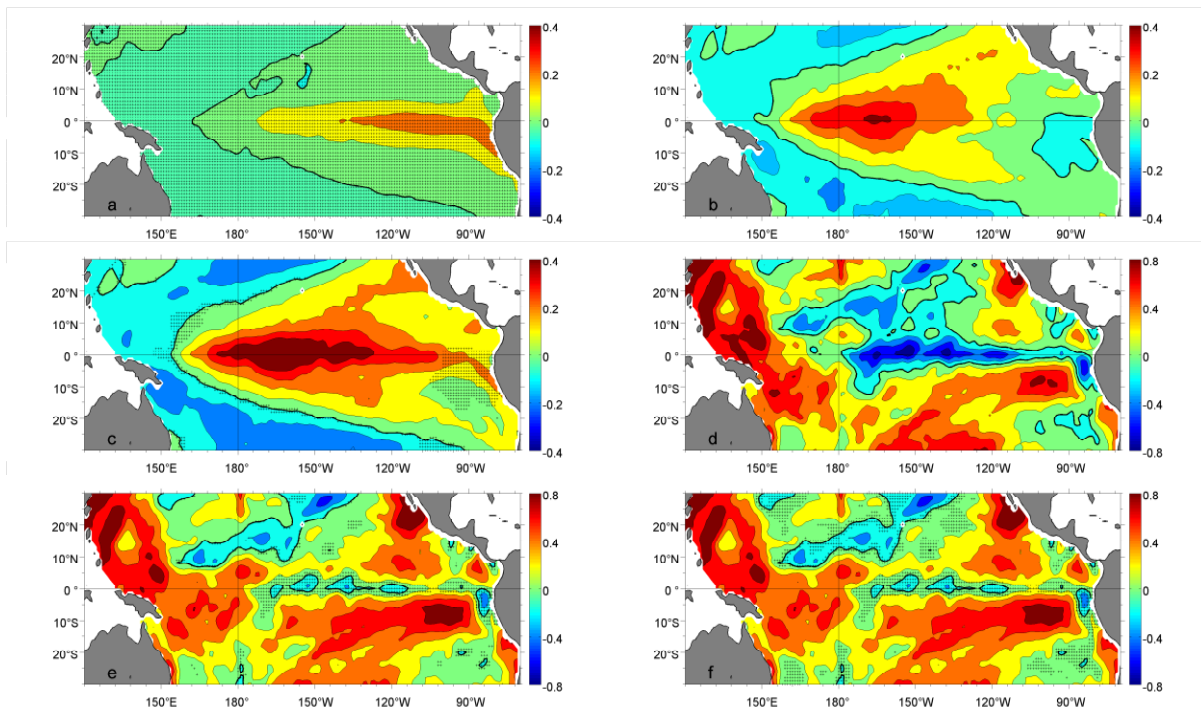


Figure 5.2 Linear trends in SST anomalies over the 1955-2008 period due to (a) EP ENSO, (b) CP ENSO, (c) EP and CP ENSO, (d) non-ENSO long-term variability, (e) EP and CP ENSO and non-ENSO long-term variability, and (f) overall long-term variability. Units are $^{\circ}\text{C}/50$ years. Regions where the trends are not significant at the 95% confidence level are hatched. Thick black contour lines in the spatial patterns denote the 0 line. Note the different color scales in the plots.

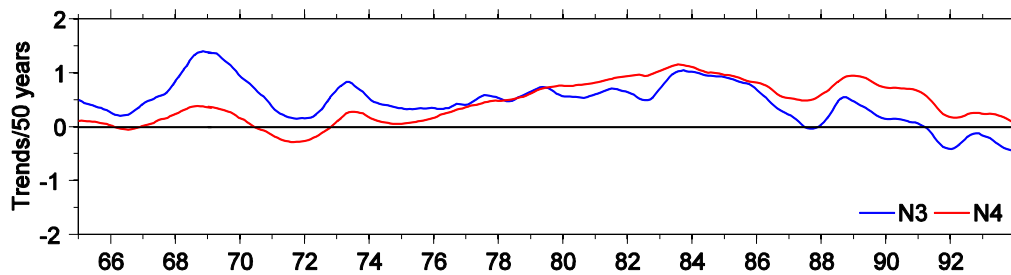


Figure 5.3 30-year running trends of mean SST anomalies in the Niño3 (150°W - 90°W , 5°S - 5°N ; in blue) and Niño4 (160°E - 150°W , 5°S - 5°N ; in red) regions over the 1950-2008 period. Units are $^{\circ}\text{C}/50$ years.

5.2.2 SSS

We apply the multivariate regression technique used in the previous section for SST to SSS data. Because information about data density is available for the SSS gridded product, a shifted pentad method was employed in calculating the trends. The results and discussion of this analysis is detailed in [Singh and Delcroix \(2011\)](#) attached at the end of this chapter. The trends due to EP ENSO and (EP+CP) ENSO, which were not shown in the above manuscript, are illustrated in [Fig. 5.4](#). The peculiar looking EP ENSO trends pattern is most likely a

consequence of the varying SSS data density over time (see [Delcroix *et al.*, 2005; 2007; 2011](#)).

Most importantly, in the above study we show the influence of EP ENSO events to be negligible, while CP El Niño events contribute to enhance the long-term freshening trends (up to 30%) in the far western equatorial Pacific and moderately reduce that freshening (up to 10%) in the SPCZ region. Our results thus suggest that the observed eastward expansion of the surface covered by low-salinity waters in the western half of the tropical Pacific ([Cravatte *et al.*, 2009](#)) is most likely due to climate change rather than to the documented possible increased occurrence and intensity of CP El Niño events (e.g., [Lee and McPhaden, 2010](#)).

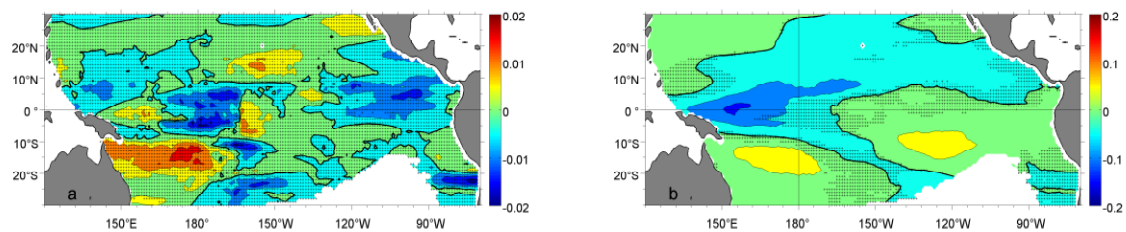


Figure 5.4 Linear trends in SSS anomalies over the 1955-2008 period due to (a) EP ENSO and (b) EP and CP ENSO. Units are pss/50 years. Regions where the trends are not significant at the 95% confidence level are hatched. Thick black contour lines in the spatial patterns denote the 0 line. Note the different color scales in the plots.

5.2.3 SL

We use the multivariate regression model with Δt set to zero in [Eq. 5.1](#) to estimate the effects of EP and CP ENSO on the long-term trends in SL over the tropical Pacific region. As expected, the spatial patterns of the regression coefficients ([Fig. 5.5](#)) for both EP and CP ENSO (discussed in detail in Chapter 3) are similar to the patterns obtained from the combined regression-EOF analysis on SL anomalies derived from Aviso (see [Fig. 3.8](#)). However, minor differences in the magnitude of the trends are apparent between the SL obtained from the Aviso, SODA and DRAKKAR products, keeping in mind that they were computed over different periods.

From the multivariate regression analysis, the SL trends ([Fig. 5.6](#)) due to EP and/or CP ENSO using the Aviso product are not significant at the 95% confidence level over the 1993-2010 period. However, it should be noted that the trends due to EP ENSO are positive (negative) in the western (eastern) tropical Pacific while the trends due to CP ENSO are almost an order of magnitude less than the EP ENSO trends. A similar result is obtained

when using SST anomalies over the 1993-2008 period; the trends due to EP and/or CP ENSO are not significant and are reversed when compared to those observed during the 1955-2008 period (Fig. 5.2). Because of the non-significant effect of ENSO, the long-term non-ENSO SL trends closely resemble the overall trends, which show positive SL trends in the north- and south-western tropical Pacific contrasted by non-significant negative trends in the eastern equatorial Pacific. This overall trends pattern is similar to those obtained in various studies using a similar product but for different periods (e.g., Carton *et al.*, 2005; Qiu and Chen, 2006; Lee and McPhaden, 2008; Becker *et al.*, 2012). Some of these studies attribute a large fraction of the positive trends in the western Pacific to ENSO (e.g., Timmermann *et al.*, 2010), while others attribute it to an intensification of the Pacific trade winds (e.g., Merrifield and Maltrud, 2011). The non-ENSO long-term and overall trends are about an order of magnitude larger than the trends related to EP and/or CP ENSO. These results are consistent with those of Merrifield (2011) who used a similar multiple regression model and altimeter data over the 1993-2009 period to study the ENSO contribution to SL trends.

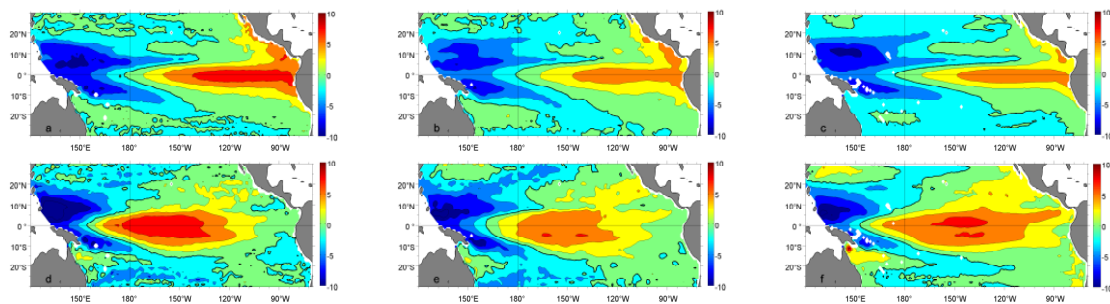


Figure 5.5 Coefficient estimates of β (top) and γ (bottom) after regressing SLA from (left column) Aviso over the 1993-2010 period, (middle column) SODA over the 1955-2008 period, and (right column) DRAKKAR over the 1958-2007 period with N_{CT} and N_{WP} indices, respectively (see Eq. 5.1). Positive values thus indicate an increase of SL during EP or CP El Niño events and vice versa during La Niña events. Units are $\text{cm } ^\circ\text{C}^{-1}$. Thick black contour lines in the spatial patterns denote the 0 line.

Using SL anomalies derived from SODA over the 1955-2008 and DRAKKAR over the 1958-2007 periods, we used the same multivariate regression analysis from above in an attempt to discriminate the effects of EP and CP ENSO on the long-term SL trends in the tropical Pacific. Prior to this, we performed a simple validation test involving SL derived from Aviso, SODA and DRAKKAR products being subjected to the multivariate regression analysis over their common period (1993-2007). The results (not shown) for each term in Eq. 5.1 are in agreement for all three products, which show similar spatial trend patterns and only slightly differ in the magnitude of the trends. Interestingly, the trends derived from SODA and

DRAKKAR are significant while those from Aviso are not. When the analysis period is extended back in time (i.e., prior to the AVISO period), the SL trend patterns from both the SODA and DRAKKAR products differ considerably from those obtained for the shorter Aviso record (Fig. 5.6; note the different color scales in the plots).

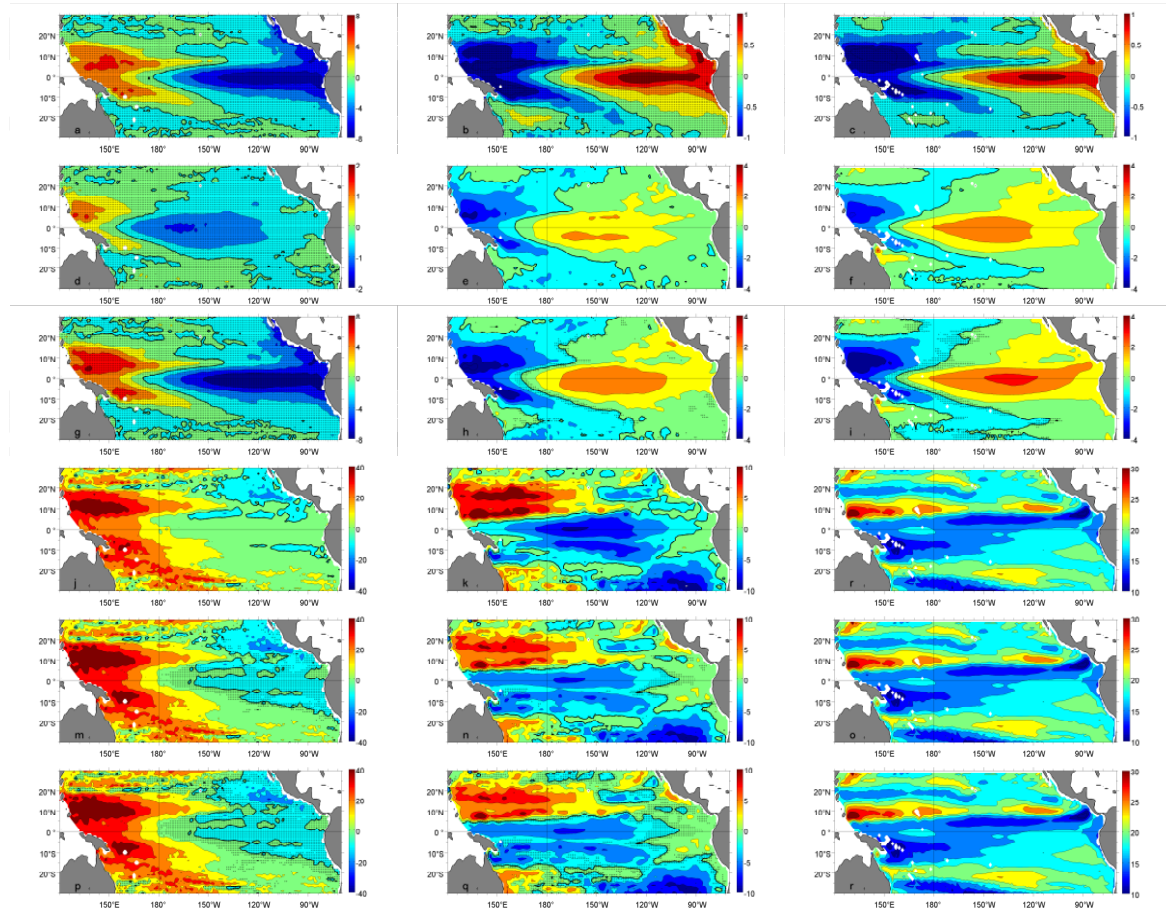


Figure 5.6 Linear trends in SL anomalies derived from (left column) Aviso over the 1993-2010 period, (middle column) SODA over the 1955-2008 period, and (right column) DRAKKAR over the 1958-2007 period due to (a-c) EP ENSO, (d-f) CP ENSO, (g-i) EP and CP ENSO, (j-l) non-ENSO long-term variability, (m-o) EP and CP ENSO and non-ENSO long-term variability, and (p-r) overall long-term variability. Units are cm/50 years. Regions where the trends are not significant at the 95% confidence level are hatched. Thick black contour lines in the spatial patterns denote the 0 line. Note the different color scales in the plots.

The trends due to EP ENSO over the extended periods from both the SODA and DRAKKAR products, although non-significant at the 95% significant level, show similar spatial patterns *but* with opposite signed trend values to those from the Aviso product. This is clearly a result of the different temporal lengths over which the analysis was performed. The same situation is obtained for the trends due to CP ENSO, except that they are significant at the 95% confidence level and therefore contains most, if not all, of the trends due to ENSO. The magnitude of the EP and/or CP ENSO trends from both SODA and DRAKKAR products are

comparable to each other. Interestingly, the non-ENSO long-term and overall trends show widespread increase in SL over the entire tropical Pacific region using the DRAKKAR product. This is not the case when using the SODA product, although the spatial trend patterns are somewhat consistent. This reminds us that the calculation of trends is sensitive to the product and period over which they are calculated (see Fig. 5.7).

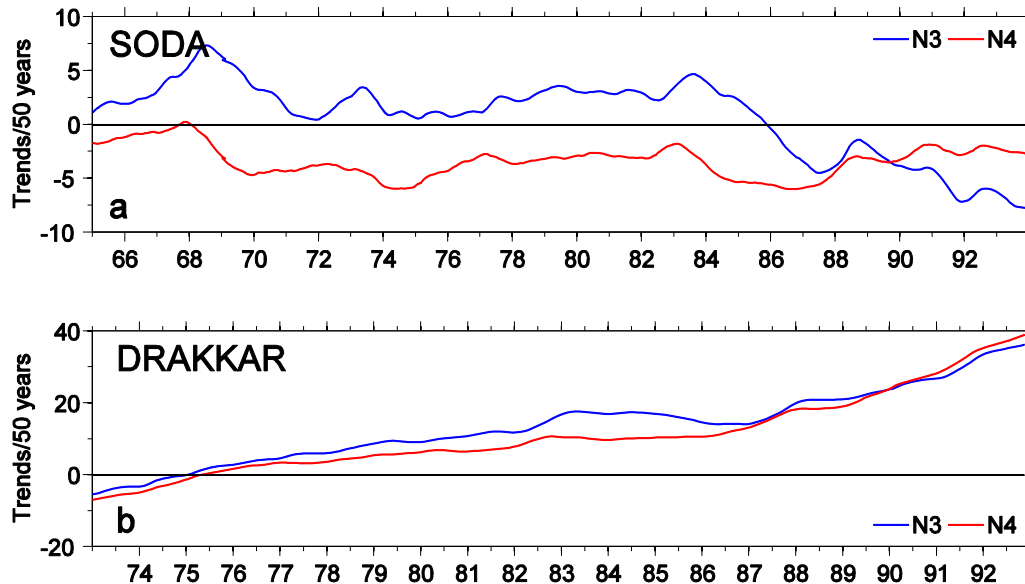


Figure 5.7 30-year running trends of mean SL anomalies derived from (a) SODA and (b) DRAKKAR in the Niño3 (150°W-90°W, 5°S-5°N; in blue) and Niño4 (160°E-150°W, 5°S-5°N; in red) regions over the 1950-2008 period in (a) and 1958-2007 period in (b). Units are cm/50 years.

Concentrating on results from the SODA product, non-ENSO long-term positive trends (>10 cm/50 years) are observed in the north western Pacific while negative trends of similar magnitude are evident between 20°S-5°N and in the southeast tropical Pacific region. Relatively weaker positive trends are observed in the eastern Pacific along the South American coast. The trends due to CP ENSO reduce the non-ENSO long-term trends in the northwestern and central Pacific regions by ~30%. This is reflected in the overall linear SL trends derived from SODA, which are consistent with those observed by [Timmermann *et al.* \(2010\)](#) using a different version of the SODA product for the period 1958-2001, and [Meysignac *et al.* \(2012\)](#) who used reconstructed SL over the 1950-2009 period. On one hand, the overall trends suggest a large scale zonal redistribution of mass in the equatorial band ([Timmermann *et al.*, 2010](#)) consistent with the ocean's response to the observed *weakening* of the Walker circulation ([Fedorov *et al.*, 2006](#); [Hansen *et al.*, 2006](#); [Vecchi *et al.*, 2006](#); [2008](#)). This is contrary to [Compo and Sardeshmukh \(2010\)](#) who hypothesized that the

observed cooling trend in the eastern equatorial Pacific (see Fig. 5.2) is due to *strengthening* of the Walker circulation (see Vecchi *et al.*, 2008 for a review of the tropical Pacific's response to global warming). On the other hand, the overall trends pattern for the entire tropical Pacific region suggests a meridional redistribution of mass with decreasing SL in the equatorial region and increasing SL in the off-equatorial regions. This spatial pattern is similar to the equatorial discharge process following an El Niño event (see Chapter 4).

5.3 Summary and Discussion

From the various simple and sophisticated methods available, we used multivariate linear regression analysis to discriminate trends due to ENSO and non-ENSO. We gain confidence in the simple regression analysis as it corroborates the different impacts of the EP and CP ENSO on SST, SSS and SL obtained from previous studies (also shown in Chapter 3). We used observational data covering the period 1955-2008 for SST and SSS and 1993-2010 for SL. To extend the SL time series, we also made use of the SODA and DRAKKAR model outputs. The contribution of the EP type of ENSO to the observed long-term SST, SSS and (modeled) SL anomaly trends was found to be insignificant in the tropical Pacific region. In comparison, the contribution of the CP type of ENSO was found to be significant for the observed SST and SSS and modeled SL anomaly trends. It is likely that the trends due to EP ENSO are negligible because EP El Niño events tend to be followed by La Niña events, while in contrast, CP El Niño events tend *not* to be followed by La Niña events (Kug *et al.*, 2009). The observed SL anomaly trends (from altimeter measurements) due to ENSO were found to be insignificant, probably due to the almost equal frequency distribution of El Niño and La Niña events over this short temporal data length (1993-2010). The long-term SL anomaly trends computed from the SODA and DRAKKAR model showed significant differences emphasizing the fact that trends are also sensitive to the product used besides their temporal lengths.

Results show that CP ENSO tends to reduce the observed long-term cooling trends in the central Pacific, and enhance the long-term freshening trends in the far western Pacific, by approximately 40% and 30%, respectively. This is consistent with the ~30% CP ENSO contribution to the positive long-term SL trends in the central Pacific region as deduced from SODA data. In addition, CP ENSO moderately reduces the saltening trends (up to 10%) in the SPCZ region. As a consequence, we can expect that the assumed increased frequency

(Yeh *et al.*, 2009) and intensity (Lee and McPhaden, 2010) of CP ENSO will strengthen the warming (freshening) trend in the central (far western) equatorial Pacific (and lessen it in the SPCZ region) in years to come. Accordingly, the expansion of the warm pool can be attributed to warming trends in the central Pacific due to CP ENSO. However, the eastward expansion of the fresh pool is *not* evident from the CP ENSO trends. Instead, the fresh pool expansion could be explained by the redistribution of SSS anomalies by mean advection and the theoretical increase of the hydrological cycle due to ocean warming (Cravatte *et al.*, 2009).

This study illustrates one possible way of estimating the contribution of the EP and CP ENSO signal to the long-term trends in SST, SSS and SL. Quoting Singh and Delcroix (2011) “it raises a number of issues. Firstly, the statistical analysis intentionally adopted here for the sake of simplicity is admittedly crude as it is based on regression of oceanic variables onto ENSO indices. It would be interesting to test more sophisticated methods as by Compo and Sardeshmukh (2010) on SSS to characterize the impacts of ENSO on the long-term salinity trends in the tropical Pacific, noting however, that these usually assumed that the dynamics of ENSO have remained unchanged, and this is probably not the case for the EP and CP types of ENSO. Secondly, it is worth noting that linear trends are very sensitive to the time-span over which they are computed. To illustrate that sensitivity, 30-year running trends were calculated for the different regions. A 30-year period is used as it has been adopted by the WMO to be the standard period for the estimation of climatic normals (WMO, 1989). In terms of SST, generally, warming trends are observed in the Niño3 and Niño4 regions over the 1950-2008 period. However, the amplitude of the warming trends change during that period and even the sign changes to cooling in the early 1990s in the Niño3 region. This could probably explain the long-term cooling trend observed in the eastern equatorial Pacific. For SSS, the trends clearly reflect a saltening before the mid-1970s and a freshening after that time in both the warm pool and SPCZ regions. It is not clear whether or not the reversed sign of the SSS trends is due to increased data density (Delcroix *et al.*, 2011), the climate shift of the late 1970s (Trenberth and Stepaniak, 2001), changes in ENSO property (Wang and An, 2001), increased occurrence and/or intensity of CP ENSO over EP ENSO (Lee and McPhaden, 2010), and/or phase reversal of the Pacific Decadal Oscillation (Mantua and Hare, 2002). Whatever its causes, this reversal in the pattern of trends warns us that our present results, although based on rather long record lengths (1955-2008), may change when choosing different time periods.”

5.4 Publication: Singh and Delcroix, 2011

The following article was published in *Geophysical Research Letters* in 2011 as part of this PhD thesis.

Singh, A., and Delcroix, T. (2011). Estimating the effects of ENSO upon the observed freshening trends of the western tropical Pacific Ocean, *Geophysical Research Letters*, **38**(L21607), doi:10.1029/2011GL049636.

Estimating the effects of ENSO upon the observed freshening trends of the western tropical Pacific Ocean

Awnesh Singh¹ and Thierry Delcroix¹

Received 9 September 2011; accepted 10 October 2011; published 8 November 2011.

[1] A significant surface freshening trend and an eastward expansion of fresh surface waters have been documented in the western tropical Pacific, consistent with the expected effects of climate change. The highest El Niño Southern Oscillation (ENSO) variability in Sea Surface Salinity (SSS) has been also documented in that region, with different quantitative signatures for the Eastern and Central Pacific ENSO events (EP and CP ENSO, respectively). This study hence analyses to what extent have the EP and CP ENSO events contributed to the long-term freshening trends, relying on 1955–2008 in situ SSS data and on EP and CP ENSO main features. We show the influence of EP ENSO events to be negligible, while CP El Niño events contribute to enhance the long-term freshening trend (up to 30%) in the far western equatorial Pacific and moderately reduce that freshening (up to 10%) in the South Pacific Convergence Zone (SPCZ). Our results thus suggest that the observed eastward expansion of the surface covered by low-salinity waters in the western half of the tropical Pacific is mostly due to climate change rather than to the documented possible increased occurrence and intensity of CP El Niño events. The sensitivity of the trend estimates to the different periodicity of the SSS data records is also discussed. **Citation:** Singh, A., and T. Delcroix (2011), Estimating the effects of ENSO upon the observed freshening trends of the western tropical Pacific Ocean, *Geophys. Res. Lett.*, 38, L21607, doi:10.1029/2011GL049636.

1. Introduction

[2] Estimates from a variety of data sources indicate that Sea Surface Temperature (SST) in the tropics and subtropics has increased by 0.4 to 1°C over the last 100 years [e.g., Deser *et al.*, 2010]. It is now unequivocal that causes of this warming trend are for the most part human activities which increase the amount of greenhouse gases in the atmosphere [Intergovernmental Panel on Climate Change, 2007]. Focusing on the tropical Pacific, the amplitude of that SST trend however differs from one region to another, and it was further shown to be sensitive to the used dataset and data span, as well as to the way low-frequency modes such as ENSO (El Niño Southern Oscillation) are considered (or not) in the computation. This proves especially visible in the eastern-central equatorial Pacific, the region of maximum ENSO variability in SST, where even the sign of the SST trend can vary depending on different data products and data processes

[e.g., Cravatte *et al.*, 2009, Table 1; Deser *et al.*, 2010, Figure 1; Compo and Sardeshmukh, 2010, Figure 8].

[3] Estimates of Sea Surface Salinity (SSS) trends are much less numerous than for SST, reflecting the relative paucity of in situ observations and the present shortness of the SMOS (Soil Moisture and Ocean Salinity) remotely-sensed SSS records. Yet, in the tropical Pacific, all studies analyzing multi-decadal SSS records (>30 years) agree on a freshening trend of the order of –0.1 to –0.4 pss over the last 50 years in the heavy precipitation regions of western Pacific warm pool and in the Inter-Tropical and South Pacific Convergence Zones (ITCZ and SPCZ, respectively [Delcroix *et al.*, 2007; Cravatte *et al.*, 2009; Durack and Wijffels, 2010; Terray *et al.*, 2011]). Interestingly, this freshening trend can be ascribed to climate change as it is found consistent with the expectation of a mean hydrological cycle increase in a warming world, in line with the wet-get-wetter paradigm [Held and Soden, 2006; Cravatte *et al.*, 2009; Terray *et al.*, 2011].

[4] The western Pacific warm pool and the SPCZ regions (and the ITCZ to a less extent), where we observed maximum freshening trends, are also regions of highest ENSO variability in SSS, with peak to peak anomalies of the order of 1 pss between El Niño and La Niña events [Delcroix and Hénin, 1991]. This raises the question as to what extent have fluctuations in the timing, amplitude, number, as well as the asymmetry of El Niño and La Niña events contributed, if any, to the observed freshening trend. That question is particularly relevant these days with the recent enhanced attention given to the two flavours of ENSO events, hereafter called Eastern and Central Pacific (EP and CP, respectively) ENSO, which have different signatures in SSS [Singh *et al.*, 2011] and were shown to potentially affect the interpretation of long-term trends in SST [Lee and McPhaden, 2010]. To answer the question, our study thus attempts to quantify the ENSO effects on long-term trends in SSS, as a possible input to the broad question of how to discriminate natural climate variability from mean climate change. The rest of the manuscript is organized as follows: section 2 describes the data and methods used to discriminate the EP and CP ENSO signature from long-term trends; section 3 describes the results; and a conclusion and discussion appear in section 4.

2. Data and Methods

[5] The SSS data were obtained from the 1° longitude by 1° latitude and 1 month gridded product of Delcroix *et al.* [2011] for the tropical Pacific region (30°S–30°N, 120°E–70°W) and from 1950 to 2008. Each grid point has an associated error indicating the confidence we can have on the SSS product. This error is given as a percentage of the interannual variance at that point. When there is no SSS data

¹LEGOS, UMR 5566, CNES, CNRS, IRD, Université de Toulouse, Toulouse, France.

available, the error is 100% and the SSS gridded value is equal to the monthly mean climatological SSS. Following Singh *et al.* [2011], we consider that we can trust the SSS gridded product value if the error is less than the 80% threshold.

[6] Various techniques have been used to discriminate the ENSO component from the long-term variability (assumed to be best represented by a linear trend). Maybe the most frequently used method to capture the ENSO component is based on least squares linear regression, lagged or not, onto ENSO indices. Some of the indices we found in the literature include the Southern Oscillation Index (SOI), the NINO3 or NINO4 SST anomalies, and the principal component(s) of Empirical Orthogonal Function (EOF) or Principal Oscillation Patterns (POP) analyses on tropical Pacific SST or 3-dimensional temperature, some indices being previously band-pass filtered [Jones, 1989; Kelly and Jones, 1996; Cane *et al.*, 1997; Latif *et al.*, 1997; Santer *et al.*, 2001; Solomon and Newman, 2011]. Other methods involve band-pass filters isolating ENSO periods (approximately within 2 to 7 years), so-called dynamic or thermodynamic models, and trend EOF analysis [Lau and Weng, 1999; Compo and Sardeshmukh, 2010; Thompson *et al.*, 2009; Barbosa and Andersen, 2009]. The long-term variability is then estimated by computing linear trends on the difference between the original record and the natural (ENSO) component(s). None of these methods are fully satisfactory [see Compo and Sardeshmukh, 2010]. Also, at the time of writing, none of the authors have diagnosed the respective impacts of the EP and CP ENSO on long term trends, with the exception of Lee and McPhaden [2010] who compared linear trends in SST for the eastern (NINO3) and western (NINO4) Pacific regions, respectively.

[7] For the sake of simplicity, we choose to use a simple multivariate least squares linear regression technique to isolate the respective effects of EP and CP ENSO on SSS from the long term variability. To distinguish between the EP and CP ENSO, we use the Niño Cold Tongue (N_{CT}) and Niño Warm Pool (N_{WP}) ENSO indices recently derived by Ren and Jin [2011]. As discussed by these authors, these new indices are the best suited to discriminate between EP and CP ENSO, especially because they are almost orthogonal in contrast to the NINO3 and NINO4 SST indices. SSS anomalies (SSSA) and N_{CT} and N_{WP} indices were first calculated relative to the 1971–2000 mean monthly climatology. The SSSA time series at each grid point (x,y) were then regressed onto a linear function of time, N_{CT} and N_{WP} for the period 1955–2008, using the following equation:

$$\underbrace{SSSA_{x,y}(t)}_I = \underbrace{\alpha_{x,y} \cdot t}_{II} + \underbrace{\beta_{x,y} \cdot N_{CT}(t - \Delta t)}_{III} + \underbrace{\gamma_{x,y} \cdot N_{WP}(t - \Delta t)}_{IV} + \underbrace{\xi_{x,y}}_V \quad (1)$$

where α , β , and γ are the coefficients obtained after regressing SSSA onto time t , N_{CT} and N_{WP} , respectively, Δt represents the lag between SSSA and the ENSO indices, and ξ is the residual obtained from the multivariate regression analysis. The lag Δt was derived from the analysis of Delcroix [1998] showing that the ENSO signature in SSS lags the one in SST by about 3 months; sensitivity tests show that using different Δt from 0 to 6 months does not significantly change our results. Trends at each grid point

were then calculated for terms I to V in equation (1), which we will refer to as the overall, non-ENSO, EP-ENSO, CP-ENSO, and residual trends, respectively. The calculation of trends were made following the works of Harrison and Carson [2007] and Cravatte *et al.* [2009] to ensure that data with large errors did not significantly affect the final result. In brief, we computed the linear trends only for the grid points that contain at least five ‘good’ SSS values (with less than 80% associated error) in each of at least 8 of the 11 pentads since 1955, starting from [1955–1959], and 7 of the 10 shifted pentads since 1958, starting from [1958–1962]. The significances of the trends were estimated at the 95% confidence level based on a Student’s t -test.

3. Results

[8] As an illustration, Figure 1d shows the combined effects of ENSO events and long-term trends on SSS changes in the western equatorial Pacific (2°N–2°S, 150°E–170°W). In general, we observe a SSS decrease during El Niño events (negative SOI; Figure 1a) and a SSS increase during La Niña events (positive SOI), together with a long-term freshening trend of the order of -0.16 pss/50 years. (The correlation coefficient between the SSS time series and the SOI is $R = 0.84$ at zero lag). Figures 1b and 1c further show the relative amplitude and the timing of the EP and CP types of ENSO, as indicated by the N_{CT} and N_{WP} indices. For instance, the N_{CT} index peaks with magnitude of 2.1°C during the very strong EP El Niño episode of 1997–98, while the N_{WP} index remains close to zero; in comparison, the N_{WP} index peaks with magnitude of 0.7°C during the CP El Niño episode of 2002–04, while the N_{CT} index remains close to zero. In both instances, we observe a SSS freshening of the order of -0.25 pss. As discussed by Singh *et al.* [2011] and below, this reflects that both EP and CP El Niño events affect the western equatorial Pacific, noting that the EP El Niño events mostly affect the eastern half of that region and the CP ENSO the western half. Also shown in Figure 1e is the time series of the averaged normalized SSS errors (se), indicating that the lack of interannual SSS variability at the beginning of the time series is spurious and actually reflects a poor data distribution (se > 80%).

[9] Values of the β and γ regression coefficients in equation (1), denoting the EP and CP ENSO signature in SSS, respectively, are shown in Figure 2. (Note that β and γ are not significantly modified when the N_{CT} and N_{WP} are band-pass filtered in the 2–7 year ENSO band.) Generally, Figure 2 indicates a decrease of SSS in the western equatorial Pacific and in the ITCZ, and an increase of SSS in the SPCZ, during both EP and CP El Niño events, and vice versa during La Niña events. These El Niño SSS changes mostly result from the anomalous eastward advection of low-salinity warm pool waters in the equatorial band, and a rainfall deficit related to the north-eastward displacement of the SPCZ [e.g., Delcroix and Picaut, 1998; Gouriou and Delcroix, 2002]. The SSS decrease in the equatorial region, centered near the dateline during EP El Niño events, is however shifted about $\sim 15^\circ$ in longitude westward and strengthened in magnitude during CP El Niño events. Moreover, the SSS increase in the SPCZ is somewhat reduced during CP El Niño events with a spatial signature inclined more to the southwest, as compared to EP El Niño events (note that the amplitude of N_{WP} is about 75% smaller

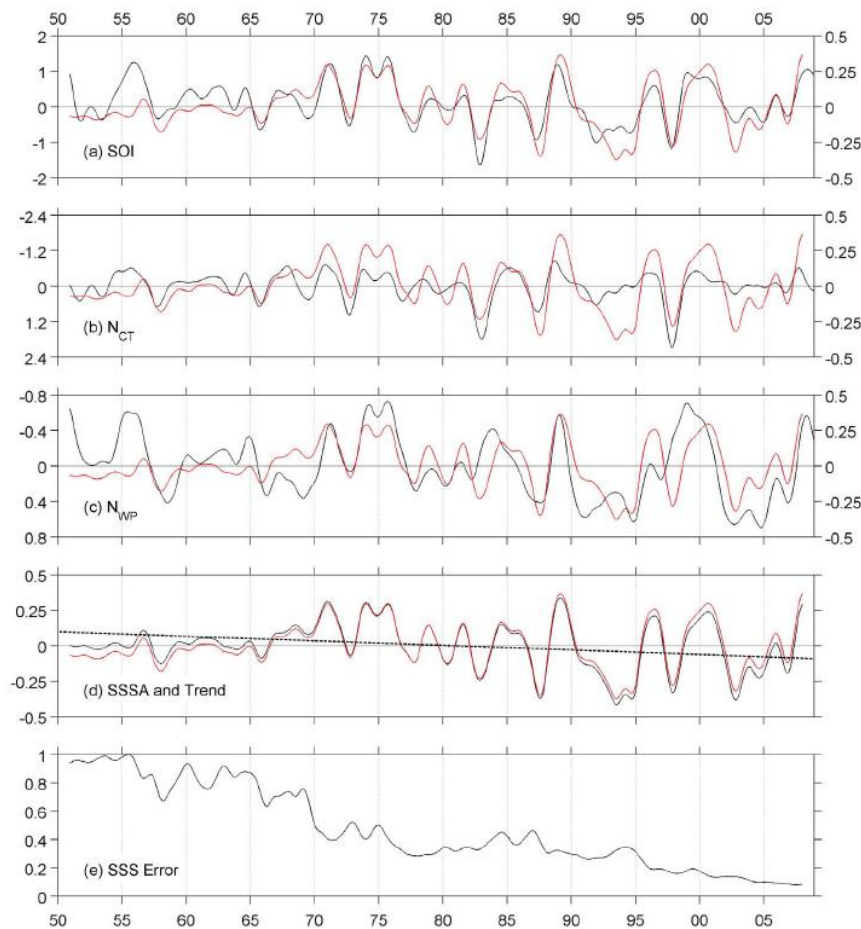


Figure 1. Time series of the (a) Southern Oscillation Index (SOI), (b) ENSO Cold Tongue Index (N_{CT}), (c) ENSO Warm Pool Index (N_{WP}), (d) SSS anomalies and linear trend, and (e) normalized SSS errors for the 1950–2008 period (black curves). Detrended SSS anomalies are scaled on the right vertical scales in Figures 1a–1c and on the left in Figure 1d (red curves). The SSS anomalies and errors were averaged in the region 150°E – 170°W and 2°S – 2°N . Anomalies in Figures 1a–1d are relative to the 1971–2000 mean monthly climatology. Values in Figures 1a–1e are smoothed using a 25-months Hanning filter for clarity. The SSS trend in Figure 1d, significant at the 95% confidence level, was computed over 1955–2008 ignoring values with SSS error greater than 0.8. Units are degree Celsius in Figures 1b and 1c, pss in Figure 1d, and percent divided by 100 in Figure 1e. Note the different and reversed vertical scales in temperature in Figures 1b and 1c.

than the amplitude of N_{CT} , see Figures 1b and 1c). These EP and CP ENSO SSS changes are remarkably consistent with those documented by *Singh et al.* [2011] from a more sophisticated AHC (Agglomerative Hierarchical Clustering)

method, reinforcing our confidence in using our simple regression analysis. As discussed by these last authors, the SSS changes during CP as compared to EP El Niño events reflect a reduced eastward advection of low-salinity warm

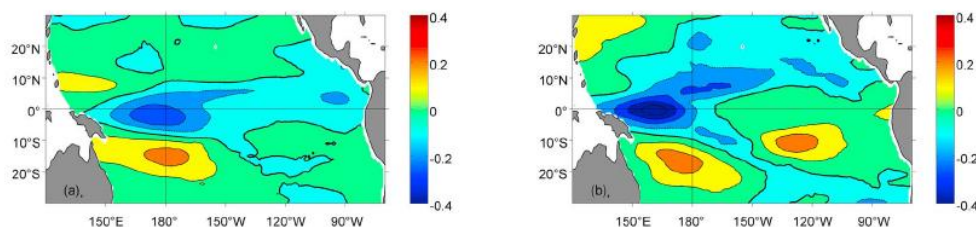


Figure 2. Coefficient estimates (a) β and (b) γ after regressing SSS anomalies with unfiltered N_{CT} and N_{WP} indices leading by 3 months, respectively (see equation (1)). Negative values thus indicate a decrease of SSS during EP or CP El Niño events and vice versa during La Niña events. Units are in pss/ $^{\circ}\text{C}$.

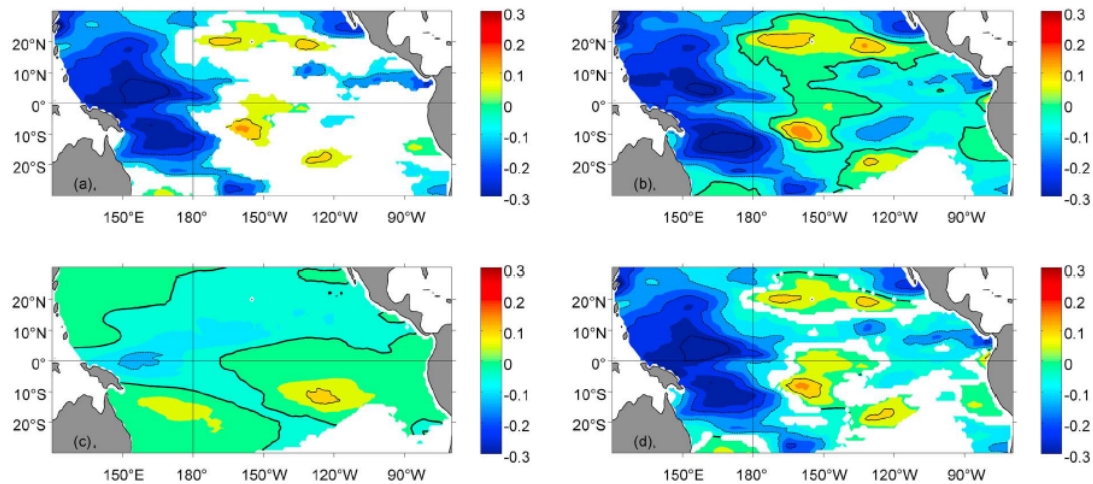


Figure 3. Linear trends in SSS anomalies over the 1955–2008 period due to (a) overall long-term variability, (b) non-ENSO long-term variability, (c) CP ENSO, and (d) EP and CP ENSO and non-ENSO long term variability (see equation (1)). Units are pss/50 years. Regions where the linear trends are not calculated due to poor data density or are not significant at the 95% confidence level are shaded in white. Thick black contour lines denote the 0 line.

pool waters in the equatorial band, and a reduced north-eastward shift of the SPCZ and associated precipitation changes.

[10] The trends obtained from terms I (overall trend), II (non-ENSO trend) and IV (CP ENSO trend) in equation (1) are shown in Figures 3a–3c, respectively. The trends obtained from terms III (EP ENSO trend) and V (residual trend) are not shown because they are one order of magnitude smaller than the other terms and both are not significant at the 95% confidence level. The overall trend (Figure 3a) shows maximum freshening concentrated in the western Pacific warm pool, including the SPCZ, with magnitudes of the order of -0.1 to -0.4 pss/50 years. Some freshening

(maximum -0.22 pss/50 years) is also visible under the ITCZ in the eastern Pacific, and there is a hint for a saltening trend in the high SSS regions of the Hawaiian and French Polynesia archipelago (with maxima reaching 0.14 and 0.16 pss/50 years, respectively), consistent with the dry-get-drier paradigm. These overall trends compare quite well in space with those determined by *Cravatte et al.* [2009] and *Durack and Wiffels* [2010] although they slightly differ in magnitude, probably due to the different periods of analysis (see the discussion of Figure 4 in Section IV). Aside from a probable influence of ocean dynamics [see *Huang et al.*, 2005], these SSS trends are qualitatively consistent with satellite-derived estimates of P-E trends [*Wentz et al.*, 2007]

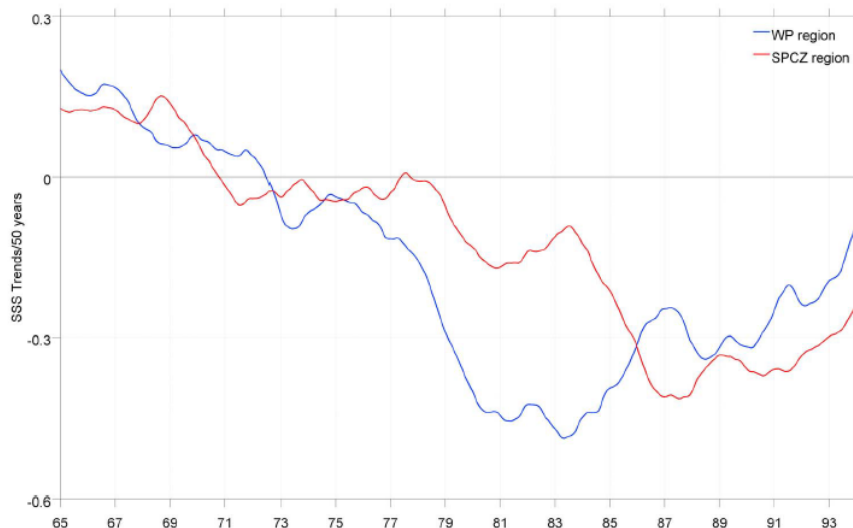


Figure 4. 30-years running trends of mean SSS anomalies in the warm pool (150°E – 170°W , 5°S – 10°N ; in blue) and SPCZ (150°E – 170°W , 20°S – 5°S ; in red) regions over the 1950–2008 period. Units are pss/50 years.

Table 1. Mean Trend Values (Computed Over 1955–2008 and Expressed in pss/50 Years) of the Reconstructed and Overall SSS anomalies in the pool (WP), SPCZ, and ITCZ Regions

	Region	CP ENSO	Non-ENSO	(EP + CP) ENSO + Non-ENSO	Overall
WP	150°E–170°W, 5°S–10°N	–0.06	–0.14	–0.21	–0.21
SPCZ	150°E–170°W, 20°S–5°S	+0.02	–0.22	–0.19	–0.20
ITCZ	150°W–90°W, 5°N–15°N	–0.02	–0.04	–0.07	–0.10

and with most of the P trends derived from rain gauge data recorded in the Pacific Islands (figures not shown).

[11] Figure 3d shows the trends from the reconstructed SSSA using the right hand side terms of equation (1) minus the residuals, ξ . The pattern and magnitude of the trends are very similar to those in Figure 3a confirming the non-significant effect of the residual trend as well as the reliability of equation (1) in efficiently extracting the main signals. The non-ENSO trend (Figure 3b) does resemble the overall trend (Figure 3a), with however some differences in amplitude, and an extension of the regions where the confidence intervals exceed 95%. The differences in amplitude are chiefly located in the far western equatorial Pacific and in the SPCZ and ITCZ regions and can largely be explained by the CP ENSO component of the trend (Figure 3c), qualitatively similar to the CP ENSO SSS pattern (Figure 2b) by construction. Noteworthy, CP ENSO events thus have a tendency to enhance the non-ENSO freshening trend in the far western equatorial Pacific and ITCZ regions (by about 30% and 20%, respectively), and to reduce the non-ENSO freshening trend in the SPCZ region (by about 10%). The 30% enhanced SSS freshening in the far western equatorial Pacific is comparable in magnitude to the 30–40% enhanced SST warming in the eastern equatorial Pacific due to ENSO [Compo and Sardeshmukh, 2010]. A quantification of mean trend values for different terms and regions are given in Table 1 for SSS.

4. Conclusion and Discussion

[12] The El Niño events generally result in a decrease of SSS in the western half of the equatorial Pacific, and an increase of SSS in the SPCZ mean area (and vice versa during La Niña events), mainly in relation to the import of low-salinity waters from the west in the equatorial band and to a rainfall deficit in the SPCZ mean area. The EP and CP types of ENSO events have however distinct quantitative impact on SSS [Singh et al., 2011]. In brief, the CP El Niño events are characterised by a westward shift (15° longitude) of the maximum SSS decrease in the equatorial band, and a reduced (50%) SSS increase in the SPCZ, as compared to EP El Niño events. In addition to the ENSO signal, there is a long-term SSS freshening trend in the precipitation-dominated regions of the western equatorial Pacific and of the SPCZ over the last 50 years, in qualitative agreement with the expected hydrological cycle increase in a warming world [Cravatte et al., 2009]. The aim of our study was thus to estimate the EP and CP ENSO contribution to the long-term SSS trends observed in the tropical Pacific.

[13] To tackle the problem, we used in situ SSS data covering the 1955–2008 period, and developed a multivariable regression analysis to discriminate ENSO and non-ENSO trends. We gain confidence in the simple regression analysis as it corroborates the different impacts of the EP and CP ENSO on SSS obtained previously from a more

sophisticated technique [Singh et al., 2011]. The contribution of the EP type of ENSO to the observed freshening trends was found to be insignificant in the western half of the tropical Pacific. In comparison, the contribution of the CP type of ENSO was found to be significant, and it tends to appreciably enhance (up to 30%) the freshening trends in the far western equatorial Pacific and moderately reduce (up to 10%) those trends under the SPCZ. As a consequence, we can expect that the assumed increased frequency [Yeh et al., 2009] and intensity [Lee and McPhaden, 2010] of CP ENSO will strengthen the freshening trend in the far western equatorial Pacific, and lessen it in the SPCZ, in the years to come.

[14] The documented eastward expansion of the surface covered by low-salinity waters in the warm pool and SPCZ regions [Cravatte et al., 2009] is not evident from the ENSO trends. The EP ENSO trend is negligible, likely because EP El Niño events tend to be followed by EP La Niña events [Kug et al., 2009]. In contrast, the CP El Niño events tend not to be followed by CP La Niña events (ibid), so that the long-term effect of CP ENSO actually induces a maximum freshening trend in the far western equatorial Pacific and a maximum saltening trend in the SPCZ. Hence, we do not expect the low-salinity waters to expand eastward due to ENSO, suggesting that the observed eastward expansion of low-salinity waters is a sign of climate change rather than just a signature of the increased occurrence, intensity and asymmetrical nature of CP ENSO events.

[15] This study illustrates one possible way of estimating the contribution of the EP and CP ENSO signal to the long-term trend in SSS. It raises a number of issues. Firstly, the statistical analysis we intentionally adopted here for the sake of simplicity is admittedly crude as it is based on regression of SSS onto ENSO indices. It would be interesting to test more sophisticated methods, as by Compo and Sardeshmukh [2010], noting however, that these usually assumed that the dynamics of ENSO have remained unchanged, and this is probably not the case for the EP and CP types of ENSO. Secondly, it is worth reminding that linear trends are very sensitive to the time-span over which they are computed. To illustrate that sensitivity with SSS data, 30-years running trends were calculated for the warm pool and SPCZ regions (Figure 4). We use a 30-year period as it has been adopted by the World Meteorological Organization (WMO) to be the standard period for the estimation of climatic normals [World Meteorological Organization, 1989]. The trends clearly reflect a saltening before the mid-1970s and a freshening after that time in both regions. It is not clear whether or not the reversed sign of the trends is due to increased data density (e.g., see Figure 1e), the climate shift of the late-1970s [Trenberth and Stepaniak, 2001], changes in ENSO property [Wang and An, 2001], increased occurrence and/or intensity of CP ENSO over EP ENSO [Lee and McPhaden, 2010], and/or phase reversal of the Pacific Decadal Oscillation [Mantua and Hare, 2002]. Whatever its causes, this

reversal in the pattern of trends warns us that our present results, although based on rather long record lengths (1955–2008), may change when choosing different time periods. Thirdly, many studies have assumed long term anthropogenic trends to be linear, and this may not be adequate [Karl *et al.*, 2000]. It would still be interesting to make use of piecewise linear trends, as by Tomé and Miranda [2004], especially in order to account for climate shifts. As a final comment, there is no doubt that long SSS (and climatic) time series must be pursued in order to ease interpretation of long-term trends from observational data.

[16] **Acknowledgments.** This work is a contribution to the GLOSCAL ESA/SMOS proposal supported by CNES. We benefited from freely available datasets, including gridded SSS field from the French SSS Observation Service (<http://www.legos.obs-mip.fr/observations/sss/>), the SOI (<http://www.cpc.ncep.noaa.gov/data/indices/soi/>), and the NINO3 and NINO4 SST anomalies (<http://www.cpc.ncep.noaa.gov/data/indices/sstoi.indices/>) from which we derived the EP and CP ENSO indices using the formula from Ren and Jin [2011]. We thank our colleagues S. Cravatte and G. Alory for their valuable comments on a draft version of this manuscript. One of us (A.S.) benefits from a PhD grant from IRD.

[17] The Editor thanks an anonymous reviewer for their assistance in evaluating this paper.

References

- Barbosa, S. M., and O. B. Andersen (2009), Trend patterns in global sea surface temperature, *Int. J. Climatol.*, *29*, 2049–2055, doi:10.1002/joc.1855.
- Cane, M. A., A. C. Clement, A. Kaplan, Y. Kushnir, D. Pozdnyakov, R. Seager, S. E. Zebiak, and R. Murtugudde (1997), Twentieth-century sea surface temperature trends, *Science*, *275*(5302), 957–960, doi:10.1126/science.275.5302.957.
- Compo, G. P., and P. D. Sardeshmukh (2010), Removing ENSO-related variations from the climate record, *J. Clim.*, *23*(8), 1957–1978, doi:10.1175/2009JCLI2735.1.
- Cravatte, S., T. Delcroix, D. Zhang, M. McPhaden, and J. Leloup (2009), Observed freshening and warming of the western Pacific Warm Pool, *Clim. Dyn.*, *33*(4), 565–589, doi:10.1007/s00382-009-0526-7.
- Delcroix, T. (1998), Observed surface oceanic and atmospheric variability in the tropical Pacific at seasonal and ENSO timescales: A tentative overview, *J. Geophys. Res.*, *103*(C9), 18,611–18,633, doi:10.1029/98JC00814.
- Delcroix, T., and C. Hénin (1991), Seasonal and interannual variations of sea surface salinity in the tropical Pacific Ocean, *J. Geophys. Res.*, *96*(C12), 22,135–22,150, doi:10.1029/91JC02124.
- Delcroix, T., and J. Picaut (1998), Zonal displacement of the western equatorial Pacific “fresh pool,” *J. Geophys. Res.*, *103*(C1), 1087–1098, doi:10.1029/97JC01912.
- Delcroix, T., S. Cravatte, and M. J. McPhaden (2007), Decadal variations and trends in tropical Pacific sea surface salinity since 1970, *J. Geophys. Res.*, *112*, C03012, doi:10.1029/2006JC003801.
- Delcroix, T., G. Alory, S. Cravatte, T. Corrège, and M. J. McPhaden (2011), A gridded sea surface salinity data set for the tropical Pacific with sample applications (1950–2008), *Deep Sea Res., Part I*, *58*(1), 38–48, doi:10.1016/j.dsr.2010.11.002.
- Deser, C., A. S. Phillips, and M. A. Alexander (2010), Twentieth century tropical sea surface temperature trends revisited, *Geophys. Res. Lett.*, *37*, L10701, doi:10.1029/2010GL043321.
- Durack, P. J., and S. E. Wijffels (2010), Fifty-year trends in global ocean salinities and their relationship to broad-scale warming, *J. Clim.*, *23*(16), 4342–4362, doi:10.1175/2010JCLI3777.1.
- Gouriou, Y., and T. Delcroix (2002), Seasonal and ENSO variations of sea surface salinity and temperature in the South Pacific Convergence Zone during 1976–2000, *J. Geophys. Res.*, *107*(C12), 3185, doi:10.1029/2001JC000830.
- Harrison, D. E., and M. Carson (2007), Is the world ocean warming? Upper-ocean temperature trends: 1950–2000, *J. Phys. Oceanogr.*, *37*(2), 174–187, doi:10.1175/JPO3005.1.
- Held, I. M., and B. J. Soden (2006), Robust responses of the hydrological cycle to global warming, *J. Clim.*, *19*, 5686–5699, doi:10.1175/JCLI3990.1.
- Huang, B., V. M. Mehta, and N. Schneider (2005), Oceanic response to idealized net atmospheric freshwater in the Pacific at the decadal time scale, *J. Phys. Oceanogr.*, *35*, 2467–2486, doi:10.1175/JPO2820.1.
- Intergovernmental Panel on Climate Change (2007), *Climate Change 2007: Synthesis Report. Contribution of Working Groups I, II and III to the Fourth Assessment Report of the Intergovernmental Panel on Climate Change*, edited by Core Writing Team, R. K. Pachauri, and A. Reisinger, Geneva, Switzerland.
- Jones, P. D. (1989), The influence of ENSO on global temperatures, *Clim. Monit.*, *17*, 80–89.
- Karl, T. R., R. W. Knight, and B. Baker (2000), Evidence for an increase in the rate of global warming?, *Geophys. Res. Lett.*, *27*(5), 719–722, doi:10.1029/1999GL010877.
- Kelly, P. M., and P. D. Jones (1996), Removal of the El Niño–Southern Oscillation signal from the gridded surface air temperature data set, *J. Geophys. Res.*, *101*(D14), 19,013–19,022, doi:10.1029/96JD01173.
- Kug, J.-S., F.-F. Jin, and S.-I. An (2009), Two types of El Niño events: Cold tongue El Niño and warm pool El Niño, *J. Clim.*, *22*(6), 1499–1515, doi:10.1175/2008JCLI2624.1.
- Latif, M., R. Kleeman, and C. Eckert (1997), Greenhouse warming, decadal variability, or El Niño? An attempt to understand the anomalous 1990s, *J. Clim.*, *10*(9), 2221–2239, doi:10.1175/1520-0442(1997)010<2221:GWDVOE>2.0.CO;2.
- Lau, K.-M., and H. Weng (1999), Interannual, decadal–interdecadal, and global warming signals in sea surface temperature during 1955–97, *J. Clim.*, *12*(5), 1257–1267, doi:10.1175/1520-0442(1999)012<1257:IDIAGW>2.0.CO;2.
- Lee, T., and M. J. McPhaden (2010), Increasing intensity of El Niño in the central–equatorial Pacific, *Geophys. Res. Lett.*, *37*, L14603, doi:10.1029/2010GL044007.
- Mantua, N. J., and S. R. Hare (2002), The Pacific Decadal Oscillation, *J. Oceanogr.*, *58*, 35–44, doi:10.1023/A:1015820616384.
- Ren, H.-L., and F.-F. Jin (2011), Niño indices for two types of ENSO, *Geophys. Res. Lett.*, *38*, L04704, doi:10.1029/2010GL046031.
- Santer, B. D., T. M. L. Wigley, C. Doutriaux, J. S. Boyle, J. E. Hansen, P. D. Jones, G. A. Meehl, E. Roeckner, S. Sengupta, and K. E. Taylor (2001), Accounting for the effects of volcanoes and ENSO in comparisons of modeled and observed temperature trends, *J. Geophys. Res.*, *106*(D22), 28,033–28,059, doi:10.1029/2000JD000189.
- Singh, A., T. Delcroix, and S. Cravatte (2011), Contrasting the flavors of El Niño Southern–Oscillation using sea surface salinity observations, *J. Geophys. Res.*, *116*, C06016, doi:10.1029/2010JC006862.
- Solomon, A., and M. Newman (2011), Decadal predictability of tropical Indo–Pacific Ocean temperature trends due to anthropogenic forcing in a coupled climate model, *Geophys. Res. Lett.*, *38*, L02703, doi:10.1029/2010GL045978.
- Terray, L., L. Corre, S. Cravatte, T. Delcroix, G. Reverdin, and A. Ribes (2011), Near-surface salinity as Nature’s rain gauge to detect human influence on the tropical water cycle, *J. Clim.*, doi:10.1175/JCLI-D-10-05025.1.
- Thompson, D. W. J., J. M. Wallace, P. D. Jones, and J. J. Kennedy (2009), Identifying signatures of natural climate variability in time series of global-mean surface temperature: Methodology and insights, *J. Clim.*, *22*(22), 6120–6141, doi:10.1175/2009JCLI3089.1.
- Tomé, A. R., and P. M. A. Miranda (2004), Piecewise linear fitting and trend changing points of climate parameters, *Geophys. Res. Lett.*, *31*, L02207, doi:10.1029/2003GL019100.
- Trenberth, K. E., and D. P. Stepaniak (2001), Indices of El Niño evolution, *J. Clim.*, *14*(8), 1697–1701, doi:10.1175/1520-0442(2001)014<1697:LIOENO>2.0.CO;2.
- Wang, B., and S.-I. An (2001), Why the properties of El Niño changed during the late 1970s, *Geophys. Res. Lett.*, *28*(19), 3709–3712, doi:10.1029/2001GL012862.
- Wentz, J. F., L. Ricciardulli, K. Hilburn, and C. Mears (2007), How much more rain will global warming bring?, *Science*, *317*(5835), 233–235, doi:10.1126/science.1140746.
- World Meteorological Organization (1989), Calculation of monthly and annual 30-year standard normals, *Rep. WCDP 10, WMO-TD 341*, Geneva, Switzerland.
- Yeh, S.-W., J.-S. Kug, B. Dewitte, M.-H. Kwon, B. P. Kirtman, and F.-F. Jin (2009), El Niño in a changing climate, *Nature*, *461*(7263), 511–514, doi:10.1038/nature08316.

T. Delcroix and A. Singh, LEGOS, UMR 5566, CNES, CNRS, IRD, Université de Toulouse, 14 av. Edouard Belin, F-31400 Toulouse CEDEX, France. (awnesh.singh@legos.obs-mip.fr)

Chapter 6

Synthesis and Discussion

Preamble

The El Niño Southern Oscillation (ENSO) event is the largest climatic signal occurring at interannual time scales. Although its existence can be traced back to the year 1525 (Quinn *et al.*, 1987), and even before in paleo-environmental records (Corrège, 2006 and references therein), its relative importance was deeply recognized after the unexpected arrival of the 1982-83 El Niño, which galvanized the scientific community in an effort to understand and predict ENSO (Wang and Picaut, 2004). It has global socioeconomic impacts and greatly affects both rich and poor countries (Goddard and Dilley, 2005). Numerous studies have hence been done in an attempt to understand the behavior of ENSO (see part of these in the references list), however, the diversity and the possible recent changing face of El Niño further complicates what is already known. The recently reported “new” flavor of El Niño is being debated deeply in the literature and it has convoluted the theories that were initially proposed to explain the existence of this dynamic phenomenon. Consequently, the aim of this study was to further shed light on this “new” flavor of ENSO using in situ, remotely-sensed and model-derived data.

6.1 ENSO flavors

Using singular, multivariate and combined regression-EOF analyses, and the more sophisticated agglomerative hierarchical clustering (AHC) and self-organizing maps (SOM) techniques, we attempted to extract coherent groups in ENSO main features and, in particular, to characterize the Eastern Pacific (EP) and Central Pacific (CP) signature of ENSO events for the observed climate variables sea surface salinity (SSS), sea surface temperature (SST), precipitation (P), zonal surface currents (U), sea level (SL) and chlorophyll (CHL). Our results for SST, P, U and SL were found to be consistent with those from previous studies, sometimes conducted using different datasets, time span, and analysis methods (e.g., Ashok *et al.*, 2007; Bosc and Delcroix, 2008; Kug *et al.*, 2009; Yeh *et al.*,

2009). However, it was for the first time that we documented the different EP and CP signatures of ENSO using SSS (Singh *et al.*, 2011) and CHL (Radenac *et al.*, 2012). These novel results were overall robust based on the different data processing techniques we employed. It should be noted that not all data analyses techniques used were successful to characterize the different signatures of ENSO. As a summary, we present in Fig. 6.1 representative examples of the 1997-98 EP and 2002-03 CP El Niño events in terms of SST, SSS, P, U, SL and CHL followed by a discussion for each event.

6.1.1 The 1997-98 EP El Niño

During EP El Niño, the “piled-up” warm waters in the western Pacific warm pool during the “normal” period are “released” in conjunction with the appearance of anomalous westerlies over the western-central Pacific and a reduction in the easterlies in the eastern Pacific. These released warm waters travel eastwards as a consequence of downwelling Kelvin waves (Fig. 6.1g) thereby shoaling the thermocline in the west and deepening it in the east (reflected in the SL anomalies in Fig. 6.1i). This leads to a thermocline which is flatter (and shallower due to poleward discharge – see Section 6.3.1) over the entire equatorial region than during normal conditions when there is a larger east-west thermocline tilt. As a result, anomalous negative SST is evidenced in the western Pacific warm pool region while positive SST anomalies occupy the eastern-central equatorial Pacific region (Fig. 6.1a). Meanwhile, the change in the surface pressure due to the change in the wind stress patterns alters the Walker circulation through ocean-atmosphere interaction, which results in an eastward shift of positive precipitation anomalies and occupies the region dominated by the positive SST anomalies (Fig. 6.1e). The SPCZ and ITCZ regions move north-eastward and southward of their normal positions, respectively. Because of this, negative SSS anomalies are found over the precipitation dominated regions of the eastern-central equatorial Pacific and positive SSS anomalies north of the equator in the warm pool and SPCZ regions (Fig. 6.1c). In the western Pacific warm pool region, zonal surface currents advect the low salinity and the nutrient poor waters eastward. This, combined with the reduced upwelling of nutrient-rich waters (due to deepening of the thermocline anomaly) in the eastern Pacific, results in negative CHL anomalies occupying the eastern-central equatorial regions (Fig. 6.1k). The positive CHL anomaly in the far western Pacific north of the equator is ascribed to the eastward advection of nutrient-rich waters from the upwelling regions of Papua New Guinea and the Solomon Islands.

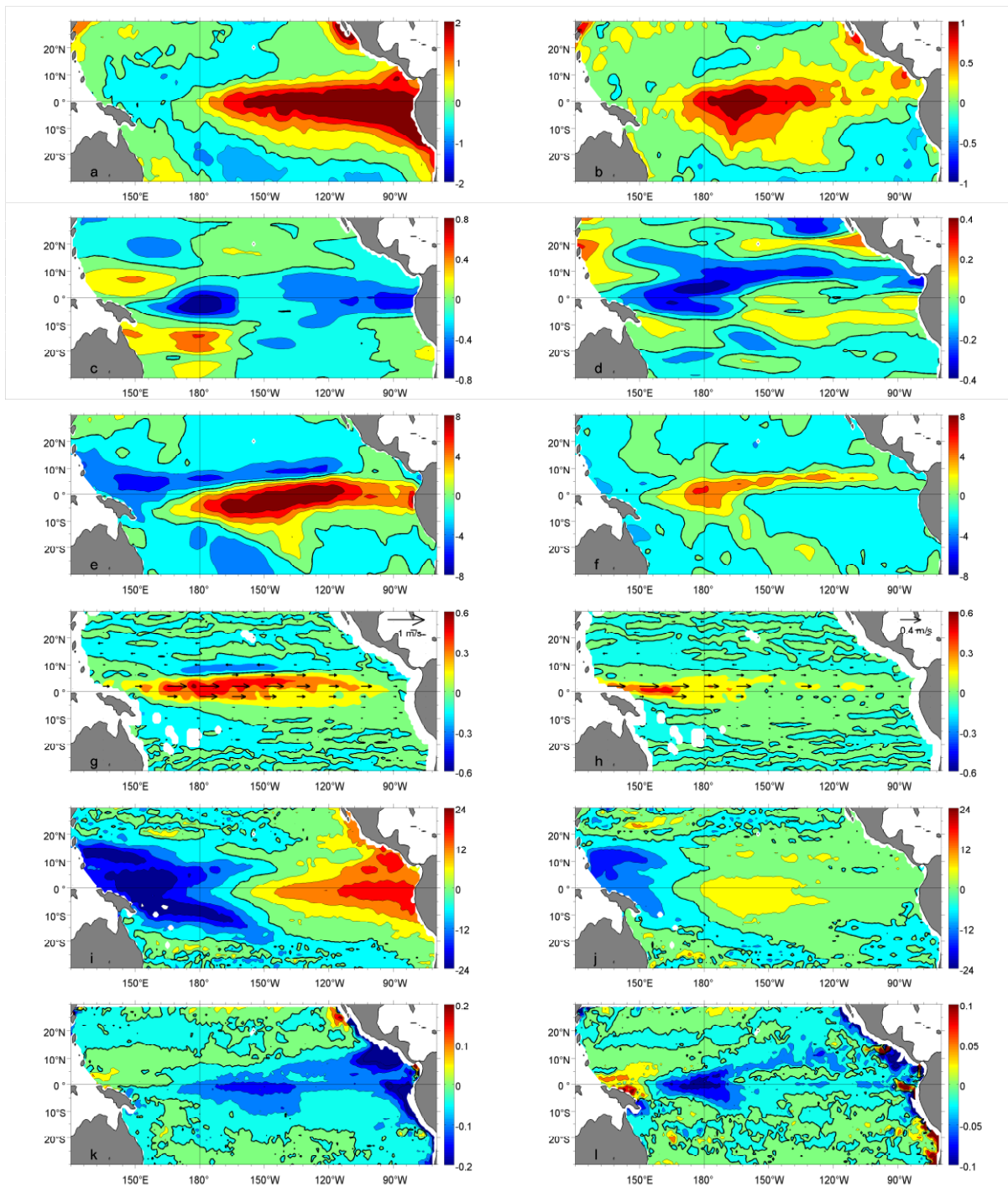


Figure 6.1 Three monthly observation-based December-January-February (DJF) composites of (a&b) SST anomalies (in $^{\circ}\text{C}$), (c&d) SSS anomalies at 3 months lag (in pss), (e&f) P anomalies (in mm day^{-1}), (g&h) U anomalies at 3 months lead (in m s^{-1}), (i&j) SL anomalies (in cm), and (k&l) CHL anomalies (in mg m^{-3}) for the 1997-98 EP El Niño (left column) and 2002-03 CP El Niño (right column). The anomalies are with respect to the mean monthly climatology over the period 1971-2000 (for SST and SSS), 1979-2008 (for P), 1993-2008 (for U), 1993-2010 (for SL) and 1998-2010 (for CHL). Thick black contour lines in the spatial patterns denote the 0 line. Note the different color scales in the plots.

6.1.2 The 2002-03 CP El Niño

The state of the tropical Pacific was found to be quite different during CP El Niño as compared to EP El Niño in terms of the signature of climate variables and the related mechanisms. The CP El Niño pattern is characterized by anomalous SST warming concentrated in the central Pacific region (Fig. 6.1b) as opposed to the central-eastern equatorial Pacific during EP El Niño. This can be explained by westerlies in the western-central Pacific, which force downwelling Kelvin waves that act to advect the warm waters of the warm pool eastwards (Fig. 6.1h). However, the presence of easterlies in the eastern Pacific suppresses the SST warming there through upwelling (and the possible generation of upwelling Kelvin waves), excess evaporation and vertical turbulent mixing (Kug *et al.*, 2009). The confinement of the positive SST anomalies to the central Pacific region is reflected in the SL anomaly patterns, which shows positive SL anomaly in the central Pacific flanked by weaker positive anomalies to the east and negative anomalies in the west (Fig. 6.1j). The region of deep atmospheric convection shifts westwards relative to that during EP El Niño. This results in a shift of the anomalous precipitation regions, which now occupy the central Pacific and ITCZ regions (Fig. 6.1f). The far western Pacific is not as dry as during EP El Niño. However, because of the $\sim 15^\circ$ westward shift of the maximum precipitation anomalies during CP El Niño as compared to EP El Niño, there is a similar westward shift (with the same magnitude) in negative SSS anomalies in the equatorial region. The SPCZ region shows positive SSS anomalies. However, the magnitude of the SSS anomalies in the western and SPCZ regions are almost 50% to those during EP El Niño (Fig. 6.1d). In addition, positive SSS anomalies now occupy the eastern equatorial Pacific. This can be explained by the reduced eastward extent of the zonal surface current anomalies in the west, which advect low salinity and oligotrophic (low chlorophyll) waters of the warm pool eastwards (Fig. 6.1i), and the hint for the presence of westward zonal surface current anomalies and negative precipitation anomalies in the east.

6.2 EP and CP ENSO vs. RD oscillator paradigm

In the beginning of our study (as summarized in Section 6.2), we contrasted the observations in climate variables during the course of EP and CP ENSO events. However, it is also important to contrast ENSO in terms of physical mechanisms and/or dynamical modes. As a first step, this was done here focusing on the recharge-discharge (RD) oscillator paradigm, which is one of the four main theories accounting for the quasi-cyclic nature of ENSO. The

RD paradigm roots on warm waters exchanged between the equatorial and off-equatorial regions. In the equatorial band, changes in Warm Water Volume (WWV) are shown to mainly result from the balance of horizontal mass transports. Hence, we investigated the horizontal transports at play during the two types of ENSO using a simple multivariate linear regression model. Our results concur with those from a similar study based on 500-year long GFDL simulation (Kug *et al.*, 2010) but we stress the use of horizontal transports in our work. We summarize our findings on EP and CP ENSO dynamics using Fig. 6.2 followed by a discussion.

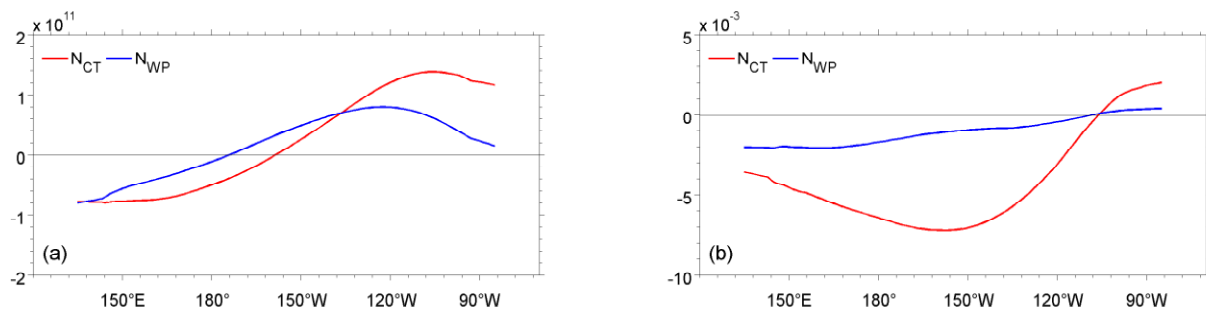


Figure 6.2 Gradients obtained from the regression of normalized Niño cold tongue (N_{CT} , in red) and Niño warm pool (N_{WP} , in blue) indices with 1958-2007 model-derived (a) mean WWV anomaly averaged between 5°S-5°N and (b) the corresponding mean WWV tendency. The regressions were performed on averages computed in running 31° longitude boxes. The abscissa is centered on the 31° longitude moving box. Note the different scales in the plots. Units are $\text{m}^3 \text{ } ^\circ\text{C}^{-1}$ in (a) and Sverdrups $^\circ\text{C}^{-1}$ per degree longitude in (b).

6.2.1 EP ENSO dynamics

The mechanisms responsible for the transition from an EP El Niño into a La Niña involves, as mentioned earlier in Chapter 4, a poleward mass discharge of warm waters from the equatorial band across the 5°N and 5°S latitudes (Fig. 6.2b; red line), with meridional discharges across the latter being relatively more pronounced. The result is upwelling of colder waters in the central Pacific and shoaling of the thermocline reminiscent of a La Niña pattern in SST, which eventually develops into an EP La Niña event through positive ocean-atmosphere feedback and consequently an increase in strength of the normal Walker circulation. There is, concurrently, a recharge of the equatorial band, which increases the warm water volume in the western Pacific and as a result, increases the east-west tilt of the thermocline (Fig. 6.2a; red line). The tropical Pacific is now in a recharged state and ready to go onto the next stage of the oscillation, EP El Niño. This cycle is similar to the one described by Jin (1997) to explain the oscillatory nature of ENSO. Here we evidenced this through the analysis of climate variables (Chapter 3) and dynamics (Chapter 4).

6.2.2 CP ENSO dynamics

The different signatures observed in the various climate variables during CP El Niño suggest that there are different mechanisms at play. An analysis of the horizontal warm water volume transports during CP El Niño indicates a recharge and discharge process occurring simultaneously; a recharge of the equatorial band in the eastern Pacific and a discharge in the western Pacific. This creates a compensating effect which results in a reduced recharge-discharge during CP ENSO (Fig. 6.2b; blue line) as when compared to EP ENSO and could explain why CP El Niño is not followed by La Niña events, in contrast to EP El Niño which are followed by La Niña events. In addition, the convergence of zonal transports during CP El Niño, which does not occur during EP Niño, could explain the geographical location of the maximum SST and SL anomalies in the central Pacific region (Fig. 6.2a; blue line).

6.2.3 Perspectives I

The above results suggest that the recharge-discharge oscillator paradigm, as proposed by Jin (1997) to explain the oscillatory nature of ENSO, applies to EP El Niño events but not to CP El Niño events. This is because of the different discharge processes occurring during these different types of events. The question then arises as to what are the origins of the different discharge processes during EP and CP El Niño events? Is it related to the different equatorial Kelvin and Rossby wave signatures (Dewitte *et al.*, 2012) that modify the zonal thermocline slope and so the geostrophic RD processes? If so, it would be interesting to test the other leading theories involving equatorial waves to explain the oscillatory nature of ENSO (see Wang and Picaut, 2004) and whether they can explain both EP and CP ENSO features.

6.3 Trends due to EP and CP ENSO

In addition, for the first time to our knowledge, we estimated the contribution of the EP and CP ENSO signatures on the long-term trends of SST, SSS and SL. Because of the different signatures of EP and CP ENSO, and the different mechanisms involved, we can expect them to have contrasting effects on the long-term trends in the tropical Pacific. Consequently, we used a simple multivariate linear regression approach using the ENSO indices N_{CT} and N_{WP} (Ren and Jin, 2011) to quantify the contribution of the EP and CP types of ENSO on the long-term SST, SSS and SL trends. Our results show that CP ENSO effects on the long-term trends for the three climate variables are significant at the 95% confidence level based on a

Student's t -test while those for EP ENSO are not. The non-significant EP ENSO trends could be due to the symmetry of EP El Niño and La Niña events and where, generally, the latter follows the former. This is not the case during CP ENSO: CP El Niño events are, generally, not followed by La Niña events. We summarize here the effects of CP ENSO on the long-term trends in SST, SSS and SL using Fig. 6.3 to illustrate the trends due to the overall long-term variability and those due to CP ENSO.

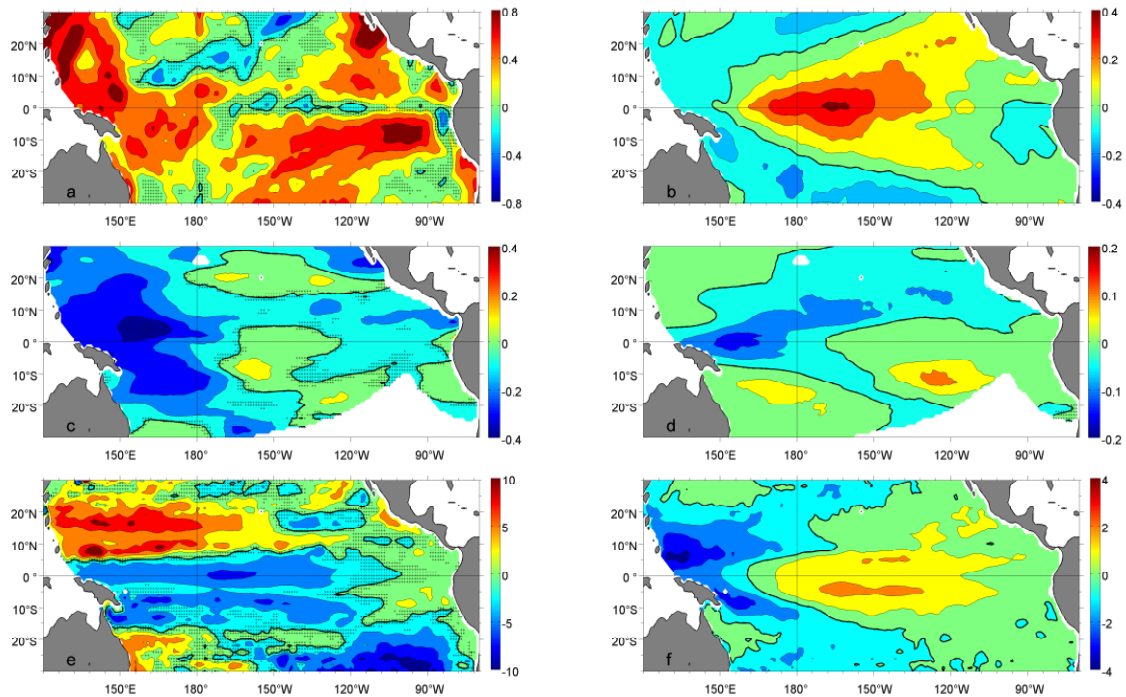


Figure 6.3 Linear trends in (a&b) SST (in $^{\circ}\text{C}/50$ years), (c&d) SSS (in pss/50years), and (e&f) SL (in cm/50 years; derived from SODA) anomalies over the 1955-2008 period due to overall long-term variability (left column) and CP ENSO variability (right column). Regions where the trends are not significant at the 95% confidence level are hatched. Thick black contour lines in the spatial patterns denote the 0 line. Note the different color scales in the plots.

6.3.1 ENSO trends in SST

The overall long-term trends in SST shows widespread warming over the entire tropical Pacific region except in the central tropical north Pacific and cold tongue regions (equatorial eastern-central Pacific) where there is an observed (but non-significant) cooling trend (Fig. 6.3a). The warming trends observed in the western Pacific are in agreement with many studies, however, the trends in the central-eastern equatorial regions are questionable as previous studies either found a cooling trend or a warming trend (see Cravatte *et al.*, 2009; their Table 1). The non-ENSO long-term cooling trends in the cold tongue regions reach magnitudes of -0.75 $^{\circ}\text{C}/50$ years. CP ENSO acts to reduce this cooling trend in the central

Pacific region by up to 40% (Fig. 6.3b). Consequently, we can anticipate the entire equatorial band to show a warming trend *assuming* an increase in frequency and intensity of CP El Niño events (Yeh *et al.*, 2009). This led Lee and McPhaden (2010) to conclude that the observed eastward expansion of the warm pool in the last decades (Cravatte *et al.*, 2009) may partly be a result of the increased occurrence of CP ENSO events.

6.3.2 ENSO trends in SSS

The overall long-term freshening trends observed in the warm pool, SPCZ and ITCZ regions are of the order ~ -0.3 pss/50 years (Fig. 6.3c). These overall trends compare quite well in space with those determined by Delcroix *et al.* (2007), Cravatte *et al.* (2009), Durack and Wijffels (2010) and Terray *et al.* (2012) although they slightly differ in magnitude, probably due to the different periods of analysis. Saltening trends are found in the high salinity regions of the Hawaiian and Tahitian archipelagos. CP ENSO enhances the non-ENSO long-term freshening trends in the warm pool and ITCZ regions by about 30% and 20%, respectively while reducing it in the SPCZ region by $\sim 10\%$ (Fig. 6.3d). The maximum freshening trends observed in the far western Pacific were found to be largely due to the effect of CP El Niño. Consequently, the observed eastward expansion of the low salinity fresh pool waters in the equatorial band and in the SPCZ cannot be attributed to CP El Niño events. Instead, the expansion could be a result of climate change, as discussed in Terray *et al.* (2012), rather than the increased occurrence, intensity and asymmetrical nature of CP ENSO events.

6.3.3 ENSO trends in SL

The long-term sea level trends are negative over the western-central Pacific between 20°S - 5°N with positive trends seen in the northern and eastern Pacific regions (Fig. 6.3e). This pattern is somewhat reminiscent of the equatorial discharge signal observed during the course of an EP El Niño in terms of SL anomalies (see Fig. 4.3c) and could possibly influence the calculation of trends due to its larger amplitude. CP ENSO tends to reduce (enhance) the negative non-ENSO long-term trends in the central equatorial (western) Pacific by $\sim 30\%$ (Fig. 6.3f). Consequently, we can expect a negative (positive) SL anomaly structure in the western (eastern) equatorial Pacific, which could be consistent with a weakening of the Walker circulation with the *assumed* increase in frequency and intensity of CP El Niño events (Yeh *et al.*, 2009; Lee and McPhaden, 2010).

6.3.4 Perspectives II

The analysis on the trends due to overall long-term variability on SST anomalies suggests a stronger equatorial zonal SST gradient because of the warming (cooling) trends in the western (eastern) equatorial Pacific. This would indicate an increase in the easterlies resulting in an increase in the strength of the Walker circulation. However, the warming trend in the central Pacific due to CP ENSO acts to reduce the long-term zonal SST gradient. Thus, we can anticipate a reduction in the increase in strength of the Walker circulation with the *assumed* increase in frequency of CP El Niño events (Yeh *et al.*, 2009). An overall weakening of the Walker circulation could probably explain the observed eastward expansion of the warm/fresh pool in the western Pacific.

The estimates of SST and SL trends in the Pacific region are unclear as many authors show contradictory results due to the different periods, methods and data used in their analyses (e.g., Carton *et al.*, 2005; Qiu and Chen, 2006; Lee and McPhaden, 2008; Cravatte *et al.*, 2009; Timmermann *et al.*, 2010; Merrifield, 2011; Merrifield and Maltrud, 2011; Becker *et al.*, 2012). Since linear trend calculations are sensitive over the period which they are computed (see Chapter 5), it may not be as straightforward as it seems to derive results that are robust. It would be interesting to make use of a sophisticated approach as that by Compo and Sardeshmukh (2010) to discriminate the effects of ENSO on the long-term trends or a method using piecewise linear trends (Tomé and Miranda, 2004), noting, however, that this method is sometimes used by climate sceptics to make ill-defined conclusions when interpreting interannual and/or decadal variability derived from too-small duration time series as ‘trends’. Furthermore, to our knowledge, there has been no study so far that isolates the effects of the different flavors of ENSO on the long-term SST, SSS and SL trends. We have attempted to estimate these trends in this study for the first time using a simple multivariate linear regression technique. It would be interesting to use other (new) methods and compare the results.

6.4 Challenging some of my results

Although the results were carefully and rigorously analyzed and subsequent conclusions derived, there were inevitably some challenges in this study. Those that come to mind are detailed below.

6.4.1 Data Length

Undoubtedly, data records need to be long and homogeneous to effectively understand the state of the climate and derive statistically robust results. In addition, it is important for data to be accurate and/or with, at least, information about its expected accuracy. With the exception of SLA data from Aviso (which however spans as much as 18 years), all datasets used here are “long enough” with regard to the 30-year standard period (in situ SSS data spans 59 years) for the estimation of climatic normals adopted by the World Meteorological Organization (WMO, 1989). To study ENSO and the recent possible changes in its behaviour, we would however need much longer time series (e.g., Giese and Ray, 2011) to derive robust statistics. Stevenson *et al.* (2010) argued that measuring ENSO variability with 90% confidence requires approximately 240 years of observations, for which we do not have even the more commonly observed SST data (about 140 years only, assuming that the early data are trustworthy). Collecting in situ data is hard work, and close to 60 years of data is relatively a lot and this is only what we have in hand. We believe that, although the statistics may not be robust, the analysis of these “short” observational time series enables us to propose new assumptions and mechanisms, and allows us to progress, aside from validating (or not) model results. We can use model data as an alternative, which obviously gives longer time series, but we are not sure if these models can correctly reproduce the ENSO flavors in SSS (e.g., see Delcroix *et al.*, 2011; their Fig. 8). Furthermore, in terms of SST, there is usually a bias with the centre of SST anomalies shifted about 20° in longitude west compared to observations (e.g., Kug *et al.*, 2010; Kim *et al.*, 2012). At this point, I would like to quote the word of M. J. McPhaden (2004), a prominent ENSO specialist and climate scientist:

“Recent observations highlight how far we have come, and how far we have yet to go, in our ability to understand and accurately predict El Niño.”

When computing trends, we did not consider the data density and/or error, except for SSS where that information was available and where we make use of the error fields and employed a shifted pentad method. Still, regarding SSS, it is worth noting that data density before the 1970s is relatively low (see Fig. 2.1; Fig. 1 in Delcroix *et al.*, 2011; Fig. 1 in Chen *et al.*, 2012). One interesting way to confirm the results (or not) would be to analyze paleosalinity data, which are available for several different locations in the Pacific (e.g., see Delcroix *et al.*, 2007; their Table 1; Durack and Wijffels, 2010; their Table 1; Kilbourne *et al.*, 2004; Gorman *et al.*, 2012), while keeping in mind that most of these paleosalinity data

are calibrated with in situ measurements when data density is sufficient. This also applies for paleo-temperature data. Also, it would be more robust to use weighted errors (e.g., [von Schuckmann and le Traon, 2011](#)) when calculating trends instead of using an error threshold.

6.4.2 EP and CP ENSO and the annual cycle

The relationship between ENSO (and a fortiori EP and CP ENSO) and the annual cycle is a long and still-debated open question (e.g., [Guilyardi, 2006](#)) that was not the purpose of our 3-year limited study. Intuitively, and as detailed in [Pezzulli *et al.* \(2005\)](#), the variability of seasonality could result actually in observed year-to-year variability that could be, for example, misinterpreted as ENSO-type variability. To “properly” remove the annual cycle, we make use of a 25-months Hanning filter rather than using a mean monthly climatology. We believe this filter to be relevant as it removes a variable (i.e., non-constant) annual cycle by assigning symmetric Gaussian-shaped weights on a sliding 25-points window. It would be interesting, however, to compare these results with those that use more sophisticated techniques, for example, the X-11 method by [Pezzulli *et al.* \(2005\)](#), with the idea to better understand how the main EP and CP ENSO features could be modified and/or reflect a modification only of the background seasonal cycle.

6.4.3 Statistical Methods

Moreover, each statistical method employed in this study has its pros and cons. These are detailed in [Table 6.1](#). Their common advantage is that they ensure a compact representation of climate data while their disadvantage is that they can be sensitive to the choice of the spatial domain and/or temporal length. Being aware of the pros and cons associated with each statistical method, which could bias the interpretation of the physics at work, it was realised that more than one method is necessary and significance tests should be done to achieve robustness in the results.

Table 6.1 Advantages and disadvantages of statistical numerical analysis methods used in this study.

Method	Advantages	Disadvantages
EOF	<ul style="list-style-type: none"> • Forces orthogonality between neighbouring EOFs • Provides a measure of variance associated with each EOF mode 	<ul style="list-style-type: none"> • Spatial pattern assumes symmetry between negative and positive phases • Only first few dominant modes of variability are utilized • Neighbouring EOFs may not be separated in a statistically significant way thus features may be mixed between EOFs or may have no physical meaning • Better results obtained with detrended data as non-detrended data may give an EOF mode that shows the trend component or the trend could be spread over several modes • Number of EOF modes equals length of data
Combined regression-EOF	<ul style="list-style-type: none"> • Extracts an EOF pattern maximally correlated to the regression index • Same as for EOF above 	<ul style="list-style-type: none"> • Uses a priori, that is, a regression index • Same as for EOF above
AHC	<ul style="list-style-type: none"> • Does not use a priori • Entire data can be represented by a few merged unique clusters 	<ul style="list-style-type: none"> • Arbitrarily defined cutting level for the dendrogram • Clusters are discrete whereas the real ocean barely skips from one state to another
NNA	<ul style="list-style-type: none"> • A common time series that can be used to extract information from any variable • Continuously trained to reach a stabilized state that shows maximum agreement between observations and neurons 	<ul style="list-style-type: none"> • Uses a priori, that is, a regression index

6.4.4 The neutral cluster

Looking at the SOI or Niño3.4 index, we see that the zero-crossing of the time series usually last for 1-3 months only, indicating the mean/neutral condition does not modulate the interannual variability. Besides, the anomalies are departures from the mean state and obtaining a neutral condition simply means that their occurrence is more frequent due to the time series curves constantly crossing the zero line to oscillate between positive and negative phases.

In using the clustering procedure, the neutral cluster was sometimes not evident. This may be because the arbitrarily defined cutting level on the dendrogram was too high and missed the neutral cluster. One solution would obviously be to lower the cutting level to obtain the neutral cluster but this may also result in other clusters being identified which may not be able to be physically explained. Hence, the choice was made of arbitrarily defining a cutting level where all the clusters obtained could be physically explained. It should be noted that the robustness of the clustering procedure was verified by comparing the clusters with the chronology of individual ENSO events, while keeping in mind that small differences may arise because of aggregation of individual maps into the cluster and also noting that no two events are quite alike ([Wyrski, 1975](#)).

6.5 Final Remarks

Personally, I have gained tremendous knowledge in understanding the dynamics of ENSO during this thesis project. I have learnt about different data analysis techniques, gained considerable knowledge on previous studies on ENSO, and above all, I have improved my scientific judgment in this area and general analytical thinking, organizational skills, endurance and perseverance for future work. Eventually it was realized that burning the midnight oil is part of daily life in doing research!

In any kind of study, one adds something to existing knowledge, while another adds something else. I believe that I have contributed a little more for those who are interested in the science of climate change and understanding ENSO. An addition, however small it may be, is a lot especially since no work of this kind has been done in this area. I conclude by quoting some of the last words of **Sir Isaac Newton (1727)**:

“I do not know what I may appear to the world, but to myself I seem to have been only a boy playing on the sea-shore, and diverting myself in now and then finding a smoother pebble or a prettier shell than ordinary, whilst the great ocean of truth lay all undiscovered before me.”

In accordance with, I have exerted all my effort into the present study in finding that smoother pebble!

References

- Adler, R. F., Huffman, G. J., Chang, A., Ferraro, R., Xie, P. P., Janowiak, J., Rudolf, B., Schneider, U., Curtis, S., Bolvin, D., Gruber, A., Susskind, J., Arkin, P., and Nelkin, E. (2003). The version-2 Global Precipitation Climatology Project (GPCP) monthly precipitation analysis (1979-present), *Journal of Hydrometeorology*, **4**(6), 1147-1167, doi:10.1175/1525-7541(2003)004<1147:tvgpscp>2.0.co;2.
- Alory, G., and Delcroix, T. (2002). Interannual sea level changes and associated mass transports in the tropical Pacific from TOPEX/Poseidon data and linear model results (1964-1999), *Journal of Geophysical Research*, **107**(C10), doi:10.1029/2001jc001067.
- Amemiya, T. (1974). Multivariate regression and simultaneous equation models when the dependent variables are truncated normal, *Econometrica*, **42**(6), 999-1012.
- Ando, K., and McPhaden, M. J. (1997). Variability of surface layer hydrography in the tropical Pacific, *Journal of Geophysical Research*, **102**(C10), 23063-23078, doi:10.1029/97JC01443.
- Ashok, K., Behera, S. K., Rao, S. A., Weng, H., and Yamagata, T. (2007). El Niño Modoki and its possible teleconnections, *Journal of Geophysical Research*, **112**(C11007), doi:10.1029/2006jc003798.
- Ashok, K., Iizuka, S., Rao, S. A., Saji, N. H., and Lee, W. J. (2009a). Processes and boreal summer impacts of the 2004 El Niño Modoki: An AGCM study, *Geophysical Research Letters*, **36**(L04703), doi:10.1029/2008gl036313.
- Ashok, K., Tam, C. Y., and Lee, W. J. (2009b). ENSO Modoki impact on the Southern Hemisphere storm track activity during extended austral winter, *Geophysical Research Letters*, **36**(L12705), doi:10.1029/2009gl038847.
- Barber, C. B., Dobkin, D. P., and Huhdanpaa, H. (1996). The Quickhull algorithm for convex hulls, *ACM Transactions on Mathematical Software*, **22**(4), 469-483, doi:10.1145/235815.235821.

-
- Barbosa, S. M., and Andersen, O. B. (2009). Trend patterns in global sea surface temperature, *International Journal of Climatology*, **29**(14), 2049-2055, doi:10.1002/joc.1855.
- Barnett, T. P., Pierce, D. W., AchutaRao, K. M., Gleckler, P. J., Santer, B. D., Gregory, J. M., and Washington, W. M. (2005). Penetration of human-induced warming into the world's oceans, *Science*, **309**(5732), 284-287, doi:10.1126/science.1112418.
- Barnier, B., Madec, G., Penduff, T., Molines, J. -M., Treguier, A. -M., le Sommer, J., Beckmann, A., Biastoch, A., Boening, C., Dengg, J., Derval, C., Durand, E., Gulev, S., Remy, E., Talandier, C., Theetten, S., Maltrud, M., McClean, J., and de Cuevas, B. (2006). Impact of partial steps and momentum advection schemes in a global ocean circulation model at eddy-permitting resolution, *Ocean Dynamics*, **56**(5-6), 543-567, doi:10.1007/s10236-006-0082-1.
- Battisti, D. S., and Hirst, A. C. (1989). Interannual variability in a tropical atmosphere ocean model – Influence of the basic state, ocean geometry and nonlinearity, *Journal of the Atmospheric Sciences*, **46**(12), 1687-1712, doi:10.1175/1520-0469(1989)046<1687:iviata>2.0.co;2.
- Becker, M., Meyssignac, B., Letetrel, C., Llovel, W., Cazenave, A., and Delcroix, T. (2012). Sea level variations at tropical Pacific Islands since 1950, *Global and Planetary Change*, **80-81**, 85-98, doi:10.1016/j.gloplacha.2011.09.004.
- Bjerknes, J. (1966). A possible response of the atmospheric Hadley circulation to equatorial anomalies of ocean temperature, *Tellus*, **18**, 820-829.
- Bjerknes, J. (1969). Atmospheric teleconnections from the equatorial Pacific, *Monthly Weather Review*, **97**, 163-172.
- Bonjean, F., and Lagerloef, G. S. E. (2002). Diagnostic model and analysis of the surface currents in the tropical Pacific Ocean, *Journal of Physical Oceanography*, **32**(10), 2938-2954, doi:10.1175/1520-0485(2002)032<2938:dmaaot>2.0.co;2.
- Bosc, C., and Delcroix, T. (2008). Observed equatorial Rossby waves and ENSO-related warm water volume changes in the equatorial Pacific Ocean, *Journal of Geophysical Research*, **113**(C06003), doi:10.1029/2007jc004613.
-

-
- Bosc, C., T. Delcroix, and C. Maes (2009). Barrier layer variability in the western Pacific warm pool from 2000 to 2007, *Journal of Geophysical Research*, **114**(C06023), doi:10.1029/2008JC005187.
- Brown, J. N., and Fedorov, A. V. (2010). Estimating the diapycnal transport contribution to warm water volume variations in the tropical Pacific Ocean, *Journal of Climate*, **23**(2), 221-237, doi:10.1175/2009jcli2347.1.
- Bunge, L., and Clarke, A. J. (2009). A verified estimation of the El Niño index Niño-3.4 since 1877, *Journal of Climate*, **22**(14), 3979-3992, doi:10.1175/2009jcli2724.1.
- Cai, W., and T. Cowan (2009). La Niña Modoki impacts Australia autumn rainfall variability, *Geophysical Research Letters*, **36**(L12805), doi:10.1029/2009GL037885.
- Cane, M. A., Clement, A. C., Kaplan, A., Kushnir, Y., Pozdnyakov, D., Seager, R., Zebiak, S. E., and Murtugudde, R. (1997). Twentieth-century sea surface temperature trends, *Science*, **275**(5302), 957-960, doi:10.1126/science.275.5302.957.
- Carton, J. A., and Giese, B. S. (2008). A reanalysis of ocean climate using Simple Ocean Data Assimilation (SODA), *Monthly Weather Review*, **136**(8), 2999-3017, doi:10.1175/2007mwr1978.1.
- Carton, J. A., Giese, B. S., and Grodsky, S. A. (2005). Sea level rise and the warming of the oceans in the Simple Ocean Data Assimilation (SODA) ocean reanalysis, *Journal of Geophysical Research*, **110**(C09006), doi:10.1029/2004jc002817.
- Chen, G., and Tam, C. -Y. (2010). Different impacts of two kinds of Pacific Ocean warming on tropical cyclone frequency over the western North Pacific, *Geophysical Research Letters*, **37**(L01803), doi:10.1029/2009gl041708.
- Chen, J., del Genio, A. D., Carlson, B. E., and Bosilovich, M. G. (2008). The spatiotemporal structure of twentieth-century climate variations in observations and reanalyses. Part I: Long-term trend, *Journal of Climate*, **21**(11), 2611-2633, doi:10.1175/2007jcli2011.1.
- Chen, J., Zhang, R., Wang, H., An, Y., Peng, P., and Zhang, W. (2012). Isolation of sea surface salinity maps of various timescales in the tropical Pacific Ocean, *Journal of Oceanography*, **68**, 687-701, doi:10.1007/s10872-012-0126-8.
-

-
- Chiodi, A. M., and Harrison, D. E. (2010). Characterizing warm-ENSO variability in the equatorial Pacific: An OLR perspective, *Journal of Climate*, **23**(9), 2428-2439, doi:10.1175/2009jcli3030.1.
- Choi, J., An, S. -I., Kug, J. -S., and Yeh, S. -W. (2011). The role of mean state on changes in El Niño's flavor, *Climate Dynamics*, **37**, 1205-1215, doi:10.1007/s00382-010-0912-1.
- Clarke, A. J. (2008). *An introduction to the dynamics of El Niño and the southern oscillation*, Amsterdam, Academic Press, 324 pp.
- Clarke, A. J., van Gorder, S., and Colantuono, G. (2007). Wind stress curl and ENSO discharge/recharge in the equatorial Pacific, *Journal of Physical Oceanography*, **37**(4), 1077-1091, doi:10.1175/jpo3035.1.
- Clement, A. C., Seager, R., Cane, M. A., and Zebiak, S. E. (1996). An ocean dynamical thermostat, *Journal of Climate*, **9**(9), 2190-2196, doi:10.1175/1520-0442(1996)009<2190:aodt>2.0.co;2.
- Collins, M., An, S. -I., Cai, W., Ganachaud, A., Guilyardi, E., Jin, F. -F., Jochum, M., Lengaigne, M., Power, S., Timmermann, A., Vecchi, G., and Wittenberg, A. (2010). The impact of global warming on the tropical Pacific Ocean and El Niño, *Nature Geoscience*, **3**(6), 391-397, doi:10.1038/ngeo868.
- Compo, G. P., and Sardeshmukh, P. D. (2010). Removing ENSO-related variations from the climate record, *Journal of Climate*, **23**(8), 1957-1978, doi:10.1175/2009jcli2735.1.
- Corrège, T. (2006). Sea surface temperature and salinity reconstruction from coral geochemical tracers, *Palaeogeography Palaeoclimatology Palaeoecology*, **232**(2-4), 408-428, doi:10.1016/j.palaeo.2005.10.014.
- Cravatte, S., Delcroix, T., Zhang, D., McPhaden, M., and Leloup, J. (2009). Observed freshening and warming of the western Pacific warm pool, *Climate Dynamics*, **33**(4), 565-589, doi:10.1007/s00382-009-0526-7.
- de Mey, P., and Menard, Y. (1989). Synoptic analysis and dynamical adjustment of GEOS-3 and SEASAT altimeter eddy fields in the northwest Atlantic, *Journal of Geophysical Research*, **94**(C5), 6221-6230, doi:10.1029/JC094iC05p06221.
-

-
- Delcroix, T. (1998). Observed surface oceanic and atmospheric variability in the tropical Pacific at seasonal and ENSO timescales: A tentative overview, *Journal of Geophysical Research*, **103**(C9), 18611-18633, doi:10.1029/98jc00814.
- Delcroix, T., and Henin, C. (1991). Seasonal and interannual variations of sea-surface salinity in the tropical Pacific Ocean, *Journal of Geophysical Research*, **96**(C12), 22135-22150, doi:10.1029/91jc02124.
- Delcroix, T., and J. Picaut (1998). Zonal displacement of the western equatorial Pacific “fresh pool”, *Journal of Geophysical Research*, **103**(C1), 1087-1098.
- Delcroix, T., McPhaden, M. J., Dessier, A., and Gouriou, Y. (2005). Time and space scales for sea surface salinity in the tropical oceans, *Deep Sea Research: Part I*, **52**(5), 787-813, doi:10.1016/j.dsr.2004.11.012.
- Delcroix, T., Cravatte, S., and McPhaden, M. J. (2007). Decadal variations and trends in tropical Pacific sea surface salinity since 1970, *Journal of Geophysical Research*, **112**(C03012), doi:10.1029/2006jc003801.
- Delcroix, T., Alory, G., Cravatte, S., Correge, T., and McPhaden, M. J. (2011). A gridded sea surface salinity data set for the tropical Pacific with sample applications (1950-2008), *Deep Sea Research: Part I*, **58**(1), 38-48, doi:10.1016/j.dsr.2010.11.002.
- Deser, C., and Wallace, J. M. (1987). El-Niño events and their relation to the southern oscillation – 1925-1986, *Journal of Geophysical Research*, **92**(C13), 14189-14196, doi:10.1029/JC092iC13p14189.
- Deser, C., Phillips, A. S., and Alexander, M. A. (2010). Twentieth century tropical sea surface temperature trends revisited, *Geophysical Research Letters*, **37**(L10701), doi:10.1029/2010gl043321.
- Dewitte, B., Vazquez-Cuervo, J., Goubanova, K., Illig, S., Takahashi, K., Cambon, G., Purca, S., Correa, D., Gutierrez, D., Sifeddine, A., and Ortlieb, L. (2012). Change in El Niño flavours over 1958-2008: Implications for the long-term trend of the upwelling off Peru, *Deep Sea Research: Part II*, **77-80**, 143-156, doi:10.1016/j.dsr2.2012.04.011.
-

-
- Ducet, N., le Traon, P. Y., and Reverdin, G. (2000). Global high-resolution mapping of ocean circulation from TOPEX/Poseidon and ERS-1 and 2, *Journal of Geophysical Research*, **105**(C8), 19477-19498, doi:10.1029/2000jc900063.
- Durack, P. J., and Wijffels, S. E. (2010). Fifty-year trends in global ocean salinities and their relationship to broad-scale warming, *Journal of Climate*, **23**(16), 4342-4362, doi:10.1175/2010jcli3377.1.
- Emery, W. J., and Thomson, R. E. (2001). *Data analysis methods in physical oceanography*, 2nd Ed., Elsevier Science Ltd., The Netherlands.
- Fedorov, A. V., and Philander, S. G. (2000). Is El Niño changing?, *Science*, **288**, 1997-2002.
- Fedorov, A. V., Dekens, P. S., McCarthy, M., Ravelo, A. C., de Menocal, P. B., Barreiro, M., Pacanowski, R. C., and Philander, S. G. (2006). The Pliocene paradox (mechanisms for a permanent El Niño), *Science*, **312**(5779), 1485-1489, doi:10.1126/science.1122666.
- Folland, C. K., Renwick, J. A., Salinger, M. J., and Mullan, A. B. (2002). Relative influences of the Interdecadal Pacific Oscillation and ENSO on the South Pacific Convergence Zone, *Geophysical Research Letters*, **29**(13), 1643, doi:10.1029/2001gl014201.
- Fyfe, J. C., Merryfield, W. J., Kharin, V., Boer, G. J., Lee, W. -S., and von Salzen, K. (2011). Skillful predictions of decadal trends in global mean surface temperature, *Geophysical Research Letters*, **38**(L22801), doi:10.1029/2011GL049508.
- GCOS (Global Climate Observing System) (2004). Implementation Plan for the Global Observing System for Climate in Support of the UNFCCC - Executive Summary, *World Meteorological Organization*, **GCOS92(ES)**(WMO/TD No. 1244), 1-29.
- Giese, B. S., and Ray, S. (2011). El Niño variability in Simple Ocean Data Assimilation (SODA), 1871-2008, *Journal of Geophysical Research*, **116**(C02024), doi:10.1029/2010jc006695.
- Gillett, N. P., Zwiers, F. W., Weaver, A. J., and Stott, P. A. (2003). Detection of human influence on sea-level pressure, *Nature*, **422**(6929), 292-294, doi:10.1038/nature01487.
-

-
- Glantz, M. H. (1996). *Currents of change. El Niño's impact on climate and society*, Cambridge University Press, 194 pp.
- Glantz, M. H., Katz, R. W., and Nicholls, N. (1991). *Teleconnections linking worldwide climate anomalies: Scientific basis and societal impact*, Cambridge University Press.
- Goddard, L., and Dilley, M. (2005). El Niño: Catastrophe or opportunity, *Journal of Climate*, **18**(5), 651-665, doi:10.1175/jcli-3277.1.
- Gorman, M. K., Quinn, T. M., Taylor, F. W., Partin, J. W., Cabioch, G., Austin, J. A., Pelletier, B., Ballu, V., Maes, C., and Saustrop, S. (2012). A coral-based reconstruction of sea surface salinity at Sabine Bank, Vanuatu from 1842 to 2007 CE, *Paleoceanography*, **27**(PA3226), doi:10.1029/2012PA002302.
- Gouriou, Y., and Delcroix, T. (2002). Seasonal and ENSO variations of sea surface salinity and temperature in the South Pacific Convergence Zone during 1976-2000, *Journal of Geophysical Research*, **107**(C12), 8011, doi:10.1029/2001jc000830.
- Gruber, A., Su, X. J., Kanamitsu, M., and Schemm, J. (2000). The comparison of two merged rain gauge-satellite precipitation datasets, *Bulletin of the American Meteorological Society*, **81**(11), 2631-2644, doi:10.1175/1520-0477(2000)081<2631:tcotmr>2.3.co;2.
- Guan, B., and Nigam, S. (2008). Pacific sea surface temperatures in the twentieth century: An evolution-centric analysis of variability and trend, *Journal of Climate*, **21**(12), 2790-2809, doi:10.1175/2007jcli2076.1.
- Guilyardi, E. (2006). El Niño-mean state-seasonal cycle interactions in a multi-model ensemble, *Climate Dynamics*, **26**, 329-348, doi:10.1007/s00382-005-0084-6.
- Guilyardi, E., Wittenberg, A., Fedorov, A., Collins, M., Wang, C. Z., Capotondi, A., van Oldenborgh, G. J., and Stockdale, T. (2009). Understanding El Niño in ocean-atmosphere general circulation models – progress and challenges, *Bulletin of the American Meteorological Society*, **90**(3), 325-340, doi:10.1175/2008bams2387.1.
- Halpern, D. (1996). Visiting TOGA's past, *Bulletin of the American Meteorological Society*, **77**(2), 233-242, doi:10.1175/1520-0477(1996)077<0233:vtp>2.0.co;2.
-

-
- Ham, J. -S., and Kug, Y. -G. (2012). How well do current climate models simulate two types of El Niño?, *Climate Dynamics*, **39**, 383-398, doi:10.1007/s00382-011-1157-3.
- Hanley, D. E., Bourassa, M. A., O'Brien, J. J., Smith, S. R., and Spade, E. R. (2003). A quantitative evaluation of ENSO indices, *Journal of Climate*, **16**(8), 1249-1258, doi:10.1175/1520-0442(2003)16<1249:aqeoei>2.0.co;2.
- Hannachi, A. (2007). Pattern hunting in climate: a new method for finding trends in gridded climate data, *International Journal of Climatology*, **27**(1), 1-15, doi:10.1002/joc.1375.
- Hansen, J., Sato, M., Ruedy, R., Lo, K., Lea, D. W., and Medina-Elizade, M. (2006). Global temperature change, *Proceedings of the National Academy of Sciences of the United States of America*, **103**(39), 14288-14293, doi:10.1073/pnas.0606291103.
- Harrison, D. E., and Larkin, N. K. (1998). El Niño-Southern Oscillation sea surface temperature and wind anomalies, 1946-1993, *Reviews of Geophysics*, **36**(3), 353-399, doi:10.1029/98rg00715.
- Harrison, D. E., and Carson, M. (2007). Is the world ocean warming? Upper-ocean temperature trends: 1950-2000, *Journal of Physical Oceanography*, **37**(2), 174-187, doi:10.1175/jpo3005.1.
- Hasegawa, T., Horii, T., and Hanawa, K. (2006). Two different features of discharge of equatorial upper ocean heat content related to El Niño events, *Geophysical Research Letters*, **33**(L02609), doi:10.1029/2005gl024832.
- Held, I. M., and Soden, B. J. (2006). Robust responses of the hydrological cycle to global warming, *Journal of Climate*, **19**(21), 5686-5699, doi:10.1175/jcli3990.1.
- Hendon, H. H., Lim, E., Wang, G., Alves, O., and Hudson, D. (2009). Prospects for predicting two flavors of El Niño, *Geophysical Research Letters*, **36**(L19713), doi:10.1029/2009gl040100.
- Hildebrandsson, H. H. (1898). Recherches sur les centres d'action de l'atmosphère, *Ciel et Terre*, **18**, 215-223.
-

-
- Hope, A. C. A. (1968). A simplified Monte Carlo significance test procedure, *Journal of the Royal Statistical Society. Series B (Methodological)*, **30**(3), 582-598.
- Horii, T., Ueki, I., and Hanawa, K. (2012). Breakdown of ENSO predictors in the 2000s: Decadal changes of recharge/discharge-SST phase relation and atmospheric intraseasonal forcing, *Geophysical Research Letters*, **39**(L10707), doi:10.1029/2012gl051740.
- Huang, B. Y., Mehta, V. M., and Schneider, N. (2005). Oceanic response to idealized net atmospheric freshwater in the Pacific at the decadal time scale, *Journal of Physical Oceanography*, **35**(12), 2467-2486, doi:10.1175/jpo2820.1.
- Huffman, G. J., Adler, R. F., Bolvin, D. T., and Gu, G. (2009). Improving the global precipitation record: GPCP version 2.1, *Geophysical Research Letters*, **36**(L17808), doi:10.1029/2009gl040000.
- IPCC (2007). Climate Change 2007: Synthesis Report. Contribution of Working Groups I, II and III to the Fourth Assessment Report of the Intergovernmental Panel on Climate Change [Core Writing Team, Pachauri, R.K and Reisinger, A. (eds.)], Geneva, Switzerland.
- Izumo, T., Vialard, J., Lengaigne, M., Montegut, C. D. B., Behera, S. K., Luo, J. -J., Cravatte, S., Masson, S., and Yamagata, T. (2010). Influence of the state of the Indian Ocean Dipole on the following year's El Niño, *Nature Geoscience*, **3**, 168-172, doi:10.1038/NGEO760.
- Janowiak, J. E., Gruber, A., Kondragunta, C. R., Livezey, R. E., and Huffman, G. J. (1998). A comparison of the NCEP-NCAR reanalysis precipitation and the GPCP rain gauge-satellite combined dataset with observational error considerations, *Journal of Climate*, **11**(11), 2960-2979, doi:10.1175/1520-0442(1998)011<2960:acotnn>2.0.co;2.
- Jin, F. -F. (1997). An equatorial ocean recharge paradigm for ENSO. Part I: Conceptual model. *Journal of the Atmospheric Sciences*, **54**(7), 811-829, doi:10.1175/1520-0469(1997)054<0811:aeorpf>2.0.co;2.
-

-
- Jin, F. -F., Neelin, J. D., and Ghil, M. (1994). El-Niño on the devils staircase – annual subharmonic steps to chaos, *Science*, **264**(5155), 70-72, doi:10.1126/science.264.5155.70.
- Jones, P. D. (1989). The influence of ENSO on global temperatures, *Climate Monitor*, **17**, 80-89.
- Jones, G. S., Tett, S. F. B., and Stott, P. A. (2003). Causes of atmospheric temperature change 1960-2000: A combined attribution analysis, *Geophysical Research Letters*, **30**(5), 1228, doi:10.1029/2002gl016377.
- Kalnay, E., Kanamitsu, M., Kistler, R., Collins, W., Deaven, D., Gandin, L., Iredell, M., Saha, S., White, G., Woollen, J., Zhu, Y., Chelliah, M., Ebisuzaki, W., Higgins, W., Janowiak, J., Mo, K. C., Ropelewski, C., Wang, J., Leetmaa, A., Reynolds, R., Jenne, and Joseph, D. (1996). The NCEP/NCAR 40-year reanalysis project, *Bulletin of the American Meteorological Society*, **77**(3), 437-471, doi:10.1175/1520-0477(1996)077<0437:tnyrp>2.0.co;2.
- Kao, H. -Y., and Yu, J. -Y. (2009). Contrasting eastern-Pacific and central-Pacific types of ENSO, *Journal of Climate*, **22**(3), 615-632, doi:10.1175/2008jcli2309.1.
- Kaplan, A., Cane, M. A., Kushnir, Y., Clement, A. C., Blumenthal, M. B., and Rajagopalan, B. (1998). Analyses of global sea surface temperature 1856-1991, *Journal of Geophysical Research*, **103**(C9), 18567-18589, doi:10.1029/97JC01736.
- Karl, T. R., Knight, R. W., and Baker, B. (2000). The record breaking global temperatures of 1997 and 1998: Evidence for an increase in the rate of global warming?, *Geophysical Research Letters*, **27**(5), 719-722, doi:10.1029/1999gl010877.
- Kelly, P. M., and Jones, P. D. (1996). Removal of the El Niño southern oscillation signal from the gridded surface air temperature data set, *Journal of Geophysical Research*, **101**(D14), 19013-19022, doi:10.1029/96jd01173.
-

-
- Kilbourne, K. H., Quinn, T. M., Taylor, F. W., Delcroix, T., and Gouriou, Y. (2004). El Niño-Southern Oscillation – related salinity variations recorded in the skeletal geochemistry of a *Porites* coral from Espiritu Santo, Vanuatu, *Climate Dynamics*, **19**(PA4002), doi:10.1029/2004PA001033.
- Kim, S. T., and Yu, J. -Y. (2012). The two types of ENSO in CMIP5 models, *Geophysical Research Letters*, **39**(L11704), doi:10.1029/2012GL052006.
- Kim, H. -M., Webster, P. J., and Curry, J. A. (2009). Impact of shifting patterns of Pacific Ocean warming on north Atlantic tropical cyclones, *Science*, **325**(5936), 77-80, doi:10.1126/science.1174062.
- Kim, J. -S., Kim, K. -Y., and Yeh, S. -W. (2012). Statistical evidence for the natural variation of the central Pacific El Niño, *Journal of Geophysical Research*, **117**(C06014), doi:10.1029/2012JC008003.
- Kohonen, T. (1989). *Self-organization and associative memory*, 3rd Ed., New York, Springer-Verlag New York Inc.
- Kug, J. -S., Jin, F. -F., and An, S. -I. (2009). Two types of El Niño events: cold tongue El Niño and warm pool El Niño, *Journal of Climate*, **22**(6), 1499-1515, doi:10.1175/2008jcli2624.1.
- Kug, J. -S., Choi, J., An, S. -I., Jin, F. -F., and Wittenberg, A. T. (2010). Warm pool and cold tongue El Niño events as simulated by the GFDL 2.1 coupled GCM, *Journal of Climate*, **23**(5), 1226-1239, doi:10.1175/2009jcli3293.1.
- Kumar, O., Naidu, C. V., and Rao, S. R. L. (2004). Influence of southern oscillation and SSTs over Niño-3.4 region on the winter monsoon rainfall over coastal Andhra Pradesh, *Proceedings of the Indian Academy of Sciences-Earth and Planetary Sciences*, **113**(3), 313-319.
- Lagerloef, G., Colomb, F. R., le Vine, D., Wentz, F., Yueh, S., Ruf, C., Lilly, J., Gunn, J., Chao, Y., de Charon, A., Feldman, G., and Swift, C. (2008). The Aquarius/SAC-D mission: designed to meet the salinity remote-sensing challenge, *Oceanography*, **21**(1), 68-81.
-

-
- Larkin, N. K., and Harrison, D. E. (2002). ENSO warm (El Niño) and cold (La Niña) event life cycles: Ocean surface anomaly patterns, their symmetries, asymmetries, and implications, *Journal of Climate*, **15**(10), 1118-1140, doi:10.1175/1520-0442(2002)015<1118:ewenoa>2.0.co;2.
- Larkin, N. K., and Harrison, D. E. (2005a). Global seasonal temperature and precipitation anomalies during El Niño autumn and winter, *Geophysical Research Letters*, **32**(L16705), doi:10.1029/2005gl022860.
- Larkin, N. K., and Harrison, D. E. (2005b). On the definition of El Niño and associated seasonal average US weather anomalies, *Geophysical Research Letters*, **32**(L13705), doi:10.1029/2005gl022738.
- Latif, M., Kleeman, R., and Eckert, C. (1997). Greenhouse warming, decadal variability, or El Niño? An attempt to understand the anomalous 1990s, *Journal of Climate*, **10**(9), 2221-2239, doi:10.1175/1520-0442(1997)010<2221:gwldvoe>2.0.co;2.
- Lau, K. M., and Weng, H. Y. (1999). Interannual, decadal-interdecadal, and global warming signals in sea surface temperature during 1955-97, *Journal of Climate*, **12**(5), 1257-1267, doi:10.1175/1520-0442(1999)012<1257:idiagw>2.0.co;2.
- Lean, J. L., and Rind, D. H. (2008). How natural and anthropogenic influences alter global and regional surface temperatures: 1889 to 2006, *Geophysical Research Letters*, **35**(L18701), doi:10.1029/2008GL034864.
- Lee, T., and McPhaden, M. J. (2008). Decadal phase change in large-scale sea level and winds in the Indo-Pacific region at the end of the 20th century, *Geophysical Research Letters*, **35**(L01605), doi:10.1029/2007gl032419.
- Lee, T., and McPhaden, M. J. (2010). Increasing intensity of El Niño in the central-equatorial Pacific, *Geophysical Research Letters*, **37**(L14603), doi:10.1029/2010gl044007.
- Leloup, J. A., Lachkar, Z., Boulanger, J. -P., and Thiria, S. (2007). Detecting decadal changes in ENSO using neural networks, *Climate Dynamics*, **28**, 147-162, doi:10.1007/s00382-006-0173-1.
-

-
- Leloup, J., Lengaigne, M., and Boulanger, J. -P. (2008). Twentieth century ENSO characteristics in the IPCC database, *Climate Dynamics*, **30**, 277-291, doi:10.1007/s00382-007-0284-3.
- Lengaigne, M., Hausmann, U., Madec, G., Menkes, C., Vialard, J., and Molines, J. M. (2012). Mechanisms controlling warm water volume interannual variations in the equatorial Pacific: diabatic versus adiabatic processes, *Climate Dynamics*, **38**, 1031-1046, doi:10.1007/s00382-011-1051-z.
- Li, G., Ren, B., Zheng, J., and Yang, C. (2011). Trend singular value decomposition analysis and its application to the global ocean surface latent heat flux and SST anomalies, *Journal of Climate*, **24**, 2931-2948, doi:10.1175/2010JCLI3743.1.
- Lian, T., and Chen, D. (2012). An evaluation of rotated EOF analysis and its application to tropical Pacific SST variability, *Journal of Climate*, **25**, 5361-5373, doi:10.1175/JCLI-D-11-00663.1.
- Lim, H. S., and Ho, C. H. (2000). Comparison of tropical rainfall between the observed GPCP data and the assimilation products of ECMWF, NCEP/NCAR, and NASA-GEOS-1, *Journal of the Meteorological Society of Japan*, **78**(5), 661-672.
- Maes, C., and Behringer, D. (2000). Using satellite-derived sea level and temperature profiles for determining the salinity variability: A new approach, *Journal of Geophysical Research*, **105**(C4), 8537-8547, doi:10.1029/1999JC900279.
- Maes, C., Ando, K., Delcroix, T., Kessler, W. S., McPhaden, M. J., and Roemmich, D. (2006). Observed correlation of surface salinity, temperature and barrier layer at the eastern edge of the western Pacific warm pool, *Geophysical Research Letters*, **33**(L06601), doi:10.1029/2005GL024772.
- Mantua, N. J., and Hare, S. R. (2002). The Pacific decadal oscillation, *Journal of Oceanography*, **58**(1), 35-44, doi:10.1023/a:1015820616384.
- McPhaden, M. J. (2003). Tropical Pacific Ocean heat content variations and ENSO persistence barriers, *Geophysical Research Letters*, **30**(9), 1480, doi:10.1029/2003gl016872.
-

-
- McPhaden, M. J. (2004). Evolution of the 2002/03 El Niño, *Bulletin of the American Meteorological Society*, **85**(5), 677-695, doi:10.1175/BAMS-85-5-677.
- McPhaden, M. J. (2008). Evolution of the 2006-2007 El Niño: the role of intraseasonal to interannual time scale dynamics, *Advances in Geosciences*, **14**, 219-230.
- McPhaden, M. J. (2012). A 21st century shift in the relationship between ENSO SST and warm water volume anomalies, *Geophysical Research Letters*, **39**(L09706), doi:10.1029/2012gl051826.
- McPhaden, M. J., and Zhang, X. (2009). Asymmetry in zonal phase propagation of ENSO sea surface temperature anomalies, *Geophysical Research Letters*, **36**(L13703), doi:10.1029/2009gl038774.
- McPhaden, M. J., Busalacchi, A. J., Cheney, R., Donguy, J. R., Gage, K. S., Halpern, D., Ji, M., Julian, P., Meyers, G., Mitchum, G. T., Niiler, P. P., Picaut, J., Reynolds, R. W., Smith, N., and Takeuchi, K. (1998). The tropical ocean global atmosphere observing system: A decade of progress, *Journal of Geophysical Research*, **103**(C7), 14169-14240, doi:10.1029/97jc02906.
- McPhaden, M. J., Zebiak, S. E., and Glantz, M. H. (2006). ENSO as an integrating concept in Earth science, *Science*, **314**(5806), 1740-1745, doi:10.1126/science.1132588.
- McPhaden, M. J., Busalacchi, A. J., and Anderson, D. L. T. (2010). A TOGA retrospective, *Oceanography*, **23**(3), 86-103.
- McPhaden, M. J., Lee, T., and McClurg, D. (2011). El Niño and its relationship to changing background conditions in the tropical Pacific Ocean, *Geophysical Research Letters*, **38**(L115709), doi:10.1029/2011GL048275.
- Mechoso, C. R., Neelin, J. D., and Yu, J. Y. (2003). Testing simple models of ENSO, *Journal of the Atmospheric Sciences*, **60**(2), 305-318, doi:10.1175/1520-0469(2003)060<0305:tsmoe>2.0.co;2.
- Meinen, C. S. (2005). Meridional extent and interannual variability of the Pacific Ocean tropical-subtropical warm water exchange, *Journal of Physical Oceanography*, **35**(3), 323-335, doi:10.1175/jpo-2694.1.
-

-
- Meinen, C. S., and McPhaden, M. J. (2000). Observations of warm water volume changes in the equatorial Pacific and their relationship to El Niño and La Niña, *Journal of Climate*, **13**(20), 3551-3559, doi:10.1175/1520-0442(2000)013<3551:oowwvc>2.0.co;2.
- Meinen, C. S., and McPhaden, M. J. (2001). Interannual variability in warm water volume transports in the equatorial Pacific during 1993-99, *Journal of Physical Oceanography*, **31**(5), 1324-1345, doi:10.1175/1520-0485(2001)031<1324:iviwwv>2.0.co;2.
- Merrifield, M. A. (2011). A shift in western tropical Pacific sea level trends during the 1990s, *Journal of Climate*, **24**(15), 4126-4138, doi:10.1175/2011jcli3932.1.
- Merrifield, M. A., and Maltrud, M. E. (2011). Regional sea level trends due to a Pacific trade wind intensification, *Geophysical Research Letters*, **38**(L21605), doi:10.1029/2011gl049576.
- Meyers, G., McIntosh, P., Pigot, L., and Pook, M. (2007). The years of El Niño, La Niña, and interactions with the tropical Indian ocean, *Journal of Climate*, **20**(13), 2872-2880, doi:10.1175/jcli4152.1.
- Meyssignac, B., Salas y Melia, D., Becker, M., Llovel, W., and Cazenave, A. (2012). Tropical Pacific spatial trend patterns in observed sea level: internal variability and/or anthropogenic signature?, *Climate of the Past*, **8**(2), 787-802, doi:10.5194/cp-8-787-2012.
- Millero, F. J., Feistel, R., Wright, D. G., and McDougall, T. J. (2008). The composition of standard seawater and the definition of the reference-composition salinity scale, *Deep Sea Research: Part I*, **55**(1), 50-72, doi:10.1016/j.dsr.2007.10.001.
- Newman, M., Shin, S. -I., and Alexander, M. A. (2011). Natural variation in ENSO flavours, *Geophysical Research Letters*, **38**(L14705), doi:10.1029/2011GL047658.
- Nicholls, N. (2008). Recent trends in the seasonal and temporal behaviour of the El Niño-Southern Oscillation, *Geophysical Research Letters*, **35**(L19703), doi:10.1029/2008GL034499.
-

-
- North, G. R., Bell, T. L., Cahalan, R. F., and Moeng, F. J. (1982). Sampling errors in the estimation of empirical orthogonal functions, *Monthly Weather Review*, **110**(7), 699-706, doi:10.1175/1520-0493(1982)110<0699:seiteo>2.0.co;2.
- Okumura, Y. M., and Deser, C. (2010). Asymmetry in the duration of El Niño and La Niña, *Journal of Climate*, **23**, 5826-5843, doi:10.1175/2010JCLI3592.1.
- Palmer, T. N., and Mansfield, D. A. (1984). Response of two atmospheric general-circulation models to sea-surface temperature anomalies in the tropical east and west Pacific, *Nature*, **310**(5977), 483-485, doi:10.1038/310483a0.
- Pezzulli, S., Stephenson, D. B., and Hannachi, A. (2005). The Variability of Seasonality, *Journal of Climate*, **18**, 71-88.
- Philander, S. G. (1990). *El Niño, La Niña, and the Southern Oscillation*, San Diego, Academic Press, 293 pp.
- Philander, S. G. (1999). El Niño and La Niña predictable climate fluctuations, *Reports on Progress in Physics*, **62**(2), 123.
- Picaut, J., and Delcroix, T. (1995). Equatorial wave sequence associated with warm pool displacements during the 1986-1989 El Niño-La Niña, *Journal of Geophysical Research*, **100**(C9), 18393-18408, doi:10.1029/95JC01358.
- Picaut, J., Ioualalen, M., Menkes, C., Delcroix, T., and McPhaden, M. J. (1996). Mechanism of the zonal displacements of the Pacific warm pool: Implications for ENSO, *Science*, **274**(5292), 1486-1489, doi:10.1126/science.274.5292.1486.
- Picaut, J., Masia, F., and du Penhoat, Y. (1997). An advective-reflective conceptual model for the oscillatory nature of the ENSO, *Science*, **277**(5326), 663-666, doi:10.1126/science.277.5326.663.
- Picaut, J., Ioualalen, M., Delcroix, T., Masia, F., Murtugudde, R., and Vialard, J. (2001). The oceanic zone of convergence on the eastern edge of the Pacific warm pool: A synthesis of results and implications for El Niño-Southern Oscillation and biogeochemical phenomena, *Journal of Geophysical Research*, **106**(C2), 2363-2386, doi:10.1029/2000jc900141.
-

-
- Picaut, J., Hackert, E., Busalacchi, A. J., Murtugudde, R., Lagerloef, G. S. E. (2002). Mechanisms of the 1997-1998 El Niño-La Niña, as inferred from space-based observations, *Journal of Geophysical Research*, **107**(C5), 1-16, doi:10.1029/2001JC000850.
- Qiu, B., and Chen, S. (2006). Decadal variability in the large-scale sea surface height field of the South Pacific Ocean: Observations and causes, *Journal of Physical Oceanography*, **36**(9), 1751-1762, doi:10.1175/jpo2943.1.
- Quinn, W. H., Neal, V. T., and de Mayolo, S. E. A. (1987). El Niño Occurrences over the past four and a half centuries, *Journal of Geophysical Research*, **92**(C13), 14449-14461, doi:10.1029/JC092iC13p14449.
- Radenac, M. -H., Léger, F., Singh, A., and Delcroix, T. (2012). Sea surface chlorophyll signature in the tropical Pacific during eastern and central Pacific ENSO events, *Journal of Geophysical Research*, **117**(C04007), doi:10.1029/2011jc007841.
- Rasmusson, E. M., and Carpenter, T. H. (1982). Variations in tropical sea-surface temperature and surface wind fields associated with the southern oscillation El-Niño, *Monthly Weather Review*, **110**(5), 354-384, doi:10.1175/1520-0493(1982)110<0354:vitsst>2.0.co;2.
- Rayner, N. A., Parker, D. E., Horton, E. B., Folland, C. K., Alexander, L. V., Rowell, D. P., Kent, E. C., and Kaplan, A. (2003). Global analyses of sea surface temperature, sea ice, and night marine air temperature since the late nineteenth century, *Journal of Geophysical Research*, **108**(D14), 4407, doi:10.1029/2002jd002670.
- Ren, H. -L., and Jin, F. -F. (2011). Niño indices for two types of ENSO, *Geophysical Research Letters*, **38**(L04704), doi:10.1029/2010gl046031.
- Roemmich, D., and Gilson, J. (2011). The global ocean imprint of ENSO, *Geophysical Research Letters*, **38**(L13606), doi:10.1029/2011GL047992.
- Roemmich, D., Johnson, G. C., Riser, S., Davis, R., Gilson, J., Owens, W. B., Garzoli, S. L., Schmid, C., and Ignaszewski, M. (2009). The Argo program observing the global ocean with profiling floats, *Oceanography*, **22**(2), 34-43.
-

-
- Santer, B. D., Wigley, T. M. L., Doutriaux, C., Boyle, J. S., Hansen, J. E., Jones, P. D., Meehl, G. A., Roeckner, E., Sengupta, S., and Taylor, K. E. (2001). Accounting for the effects of volcanoes and ENSO in comparisons of modeled and observed temperature trends, *Journal of Geophysical Research*, **106**(D22), 28033-28059, doi:10.1029/2000jd000189.
- Santer, B. D., Wehner, M. F., Wigley, T. M. L., Sausen, R., Meehl, G. A., Taylor, K. E., Ammann, C., Arblaster, J., Washington, W. M., Boyle, J. S., and Bruggemann, W. (2003). Contributions of anthropogenic and natural forcing to recent tropopause height changes, *Science*, **301**(5632), 479-483, doi:10.1126/science.1084123.
- Singh, A., and Aung, T. (2005). Effect of barometric pressure on sea level variations in the Pacific region, *The South Pacific Journal of Natural and Applied Sciences*, **23**(1), 9-15, doi:10.1071/SP05002.
- Singh, A., and Delcroix, T. (2011). Estimating the effects of ENSO upon the observed freshening trends of the western tropical Pacific Ocean, *Geophysical Research Letters*, **38**(L21607), doi:10.1029/2011gl049636.
- Singh, A., and Delcroix, T. (2012). Eastern and Central Pacific ENSO and their relationships to the recharge/discharge oscillator paradigm. *Deep Sea Research: Part I*, submitted.
- Singh, A., Delcroix, T., and Cravatte, S. (2011). Contrasting the flavours of El Niño-Southern Oscillation using sea surface salinity observations, *Journal of Geophysical Research*, **116**(C06016), doi:10.1029/2010jc006862.
- Smith, T. M., and Reynolds, R. W. (2003). Extended reconstruction of global sea surface temperatures based on COADS data (1854-1997), *Journal of Climate*, **16**(10), 1495-1510, doi:10.1175/1520-0442-16.10.1495.
- Solomon, A., and Newman, M. (2011). Decadal predictability of tropical Indo-Pacific Ocean temperature trends due to anthropogenic forcing in a coupled climate model, *Geophysical Research Letters*, **38**(L02703), doi:10.1029/2010gl045978.
-

-
- Stevenson, S., Fox-Kemper, B., Jochum, M., Rajagopalan, B., and Yeager, S. (2010). ENSO model validation using wavelet probability analysis, *Journal of Climate*, **23**, 5540-5547, doi:10.1175/2010JCLI3609.1.
- Suarez, M. J., and Schopf, P. S. (1988). A delayed action oscillator for ENSO, *Journal of the Atmospheric Sciences*, **45**(21), 3283-3287, doi:10.1175/1520-0469(1988)045<3283:adaofe>2.0.co;2.
- Sudre, J., and Morrow, R. A. (2008). Global surface currents: a high-resolution product for investigating ocean dynamics, *Ocean Dynamics*, **58**(2), 101-118, doi:10.1007/s10236-008-0134-9.
- Terray, L., Corre, L., Cravatte, S., Delcroix, T., Reverdin, G., and Ribes, A. (2012). Near-surface salinity as nature's rain gauge to detect human influence on the tropical water cycle, *Journal of Climate*, **25**(3), 958-977, doi:10.1175/jcli-d-10-05025.1.
- Thompson, B. (1993). The use of statistical significance tests in research: bootstrap and other alternatives. *Journal of Experimental Education*, **61**(4), 361-377.
- Thompson, D. W. J., Wallace, J. M., Jones, P. D., and Kennedy, J. J. (2009). Identifying signatures of natural climate variability in time series of global-mean surface temperature: Methodology and insights, *Journal of Climate*, **22**(22), 6120-6141, doi:10.1175/2009jcli3089.1.
- Timmermann, A., McGregor, S., and Jin, F. -F. (2010). Wind effects on past and future regional sea level trends in the southern Indo-Pacific, *Journal of Climate*, **23**(16), 4429-4437, doi:10.1175/2010jcli3519.1.
- Tomé, A. R., and Miranda, P. M. A. (2004). Piecewise linear fitting and trend changing points of climate parameters, *Geophysical Research Letters*, **31**(2), L02207, doi:10.1029/2003gl019100.
- Trenberth, K. E. (1984). Signal versus noise in the southern oscillation, *Monthly Weather Review*, **112**(2), 326-332, doi:10.1175/1520-0493(1984)112<0326:svnits>2.0.co;2.
- Trenberth, K. E. (1997). The definition of El Niño, *Bulletin of the American Meteorological Society*, **78**(12), 2771-2777, doi:10.1175/1520-0477(1997)078<2771:tdoen>2.0.co;2.
-

-
- Trenberth, K. E., and Stepaniak, D. P. (2001). Indices of El Niño evolution, *Journal of Climate*, **14**(8), 1697-1701, doi:10.1175/1520-0442(2001)014<1697:lioeno>2.0.co;2.
- van Oldenborgh, G. J., Philip, S. Y., and Collins, M. (2005). El Niño in a changing climate: A multi-model study, *Ocean Science*, **1**, 81-95, doi:10.5194/os-1-81-2005.
- Vecchi, G. A., and Harrison, D. E. (2003). On the termination of the 2002-03 El Niño event, *Geophysical Research Letters*, **30**(18), doi:10.1029/2003GL017564.
- Vecchi, G. A., and Wittenberg, A. T. (2010). El Niño and our future climate: where do we stand?, *Wiley Interdisciplinary Reviews: Climate Change*, **1**(2), 260-270, doi:10.1002/wcc.33.
- Vecchi, G. A., Soden, B. J., Wittenberg, A. T., Held, I. M., Leetmaa, A. and Harrison, M. J. (2006). Weakening of tropical Pacific atmospheric circulation due to anthropogenic forcing, *Nature*, **44**, 73-76, doi:10.1038/nature04744.
- Vecchi, G. A., Clement, A., and Soden, B. J. (2008). Examining the tropical Pacific's response to global warming, *Eos Transactions AGU*, **89**(9), doi:10.1029/2008eo090002.
- Vialard, J., Delecluse, P., and Menkes, C. (2002). A modeling study of salinity variability and its effects in the tropical Pacific Ocean during the 1993-1999 period, *Journal of Geophysical Research*, **107**(C12), 1-14, doi:10.1029/2000JC000758.
- Vincent, D. G. (1994). The South-Pacific Convergence Zone (SPCZ) – A review, *Monthly Weather Review*, **122**(9), 1949-1970, doi:10.1175/1520-0493(1994)122<1949:tspcza>2.0.co;2.
- Vincent, E. M., Lengaigne, M., Menkes, C. E., Jourdain, N. C., Marchesiello, P., and Madec, G. (2009). Interannual variability of the South Pacific Convergence Zone and implications for tropical cyclone genesis, *Climate Dynamics*, **36**(9-10), 1881-1896, doi:10.1007/s00382-009-0716-3.
- von Schuckmann, K., and le Traon, P. -Y. (2011). How well can we derive Global Ocean Indicators from Argo data?, *Ocean Science*, **7**, 783-791, doi:10.5194/os-7-783-2011.
-

-
- Walker, G. T. (1923). Correlation in seasonal variations of weather. VIII. A preliminary study of world-weather, *Memoirs of the Indian Meteorological Department*, **24**(Part 4), 75-131.
- Walker, G. T. (1924). Correlation in seasonal variations of weather, IX. A further study of world weather, *Memoirs of India Meteorological Department*, **24**(9), 275-332.
- Walker, G. T. (1928). World weather, III, *Memoirs of India Meteorological Department*, **2**, 97-106.
- Walker, G. T., and Bliss, E. W. (1930). World weather, IV, *Memoirs of Royal Meteorological Society*, **3**, 81-95.
- Walker, G. T., and Bliss, E. W. (1932). World weather, V, *Memoirs of Royal Meteorological Society*, **4**, 53-84.
- Walker, G. T., and Bliss, E. W. (1937). World weather, VI, *Memoirs of Royal Meteorological Society*, **4**, 119-139.
- Wang, B. (1995). Interdecadal changes in El Niño onset in the last 4 decades, *Journal of Climate*, **8**(2), 267-285, doi:10.1175/1520-0442(1995)008<0267:icieno>2.0.co;2.
- Wang, C. (2001). A unified oscillator model for the El Niño-Southern Oscillation, *Journal of Climate*, **14**, 98-115, doi:10.1175/1520-0442(2001)014<0098:AUOMFT>2.0.CO;2.
- Wang, B., and An, S. I. (2001). Why the properties of El Niño changed during the late 1970s, *Geophysical Research Letters*, **28**(19), 3709-3712, doi:10.1029/2001gl012862.
- Wang, C. Z., and Picaut, J. (2004). Understanding ENSO physics – A review, *Earth's Climate: the Ocean-Atmosphere Interaction*, **147**, 21-48.
- Ward, J. H. (1963). Hierarchical grouping to optimize an objective function, *Journal of the American Statistical Association*, **58**(301), 236-244.
- Weisberg, R. H., and Wang, C. Z. (1997). A western Pacific oscillator paradigm for the El Niño Southern Oscillation, *Geophysical Research Letters*, **24**(7), 779-782, doi:10.1029/97gl00689.
-

-
- Weng, H., Ashok, K., Behera, S. K., Rao, S. A., and Yamagata, T. (2007). Impacts of recent El Niño Modoki on dry/wet conditions in the Pacific rim during boreal summer, *Climate Dynamics*, **29**(2-3), 113-129, doi:10.1007/s00382-007-0234-0.
- Weng, H., Behera, S. K., and Yamagata, T. (2009). Anomalous winter climate conditions in the Pacific rim during recent El Niño Modoki and El Niño events, *Climate Dynamics*, **32**, 663-674, doi:10.1007/s00382-008-0394-6.
- Wentz, J. F., Ricciardulli, L., Hilburn, K., and Mears, C. (2007). How much more rain will global warming bring? *Science*, **317**(5835), 233-235, doi:10.1126/science.1140746.
- Wolter, K., and Timlin, M. S. (1998). Measuring the strength of ENSO events: How does the 1997/98 rank?, *Weather*, **53**(9), 315-324.
- WMO (World Meteorological Organization), (1989). Calculation of monthly and annual 30-year standard normals, **WCDP-No. 10**(WMO-TD/No. 341).
- Wyrтки, K. (1975). El Niño – The dynamic-response of equatorial Pacific Ocean to atmospheric forcing, *Journal of Physical Oceanography*, **5**(4), 572-584, doi:10.1175/1520-0485(1975)005<0572:entdro>2.0.co;2.
- Wyrтки, K. (1981). An estimate of equatorial upwelling in the Pacific, *Journal of Physical Oceanography*, **11**(9), 1205-1214, doi:10.1175/1520-0485(1981)011<1205:aeoeui>2.0.co;2.
- Wyrтки, K. (1985). Water displacements in the pacific and the genesis of El-Niño cycles, *Journal of Geophysical Research*, **90**(NC4), 7129-7132, doi:10.1029/JC090iC04p07129.
- Wyrтки, K., and Kilonsky, B. (1984). Mean water and current structure during the Hawaii-to-Tahiti shuttle experiment, *Journal of Physical Oceanography*, **14**(2), 242-254, doi:10.1175/1520-0485(1984)014<0242:mwacsd>2.0.co;2.
- Xiang, B., Wang, B., and Li, T. (2012). A new paradigm for the predominance of standing Central Pacific Warming after the late 1990s, *Climate Dynamics*, 1-14, doi:10.1007/s00382-012-1427-8.
-

-
- Xie, P. P., and Arkin, P. A. (1997). Global precipitation: A 17-year monthly analysis based on gauge observations, satellite estimates, and numerical model outputs, *Bulletin of the American Meteorological Society*, **78**(11), 2539-2558, doi:10.1175/1520-0477(1997)078<2539:gpayma>2.0.co;2.
- Xie, P. P., Janowiak, J. E., Arkin, P. A., Adler, R., Gruber, A., Ferraro, R., Huffman, G. J., and Curtis, S. (2003). GPCP pentad precipitation analyses: An experimental dataset based on gauge observations and satellite estimates, *Journal of Climate*, **16**(13), 2197-2214, doi:10.1175/2769.1
- Yeh, S. -W., Kug, J. -S., Dewitte, B., Kwon, M. -H., Kirtman, B. P., and Jin, F. -F. (2009). El Niño in a changing climate, *Nature*, **461**(7263), 511-514, doi:10.1038/nature08316.
- Yeh, S. -W., Kirtman, B. P., Kug, J. -S., Park, W., and Latif, M. (2011). Natural variability of the central Pacific El Niño event on multi-centennial timescales, *Geophysical Research Letters*, **38**(L02704), doi:10.1029/2010gl045886.
- Yu, L. (2007). Global variations in oceanic evaporation (1958-2005): The role of the changing wind speed, *Journal of Climate*, **20**, 5367-5390, doi:10.1175/2007JCLI1714.1.
- Yu, J. -Y., and Kim, S. T. (2010). Three evolution patterns of Central-Pacific El Niño, *Geophysical Research Letters*, **37**(L08706), doi:10.1029/2010gl042810.
- Yu, J. -Y., and Kim, S. T. (2011). Reversed spatial asymmetries between El Niño and La Niña and their linkage to decadal ENSO modulation in CMIP3 models, *Journal of Climate*, **24**, 5423-5434, doi:10.1175/JCLI-D-11-00024.1.
- Yu, J. -Y., Kao, H. -Y., and Lee, T. (2010a). Subtropics-related interannual sea surface temperature variability in the central equatorial Pacific, *Journal of Climate*, **23**(11), 2869-2884, doi:10.1175/2010jcli3171.1.
- Yu, J. -Y., Kao, H. -Y., Lee, T., and Kim, S. T. (2010b). Subsurface ocean temperature indices for Central-Pacific and Eastern-Pacific types of El Niño and La Niña events, *Theoretical and Applied Climatology*, **103**(3-4), 337-344, doi:10.1007/s00704-010-0307-6.
-

Zhang, X., Zwiers, F. W., Hegerl, G. C., Lambert, F. H., Gillett, N. P., Solomon, S., Stott, P. A., and Nozawa, T. (2007). Detection of human influence on twentieth-century precipitation trends, *Nature*, **448**(7152), 461-464, doi:10.1038/nature06025.

Appendix II Publication: Radenac *et al.*, 2012

The following article was published in *Journal of Geophysical Research* in 2012 as a parallel study for this PhD thesis.

Radenac, M. H., Léger, F., Singh, A., and Delcroix, T. (2012). Sea surface chlorophyll signature in the tropical Pacific during Eastern and Central Pacific ENSO events, *Journal of Geophysical Research*, **117**(C04007), doi:10.1029/2011JC007841.

Sea surface chlorophyll signature in the tropical Pacific during eastern and central Pacific ENSO events

Marie-Hélène Radenac,¹ Fabien Léger,¹ Awnesh Singh,¹ and Thierry Delcroix¹

Received 16 December 2011; revised 7 February 2012; accepted 9 February 2012; published 4 April 2012.

[1] Recent analyses of physical measurements show the existence of a central Pacific type of El Niño (CPEN) with a sea surface temperature warming pattern distinct from that of the “classical” eastern Pacific El Niño (EPEN). In this study, we analyze the surface chlorophyll signature of El Niño-Southern Oscillation (ENSO), using monthly maps of satellite-derived chlorophyll anomalies between September 1997 and December 2010. We identify five typical ENSO structures. The first structure describes the lonely 1997–1998 EPEN of the period, the second and third represent La Niña, the fourth illustrates intermediate conditions, and the fifth characterizes CPEN. During the 1997–1998 EPEN, a large eastward shift of the oligotrophic warm pool and a reduction of equatorial upwelling result in negative chlorophyll anomalies east of 170°E between 10°S and 10°N. During the four CPEN events, a reduced eastward shift yields negative chlorophyll anomalies in the equatorial band, within about 160°E and 160°W only. Westward surface current in the central basin limits the expansion of the anomaly core. Negative chlorophyll anomalies that extend eastward from the equatorial anomaly core probably result from reduced upward iron fluxes linked to the deepening of the Equatorial Undercurrent. During La Niña, the westward expansion of the equatorial upwelling results in positive chlorophyll anomalies west of the date line. Away from the equatorial band, advection of oligotrophic warm pool waters by enhanced eastward countercurrents drives negative anomalies within 8–10°N and toward the Marquesas Islands during CPEN, while reduced countercurrents lead to positive chlorophyll anomaly during La Niña.

Citation: Radenac, M.-H., F. Léger, A. Singh, and T. Delcroix (2012), Sea surface chlorophyll signature in the tropical Pacific during eastern and central Pacific ENSO events, *J. Geophys. Res.*, 117, C04007, doi:10.1029/2011JC007841.

1. Introduction

[2] It is now well established that El Niño-Southern Oscillation (ENSO) events account for an important part of the global climate variability on interannual timescales with notable impacts on environment, ecosystems, economy, and society [Glantz, 2000; McPhaden *et al.*, 2006]. Numerous studies have shown that sea surface temperatures (SST) warmer than seasonal values invade the central and, sometimes, the eastern equatorial Pacific during the warm phase (El Niño) of the ENSO cycle. However, many differences have been observed among the various El Niño events. Among those differences, warm SST anomalies occur both in the eastern and central Pacific during the conventional El Niño, also referred to as canonical, cold tongue, or eastern Pacific El Niño, while warm SST anomalies remain confined only in the central Pacific during most of the events observed in recent years [Trenberth and Stepaniak, 2001; Ashok *et al.*, 2007; Kug *et al.*, 2009; Kao and Yu, 2009]. Interestingly, this latter type of events, referred to as central Pacific El Niño,

dateline El Niño, or El Niño Modoki, has been shown to be more intense in recent decades [Lee and McPhaden, 2010] and could be more frequent in a warming world [Yeh *et al.*, 2009]. Some studies argue that this later type of events differs from conventional ENSO [Ashok *et al.*, 2007] while other studies argue that both types belong to an overall non-linear phenomenon [Takahashi *et al.*, 2011]. In this study, we will refer to these two types of El Niño as eastern Pacific (EP) and central Pacific (CP) El Niño.

[3] Based on atmospheric observations, the well known Southern Oscillation Index (SOI) is often used to identify the warm and cold phases of ENSO. Based on oceanic observations, several SST indices were further proposed to distinguish the EP and CP El Niño. These mainly rely on comparisons between SST anomalies, normalized or not, in the Niño3 (5°S–5°N, 150°W–90°W) and Niño4 (5°S–5°N, 160°E–150°W) regions [Kug *et al.*, 2009; Yeh *et al.*, 2009; Kim *et al.*, 2009]. Some studies also rely on other possible El Niño indices such as the Trans-Niño Index (TNI) [Trenberth and Stepaniak, 2001], El Niño Modoki Index (EMI) [Ashok *et al.*, 2007], and other metrics [e.g., Kao and Yu, 2009; Takahashi *et al.*, 2011; Ren and Jin, 2011]. Singh *et al.* [2011] also proposed ENSO indices based on differences of sea surface salinity (SSS) anomaly in two equatorial regions

¹LEGOS, UMR 5566, CNRS/IRD/CNES/UPS, Toulouse, France.

Table 1. Classification of ENSO Events as Central Pacific (CP) or Eastern Pacific (EP) El Niño (EN) or La Niña (LN)^a

	Years											
	97–98	98–99	99–00	00–01	02–03	04–05	05–06	06–07	07–08	08–09	09–10	10
<i>Ashok et al.</i> [2007]					CPEN	CPEN						
<i>Kim et al.</i> [2009]	EPEN	EPLN	EPLN		CPEN	CPEN						
<i>Yeh et al.</i> [2009]	EPEN				CPEN	CPEN		EPEN				
<i>Kao and Yu</i> [2009]	EPEN	CPLN	CPLN		CPEN	CPEN	EPLN					
<i>Kug et al.</i> [2009]	EPEN	LN	LN	LN	CPEN	CPEN	LN					
<i>Lee and McPhaden</i> [2010]	EPEN	LN			CPEN	CPEN		EPEN	LN		CPEN	
<i>Ren and Jin</i> [2011]	EPEN	LN	LN		CPEN	CPEN		CPEN	LN		CPEN	
<i>Singh et al.</i> [2011]	EPEN	CPLN	EPLN	EPLN	CPEN	CPEN	EPLN	CPEN	EPLN	EPLN		
<i>McPhaden et al.</i> [2011]	EPEN				CPEN	CPEN		EPEN			CPEN	
This study	EPEN	LN	LN	LN	CPEN	CPEN		CPEN	LN	LN	CPEN	LN

^aAll studies used SST except *Singh et al.* [2011] used SSS and this study used chlorophyll to characterize ENSO.

and in the South Pacific Convergence Zone (SPCZ). Identifications of EP and CP events following several of these methods are fairly consistent. Some discrepancies however exist and reflect the complexity of the problem as events may evolve from one type to the other [*Yu and Kim*, 2010; *Takahashi et al.*, 2011] or may have patterns intermediate between the EP and CP types [*Kug et al.*, 2009]. Table 1 summarizes the classification of EP and CP ENSO events since the strong El Niño in 1997–1998 (see also *Singh et al.* [2011, Table 1] for previous years).

[4] Although physical processes responsible for SST anomaly patterns during CP El Niño are, by far, not completely understood, they seem to differ from the ones leading to EP El Niño. Basically, during EP El Niño, the weakening of the trade winds and basin wide variations of thermocline depth lead to warming in the eastern equatorial Pacific while positive SST anomalies in the central basin result from eastward advection of the warm pool [*Picaut et al.*, 2001; *Vialard et al.*, 2001; *Kao and Yu*, 2009; *Kug et al.*, 2009]. For CP El Niño, local atmospheric forcing and zonal advection are likely mechanisms involved in the development, confinement, and decay of anomalies in the central basin [*Kao and Yu*, 2009; *Kug et al.*, 2009; *Singh et al.*, 2011]. The so-called thermocline and advection feedbacks would then be at work during EP El Niño, while the advection feedback would mostly be at work during CP El Niño.

[5] Mechanisms that control the SST warming during EP El Niño apparently account for the decrease of biological production in the equatorial Pacific. During the 1997–1998 El Niño, nutrient- and phytoplankton-poor (surface chlorophyll lower than 0.1 mg m^{-3}) waters of the warm pool were advected eastward to the central and eastern basins while vertical inputs of nutrients decreased in the east because of the thermocline deepening and the reduction of the upward vertical velocity [*Chavez et al.*, 1998; *Radenac et al.*, 2001]. The ecosystem of the equatorial upwelling region is iron-limited [*Landry et al.*, 1997] and the thermocline deepening is associated with the depression of the Equatorial Undercurrent (EUC) that transports iron across the basin from the western Pacific [*Gordon et al.*, 1997; *Wells et al.*, 1999; *Lacan and Jeandel*, 2001]. As biologically available iron in the photic layer is mainly upwelled from the EUC [*Gordon et al.*, 1997], strong reduction of the iron fluxes ensues from the depression of the EUC during El Niño [*Barber et al.*, 1996; *Gordon et al.*, 1997; *Chavez et al.*, 1999; *Friedrichs and Hofmann*, 2001]. The result is a collapse of

new and primary production in the equatorial Pacific during the 1997–1998 [*Chavez et al.*, 1999; *Strutton and Chavez*, 2000; *Radenac et al.*, 2001; *Turk et al.*, 2001] and previous EP El Niño events [*Barber and Kogelschatz*, 1990; *Barber et al.*, 1996]. However, to our knowledge, no study characterizes the response of the equatorial ecosystems to the subsequent CP El Niño events in 2002–2003, 2004–2005, 2006–2007, and 2009–2010, apart from the recent paper by *Turk et al.* [2011]. This is the goal of this study. The occurrence and strength of CP El Niño have increased since the 1990s [*Lee and McPhaden*, 2010]) and their frequency may still increase in future as stressed by *Yeh et al.* [2009]. Therefore, further investigations are necessary to better understand ENSO related physical-biological interactions and their impacts on biological fields and dynamics up to top predators.

[6] The manuscript is organized as follows. Section 2 describes the satellite-derived data that allow us to describe the 1997–2010 changes in surface chlorophyll on basin scale. To set the context, section 3 compares the SST, SSS, and surface chlorophyll anomalies in the equatorial band. Then, section 4 contrasts the surface chlorophyll anomaly signatures characterizing the EP and CP El Niño, and section 5 analyzes the possible impacts of changes in surface circulation and thermocline depth on the surface chlorophyll distribution. A discussion and conclusion appear in the last section.

2. Data and Methods

[7] Surface chlorophyll concentrations were derived from Sea-viewing Wide Field-of-view Sensor (SeaWiFS) measurements and from the Moderate Resolution Imaging Spectroradiometer (MODIS) measurements aboard the Aqua satellite. SeaWiFS data are available between September 1997 and December 2010 and MODIS data since July 2002. We used 9 km resolution monthly composites computed by the NASA Goddard Space Flight Center (GSFC) Distributed Active Archive Center (DAAC) [*McClain et al.*, 2004]. When a SeaWiFS monthly map was not available or had less than 60% of data available (7 maps, i.e., 4.4% of the time), we used the Aqua MODIS map in order to obtain a complete chlorophyll time series from September 1997 to December 2010. For each location, chlorophyll values higher than 3 mg m^{-3} and/or that were more than five standard deviations away from the 1997–2010 mean were treated as missing [*Messié and Radenac*, 2006]. In the calculations, we

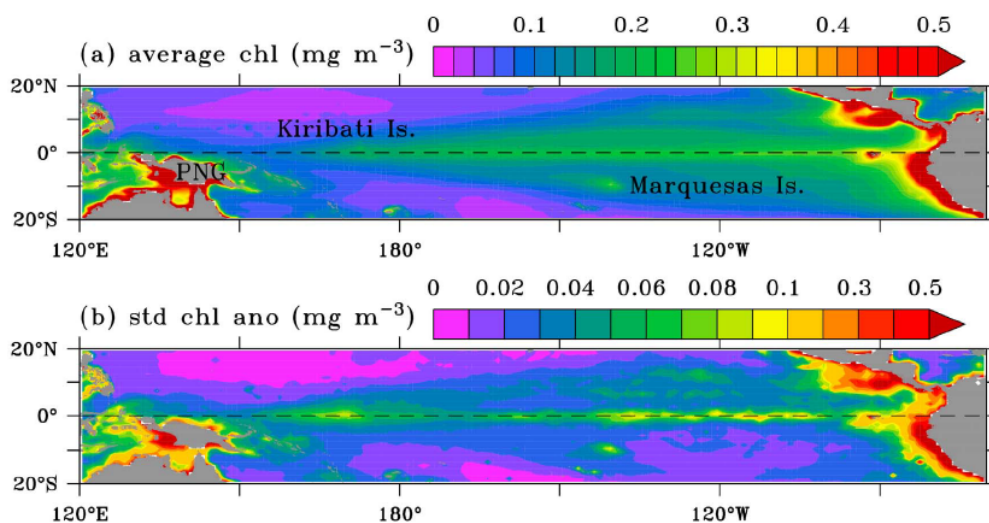


Figure 1. Maps of (a) average and (b) interannual standard deviation of the surface chlorophyll computed over the September 1997 to December 2010 period. PNG stands for Papua New Guinea.

interpolated the data onto a $1^\circ \times 1^\circ$ grid following the method of *Yoder and Kennelly* [2003]. First, we computed $0.25^\circ \times 0.25^\circ$ maps using the maximum likelihood estimator [*Campbell et al.*, 1995]. Then, most of the data gaps due to sparse clouds were filled by taking the median of every $1^\circ \times 1^\circ$ cell. The remaining missing data were filled by taking the median of the first neighbors. The chlorophyll anomalies we present are relative to a mean seasonal cycle calculated between 1998 and 2010. We also used monthly maps of Photosynthetically Available Radiation (PAR) estimates derived from SeaWiFS and MODIS [*Frouin et al.*, 2003].

[8] SST data was provided by the Hadley Centre for Climate Prediction and Research Sea Ice and Sea Surface Temperature HadISST1 data set [*Rayner et al.*, 2003]. Monthly SST maps are available since 1870 on a $1^\circ \times 1^\circ$ grid. SSS data came from the recently updated *Delcroix et al.* [2011] product for the tropical Pacific. Monthly SSS data are available on a $1^\circ \times 1^\circ$ grid and span from 1950 to 2009. Monthly near surface currents were obtained from the Ocean Surface Current Analysis - Real time (OSCAR) $1^\circ \times 1^\circ$ product; the geostrophic, wind-driven, and thermal-wind components of which are derived from satellite data [*Bonjean and Lagerloef*, 2002]. Monthly anomalies of wind speed and depth of the 20°C ($Z_{20^\circ\text{C}}$) isotherms are derived from time series recorded at the Tropical Atmosphere Ocean/Triangle Trans Ocean Buoy Network (TAO/TRITON) [*McPhaden et al.*, 1998] moorings. We also used time series of the SOI and EMI [*Ashok et al.*, 2007].

[9] Different statistical procedures have been used in the literature to discriminate ENSO features. To name a few, these include regression of anomaly onto specific ENSO indices [*Trenberth and Stepaniak*, 2001; *Ren and Jin*, 2011; *Takahashi et al.*, 2011; *Singh and Delcroix*, 2011], Empirical Orthogonal Functions (EOF) analyses [*Ashok et al.*, 2007; *Park et al.*, 2011], combined regression-EOF analyses [*Kao and Yu*, 2009], neural network [*Hsieh*, 2001; *Leloup et al.*, 2008], and Agglomerative Hierarchical Clustering (AHC)

analysis [*Kao and Yu*, 2009; *Singh et al.*, 2011]. We tested here the EOF and AHC analyses on chlorophyll in the tropical Pacific. The EOF analysis of the chlorophyll anomaly indicates that the CP El Niño signal is distributed over at least the first, third, and fourth modes (not shown). Hence, the EOF technique does not distinguish properly EP and CP El Niño. A similar leakage of the signal was found for the EOF analysis of SSS in the tropical Pacific [*Singh et al.*, 2011]. Therefore, we chose to perform an AHC analysis on the monthly surface chlorophyll anomalies to characterize ENSO related signatures. In this nonlinear composite procedure, maps are merged into clusters according to their similarity, estimated from the smallest Euclidean distance (defined as the root-mean squared distance between each pair of maps). The clustering procedure can be represented by a dendrogram tree that illustrates combinations made at each successive step of the analysis. This technique has been successfully performed on SST [*Kao and Yu*, 2009], SSS [*Singh et al.*, 2011], and South Pacific Convergence Zone (SPCZ) location [*Vincent et al.*, 2009] to separate ENSO signatures in the tropical Pacific. In this study, we applied the AHC method to monthly maps of surface chlorophyll anomalies for the region between 130°E – 70°W and 10°S – 10°N . The Indonesian Throughflow region and Central and South America coastal upwellings were excluded as regional effects may mask the basin-scale ENSO signature (Figure 1).

3. Comparing SST, SSS, and Surface Chlorophyll Anomalies in the Equatorial Band

[10] The mean chlorophyll distribution and its interannual variability are presented first to set the context (Figure 1). The mean values were computed by averaging all monthly values covering the 1997–2010 period, and the interannual variability was defined as the standard deviation of the chlorophyll anomalies (relative to the mean seasonal cycle). Figure 1a shows that the mean chlorophyll is lower than

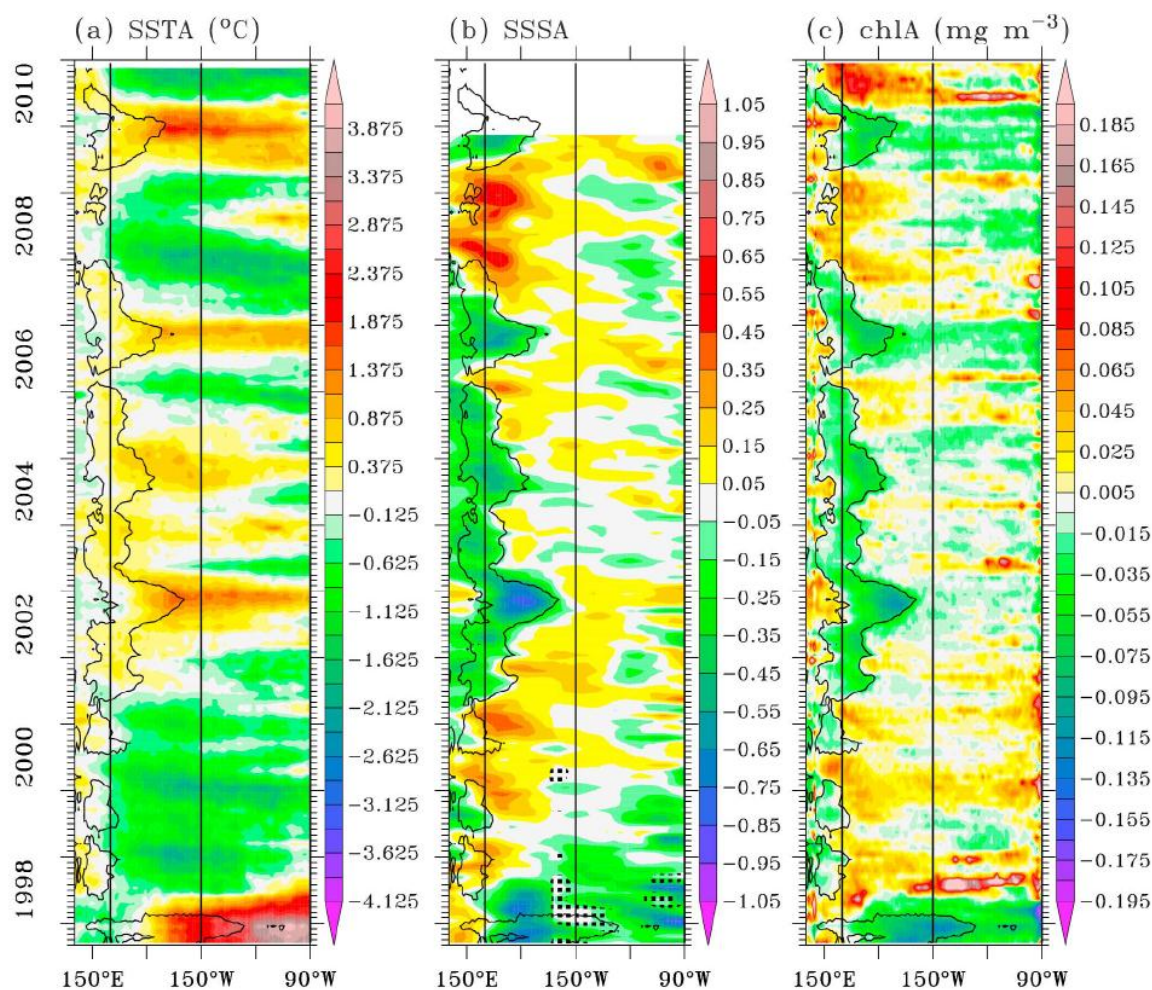


Figure 2. Longitude-time distribution of the anomaly of (a) SST, (b) SSS, and (c) surface chlorophyll averaged between 5°S and 5°N . The black contour encloses the region with surface chlorophyll lower than 0.1 mg m^{-3} . Vertical lines indicate the zonal boundaries of the Niño3 (150°W , 90°W) and Niño4 (160°E , 150°W) boxes. Regions with dots in Figure 2b indicate normalized SSS errors larger than 0.80.

0.3 mg m^{-3} outside the Central and South America upwelling regions, with well-marked maxima in a huge equatorial region spreading westward from the South American coast. These values are mostly due to the equatorial upwelling which brings cool, salty, and nutrient-rich waters toward the surface. Although the surface nitrate concentration is high in the upwelling, the chlorophyll content remains moderate (less than 0.2 mg m^{-3} on average) because of an iron-limited and grazing-balanced ecosystem [Landry *et al.*, 1997]. Mesotrophic waters of the equatorial upwelling are surrounded by oligotrophic waters ($[\text{chl}] < 0.1 \text{ mg m}^{-3}$) of the warm pool to the west and of subtropical gyres poleward (note also the moderate mesotrophic waters north of Papua New Guinea and near the Solomon Sea). The interannual variability (Figure 1b) is high between 10°S and 10°N , especially along the equator, in the North Equatorial Countercurrent (NECC) region, around Papua New Guinea, and in the Central and South America coastal upwelling regions.

[11] Looking at the regions of maximum interannual variability, the longitude-time distributions of the 5°N – 5°S averaged SST, SSS, and surface chlorophyll anomalies are shown in Figure 2. For all El Niño events, the maximum positive SST anomaly occurs during boreal winter, between September and February (Figure 2a). The location and amplitude of the anomaly differ from one event to the other. The 1997–1998 (EP, see Table 1 and below) El Niño is the only one with very warm SST anomaly ($\text{SSTA} > 3^{\circ}\text{C}$) that peaks east of 120°W and extends toward the central basin. During the following (CP, see Table 1 and below) El Niño events, the maximum SST anomaly is lower (sometimes less than 1°C) and mostly situated in the central-western basin, at least in 2002–2003, 2004–2005, and 2009–2010. The strongest warming (SST anomaly close to 2°C) during a CP El Niño event is reached during the mature phase of the 2009–2010 event, in agreement with Lee and McPhaden [2010].

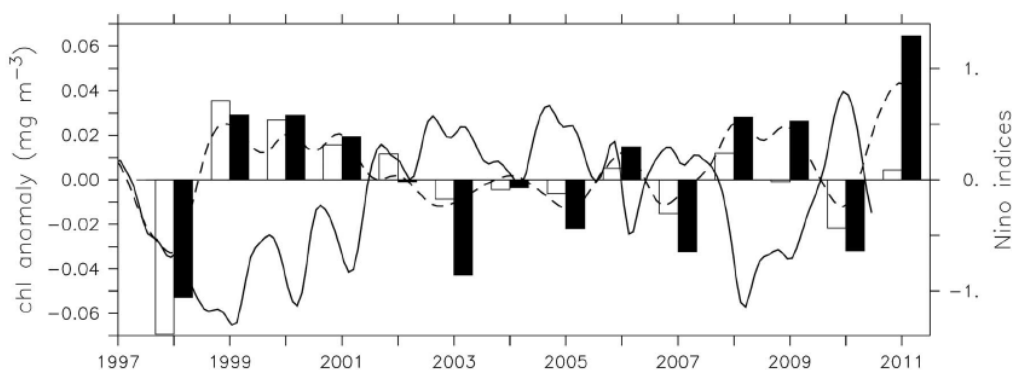


Figure 3. Surface chlorophyll anomaly averaged between September and February in the Niño3 (150°W–90°W, 5°S–5°N; hollow bars) and Niño4 (160°E–150°W, 5°S–5°N; filled bars) boxes. EMI (full line) and $0.25 \times$ SOI (dashed line) are scaled on the right axis.

[12] The strongest negative SSS anomalies (Figure 2b) appear to be located west of the maximum positive SST anomalies. During the 1997–1998 EP El Niño, the SSS anomaly is negative east of 160°E, with a maximum freshening near the date line. During the following CP El Niño events, the maximum negative anomalies tend to be displaced westward by 10 to 15° of longitude, except in 2002–2003, in agreement with *Singh et al.* [2011].

[13] The time series of surface chlorophyll anomaly (Figure 2c) is reminiscent of the SSS anomaly time series as strong negative chlorophyll anomalies tend to be located west of the warm El Niño-related SST anomalies. In 1997–1998, the strong anomaly core ($< -0.12 \text{ mg m}^{-3}$) is near 150°W and the surface chlorophyll concentration is below the mean seasonal value from 150°E to the American coast. During the following events, the negative anomaly core (-0.08 to -0.10 mg m^{-3}) is located in the central-western basin, between about 150°E and 180°, while the moderate anomalies observed eastward range between less than -0.02 mg m^{-3} in 2002–2003 and 2004–2005 to -0.04 mg m^{-3} in 2006–2007 and 2009–2010.

[14] Oligotrophic waters ($[\text{chl}] < 0.1 \text{ mg m}^{-3}$) have been shown to be quasi-persistent in the eastern part of the equatorial warm pool while moderate mesotrophic waters (surface chlorophyll concentration slightly higher than 0.1 mg m^{-3}) were often observed in its western part [*Radenac et al.*, 2010]. This oligotrophic region is delimited by the black contour in Figures 2a, 2b, and 2c. The easternmost limit of this zone characterizes the eastern edge of the warm pool [*Murtugudde et al.*, 1999; *Stoens et al.*, 1999; *Radenac et al.*, 2010] that separates waters of the eastern warm pool ($[\text{chl}] < 0.1 \text{ mg m}^{-3}$) from upwelled waters ($[\text{chl}] > 0.1 \text{ mg m}^{-3}$). Large zonal displacements of the eastern edge of the warm pool occur at interannual timescales and its longitudinal position is related to the phases of ENSO [*Picaut and Delcroix*, 1995; *Le Borgne et al.*, 2002]. It reaches 130°W during the 1997–1998 EP El Niño and lies between the dateline and 160°W during CP events. Interestingly, the oligotrophic waters of the eastern part of the warm pool follow these movements (Figure 2c). Thus, the maximum negative chlorophyll and SSS anomaly cores are both located west of the warmest SST anomalies.

[15] Several La Niña years interleave between El Niño years (Table 1). When La Niña events reach their mature phase in boreal winter (e.g., in early 2008), SST in the central and eastern basins are cooler while becoming slightly warmer west of 160°E (Figure 2a). Strong positive anomalies of SSS and surface chlorophyll are closely related west of 150°W (Figures 2b and 2c). They are located at the western limit of the cool SST anomaly, in the region of zonal displacements of the eastern edge of the warm pool. Chlorophyll anomalies exceed 0.10 mg m^{-3} in 2010 and range between 0.05 and 0.08 mg m^{-3} during the other La Niña years. A moderate increase of chlorophyll ($< 0.03 \text{ mg m}^{-3}$) is observed eastward of these maxima.

[16] Figure 2c shows that the chlorophyll anomalies are negative all along the equator in 1997–1998 while the core of chlorophyll anomaly remains west of 150°W during the following boreal winters (see also spatial patterns from the cluster analysis below). Therefore, comparing the chlorophyll anomalies averaged over the Niño3 and Niño4 regions during the peak period of the events (September–February; Figure 3) mostly concurs with the classification of La Niña and CP and EP El Niño events. Chlorophyll anomalies are negative in both regions during El Niño years ($\text{SOI} < 0$) and positive during La Niña years ($\text{SOI} > 0$). Also, differences between the anomalies in each region are consistent with the CP El Niño as depicted by the EMI (Figure 3). The amplitude of the chlorophyll anomaly indeed tends to be greater in Niño4 than in Niño3 during CP El Niño ($\text{EMI} > 0$). Following these results, the 2006–2007 El Niño is identified here as a CP event as in the SSS study [*Singh et al.*, 2011] and in contrast to most of the SST studies (Table 1). The 2009–2010 event, acknowledged as the warmest CP El Niño during the last decades [*Lee and McPhaden*, 2010], yields chlorophyll anomalies in Niño4 weaker than during the 2002–2003 event. Actually, the magnitude of the chlorophyll decrease in Niño4 is linked to the eastward expansion of the oligotrophic warm pool (Figure 2c) whereas warming in Niño4 is not (Figure 2a). During La Niña winters, the chlorophyll anomaly in Niño4 is always larger than in Niño3 (except in 1998–1999), suggesting that the strongest increase of chlorophyll occur in the region of zonal shifts of

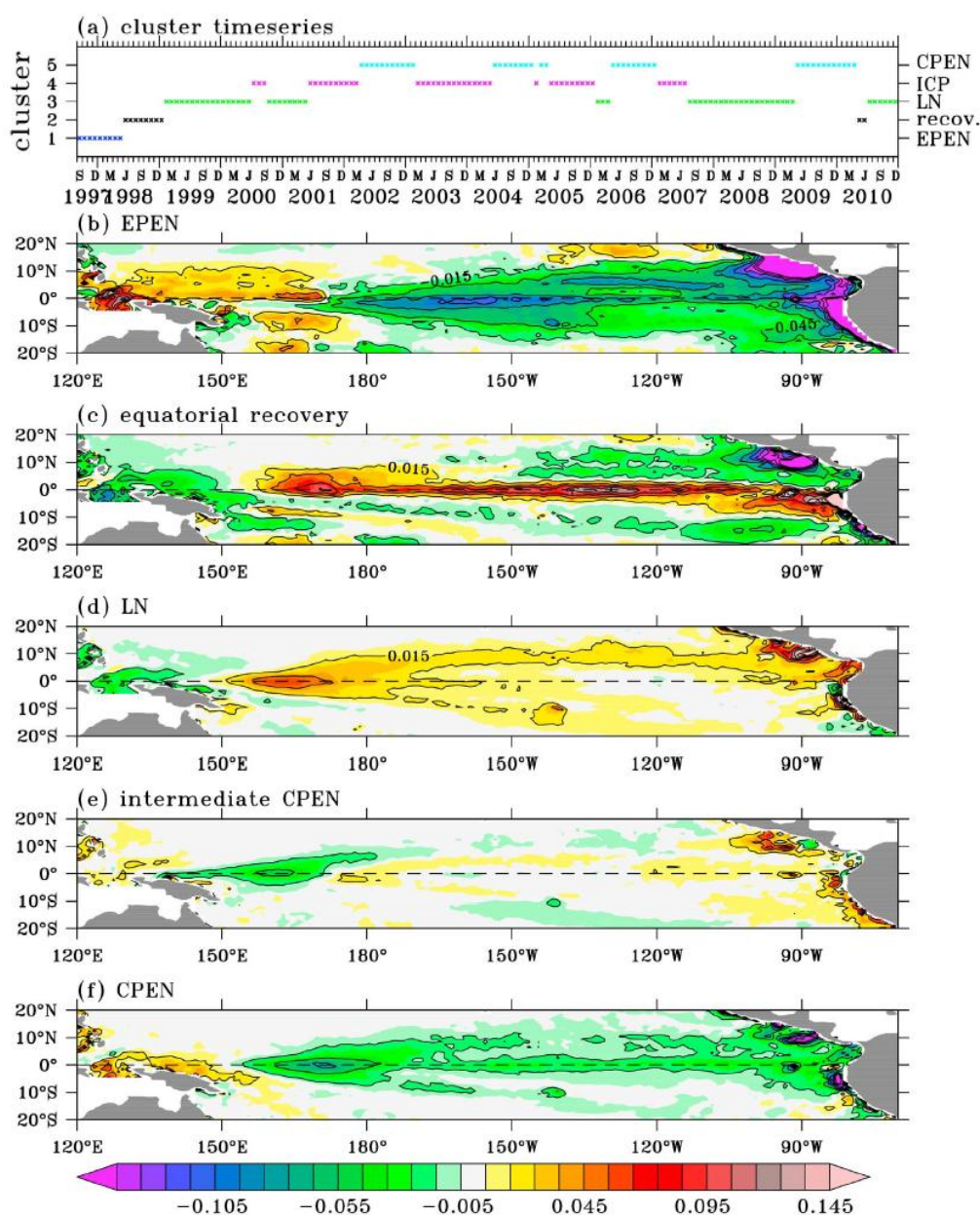


Figure 4. (a) Time series of the cluster analysis. Spatial patterns of the corresponding surface chlorophyll anomaly during the so-called (b) eastern Pacific El Niño (EPEN), (c) equatorial recovery conditions (recov), (d) La Niña (LN), (e) intermediate central Pacific period (ICP), and (f) central Pacific El Niño (CPEN). Chlorophyll anomaly contours are every 0.03 mg m⁻³. The 0 mg m⁻³ contour is omitted.

the eastern edge of the warm pool. The greatest winter increase reached in the Niño4 region is in 2010–2011.

4. Describing the Spatial Patterns of ENSO-Related Surface Chlorophyll Anomalies

[17] Using the AHC analysis described in section 2, we identified five clusters out of 160 monthly maps during the

September 1997–December 2010 period. As detailed below, we believe they are representative of EP El Niño, equatorial recovery, La Niña, intermediate CP El Niño, and CP El Niño conditions. They occur about 6%, 6%, 34%, 28%, and 26% of the time, respectively. The associated time series and the derived composite maps are presented in Figure 4. Occurrences of EP El Niño (1997–1998), CP El Niño (2002–2003, 2004–2005, 2006–2007, 2009–2010), and La Niña events

(1998–1999, 1999–2000, 2000–2001, 2007–2008, 2008–2009, 2010–2011) are consistent with those found in previous studies using SST or SSS indices (Table 1) and with the comparison of chlorophyll anomalies in the Niño3 and Niño4 regions (Figure 3). Of note, the cluster analysis does not classify the end of 1998 as typical La Niña conditions although that period has been described as a La Niña year from the surface chlorophyll distribution [Murtugudde et al., 1999; Radenac et al., 2001; Ryan et al., 2002] and from other variables (Figure 3 and Table 1): the reason for this is discussed below. Intermediate CP El Niño periods occur in 2001–2002, 2003–2004, 2005–2006, and 2007 near CP El Niño years when the SOI or EMI is weak (Figure 3).

[18] Aside from the “all-month” AHC analysis we present, we also performed an AHC analysis using September to February months only (not shown) because CP and EP El Niño and La Niña events reach their mature phase in boreal winter for most climate variables [Kao and Yu, 2009] and for chlorophyll changes [Chavez et al., 1999; Strutton and Chavez, 2000; Radenac et al., 2001] (see also Figure 2). In that case, we obtained similar patterns for the CP and EP El Niño, and La Niña clusters. The strong equatorial signal (Figure 4c) however did not show up as elevated chlorophyll concentration along the equator was observed in boreal spring and summer. Caution is thus required when selecting some months per year only in analyzing ENSO features.

[19] Cluster 1 captures the spatial pattern of the only EP El Niño event over the study period (Figure 4b). Given the strength of this event, it is not surprising that its spatial pattern resembles that of the EOF analysis performed on the 1997–1999 chlorophyll data [Wilson and Adamec, 2001]. The chlorophyll anomaly is negative over a broad region from 170°E to the American coast and maximum along the equator. The northern limit of the negative anomaly region is sharp and almost zonally oriented near 8°N while the southern limit may look smoother and extends south of 10°S (except west of the dateline). Unlike the SST anomaly pattern during EP El Niño, which is strongest near the American coast and extends westward along the equator [Rasmusson and Carpenter, 1982; Kao and Yu, 2009; Kug et al., 2009], the chlorophyll anomaly seems to have two distinct cores (lower than -0.075 mg m^{-3}). One core is found between the date line and 140°W and the other one east of 110°W in the equatorial region. The chlorophyll anomaly is positive in the western basin mostly between the equator and 10° latitudes.

[20] Characteristics of surface chlorophyll during the four CP El Niño events are represented by cluster 5 (Figure 4f). The negative anomaly pattern has an arrow shape whose head would be the core of the largest negative anomaly (less than -0.08 mg m^{-3}) located at the equator around 170°E. Thin bands of negative chlorophyll anomaly (-0.02 to -0.01 mg m^{-3}) stretches from the anomaly core along 8–10°N to the Central American coast, while another of lower magnitude extends to the Marquesas Islands at 140°W, 10°S. The tail of the arrow would be the narrow band of moderate negative anomaly (-0.03 to -0.02 mg m^{-3}) along the equator from the anomaly core to the American coast. The core of maximum negative surface chlorophyll anomaly matches the core of maximum negative SSS anomaly [Singh et al., 2011] during both El Niño types, and in the same way as the SST anomaly, it is shifted westward during

CP El Niño compared to EP El Niño. The three zonal bands of moderate negative chlorophyll anomaly that stretch eastward from the equatorial minimum anomaly core are specific to the chlorophyll signature. In the western Pacific, north of Papua New Guinea and Solomon Islands, chlorophyll anomalies are positive during CP El Niño events.

[21] The timing of La Niña years, captured by cluster 3 (Figure 4a), are consistent with the occurrence of positive SOI (Figure 3). The La Niña patterns (Figure 4d) somewhat mirror the CP El Niño patterns (Figure 4f) in the western half of the basin, although the maximum anomaly is stronger and extends 5° to 10° longitude further to the west during La Niña. In agreement with Figure 3, cluster 3 thus shows that the positive chlorophyll anomalies in Niño4 region are larger than in Niño3 (Figure 4d). Narrow bands of positive anomaly stretch from the high positive anomaly core along the equator and 6°N–7°N toward the American coast and to the Marquesas Islands. Cluster 2 captures a strong enhancement of the surface chlorophyll concentration ($>0.05 \text{ mg m}^{-3}$) in a narrow equatorial band by the end of 1998 and mid-2010 (Figures 4a and 4c) during the strong La Niña events that followed the strong 1997–1998 EP El Niño and 2009–2010 CP El Niño. Two cores with chlorophyll anomaly higher than 0.08 mg m^{-3} are located west of the Kiribati Islands (175°E) and between 140°W and 120°W. Anomalies are negative between 10°S and 10°N in the western basin and poleward of 5° in the east.

[22] Surface chlorophyll distribution captured by cluster 4 (Figures 4a and 4e) appears when the SOI and chlorophyll anomalies in the Niño3 and Niño4 regions are weak (Figure 2). The main feature is a negative anomaly zone in the western equatorial basin.

5. Analyzing Possible Drivers of Surface Chlorophyll Changes During El Niño Events

[23] In this section, we investigate mechanisms that could possibly constrain the overall spatial structure of surface chlorophyll anomaly during El Niño events, relying on changes in surface zonal current, wind, and thermocline depth (assumed to be the 20°C isotherm depth, $Z_{20^\circ\text{C}}$). We first recall the main results obtained for the 1997–1998 EP El Niño [Chavez et al., 1999; Murtugudde et al., 1999; Stoens et al., 1999; Wilson and Adamec, 2001; Strutton and Chavez, 2000; Radenac et al., 2001, 2005]. Then, we choose to describe the spatial evolution of chlorophyll anomaly during CP El Niño, with a slight focus on the fairly representative 2002–2003 event, rather than on a composite, in order to preserve tiny structures whose positions are slightly different among events. Figure 5 shows the time evolution of the anomalies of zonal wind speed, $Z_{20^\circ\text{C}}$, and surface zonal current along the equator from September 1997 to December 2010. The limits of the oligotrophic region are indicated by the black contour in each panel. Anomalies of the surface current are superimposed on the surface chlorophyll anomalies during the peak period (September–February) of the 1997–1998 EP El Niño (Figure 6) and 2002–2003 CP El Niño (Figure 7).

5.1. The 1997–1998 EP El Niño Event

[24] During boreal fall of 1997, strong anomalous eastward currents dominate the equatorial Pacific (Figures 5c

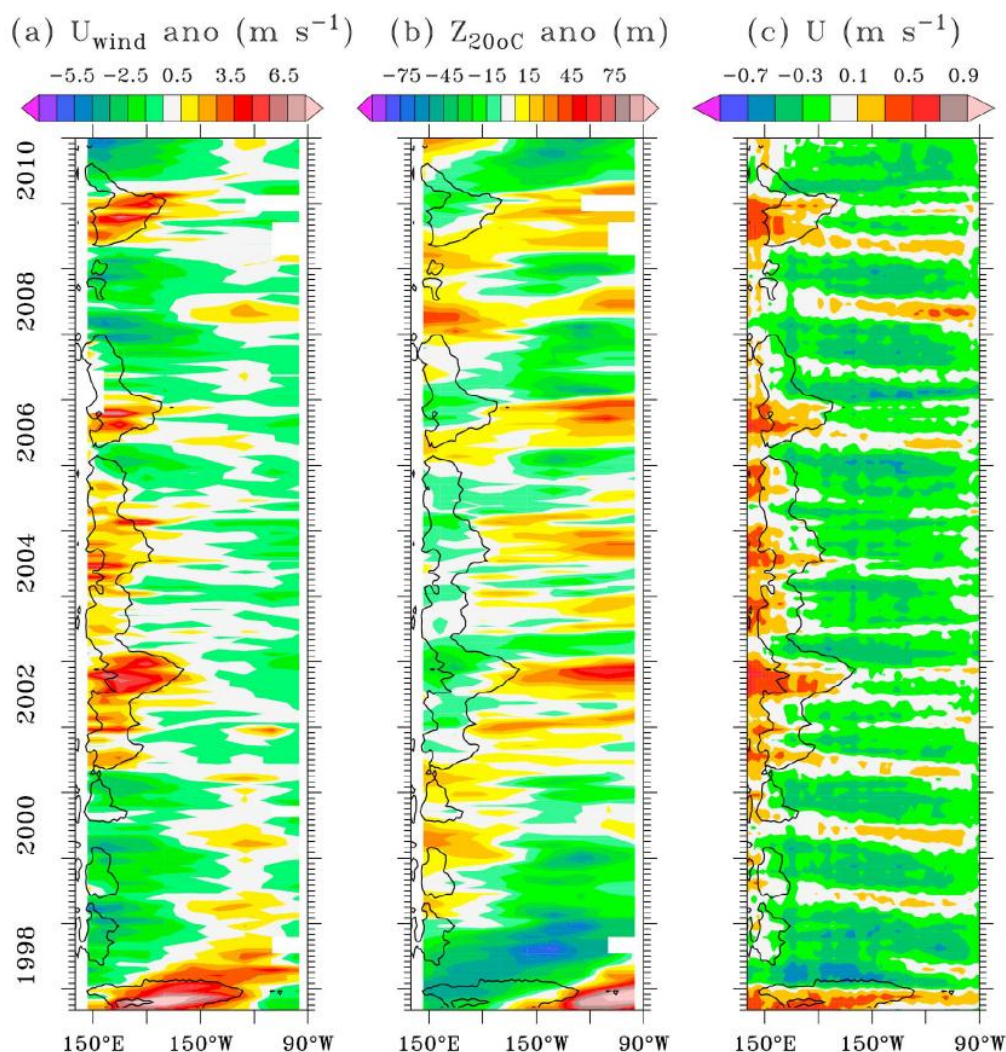


Figure 5. Longitude-time distribution along the equator of (a) zonal wind speed anomaly (positive eastwards; colors; m s^{-1}), (b) 20°C isotherm depth anomaly (positive downward; m), and (c) zonal surface current (positive eastwards; m s^{-1}). The black contours in Figures 5a–5c enclose the region with surface chlorophyll lower than 0.1 mg m^{-3} .

and 6a–6d) as a consequence of anomalous westerly winds (Figure 5a) and forced downwelling Kelvin waves [Delcroix *et al.*, 2000]. The South Equatorial Current (SEC) is weak or reversed and the NECC is stronger and shifted southwards [Johnson *et al.*, 2000]. As a result, nutrient-poor warm pool waters are advected eastward and reach 130°W during the mature phase in November 1997–January 1998 [Radenac *et al.*, 2001]. The core of high negative chlorophyll anomaly is in the eastern part of the warm pool (Figures 2c and 4b) where eastward surface currents are strong (Figure 5c). Meanwhile, vertical supplies of nitrate and iron decrease or cease because of the reduction of the upwelling and the deepening of the nitracline and EUC (Figure 5b) [Chavez *et al.*, 1999; Strutton and Chavez, 2000; Wilson and Adamec,

2001; Radenac *et al.*, 2001, 2005]. A combination of these processes lead to a dramatic decrease of the surface chlorophyll and of the biological production in the central and eastern basins. The northern and southern limits of the negative chlorophyll anomaly closely match the extent of the eastward surface current anomaly until the peak period in December 1997 (Figures 6a–6d). Starting in January 1998, the surface chlorophyll anomaly weakens as strong westward surface currents begin to develop (Figures 6d–6e).

[25] In the warm pool, the overall chlorophyll increase (Figures 6a–6f) has been ascribed to the thermocline rise (Figure 5b) allowing nutrient input toward the lighted layer [Wilson and Adamec, 2001; Radenac *et al.*, 2001; Turk *et al.*, 2001]. Part of it, between 5°N and 10°N , results from

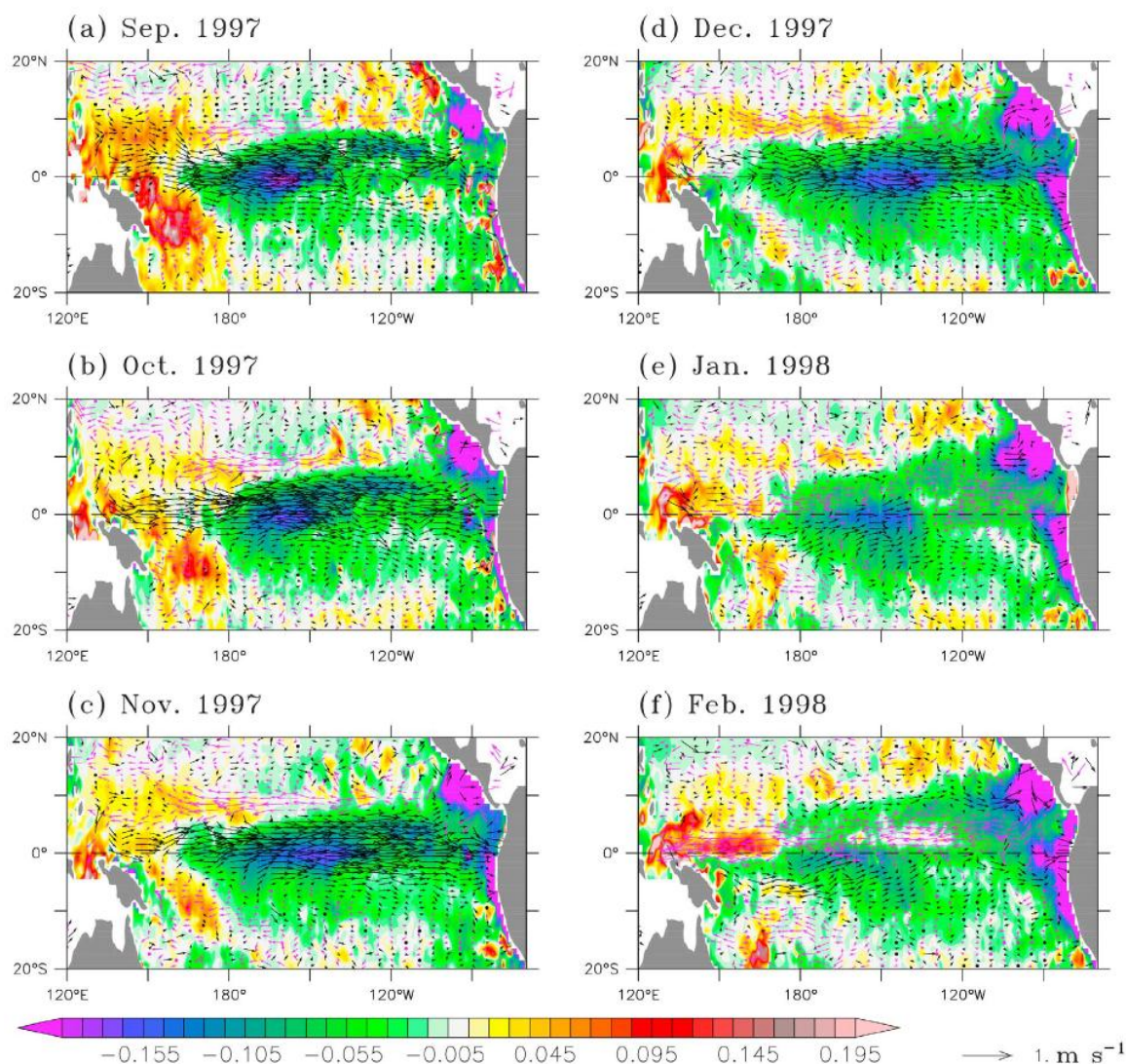


Figure 6. Maps of monthly surface chlorophyll anomaly (colors; mg m^{-3}) and surface layer current anomaly (vectors; m s^{-1}) during the 1997–1998 eastern Pacific El Niño. Current vectors with eastward (westward) zonal component are in black (purple).

enhanced chlorophyll concentration in the meanders of the nascent NECC observed seasonally between January and June and that were strong at the end of the 1997–1998 El Niño [Christian *et al.*, 2004; Messié and Radenac, 2006]. Upwelling that develops along the coast of Papua New Guinea and Solomon Islands during favorable periods of westerly wind [Webster and Lukas, 1992; Kuroda, 2000; Ueki *et al.*, 2003] also contributes to the chlorophyll increase in the warm pool south of the equator [Messié, 2006; Radenac *et al.*, 2010].

5.2. The CP El Niño Events

[26] During CP El Niño events, the eastward shift of the warm pool (see the black contours in Figure 5a) in response

to westerly winds is of lesser magnitude than during EP El Niño. The associated equatorial eastward surface currents contribute to the development of negative chlorophyll anomaly as a consequence of the penetration of the oligotrophic waters of the warm pool toward the mesotrophic waters of the upwelling (Figure 5c). The core of high chlorophyll anomaly remains within the zone of quasi-persistent oligotrophic waters enclosed by the 0.1 mg m^{-3} surface chlorophyll isoline in the eastern part of the warm pool (Figure 2c), near the zone of convergence between the eastward surface current in the warm pool and the westward SEC east of it (Figure 5c). The importance of this current convergence has been raised by Kug *et al.* [2009] and Singh

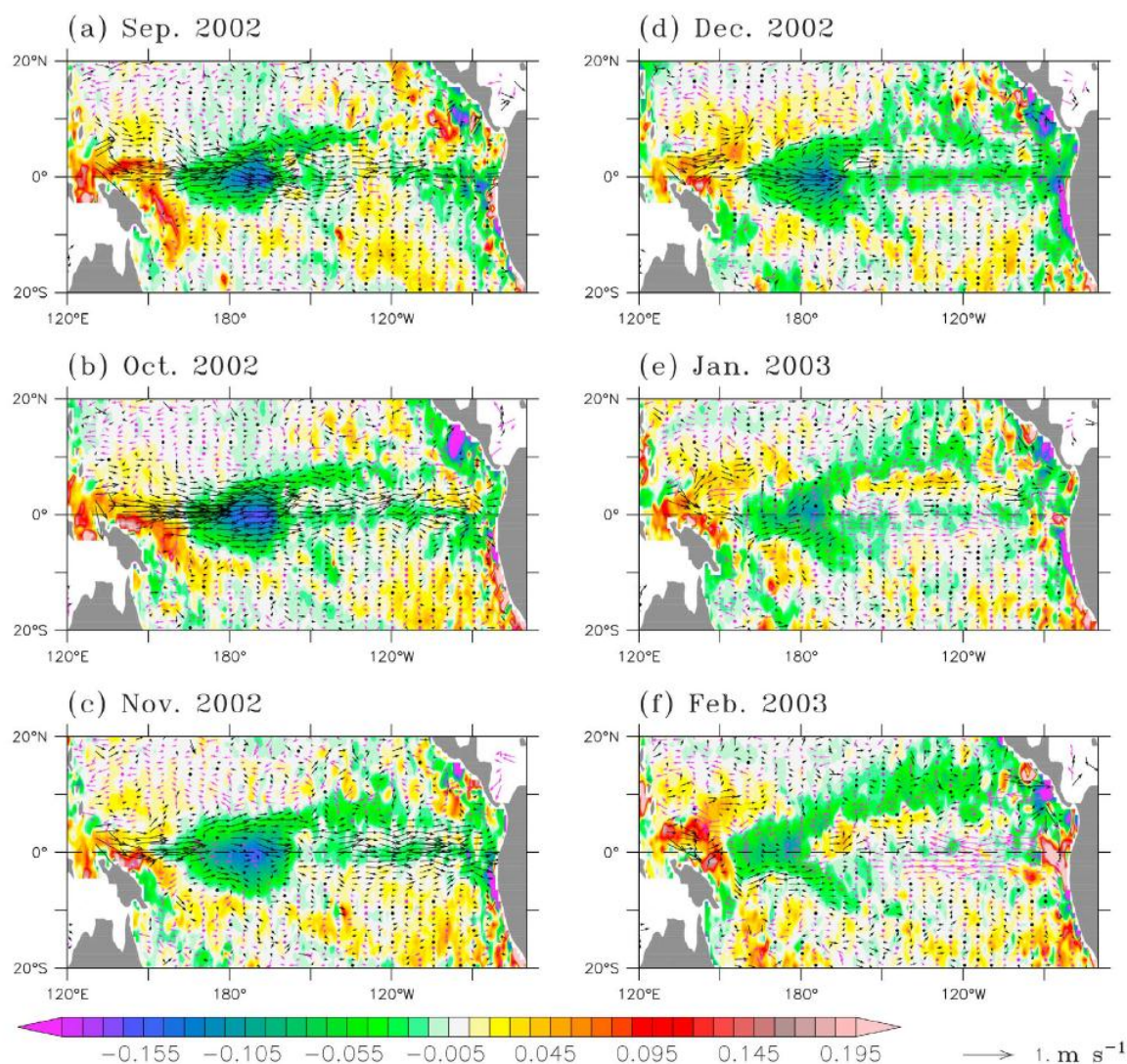


Figure 7. Maps of monthly surface chlorophyll anomaly (colors; mg m^{-3}) and surface layer current anomaly (vectors; m s^{-1}) during the 2002–2003 central Pacific El Niño. Current vectors with eastward (westward) zonal component are in black (purple).

et al. [2011] to explain how SST and SSS anomaly cores could remain confined in the central basin during CP El Niño.

[27] During the 2002–2003 CP El Niño, the maximum negative chlorophyll anomaly is situated around 170°E in June, 180°E in August, and it stays at 170°W between September and December 2002 (Figures 2c and 7a–7d). It starts to move back to the west in January 2003 when strong westward anomalies develop. The monthly maps of surface chlorophyll and current (Figures 7a–7c) also suggest that anomalous eastward currents partly contribute to the equatorial chlorophyll decrease toward the American coast.

[28] As discussed above for CP El Niño, negative anomalies (weaker than -0.015 mg m^{-3}) are constrained within 2° of the equator east of the high chlorophyll anomaly

core (Figure 4f). The zonal wind anomaly is slightly westward in the eastern basin during the CP El Niño years (Figure 5a) and so cannot be responsible for a collapse of the upwelling in this region. Besides, variations of the vertical supply of nitrate, depending on the nutrient pool depth represented by the 20°C isotherm depth ($Z_{20^\circ\text{C}}$), will not impact the phytoplankton growth as nitrate is usually in excess in this region. The equatorial chlorophyll decrease would rather be the result of vertical displacements of the EUC that contribute modulating vertical iron fluxes and the phytoplankton growth in the iron limited ecosystem of the central and eastern equatorial Pacific. The temporal variability of the $Z_{20^\circ\text{C}}$ anomaly can be used as an indicator of the EUC depth (Z_{EUC}) anomaly [Izumo, 2005]. When

ADCP currents are available at the equatorial mooring sites, the bias between Z_{EUC} (calculated as the depth of the maximum eastward velocity) and $Z_{20^\circ C}$ is lower than 4 m at $170^\circ W$ and $140^\circ W$ and the correlation coefficient is 0.72 at both sites. Therefore, the variations of $Z_{20^\circ C}$ reliably represent the variations of Z_{EUC} that deepens by 20–40 m during CP El Niño (Figure 5b) and could drive a significant decrease of the vertical iron flux [Chavez *et al.*, 1999]. A strip of maximum anomaly confined to the equator is consistent with the structure of meridional velocity and a narrow band of strong divergence roughly centered along the equator [Poulain, 1993]. This further suggests that biology along the equator is sensitive to the EUC depth and iron concentration.

[29] Off the equator, the narrow zonal band of negative chlorophyll anomaly between $5^\circ N$ and $10^\circ N$ is observed during the four CP El Niño events. During the 2002–2003 CP El Niño event, it appears during August–September (Figure 7a) and starts to break up during January–February (Figure 7e). The negative chlorophyll anomaly strip follows the position of the eastward surface current anomaly (Figures 7a–7d), suggesting that nutrient- and phytoplankton-poor water from the warm pool is advected eastward by the strong NECC. Messié and Radenac [2006] showed the significant impact of the NECC variations on the surface chlorophyll seasonal variability in the western Pacific. During El Niño events, it is a basin-wide feature that participates in setting up the sharp chlorophyll front at the northern edge of the upwelling. In monthly chlorophyll maps, it is seen as a narrow band of oligotrophic waters extending from the warm pool to the Central American coast during October–December of all El Niño years (not shown). South of the equator, negative chlorophyll anomalies coincide with a region of southeastward surface currents that transport nutrient- and phytoplankton-poor waters toward the Marquesas Islands (Figures 7a–7f). This feature is observed during September–February 2002–2003, 2004–2005, and 2006–2007. It develops later during February–April during the 2009–2010 CP El Niño event (not shown).

6. Summary and Discussion

[30] Enhanced attention has been given to global climate changes related to differences in the location of SST anomalous warming in the tropical Pacific in recent years [Trenberth and Stepaniak, 2001; Ashok *et al.*, 2007; Kug *et al.*, 2009; Kao and Yu, 2009; Yeh *et al.*, 2009; Lee and McPhaden, 2010]. To our knowledge, no attempt has been made so far to contrast the biological conditions featuring the EP and CP El Niño, except for the recent study by Turk *et al.* [2011]. To fulfill this gap, the goal of our study was to contrast and tentatively explain the signature in chlorophyll of the EP and CP ENSO, for the 1997–2010 period.

[31] During the SeaWiFS years, an AHC analysis of the surface chlorophyll anomaly shows that EP El Niño occurred in 1997–1998, CP El Niño in 2002–2003, 2004–2005, 2006–2007, and 2009–2010, while La Niña lasted from 1998 to 2001 and from 2007 to 2009, consistent with previous studies based on SST and SSS analyses (Table 1). Both types of El Niño events are associated with an overall decrease of surface chlorophyll in the $10^\circ S$ – $10^\circ N$ region. Yet, spatial patterns differ between events.

[32] During the 1997–1998 EP El Niño event, negative anomalies occupy most of the equatorial basin between $10^\circ S$ and $10^\circ N$, except for a chlorophyll increase in the western basin. A strong negative chlorophyll anomaly ($< -0.075 \text{ mg m}^{-3}$) is located at the equator between the date line and $150^\circ W$ and the oligotrophic warm pool is displaced eastward and reaches $130^\circ W$.

[33] During the CP El Niño events, the equatorial anomaly is weaker ($< -0.045 \text{ mg m}^{-3}$), shifted westward by about 20° of longitude, and the eastern edge of the oligotrophic warm pool is confined west of $160^\circ W$. So, as already found for SST and SSS [Kug *et al.*, 2009; Singh *et al.*, 2011], the region of strong chlorophyll anomaly is clearly shifted westward during CP El Niño relative to EP El Niño. The location of these strong negative anomalies in the eastern part of the warm pool suggests that oligotrophic waters of the warm pool replace mesotrophic waters of the upwelling in the central basin, and that zonal advection is a major process responsible for this signature. During CP El Niño, westward surface currents in the eastern and central basins probably limit the eastward spreading of the negative chlorophyll anomaly core.

[34] Other mechanisms affecting nutrient or light availability could also lead to a chlorophyll decrease in the central equatorial basin. One of them is the depth of the nutrient pool. The core of high chlorophyll anomaly matches the maximum sea level anomaly [Kug *et al.*, 2009; Bosc *et al.*, 2009] which reflects a strong depression of the thermocline [Rébert *et al.*, 1985], closely related to the depth of the nitracline in the oligotrophic warm pool. Besides, barrier layer tends to be thick in the eastern edge of the warm pool [Maes *et al.*, 2004; Bosc *et al.*, 2009] and to further isolate the deep nutrient pool from the lighted surface layer [Mackey *et al.*, 1995; Eldin *et al.*, 1997; Murtugudde *et al.*, 1999; Turk *et al.*, 2001]. The nutrient pool is deep on average in the oligotrophic warm pool and the depression of the nitracline in the eastern part of the warm pool is probably a second order factor on surface chlorophyll changes compared to the impact of advection.

[35] Another factor accounting for chlorophyll changes during EP and CP El Niño could be the reduction of incident light in the central Pacific as suggested by Park *et al.* [2011]. Zonal extension of oligotrophic conditions is linked to the zonal extension of the warm pool, which is the site of convective activity and moves eastward during El Niño. The average monthly value of the satellite derived Photosynthetically Available Radiation (PAR) is $44.7 \pm 4.4 \text{ Einstein m}^{-2} \text{ d}^{-1}$ in the eastern part of the warm pool while it is $48.6 \pm 2.2 \text{ Einstein m}^{-2} \text{ d}^{-1}$ in the upwelling region at $140^\circ W$. The eastward shift of the convection zone leads to PAR anomaly around $10 \text{ Einstein m}^{-2} \text{ d}^{-1}$ in the strong chlorophyll anomaly region in 1997–1998 and close to or less than $5 \text{ Einstein m}^{-2} \text{ d}^{-1}$ during the following El Niño events. These relatively weak PAR variations, three to ten times weaker than variations at mid and high latitudes [Letelier *et al.*, 2004; Goes *et al.*, 2004], suggest a weak impact on the phytoplankton growth. Therefore, zonal advection and the resulting change of ecosystem in the central Pacific are probably the dominant mechanisms responsible for the strong chlorophyll anomaly, as also proposed by M. Messié and F. Chavez (Global synchrony

associated with ENSO: The oceans biological response to physical forcing, submitted to *Journal of Geophysical Research*, 2012). Mesotrophic waters of the upwelling with surface chlorophyll concentration around 0.2 mg m^{-3} are replaced by oligotrophic waters of the eastern part of the warm pool with surface chlorophyll concentration lower than 0.07 mg m^{-3} [Radenac et al., 2010]. However, separating the impact of the ecosystem change and of the light attenuation is not simple as oligotrophic waters move simultaneously to the convection zone, and a process study is needed to estimate each influence.

[36] We suggest that the chlorophyll decrease along the equator east of the strong central Pacific anomaly is the consequence of reduced vertical iron fluxes linked to the deepening of the EUC during El Niño [Barber et al., 1996; Chavez et al., 1999; Wilson and Adamec, 2001; Friedrichs and Hofmann, 2001]. Changes in the iron content of the EUC could also impact biology in the central and eastern Pacific. Ryan et al. [2006] hypothesized that the strengthening of the New Guinea Coastal Undercurrent (NGCUC), flowing northwestward along the northern coast of Papua New Guinea, favored transport of iron from shelf sediments that feeds the EUC during El Niño years, which in turn favored phytoplankton blooms observed in the central Pacific following El Niño events. In contrast, setting the iron concentration proportional to the NGCUC speed in the source region did not change the intensity of eastern equatorial Pacific blooms in a simulation based study [Gorgues et al., 2010]. Thus, although the impact of a continental iron source in the western equatorial Pacific on the biogeochemistry of the equatorial upwelling region has been shown in several modeling studies [Christian et al., 2001; Vichi et al., 2008; Slemmons et al., 2010; Gorgues et al., 2010], the influence of a variable iron supply into the EUC on the ecosystems of the central and eastern basins is still unclear. So is the role of tropical instability waves (TIW). Because of vigorous horizontal processes as well as upwelling and downwelling, localized maximum and minimum of phytoplankton biomass characterize TIW [Yoder et al., 1994; Strutton et al., 2001; Menkes et al., 2002]. Their net impact on phytoplankton biomass has been estimated to be positive [Barber et al., 1996; Friedrichs and Hofmann, 2001; Strutton et al., 2001] or negative [Gorgues et al., 2005]. Other studies show an enhancement or decrease of the phytoplankton biomass depending on interactions between the large scale thermocline/ferricline depth and the intensity of the local TIW dynamics [Vichi et al., 2008; Evans et al., 2009]. The reduction or absence of TIW activity during El Niño [Legeckis, 1977; Friedrichs and Hofmann, 2001; Evans et al., 2009] can also possibly contribute to the chlorophyll decrease observed along the equator.

[37] The AHC analysis of the 1997–2010 surface chlorophyll anomaly data set does not separate La Niña events into EP and CP events. Chlorophyll increases in the equatorial western basin and near $8\text{--}10^\circ\text{N}$ and toward the Marquesas Islands are common patterns to La Niña maps. Nevertheless, the location of the equatorial core of positive anomalies and its magnitude change (much stronger in 2010 than during other events) and an equatorial increase in the central and eastern basins may not be observed. The average location of chlorophyll anomaly of the six La Niña events seen by SeaWiFS is situated west of the EP and CP El Niño

anomalies. This is consistent with the La Niña signature as reported by Kug et al. [2009] and Kug and Ham [2011] who do not separate CP and EP cold events in terms of SST anomaly. Besides, the chlorophyll anomaly analysis does not evidence any symmetry between the warm and cold phases of ENSO events as suggested by Kao and Yu [2009] and Yu et al. [2010] analyses. The distinct EP and CP La Niña patterns mentioned by Singh et al. [2011] are based on a cluster analysis of SSS that captures a signal in the SPCZ region that does not show up in the chlorophyll analysis.

[38] During La Niña years, the equatorial core of positive anomaly results from the westward expansion of the upwelling mesotrophic waters in a region where the usual surface chlorophyll concentration does not exceed 0.1 mg m^{-3} (Figure 2c). The weak nutrient supply to the euphotic layer in the Niño4 region results from horizontal advection of nutrient-rich waters from the east and upward advection [Stoens et al., 1999]. During La Niña events, observational and modeling studies have shown that upwelling led to increased surface chlorophyll concentration in the western Pacific [Blanchot et al., 1992; Radenac and Rodier, 1996; Radenac et al., 2001]. East of the strong anomaly core, the iron limitation and the grazing pressure (small phytoplankton and zooplankton species dominate the ecosystem and microzooplankton can quickly respond to changes in nano- and pico-phytoplankton biomass) control the ecosystem resulting in a monotonously low phytoplankton biomass in the equatorial divergence [Chavez et al., 1991; Le Bouteiller and Blanchot, 1991; Strutton et al., 2008]. This special feature of the equatorial upwelling ecosystem could explain why no strong chlorophyll increase characterizes the overall La Niña distribution of chlorophyll anomaly along the equator east of the anomaly core (Figure 4d). An asymmetry between El Niño and La Niña has also been observed in terms of temperature [Larkin and Harrison, 2002; An and Jin, 2004]. The warm phase of ENSO is often stronger than its cold phase. Nonlinear dynamical processes could impact nutrient (iron) supply and cause an asymmetry of the ENSO-related biological response as they impact the ENSO-related heat budget [An and Jin, 2004]. More investigations remain to be done on this issue, especially during the CP El Niño events that dominate during the recent years. Cluster 2 in the AHC analysis (Figures 4a and 4c) captured exceptions to this uniformity. 80% of the maps that compose this cluster come from the 1998 La Niña year when unusual large-scale blooms [Ryan et al., 2002] were observed in the equatorial Pacific after the major 1997–1998 EP El Niño event. Chlorophyll increases subsequent to island mass effect generated by the Kiribati Islands, which behave as an obstacle to both the SEC and the EUC between February and June 1998 [Ryan et al., 2002; Messié et al., 2006] may contribute to the positive anomaly observed west of the dateline. A second bloom, the longest and more intense one with chlorophyll concentration higher than 0.8 mg m^{-3} , developed between 160°W and 140°W and then spread eastward from June to September [Chavez et al., 1999; Ryan et al., 2002; Gorgues et al., 2010]. The last bloom was observed around 130°W during November–December 1998 [Ryan et al., 2002]. Reasons for these blooms can be both large-scale and local dynamics, such as, enhanced iron vertical fluxes because of a shallower thermocline and more active TIW during La Niña. A similar but

somewhat weaker situation seemed to occur in mid-2010. Interestingly, these equatorial recovery conditions occur when strong El Niño events turn swiftly into strong La Niña: from the major 1997–1998 EP El Niño to the strong 1998–1999 La Niña [Chavez et al., 1999; Ryan et al., 2002; Radenac et al., 2010] and from the strong 2009–2010 CP El Niño to the strong 2010–2011 La Niña [Kim et al., 2011]. These periods coincide with phases of reduced grazing pressure as a response to El Niño related reduced phytoplankton biomass and productivity. Therefore, momentarily low grazing pressure probably combines to dynamical impacts leading to enhanced phytoplankton growth to drive high phytoplankton biomass during these recovery periods after strong El Niño events [Strutton and Chavez, 2000; Friedrichs and Hofmann, 2001; Gorgues et al., 2010].

[39] While increased eastward advection was responsible for the chlorophyll decreases along 8–10°N and toward the Marquesas Islands during CP El Niño, the chlorophyll increases at the same locations during La Niña coincide with increased westward and poleward surface currents suggesting the influence of horizontal advection.

[40] Situations that occurred in 2001–2002, 2003–2004, 2005–2006, and 2007 close to CP El Niño years (Figures 4a and 4e) were called intermediate CP El Niño conditions. Their spatial structure (Figure 4e) is characterized by an anomaly core of about -0.04 mg m^{-3} located near 160°E. The persistent negative chlorophyll anomaly in the western Pacific could be specific to the period we study (recurring CP El Niño conditions) and this is why we do not refer to it as neutral conditions.

[41] The SeaWiFS archive spans over more than 13 years during which 5 El Niño events occur. Interestingly, the AHC analysis we performed on the monthly surface chlorophyll anomaly maps separates the 1997–1998 EP episode from the other CP El Niño episodes. These results need to be refined with the help of longer observational time series, modeling outputs, and theoretical work. An improve understanding of the phytoplankton distribution and its temporal variability is actually essential to anticipate biogeochemical climate-driven shifts and their consequences on ocean dynamics, carbon cycle, and marine resources. Different phytoplankton distribution during CP and EP El Niño events could actually impact the distribution and abundance of exploited fish species such as tuna, whose fishery in the central and western tropical Pacific is one of the largest industrial fisheries of the world [Lahodey et al., 2011]. Complementing our qualitative analysis, we also need to quantify how physical and/or biological processes lead to the contrasted patterns we evidenced.

[42] **Acknowledgments.** We acknowledge the SeaWiFS Project at GSFC (<http://oceancolor.gsfc.nasa.gov>), the Hadley Centre for Climate Prediction and Research Sea Ice and Sea Surface Temperature (<http://www.metoffice.gov.uk/hadobs/hadisst>), OSCAR (<http://www.oscar.noaa.gov>), the SSS Observation Service (<http://www.legos.obs-mip.fr/observations/sss>), and the TOGA-TAO Project Office of NOAA/PMEL (<http://www.pmel.noaa.gov/tao>) for sharing the freely available data we used. We also used time series of the Southern Oscillation Index (<http://www.cpc.ncep.noaa.gov/data/indices/soi>) and of the El Niño Modoki Index (http://www.jamstec.go.jp/frgc/research/d1/iod/modoki_home.html.en). This work was supported by CNES in the frame of the Ocean Surface Topography Science Team program. F.L. benefited from CNES funding and A.S. benefits from a PhD grant from the Institut de Recherche pour le Développement (IRD). We thank the two reviewers for their useful comments.

References

- An, S.-I., and F.-F. Jin (2004), Nonlinearity and asymmetry of ENSO, *J. Clim.*, *17*, 2399–2412, doi:10.1175/1520-0442(2004)017<2399:NAAOE>2.0.CO;2.
- Ashok, K., S. K. Behera, S. A. Rao, H. Weng, and T. Yamagata (2007), El Niño Modoki and its teleconnection, *J. Geophys. Res.*, *112*, C11007, doi:10.1029/2006JC003798.
- Barber, R. T., and J. E. Kogelschatz (1990), Nutrients and productivity during the 1982/83 El Niño, in *Global Ecological Consequences of the 1982–83 El Niño–Southern Oscillation*, edited by P. W. Glynn, pp. 21–53, Elsevier, Amsterdam, doi:10.1016/S0422-9894(08)70032-1.
- Barber, R. T., M. P. Sanderson, S. T. Lindley, F. Chai, J. Newton, C. C. Trees, D. G. Foley, and F. P. Chavez (1996), Primary productivity and its regulation in the equatorial Pacific during and following the 1991–1992 El Niño, *Deep Sea Res., Part II*, *43*, 933–969, doi:10.1016/0967-0645(96)00035-5.
- Blanchot, J., M. Rodier, and A. Le Bouteiller (1992), Effect of El Niño Southern Oscillation events on the distribution and abundance of phytoplankton in the western Pacific Ocean along 165°E, *J. Plankton Res.*, *14*, 137–156, doi:10.1093/plankt/14.1.137.
- Bonjean, F., and G. S. E. Lagerloef (2002), Diagnostic model and analysis of the surface currents in the tropical Pacific Ocean, *J. Phys. Oceanogr.*, *32*, 2938–2954, doi:10.1175/1520-0485(2002)032<2938:DMAOT>2.0.CO;2.
- Bosc, C., T. Delcroix, and C. Maes (2009), Barrier layer variability in the western Pacific warm pool from 2000 to 2007, *J. Geophys. Res.*, *114*, C06023, doi:10.1029/2008JC005187.
- Campbell, J. W., J. M. Blaisdell, and M. Darzi (1995), Level-3 SeaWiFS data products: Spatial and temporal binning algorithms, *NASA Tech. Memo. TM-104566*, vol. 32, 80 pp., Goddard Space Flight Cent., Greenbelt, Md.
- Chavez, F. P., K. R. Buck, K. H. Coale, J. H. Martin, G. R. DiTullio, N. A. Welschmeyer, A. C. Jacobson, and R. T. Barber (1991), Growth rates, grazing, sinking, and iron limitation of equatorial Pacific phytoplankton, *Limnol. Oceanogr.*, *36*, 1816–1833, doi:10.4319/lo.1991.36.8.1816.
- Chavez, F. P., P. G. Strutton, and M. J. McPhaden (1998), Biological-physical coupling in the central Pacific during the onset of the 1997–98 El Niño, *Geophys. Res. Lett.*, *25*, 3543–3546, doi:10.1029/98GL02729.
- Chavez, F. P., P. G. Strutton, G. E. Friederich, R. A. Feely, G. C. Feldman, D. G. Foley, and M. J. McPhaden (1999), Biological and chemical response of the equatorial Pacific Ocean to the 1997–98 El Niño, *Science*, *286*, 2126–2131, doi:10.1126/science.286.5447.2126.
- Christian, J. R., M. A. Verschell, R. Murtugudde, A. J. Busalacchi, and C. R. McClain (2001), Biogeochemical modelling of the tropical Pacific Ocean. II. Iron biogeochemistry, *Deep Sea Res., Part II*, *49*, 545–565, doi:10.1016/S0967-0645(01)00111-4.
- Christian, J. R., R. Murtugudde, J. Ballabrera-Poy, and C. R. McClain (2004), A ribbon of dark water: Phytoplankton blooms in the meanders of the Pacific North Equatorial Countercurrent, *Deep Sea Res., Part II*, *51*, 209–228, doi:10.1016/j.dsr2.2003.06.002.
- Delcroix, T., B. Dewitte, Y. duPenhoat, F. Masia, and J. Picaut (2000), Equatorial waves and warm pool displacements during the 1992–1998 El Niño Southern Oscillation events: Observation and modeling, *J. Geophys. Res.*, *105*, 26,045–26,062, doi:10.1029/2000JC900113.
- Delcroix, T., G. Alory, S. Cravatte, T. Corrége, and M. J. McPhaden (2011), A gridded sea surface salinity data set for the tropical Pacific with sample applications (1950–2008), *Deep Sea Res., Part I*, *58*, 38–48, doi:10.1016/j.dsr.2010.11.002.
- Eldin, G., M. Rodier, and M. H. Radenac (1997), Physical and nutrient variability in the upper equatorial Pacific associated with westerly wind forcing and wave activity in October 1994, *Deep Sea Res., Part II*, *44*, 1783–1800, doi:10.1016/S0967-0645(97)00023-4.
- Evans, W., P. G. Strutton, and F. P. Chavez (2009), Impact of tropical instability waves on nutrient and chlorophyll distributions in the equatorial Pacific, *Deep Sea Res., Part I*, *56*, 178–188, doi:10.1016/j.dsr.2008.08.008.
- Friedrichs, M. A. M., and E. E. Hofmann (2001), Physical control of biological processes in the central equatorial Pacific Ocean, *Deep Sea Res., Part I*, *48*, 1023–1069, doi:10.1016/S0967-0637(00)00079-0.
- Frouin, R., B. A. Franz, and P. J. Werdell (2003), The SeaWiFS PAR product, in *Algorithm Updates for the Fourth SeaWiFS Data Reprocessing*, edited by S. B. Hooker and E. R. Firestone, *NASA Tech. Memo. NASA/TM-2003-206892*, pp. 46–50, Goddard Space Flight Cent., Greenbelt, Md.
- Glantz, M. H. (2000), *Currents of Change: Impacts of El Niño and La Niña on Climate and Society*, 266 pp., Cambridge Univ. Press, Cambridge, U. K.
- Goes, J. I., K. Sasaoka, H. Do, R. Gomes, S.-I. Saitoh, and T. Saino (2004), A comparison of the seasonality and interannual variability of phytoplankton biomass and production in the western and eastern gyres of

- the subarctic Pacific using multi-sensor satellite data, *J. Oceanogr.*, *60*, 75–91, doi:10.1023/B:JOCE.0000038320.94273.25.
- Gordon, R. M., K. H. Coale, and K. S. Johnson (1997), Iron distribution in the equatorial Pacific: Implications for new production, *Limnol. Oceanogr.*, *42*, 419–431, doi:10.4319/lo.1997.42.3.0419.
- Gorgues, T., C. Menkes, O. Aumont, J. Vialard, Y. Dandonneau, and L. Bopp (2005), Biogeochemical impact of tropical instability waves in the equatorial Pacific, *Geophys. Res. Lett.*, *32*, L24615, doi:10.1029/2005GL024110.
- Gorgues, T., C. Menkes, L. Slemmons, O. Aumont, Y. Dandonneau, M.-H. Radenac, S. Alvain, and C. Moulin (2010), Revisiting the La Niña 1998 phytoplankton blooms in the equatorial Pacific, *Deep Sea Res., Part I*, *57*, 567–576, doi:10.1016/j.dsr.2009.12.008.
- Hsieh, W. W. (2001), Nonlinear canonical correlation analysis of the tropical Pacific climate variability using a neural network approach, *J. Clim.*, *14*, 2528–2539, doi:10.1175/1520-0442(2001)014<2528:NCCAOT>2.0.CO;2.
- Izumo, T. (2005), The equatorial undercurrent, meridional overturning circulation, and their roles in mass and heat exchanges during El Niño events in the tropical Pacific ocean, *Ocean Dyn.*, *55*, 110–123, doi:10.1007/s10236-005-0115-1.
- Johnson, G. C., M. J. McPhaden, G. D. Rowe, and K. E. McTaggart (2000), Upper equatorial Pacific ocean current and salinity variability during the 1996–1998 El Niño–La Niña cycle, *J. Geophys. Res.*, *105*, 1037–1053, doi:10.1029/1999JC900280.
- Kao, H.-Y., and J.-Y. Yu (2009), Contrasting eastern-Pacific and central-Pacific types of ENSO, *J. Clim.*, *22*, 615–632, doi:10.1175/2008JCLI2309.1.
- Kim, H.-M., P. J. Webster, and J. A. Curry (2009), Impact of shifting patterns of Pacific Ocean warming on north Atlantic tropical cyclones, *Science*, *325*(5936), 77–80, doi:10.1126/science.1174062.
- Kim, W., S.-W. Yeh, J.-H. Kim, J.-S. Kug, and M. Kwon (2011), The unique 2009–2010 El Niño event: A fast phase transition of warm pool El Niño to La Niña, *Geophys. Res. Lett.*, *38*, L15809, doi:10.1029/2011GL048521.
- Kug, J.-S., and Y.-G. Ham (2011), Are there two types of La Niña?, *Geophys. Res. Lett.*, *38*, L16704, doi:10.1029/2011GL048237.
- Kug, J.-S., F.-F. Jin, and S.-I. An (2009), Two types of El Niño events: Cold tongue El Niño and warm pool El Niño, *J. Clim.*, *22*, 1499–1515, doi:10.1175/2008JCLI2624.1.
- Kuroda, Y. (2000), Variability of currents off the northern coast of New Guinea, *J. Oceanogr.*, *56*, 103–116, doi:10.1023/A:1011122810354.
- Lacan, F., and C. Jeandel (2001), Tracing Papua New Guinea imprint on the central equatorial Pacific Ocean using neodymium isotopic compositions and rare earth element patterns, *Earth Planet. Sci. Lett.*, *186*, 497–512, doi:10.1016/S0012-821X(01)00263-1.
- Landry, M. R., et al. (1997), Iron and grazing constraints on primary production in the central equatorial Pacific: An EqPac synthesis, *Limnol. Oceanogr.*, *42*, 405–418, doi:10.4319/lo.1997.42.3.0405.
- Larkin, N. K., and D. E. Harrison (2002), ENSO warm (El Niño) and cold (La Niña) event life cycles: Ocean surface anomaly patterns, their symmetries, asymmetries, and implications, *J. Clim.*, *15*, 1118–1140, doi:10.1175/1520-0442(2002)015<1118:EWENOA>2.0.CO;2.
- Le Borgne, R., R. T. Barber, T. Delcroix, H. Y. Inoue, D. J. Mackey, and M. Rodier (2002), Pacific warm pool and divergence: Temporal and zonal variations on the equator and their effects on the biological pump, *Deep Sea Res., Part II*, *49*, 2471–2512, doi:10.1016/S0967-0645(02)00045-0.
- Le Bouteiller, A., and J. Blanchot (1991), Size distribution and abundance of phytoplankton in the Pacific equatorial upwelling, *La Mer*, *29*, 175–179.
- Lee, T., and M. J. McPhaden (2010), Increasing intensity of El Niño in the central-equatorial Pacific, *Geophys. Res. Lett.*, *37*, L14603, doi:10.1029/2010GL044007.
- Legeckis, R. (1977), Long waves in the eastern equatorial Pacific Ocean: A view from a geostationary satellite, *Science*, *197*, 1179–1181, doi:10.1126/science.197.4309.1179.
- Lehodey, P., et al. (2011), Vulnerability of oceanic fisheries in the tropical Pacific to climate change, in *Vulnerability of Tropical Pacific Fisheries and Aquaculture to Climate Change*, edited by J. D. Bell, J. E. Johnson, and A. J. Hobday, pp. 433–492, Secr. of the Pac. Community, Noumea, New Caledonia.
- Leloup, J., M. Lengaigne, and J.-P. Boulanger (2008), Twentieth century ENSO characteristics in the IPCC database, *Clim. Dyn.*, *30*, 277–291, doi:10.1007/s00382-007-0284-3.
- Letelier, R. M., D. M. Karl, M. R. Abbott, and R. R. Bidigare (2004), Light driven seasonal patterns of chlorophyll and nitrate in the lower euphotic zone of the north Pacific subtropical gyre, *Limnol. Oceanogr.*, *49*, 508–519, doi:10.4319/lo.2004.49.2.0508.
- Mackey, D. J., J. Parslow, H. W. Higgins, F. B. Griffiths, and J. E. O'Sullivan (1995), Plankton productivity and biomass in the western equatorial Pacific: Biological and physical controls, *Deep Sea Res., Part II*, *42*, 499–533, doi:10.1016/0967-0645(95)00038-R.
- Maes, C., J. Picaut, Y. Kuroda, and K. Ando (2004), Characteristics of the convergence zone at the eastern edge of the Pacific warm pool, *Geophys. Res. Lett.*, *31*, L11304, doi:10.1029/2004GL019867.
- McClain, C. R., G. C. Feldman, and S. B. Hooker (2004), An overview of the SeaWiFS project and strategies for producing a climate research quality global ocean bio-optical time series, *Deep Sea Res., Part II*, *51*, 5–42, doi:10.1016/j.dsr.2003.11.001.
- McPhaden, M. J., et al. (1998), The Tropical Ocean–Global Atmosphere observing system: A decade of progress, *J. Geophys. Res.*, *103*, 14,169–14,240, doi:10.1029/97JC02906.
- McPhaden, M. J., S. E. Zebiak, and M. H. Glantz (2006), ENSO as an integrating concept in earth science, *Science*, *314*(5806), 1740–1745, doi:10.1126/science.1132588.
- McPhaden, M. J., T. Lee, and D. McClurg (2011), El Niño and its relationship to changing background conditions in the tropical Pacific Ocean, *Geophys. Res. Lett.*, *38*, L15709, doi:10.1029/2011GL048275.
- Menkes, C., et al. (2002), A whirling ecosystem in the equatorial Atlantic, *Geophys. Res. Lett.*, *29*(11), 1553, doi:10.1029/2001GL014576.
- Messié, M. (2006), Contrôle de la dynamique de la biomasse phytoplanctonique dans le Pacifique tropical ouest, PhD thesis, 263 pp., Univ. Toulouse 3, Toulouse, France.
- Messié, M., and M.-H. Radenac (2006), Seasonal variability of the surface chlorophyll in the western tropical Pacific from SeaWiFS data, *Deep Sea Res., Part I*, *53*(10), 1581–1600, doi:10.1016/j.dsr.2006.06.007.
- Messié, M., M.-H. Radenac, J. Lefèvre, and P. Marchesio (2006), Chlorophyll bloom in the western Pacific at the end of the 1997–98 El Niño: The role of Kiribati Islands, *Geophys. Res. Lett.*, *33*, L14601, doi:10.1029/2006GL026033.
- Murtugudde, R. G., S. R. Signorini, J. R. Christian, A. J. Busalacchi, C. R. McClain, and J. Picaut (1999), Ocean color variability of the tropical Indo-Pacific basin observed by SeaWiFS during 1997–98, *J. Geophys. Res.*, *104*, 18,351–18,366, doi:10.1029/1999JC900135.
- Park, J.-Y., J.-S. Kug, J.-S. Park, S.-W. Yeh, and C. J. Jang (2011), Variability of chlorophyll associated with ENSO and its possible biological feedback in the equatorial Pacific, *J. Geophys. Res.*, *116*, C10001, doi:10.1029/2011JC007056.
- Picaut, J., and T. Delcroix (1995), Equatorial wave sequence associated with warm pool displacement during the 1986–1989 El Niño–La Niña, *J. Geophys. Res.*, *100*, 18,393–18,408, doi:10.1029/95JC01358.
- Picaut, J., M. Ioualalen, T. Delcroix, F. Masia, R. Murtugudde, and J. Vialard (2001), The oceanic zone of convergence on the eastern edge of the Pacific warm pool: A synthesis of results and implications for El Niño–Southern Oscillation and biogeochemical phenomena, *J. Geophys. Res.*, *106*, 2363–2386, doi:10.1029/2000JC900141.
- Poulain, P.-M. (1993), Estimates of horizontal divergence and vertical velocity in the equatorial Pacific, *J. Phys. Oceanogr.*, *23*, 601–607, doi:10.1175/1520-0485(1993)023<0601:EOHDAV>2.0.CO;2.
- Radenac, M.-H., and M. Rodier (1996), Nitrate and chlorophyll distributions in relation to thermohaline and current structures in the western tropical Pacific during 1985–1989, *Deep Sea Res., Part II*, *43*, 725–752, doi:10.1016/0967-0645(96)00025-2.
- Radenac, M.-H., C. Menkes, J. Vialard, C. Moulin, Y. Dandonneau, T. Delcroix, C. Dupouy, A. Stoens, and P.-Y. Deschamps (2001), Modeled and observed impacts of the 1997–1998 El Niño on nitrate and new production in the equatorial Pacific, *J. Geophys. Res.*, *106*, 26,879–26,898, doi:10.1029/2000JC000546.
- Radenac, M.-H., Y. Dandonneau, and B. Blanke (2005), Displacements and transformations of nitrate-rich and nitrate-poor water masses in the tropical Pacific during the 1997 El Niño, *Ocean Dyn.*, *55*, 34–46, doi:10.1007/s10236-005-0111-5.
- Radenac, M.-H., P. E. Plimpton, A. Lebourges-Dhaussy, L. Commien, and M. J. McPhaden (2010), Impact of environmental forcing on the acoustic backscattering strength in the equatorial Pacific: Diurnal, lunar, intraseasonal, and interannual variability, *Deep Sea Res., Part I*, *57*, 1314–1328, doi:10.1016/j.dsr.2010.06.004.
- Rasmusson, E. M., and T. H. Carpenter (1982), Variations in tropical sea surface temperature and surface wind fields associated with the Southern Oscillation/El Niño, *Mon. Weather Rev.*, *110*, 354–384, doi:10.1175/1520-0493(1982)110<0354:VITSST>2.0.CO;2.
- Rayner, N. A., D. E. Parker, E. B. Horton, C. K. Folland, L. V. Alexander, D. P. Rowell, E. C. Kent, and A. Kaplan (2003), Global analyses of sea surface temperature, sea ice, and night marine air temperature since the late nineteenth century, *J. Geophys. Res.*, *108*(D4) 4407, doi:10.1029/2002JD002670.
- Rébert, J.-P., J.-R. Donguy, G. Eldin, and K. Wyrtki (1985), Relations between sea-level, thermocline depth, heat content, and dynamic height in

- the tropical Pacific, *J. Geophys. Res.*, *90*, 11,719–11,725, doi:10.1029/JC090iC06p11719.
- Ren, H.-L., and F.-F. Jin (2011), Niño indices for two types of ENSO, *Geophys. Res. Lett.*, *38*, L04704, doi:10.1029/2010GL046031.
- Ryan, J. P., P. S. Polito, P. G. Strutton, and F. P. Chavez (2002), Unusual large-scale phytoplankton blooms in the equatorial Pacific, *Prog. Oceanogr.*, *55*, 263–285, doi:10.1016/S0079-6611(02)00137-4.
- Ryan, J. P., I. Ueki, Y. Chao, H. Zhang, P. S. Polito, and F. P. Chavez (2006), Western Pacific modulation of large phytoplankton blooms in the central and eastern equatorial Pacific, *J. Geophys. Res.*, *111*, G02013, doi:10.1029/2005JG000084.
- Singh, A., and T. Delcroix (2011), Estimating the effects of ENSO upon the observed freshening trends of the western tropical Pacific Ocean, *Geophys. Res. Lett.*, *38*, L21607, doi:10.1029/2011GL049636.
- Singh, A., T. Delcroix, and S. Cravatte (2011), Contrasting the flavors of El Niño–Southern Oscillation using sea surface salinity observations, *J. Geophys. Res.*, *116*, C06016, doi:10.1029/2010JC006862.
- Slemons, L. O., J. W. Murray, J. Resing, B. Paul, and P. Dutrieux (2010), Western Pacific coastal sources of iron, manganese, and aluminum to the Equatorial Undercurrent, *Global Biogeochem. Cycles*, *24*, GB3024, doi:10.1029/2009GB003693.
- Stoens, A., et al. (1999), The coupled physical–new production system in the equatorial Pacific during the 1992–1995 El Niño, *J. Geophys. Res.*, *104*, 3323–3339, doi:10.1029/98JC02713.
- Strutton, P. G., and F. P. Chavez (2000), Primary productivity in the equatorial Pacific during the 1997–98 El Niño, *J. Geophys. Res.*, *105*, 26,089–26,101, doi:10.1029/1999JC000056.
- Strutton, P. G., J. P. Ryan, and F. P. Chavez (2001), Enhanced chlorophyll associated with tropical instability waves in the equatorial Pacific, *Geophys. Res. Lett.*, *28*, 2005–2008, doi:10.1029/2000GL012166.
- Strutton, P. G., W. Evans, and F. P. Chavez (2008), Equatorial Pacific chemical and biological variability, 1997–2003, *Global Biogeochem. Cycles*, *22*, GB2001, doi:10.1029/2007GB003045.
- Takahashi, K., A. Montecinos, K. Goubanova, and B. Dewitte (2011), ENSO regimes: Reinterpreting the canonical and Modoki El Niño, *Geophys. Res. Lett.*, *38*, L10704, doi:10.1029/2011GL047364.
- Trenberth, K. E., and D. P. Stepaniak (2001), Indices of El Niño evolution, *J. Clim.*, *14*, 1697–1701, doi:10.1175/1520-0442(2001)014<1697:LIOENO>2.0.CO;2.
- Turk, D., M. R. Lewis, G. W. Harrison, T. Kawano, and I. Asanuma (2001), Geographical distribution of new production in the western/central equatorial Pacific during El Niño and non–El Niño conditions, *J. Geophys. Res.*, *106*, 4501–4515, doi:10.1029/1999JC000058.
- Turk, D., C. S. Meinen, D. Antoine, M. J. McPhaden, and M. R. Lewis (2011), Implications of changing El Niño patterns for biological dynamics in the equatorial Pacific Ocean, *Geophys. Res. Lett.*, *38*, L23603, doi:10.1029/2011GL049674.
- Ueki, I., Y. Kashino, and Y. Kuroda (2003), Observation of current variations off the New Guinea coast including the 1997–1998 El Niño period and their relationship with Sverdrup transport, *J. Geophys. Res.*, *108*(C7), 3243, doi:10.1029/2002JC001611.
- Vialard, J., C. Menkes, J.-P. Boulanger, P. Delecluse, E. Guilyardi, M. J. McPhaden, and G. Madec (2001), A model study of oceanic mechanisms affecting equatorial Pacific sea surface temperature during the 1997–98 El Niño, *J. Phys. Oceanogr.*, *31*, 1649–1675, doi:10.1175/1520-0485(2001)031<1649:AMSOOM>2.0.CO;2.
- Vichi, M., S. Masina, and F. Nencioli (2008), A process-oriented model study of equatorial Pacific phytoplankton: The role of iron supply and tropical instability waves, *Prog. Oceanogr.*, *78*, 147–162, doi:10.1016/j.pcean.2008.04.003.
- Vincent, E. M., M. Lengaigne, C. E. Menkes, N. C. Jourdain, P. Marchesio, and G. Madec (2009), Interannual variability of the South Pacific Convergence Zone and implications for tropical cyclone genesis, *Clim. Dyn.*, *36*, 1881–1896, doi:10.1007/s00382-009-0716-3.
- Webster, P. J., and R. Lukas (1992), TOGA-COARE: The Coupled Ocean–Atmosphere Response Experiment, *Bull. Am. Meteorol. Soc.*, *73*, 1377–1416, doi:10.1175/1520-0477(1992)073<1377:TCTCOR>2.0.CO;2.
- Wells, M. L., G. K. Vallis, and E. A. Silver (1999), Tectonic processes in Papua New Guinea and past productivity in the eastern equatorial Pacific Ocean, *Nature*, *398*(6728), 601–604, doi:10.1038/19281.
- Wilson, C., and D. Adamec (2001), Correlations between surface chlorophyll and sea surface height in the tropical Pacific during the 1997–1999 El Niño–Southern Oscillation event, *J. Geophys. Res.*, *106*, 31,175–31,188, doi:10.1029/2000JC000724.
- Yeh, S.-W., J.-S. Kug, B. Dewitte, M.-H. Kwon, B. P. Kirtman, and F.-F. Jin (2009), El Niño in a changing climate, *Nature*, *461*, 511–514, doi:10.1038/nature08316.
- Yoder, J. A., and M. Kennelly (2003), Seasonal and ENSO variability in global ocean phytoplankton chlorophyll derived from 4 years of SeaWiFS measurements, *Global Biogeochem. Cycles*, *17*(4), 1112, doi:10.1029/2002GB001942.
- Yoder, J. A., S. G. Ackleson, R. T. Barber, P. Flament, and W. M. Balch (1994), A line in the sea, *Nature*, *371*, 689–692, doi:10.1038/371689a0.
- Yu, J.-Y., and S. T. Kim (2010), Identification of central-Pacific and eastern-Pacific types of ENSO in CMIP3 models, *Geophys. Res. Lett.*, *37*, L15705, doi:10.1029/2010GL044082.
- Yu, J.-Y., H.-Y. Kao, T. Lee, and S. T. Kim (2010), Subsurface ocean temperature indices for central-Pacific and eastern-Pacific types of El Niño and La Niña events, *Theor. Appl. Climatol.*, *103*, 337–344, doi:10.1007/s00704-010-0307-6.

T. Delcroix, F. Léger, M.-H. Radenac, and A. Singh, LEGOS, UMR 5566, CNRS/IRD/CNES/UPS, 14 avenue Edouard Belin, F-31400 Toulouse, France. (marie-helene.radenac@legos.obs-mip.fr)

Appendix III Scientific News Sheet, IRD, 2012

Actualité scientifique

Scientific news

Actualidad científica



N° 405

Mai 2012

Le nouveau visage d'El Niño

El Niño change de visage. Ce perturbateur climatique prend de plus en plus souvent la forme d'une variante appelée Modoki, « semblable mais différent » en japonais. Le cœur du phénomène se déplace alors de l'est du Pacifique tropical vers le centre du bassin océanique. De nouveaux travaux de chercheurs de l'IRD et de leurs partenaires du laboratoire Legos¹ décrivent Modoki sur le plan biologique en zone équatoriale. Un tel épisode appauvrit en phytoplancton la partie centrale du Pacifique : les images satellitaires analysées de 1997 à 2010 révèlent des eaux beaucoup moins vertes lors des événements de 2002 à 2007 et 2009-2010. Cette couleur traduit la teneur réduite en algues marines en surface, synonyme d'une faible activité biologique. Une autre étude avec des chercheurs péruviens² et du laboratoire Locean³ révèle que Modoki, à l'inverse de son grand cousin, pourrait favoriser l'*upwelling*⁴ le long de la côte sud-américaine. Une simulation océanique haute résolution, confrontée aux données satellites et historiques de l'Imarpe⁵, indique un renforcement de cette remontée d'eaux froides et chargées en éléments nutritifs au cours des récents épisodes. L'augmentation annoncée de la fréquence de Modoki⁶ pourrait ainsi influencer les pêches dans la zone.



Les El Niño de type Modoki, qui prennent naissance au-dessus du Pacifique équatorial (ici au large des Îles Salomon), sont de plus en plus fréquents par rapport aux épisodes classiques.

Prenant naissance tous les deux à sept ans dans le Pacifique équatorial, El Niño sème le désordre sur l'ensemble du globe et dans l'économie mondiale. Mais, depuis dix ans, il change de visage. Il revêt de plus en plus souvent des allures de Modoki, « semblable mais différent » en japonais, comme l'a baptisé l'équipe nipponne qui a découvert ce cousin moins tumultueux qui provoque des sécheresses en Inde ou en Australie. De récents travaux ont décrit les manifestations physiques de cette variante d'El Niño, avec un déplacement du cœur du phénomène de l'est vers le centre du bassin Pacifique. Restait à examiner ses impacts sur la biologie marine et son influence probable sur les pêches. Pour ce faire, des chercheurs de l'IRD et leurs partenaires des laboratoires Legos¹ et Locean³ ont étudié ses conséquences sur les tous premiers maillons de la chaîne alimentaire.

Moins de vie aquatique au centre du Pacifique

De façon analogue aux mécanismes physiques, les épisodes de type Modoki consistent d'un point de vue biologique en un déplacement des manifestations du

phénomène. On n'assiste plus en effet, comme lors d'un El Niño classique, à un appauvrissement des eaux en phytoplancton de manière très étalée vers l'est du Pacifique, mais de façon plus localisée dans la partie centrale du bassin.

Les océanographes ont observé la couleur du Pacifique grâce aux images satellitaires « couleur de l'eau » de 1997 à 2010. La couleur bleue ou verte de l'océan contemplée depuis l'espace reflète en effet les variations de la concentration en chlorophylle de surface. Lors des événements Modoki survenus en 2002-2003, 2004-2005, 2006-2007 et 2009-2010, les scientifiques ont ainsi observé au centre du bassin Pacifique de faibles teneurs en chlorophylle, inférieures à 0,1 mg par m³. Ce pigment vert permet aux végétaux, et notamment aux algues marines, d'effectuer la photosynthèse. Sa concentration constitue donc un indicateur de la biomasse en phytoplancton à la surface de l'océan. Les valeurs observées dans la partie centrale du bassin au cours des récents El Niño Modoki traduisent alors la pauvreté des eaux en éléments nutritifs nécessaires au développement végétal et donc à la vie marine.

Quand El Niño se mêle de la météo

En temps « normal » au-dessus du Pacifique, les vents alizés soufflent fortement d'est en ouest. Ils accumulent et confinent ainsi dans la partie occidentale de l'océan les eaux chaudes et pauvres de surface qui constituent la « *warm pool* ». Ce gigantesque réservoir d'eau chaude de plus de 28°C alimente les flux de chaleur et d'humidité de la majeure partie de l'atmosphère terrestre, telle la « pompe à chaleur » de la planète. Lorsque se déclenche un épisode El Niño classique, les alizés faiblissent brutalement et le phénomène d'*upwelling*¹ qui est induit le long de l'équateur par la force de Coriolis ralentit. L'immense réservoir se répand alors dans le Pacifique vers l'est et les eaux s'appauvrissent.

En revanche, quand vient le tour de Modoki, les alizés faiblissent peu. On observe alors un ralentissement moindre de l'*upwelling* équatorial et un blocage des eaux de la « *warm pool* », ce qui explique un appauvrissement beaucoup plus localisé dans le centre de l'océan.

Des eaux plus froides et plus riches à l'est

Une autre étude récente, réalisée en partenariat avec des chercheurs péruviens², vient de montrer que les événements de type Modoki pourraient favoriser le phénomène d'*upwelling* qui se produit cette fois le long des côtes sud-américaines.

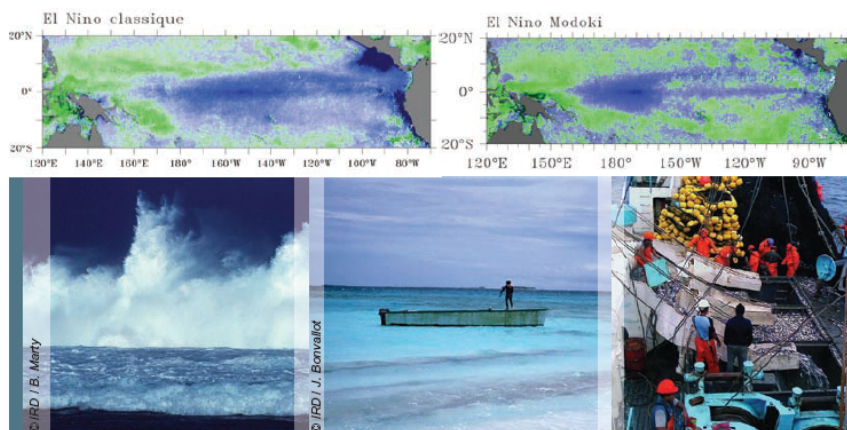
Au cours de ces travaux, l'équipe de recherche s'est intéressée à la température de surface de

l'océan, toujours observée depuis l'espace et simulée à partir d'un modèle océanique haute-résolution. Pour ce faire, les scientifiques ont analysé les images satellite au large du Pérou depuis 1981 et une simulation haute résolution depuis 1958. Ils montrent ainsi un refroidissement des eaux à proximité des côtes péruviennes, traduisant un renforcement de l'*upwelling*, lié à l'augmentation de la fréquence des événements Modoki. Cette remontée d'eaux profondes froides et chargées en éléments nutritifs favorise la productivité des eaux dans la région. La nouvelle facette d'El Niño pourrait donc avoir un effet sur la ressource halieutique au large de l'Amérique du Sud.

D'abord perçu par les scientifiques comme un phénomène nouveau, Modoki est apparu au fil des recherches comme une variante d'El Niño. En effet, Modoki n'est pas récent. Les chercheurs ont retrouvé sa trace dans des enregistrements climatiques au cours des 120 dernières années⁶. Mais, si le lien avec le changement climatique n'est pas fermement établi, sa fréquence pourrait être multipliée par cinq à l'horizon 2050⁶. Les épisodes classiques majeurs de 1982-1983 et 1997-1998 ont fait chuter les stocks des poissons notamment péruviens. Qu'en sera-t-il de Modoki ? Avec quelle ampleur il influencera les pêches reste désormais à déterminer.

Rédaction – DIC, Gaëlle Courcoux

1. Laboratoire d'études en géophysique et océanographie spatiales (UMR IRD / CNRS / UPS Toulouse 3)
2. du LMI DiscOH (Imarpe, IGP et Senamhi)
3. Laboratoire d'océanographie et du climat : expérimentations et approches numériques (UMR IRD / CNRS / MNHN / UPMC Paris 6)
4. Un *upwelling* est une zone de remontée d'eaux plus froides et riches en éléments nutritifs vers la surface. Le long de l'équateur, du fait de la force de Coriolis, les masses d'eau entraînées par les alizés sont repoussées vers les pôles et remplacées par des eaux profondes.
5. *Instituto del Mar del Perú*
6. *Nature*, 2009, 461 (7263), p. 511-514. fdi:010048207



Lors d'un épisode Modoki, les eaux appauvries en phytoplancton (en bleu sur l'image satellitaire) se concentrent dans la partie centrale de l'océan. Cette autre facette d'El Niño pourrait ainsi avoir un impact sur les stocks de pêches de subsistance (en Polynésie au centre) ou industrielles (au Pérou à droite) du Pacifique tropical.

Abonnez-vous aux fiches d'actualité de l'IRD : fichesactu@ird.fr

POUR EN SAVOIR PLUS

Contacts

MARIE-HÉLÈNE RADENAC, chercheuse à l'IRD
Tél. : +33 (0)5 61 33 30 00
marie-helene.radenac@ird.fr

THIERRY DELCROIX, chercheur à l'IRD
thierry.delcroix@ird.fr

BORIS DEWITTE, chercheur à l'IRD
Tél. : +33 (0)5 61 33 30 05
boris.dewitte@ird.fr

UMR Legos (IRD / CNES / CNRS / Université Paul Sabatier - Toulouse 3)

Adresse

Legos
14, avenue Édouard-Belin
31400 Toulouse cedex 9

Références

RADENAC MARIE-HÉLÈNE, LÉGER F., SINGH AWNESH AND DELCROIX THIERRY, Sea surface chlorophyll signature in the tropical Pacific during eastern and central Pacific ENSO events, *Journal of Geophysical Research*, 2012, 117, C04007. fdi:010055078.

DEWITTE BORIS, VASQUEZ-CUERO J., GOUBANOVA K., ILLIG SÉRÉNA, TAKAHASHI K., CAMBON GILDAS, PURCA S., CORREA D., GUTIERREZ D., SIFEDDINE ABDEL AND ORTLIEB LUC, Change in El Niño flavours in 1958-2008: Implications for long term upwelling trend off Peru. *Deep Sea Research*, 2012, in press. <http://dx.doi.org/10.1016/j.dsr2.2012.04.011>

Mots clés

El Niño Modoki, Pacifique équatorial, phytoplancton, pêche

Coordination

Gaëlle COURCOUX
Direction de l'Information et de la culture scientifiques pour le Sud
Tél. : +33 (0)4 91 99 94 90
Fax : +33 (0)4 91 99 92 28
fichesactu@ird.fr
www.ird.fr/la-mediathèque



Relations avec les médias

Cristelle DUOS
+33 (0)4 91 99 94 87
presse@ird.fr

Indigo, photothèque de l'IRD

Daina RECHNER
+33 (0)4 91 99 94 81
indigo@ird.fr
Retrouvez les photos de l'IRD concernant cette fiche, libres de droit pour la presse, sur :
www.Indigo.Ird.fr



Institut de recherche pour le développement
44 boulevard de Dunkerque,
CS 90009
13572 Marseille Cedex 02
France

Appendix IV Résumé étendu

Le phénomène El Niño Oscillation Australe (ENOA) est le signal climatique le plus fort de la planète à l'échelle interannuelle. Comprendre les mécanismes moteurs et pouvoir anticiper l'impact environnemental de ce phénomène constituent donc des enjeux scientifiques et sociétaux de première importance, notamment pour les Pays Emergents. Des progrès considérables ont été réalisés ces dernières années quant à l'observation, la compréhension et la prévision d'ENOA, grâce à la mise en place, au maintien et à l'amélioration de systèmes d'observations in situ et satellitaires, au développement de théories nouvelles pouvant rendre compte de sa nature quasi-cyclique, à la modélisation numérique et à l'assimilation de données. Des travaux récents suggèrent cependant que certaines des caractéristiques majeures d'ENOA pourraient être en train de changer avec, en particulier, la mise en évidence d'un 'nouveau type' d'El Niño, appelé selon les auteurs El Nino modoki, Central Pacific El Niño ou Warm Pool El Niño. Faisant suite et en complément à ces travaux, les objectifs de ce travail de thèse sont d'analyser:

1. la signature des différents types d'ENOA pour plusieurs variables climatiques essentielles (température et salinité de surface, niveau de la mer, courant de surface, précipitation, vent de surface, ...);
2. la pertinence de la théorie dite de recharge / décharge, une des quatre théories majeures d'ENOA, à rendre compte ou non de la nature quasi oscillatoire des différents types d'ENOA; et
3. l'impact potentiel des modifications des caractéristiques majeures d'ENOA sur notre interprétation des tendances climatiques à 'long' terme pour plusieurs variables climatiques essentielles.

Une analyse en clusters nous a permis d'identifier la signature des événements ENOA de type canonique et modoki pour les variables climatiques essentielles répertoriées ci-dessus. A titre d'exemple, en salinité de surface, grâce à des observations collectées entre 1977 et 2008, nous mettons en évidence l'existence de trois événements El Niño canoniques (1982-83, 1991-92 et 1997-98), de sept événements El Niño modoki (1977-78, 1986-88, 1990-91, 1992-95, 2002-03, 2004-05 et 2006-07), de six événements La Niña canoniques (1985-86, 1988-89, 1995-96, 1999-2001, 2005-06 et 2007-08) et de deux événements La Niña modoki (1983-

84 et 1998-99). Les événements El Niño canoniques se caractérisent par un déplacement vers l'Est (sur plus de 3000 km) du bord Est de la warm/fresh pool dans la bande équatoriale, ce qui se traduit par une baisse maximum de salinité de surface de l'ordre de -1 au voisinage de la ligne de changement de date. Ils se caractérisent également par une augmentation de la salinité de surface de l'ordre de +1 sous la position moyenne de la Zone de Convergence du Pacifique Sud (ZCPS). Les déplacements du bord Est de la warm/fresh pool et l'augmentation de la salinité de surface sous la ZCPS se trouvent réduits de moitié pendant les événements El Niño modoki, la région de baisse maximum de la salinité de surface se situant quant à elle environ 1500 km plus à l'Ouest dans la bande équatoriale. Une analyse qualitative basée sur des observations in situ et satellitaires de courant de surface et de précipitation suggère que les anomalies observées de salinité de surface ainsi que le contraste entre les événements ENOA canonique et modoki sont régis essentiellement par des modifications de la circulation océanique zonale et des précipitations.

Une analyse contrastant les différents types d'ENOA est également conduite en termes de dynamique océanique, l'accent étant mis sur le paradigme de Recharge Décharge (RD). La pertinence de ce paradigme est évaluée en étudiant la variabilité du volume d'eau chaude (température > 20°C) de la bande équatoriale, estimée à la fois à partir de données de niveau de la mer issues de mesures satellitaires sur la période 1993-2000 et de données hydrologiques issues du modèle de circulation océanique Drakkar sur la période 1958-2007. L'analyse du volume d'eau chaude (observé et modélisé) et de la température de surface de l'océan correspondante montre clairement l'existence de quatre situations types caractérisant les événements El Niño et La Niña canonique et modoki. Elle montre également une décharge en volume d'eau chaude de la bande équatoriale pendant les événements El Niño canoniques, en accord avec le paradigme de RD, celle-ci devenant quasi inexistante pendant les événements El Niño modoki. Nous montrons que la décharge de la bande équatoriale pendant les événements El Niño canoniques est liée à un transport d'eaux chaudes en direction des pôles se produisant sur la quasi-totalité du Pacifique. Ce transport vers les pôles n'apparaît que dans la moitié Ouest du Pacifique et se trouve compensé par un transport vers l'équateur dans la moitié Est pendant les événements El Niño modoki, en lien avec la structure zonale de la pente de la thermocline. Le paradigme de RD ne semble donc pas s'appliquer aux événements El Niño modoki.

Le rôle potentiel des différents types d'ENOA et de leurs caractéristiques respectives sur le calcul des tendances climatiques est analysé pour plusieurs variables climatiques essentielles. En salinité de surface, par exemple, nous montrons qu'au cours de la période 1955-2008 les événements ENOA canoniques n'ont pas d'effet sensible sur la mise en évidence récente (attribuée au changement climatique) de l'expansion vers l'Est des eaux de faible salinité de la warm/fresh pool et sur la diminution de la salinité de surface dans cette région. Nous montrons, a contrario, que les événements de type modoki contribuent à augmenter la désalinisation de la partie ouest de la warm/fresh pool et à augmenter la salinité de surface sous la ZCPS. Ces événements modoki tendent ainsi à minimiser la baisse observée de la salinité de surface à long terme (>30 ans) dans la moitié Ouest du Pacifique tropical, cette dernière ne pouvant donc être attribuée aux changements des caractéristiques d'ENOA. Nous soulignons par ailleurs la sensibilité du calcul des tendances à long terme en salinité de surface à la durée des observations. Des analyses similaires sont conduites pour la température de surface et le niveau de la mer.

Mots-clés

ENSO, ENOA, El Niño, La Niña, Océan Pacifique Tropical, *warm pool*, *SPCZ*, ZCPS, température de surface, salinité de surface, niveau de la mer, volume d'eau chaude, oscillateur rechargé/déchargé

Appendix V Thesis Journey

During the course of this project, three seminars, two posters and one oral presentation at scientific meetings, three peer-reviewed publications and participation in a summer school were realized. In addition, a paper has been submitted for possible publication. These are itemized below.

Publications

- Singh, A., Delcroix, T., and Cravatte, S. (2011). Contrasting the flavors of El Niño-Southern Oscillation using sea surface salinity observations, *Journal of Geophysical Research*, **116**(C06016), doi:10.1029/2010JC006862.
- Singh, A., and Delcroix, T. (2011). Estimating the effects of ENSO upon the observed freshening trends of the western tropical Pacific Ocean, *Geophysical Research Letters*, **38**(L21607), doi:10.1029/2011GL049636.
- Radenac, M. H., Léger, F., Singh, A., and Delcroix, T. (2012). Sea surface chlorophyll signature in the tropical Pacific during Eastern and Central Pacific ENSO events, *Journal of Geophysical Research*, **117**(C04007), doi:10.1029/2011JC007841.
- Singh, A., and Delcroix, T. (2012). Eastern and Central Pacific ENSO and their relationships to the recharge/discharge oscillator paradigm, *Deep Sea Research: Part I*, submitted, manuscript number: DSR1-D-12-00158.

Seminars

- *Climatic changes in the tropical Pacific region and contrasting El Niño events using Sea Surface Salinity observations* presented at the University of the South Pacific, Suva, Fiji, 16 August 2010.
- *ENSO-related sea surface salinity changes and long-term freshening trends* presented at the Journées Scientifiques du LEGOS, Toulouse, France, 1 February 2011.
- *Climate Change: El Niño Modoki and Sea Surface Salinity in the Tropical Pacific* presented at the University of the South Pacific, Suva, Fiji, 19 August 2011.

Meetings

- Singh, A., T. Delcroix, and S. Cravatte. *Contrasting El Niño Southern Oscillation events in the western tropical Pacific using Sea Surface Salinity Observations*. Poster presentation, AGU Fall Meeting, San Francisco, USA, 13-17 December 2010.
- Singh, A., T. Delcroix, and S. Cravatte. *Contrasting El Niño Southern Oscillation events in the tropical Pacific using Sea Surface Salinity Observations*. Poster presentation, EGU General Assembly, Vienna, Austria, 3-8 April 2011. Received an Outstanding Poster Award in the Nonlinear Processes in Geosciences Division of the EGU.
- Singh, A., T. Delcroix, and S. Cravatte. *ENSO-related sea surface salinity changes and long-term freshening trends in the western tropical Pacific*. Oral presentation, 10th International Conference on Southern Hemisphere Meteorology and Oceanography, Noumea, New Caledonia, 23-27 April 2012.
- Delcroix, T., F. Léger, M.-H. Radenac, and A. Singh. *Seasonal sea surface salinity and temperature changes in the western Solomon and Bismarck Sea*. Oral presentation by the first author, 10th International Conference on Southern Hemisphere Meteorology and Oceanography, Noumea, New Caledonia, 23-27 April 2012.
- Singh, A., and T. Delcroix. *Testing the applicability of the ENSO recharge/discharge oscillator paradigm with altimetry- and model-derived sea level*, Oral presentation, 20 Years of Progress in Radar Altimetry 2012, Venice, Italy, 24-29 September 2012.
- Singh, A., and T. Delcroix. *Eastern and Central Pacific ENSO and their relationships to the recharge/discharge oscillator paradigm*. Oral presentation, AGU Fall Meeting, San Francisco, USA, 3-7 December 2012.

Other

- Summer school on *Physics of the Ocean* supported by Deutsche Physikalische Gesellschaft (DPG) and Wilhelm and Else Heraeus Foundation and held at Physikzentrum Bad Honnef, Germany from 11-16 September 2011.
- Research cruise termed *Pandora* on board *RV L'Atalante* to measure oceanic parameters in the *Coral* and *Solomon Seas*, 28 June - 6 August 2012.

AUTHOR:

Awnesh SINGH

TITLE:

Contrasting the flavors of ENSO and related trends in the tropical Pacific Ocean in recent decades

THESIS SUPERVISOR:

Thierry DELCROIX

DEFENSE:

LEGOS, 25 October, 2012

ABSTRACT

The main features of the Eastern (EP) and Central (CP) Pacific El Niño Southern Oscillation (ENSO) events are analyzed using 1950-2010 observed and modeled data. Using various analysis techniques, we found that the CP El Niño differs from the canonical EP El Niño in terms of amplitude and location of maximum/minimum sea surface temperature, sea surface salinity and sea level anomalies, and the recharge/discharge (R/D) dynamical mode. The distinctive R/D features are characterized by different transport mechanisms: during EP El Niño, there is a mass discharge of warm waters ($>20^{\circ}\text{C}$) over the entire equatorial band resulting in a change from El Niño to La Niña conditions. Whereas during CP El Niño, there is a compensating effect ensuing in relatively no overall discharge. Furthermore, the long-term trends due to ENSO are mostly because of the influence of CP El Niño, which for example, accounts up to 30% of the warming/freshening trends in the western-central equatorial Pacific.

KEYWORDS

ENSO, El Niño, La Niña, tropical Pacific, warm pool, SPCZ, sea surface temperature, sea surface salinity, sea level, warm water volume, recharge-discharge oscillator

DISCIPLINE: Physical Oceanography

LEGOS, 14 Avenue Edouard Belin, 31400 Toulouse, France

